CARBON FORMATION AND REMOVAL IN THE CONTEXT OF NICKEL CATALYSTS

by

CARLOS ANTÓNIO ALVES BERNARDO

A Thesis Submitted for
the Degree of Doctor of Philosophy
of the University of London

December, 1977

Department of Chemical Engineering and Chemical Technology
Imperial College, London SW7

A meus Pais, Maria e António

ABSTRACT

The formation of carbon from various hydrocarbons on nickel catalysts has been studied, in the absence and presence of steam, over the range of temperatures 400 - 800°C. The studies covered both the kinetics of the deposition and the structure and properties of the deposits formed. The gasification of the carbon deposits by steam, carbon dioxide and hydrogen has also been studied over the same temperature range.

The kinetic experiments were carried out using both a static system and a differential flow reactor fitted with a microbalance and an on-line chromatograph. Carbon formation and gasification on nickel foils and supported nickel catalysts was studied either at fixed conditions or by changing the reaction temperature and the partial pressure of the reactants. The structure and the composition of the deposits formed was studied using optical and electron microscopes, by electron and X-ray diffraction and by analytical techniques.

A detailed investigation of acetylene decomposition on polycrystalline foils and nickel single crystals was performed under batch and flow conditions for temperatures between 450 and 600°C. The effect of surface irregularities, grain boundaries and crystal orientation was studied: carbon formation was greatly enhanced if the surface was rough and there were grain boundaries present. Grain boundaries were shown to be involved in the process of carbon diffusion in nickel.

The curves of rate versus conversion obtained in batch conditions showed two maxima. The first was interpreted in terms of a combined effect of carbon nucleation and poisoning of the catalyst, while the second could be explained by the autocatalytic effect of the hydrogen produced in the reaction. The kinetic results obtained at low temperatures are in agreement with a previously proposed mechanism for the process, that supposes carbon diffusion through nickel to be the rate controlling step below 500°C. The kinetics of the deposition from aliphatic and aromatic hydrocarbons could not be explained by the same mechanism. The results seem to indicate control by surface reaction at these temperatures.

With all hydrocarbons, the rate of carbon deposition decreased when the temperature increased above 550 - 600°C. In the case of acetylene, ethylene and 1-butene, the kinetics determined for these conditions

were successfully explained by a theoretical model that supposed the surface reaction to be the rate controlling step of the process. The negative apparent activation energies were shown to be due to the effect of enhanced desorption of the reactants. A general discussion of the causes of the decrease in rate with temperature in the different systems is presented.

Nickel was found to be an effective catalyst for the gasification of carbon deposits. The kinetics of gasification by steam, carbon dioxide and hydrogen have been determined in the temperature range 475-850°C. The similarity of the main features of deposition and gasification of carbon indicates that the process of carbon diffusion through nickel may be operative in both reactions. This was used to explain the high reactivity of the present systems as compared to previous results on the gasification of nickel doped carbons. The relative efficacies of the three gases was also determined. Steam was found to be the more effective gasifying agent across the whole temperature range. Carbon dioxide is more reactive than hydrogen below 500 and above 700°C, but less reactive between 525-675°C. The reversal of the order of reactivity at high temperatures is thought to be due to equilibrium limitations that affect the reaction with hydrogen but are not important in the case of carbon dioxide.

The reaction of n-hexane with steam was usually accompanied by the deposition of carbon on the catalyst without apparent loss of catalytic activity. The rates of carbon formation in the presence and the absence of steam were compared with the rate of steam gasification to clarify the mechanism of coking of steam reforming catalysts. The results suggest that an adsorbed hydrocarbon intermediate acts as a precursor for both the coking and the steam reforming reactions.

ACKNOWLEDGEMENTS

My thanks are due to Dr. D.L. Trimm for his interest and guidance during the supervision of this research project; to Dr. K.C. Pratt for his help in the last part of the project; to Dr. G. Parry for advice in the interpretation of the X-ray results; to the Universidade do Minho for leave of absence and to the Comissao Permanente Invotan for the award of a generous scholarship. My special thanks to Dr. L.S. Lobo, whose friendship and enthusiasm made me decide to undertake this long period of research.

I would also like to express my gratitude to the British Gas Corporation, London Research Station, for providing catalysts, and helping in various ways; to the Departmental staff who assisted in carrying out this work; to my colleagues in the Laboratory, past and present, for their sense of humour and stimulating discussions. Particularly, I am indebted to Manuel Jerónimo who helped with computing and to José Luis Figueiredo who read critically some parts of the manuscript.

Finally I am grateful to Arlete and Miguel for making it all worthwhile.

CONTENTS

		Page
CHAPTER 1	INTRODUCTION	1
CHAPTER 2	EXPERIMENTAL	29
CHAPTER 3	RESULTS	55
CHAPTER 4	DISCUSSION	155
CONCLUSIONS		202
APPENDIX		206
REFERENCES		211

CHAPTER 1

INTRODUCTION

		Page
1.1	GENERAL	1
1.2	THE FORMATION OF CARBON	4
1.2.1	Thermodynamics of carbon formation	4
1.2.2	The kinetics of nucleation	6
1.2.3	The structure of carbon	9
1.2.4	The formation and properties of carbon	9
1.2.4.1	The influence of the metal substrate	12
1.2.5	The kinetics and mechanism of catalytic carbon formation from hydrocarbons	14
1.3	THE GASIFICATION OF CARBON DEPOSITS	20
1.4	THE DEPOSITION OF CARBON ON STEAM REFORMING CATALYSTS	25

CHAPTER 1

INTRODUCTION

1.1 GENERAL

The present work is concerned with the processes of carbon deposition and removal from nickel based catalysts. These catalysts are used in a wide range of industrial reactions that involve hydrocarbon processing, where formation of elemental carbon is an undesirable side reaction (1). The lay-down of carbon causes the deactivation of the catalysts by coverage of the surface or blockage of the pore "mouths" and its accumulation will also bring about an increase of the pressure drop through the reactor. This is a common problem of many processes of great economic significance, some of which are listed in Table 1.1.

The growth of carbon on hot metallic surfaces can also cause plugging and fouling of the other pieces of equipment, such as heat exchangers. Some processes suffer ill-effects in more than one operating region. For example, carbon can be deposited on either the inlet or the outlet of the reactor during the steam reforming of light hydrocarbons (2).

It is clearly of importance to understand the mechanism of carbon formation in order to be able to minimise these problems, and to avoid the deactivation of the catalysts. The present work is mainly concerned with catalyst deactivation by carbon deposition. It attempts to elucidate the process of carbon formation on metallic surfaces by coupling kinetic information with the observation of the morphology of the deposits.

The coking of industrial catalysts has been the subject of many publications. The various empirical equations proposed to describe the process have been reviewed by Szepe and Levenspiel (3). They showed that an equation of the type $-\frac{da}{dt} = k(T)a^n$, where: a - activity of the catalyst; t - time; k(T) - specific rate of deactivation; n - constant, generalizes most of the proposed deactivation laws. The effect of fouling on selectivity was reviewd by Satterfield (4) and Thomas and Thomas (5).

Table 1.1 Industrial processes affected by fouling

PROCESS	FEED	CATALYST	PRESSURE (atm)	TEMPERATURE (^{o}C)
Steam-Reforming	H_2O + CH_4 or higher hydrocarbons	Ni on Al_2O_3, MgO + a neutralizer	3 - 40	450 - 1000
Reforming	Naphthas	Pt/Al_2O_3 or MoO_3/Al_2O_3	10 - 40	450 - 530
Cracking	Heavy gas-oils	SiO_2-Al_2O_3 or zeolites	2 - 4	450 - 530
Dehydro-genation	Light hydro-carbons, ethyl benzene	$Ca_8Ni(PO_4)_6$, Al_2O_3-Cr_2O_3, Fe_2O_3	1 - 3	550 - 650
Fischer-Tropsch	CO + H_2	$Fe_2C/Fe_3O_4/Fe$; also Co or Ni based	17 - 25	220 - 350
Methana-tion	CO or CO_2 + H_2	Ni/Al_2O_3	1 - 30	230 - 450
Water-gas Shift	CO + H_2O	Fe_3O_4-Cr_2O_3	1 - 30	315 - 485

(Adapted from (7))

However, there are a number of problems that need further investigation. For instance, it is known that imperfections in metallic surfaces are centres of enhanced carbon deposition. This is thought to be related with the ease of nucleation of carbon in zones of energetic heterogeneity such as grain boundaries at their intersection with the surface (6). A better understanding of the role of grain boundaries on the process of carbon nucleation and growth seems to be necessary. This could be achieved by studying the deposition of carbon in the absence and in the presence of grain boundaries. Thus, studies of carbon formation on polycrystalline foils and single crystals of nickel of different finishings were performed. Another problem that needs clarification is the effect of hydrogen in the prevention of catalyst deactivation by coking at intermediate and high temperatures (relevant to the steam reforming and cracking processes) (7). This effect was also studied in order to find a mechanism for the deactivation at these temperatures.

The deactivation of catalysts poses problems of regeneration and optimum operation control. The regeneration of fouled catalysts is mainly achieved by burning-off the carbon with air, steam or mixtures of both. This subject has been reviewed by Satterfield (4). When the operation is carried out in fixed bed reactors, the regeneration takes place within a burning zone that moves slowly throughout the reactor. Control of the maximum temperature in this zone is critical if further deactivation of the catalyst by sintering is to be prevented. Sometimes, complete regeneration is not possible and the catalyst has to be replaced. This is particularly the case in the event of disintegration, due to carbon accumulation within the catalyst porous structure. Thus, it is important to define the operating conditions that promote the formation of desired products while supressing the formation of carbon. For instance, in the steam reforming of hydrocarbons, this could be achieved by enhancing the removal of the coke deposited on the catalyst by some of the gases present in the system. Either steam or some of the main reforming products could react with carbon to yield hydrogen, carbon monoxide and methane. With these ideas in mind, the study of the gasification of carbon deposited on nickel catalysts by steam, hydrogen and carbon dioxide was undertaken. It was thought that the knowledge of the kinetics of the gasification would allow the definition of conditions where carbon deposition could be minimized. These studies can also throw some light on the mechanism of coking of steam reforming catalysts.

The introduction chapter aims at providing a background for the various processes studied, including a review of the pertinent literature. The process of carbon formation is discussed first. The thermodynamics of carbon formation, the kinetics of nucleation and the structure of carbon are briefly described. Emphasis is given to the formation of carbon catalysed by metals. The catalytic carbon gasification and the coking of steam reforming catalysts are discussed next.

1.2 THE FORMATION OF CARBON

1.2.1 Thermodynamics of carbon formation

The standard free energies of formation represented in Fig. 1.1, show that the decomposition of hydrocarbons to give carbon and hydrogen can occur spontaneously at room temperature and above. High temperatures favour the decomposition of high paraffins. Paraffins with low molecular weights are stable at low and intermediate temperatures (methane, for instance, is thermodynamically stable until 570°C). The figure also shows that, at low temperatures, olefins can be hydrogenated to the corresponding paraffins, whilst high temperatures favour the reverse reaction. Acetylene, olefins and aromatic hydrocarbons will decompose spontaneously over the whole temperature range.

The fact that carbon formation is thermodynamically favoured does not mean that direct equilibria between hydrocarbon and carbon is always feasible. In most cases, intermediate steps are involved in the reaction, one of which is partial dehydrogenation. Direct equilibrium is only possible in the case of methane and this system has been studied by several workers (Fig. 1.2). The constants determined for the equilibrium have consistently deviated from those derived from graphite data (8,9). This subject has been investigated recently by Rostrup-Nielsen (10) and Renaud et al. (11). The deviations were explained in terms of the structural imperfectness of the carbon formed (compared with the ideal structure of graphite) and a contribution of the surface energy. A good correlation was observed between these deviations and the maxima crystallite sizes of the catalysts (10). The data obtained can be used, with certain limitations, to estimate the area of the metallic particles dispersed in the carbon.

Besides carbon and metal, other solid phases may be involved in the process of catalytic carbon formation. Namely, the presence of metal carbides has often been detected in the decomposition of hydrocarbons on transition metal catalysts (13). This fact complicates the

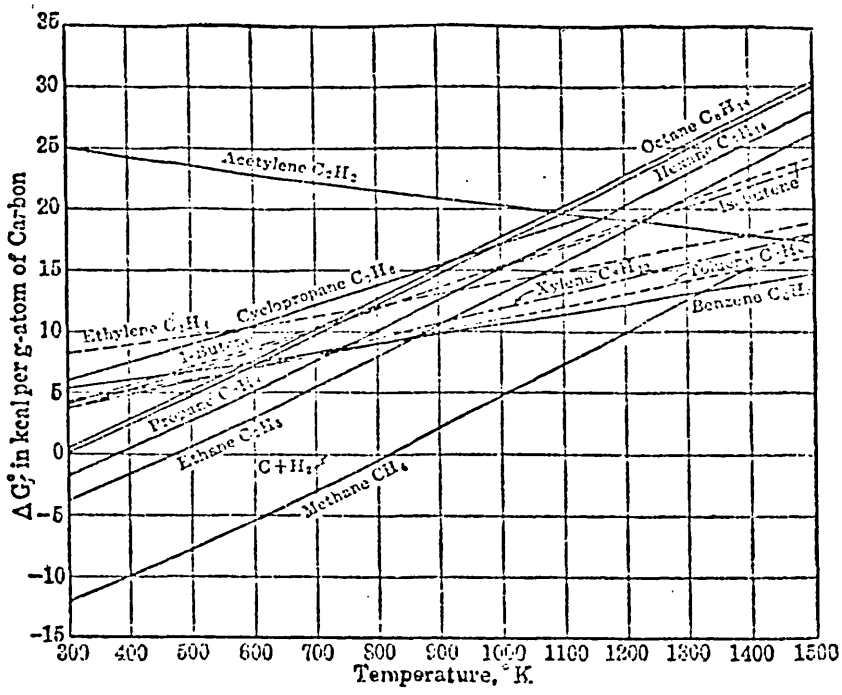

Fig. 1.1 Free energy of formation of hydrocarbons (From Reference 12)

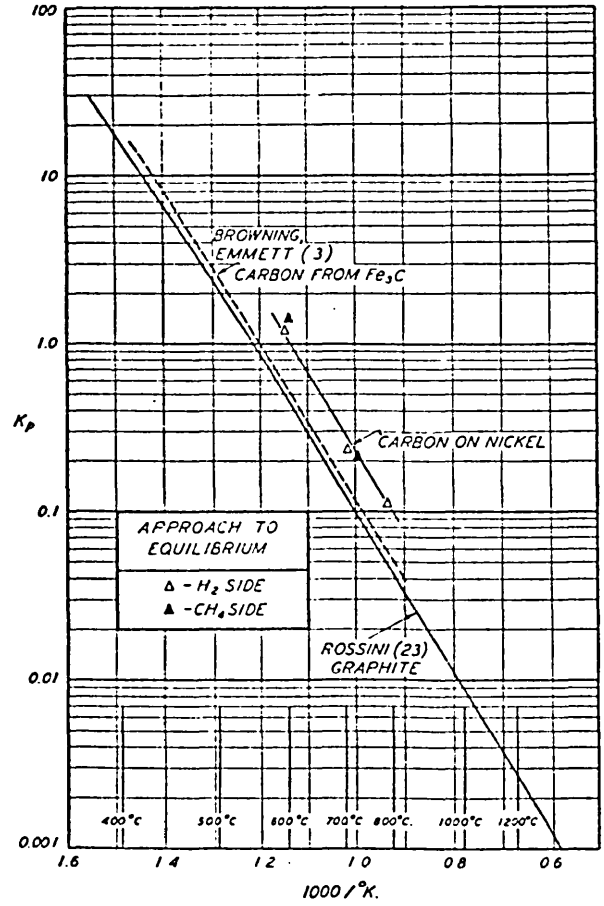

Fig. 1.2 Carbon-Hydrogen-Methane Equilibrium (From Reference 9)

study of the chemical equilibrium, since the phases involved are often unknown.

1.2.2 The kinetics of nucleation

Nucleation is the precondition for the growth of any solid phase. The nuclei grow by addition of free atoms or molecules, which initially causes an increase in ΔG_i, the free energy of the system. When the cluster reaches a critical size, further growth occurs with a decrease in free energy due to a strong contribution of the surface energy, γ, which is negligible in macroscopic particles. Thus, clusters larger than the critical size are stable and have a tendency to grow.

Several reviews have been published on the kinetics of homogeneous and heterogeneous nucleation (14-17). If nucleation occurs at any random point within a system it is considered homogeneous. This is only possible in an "ideal" system, chemically homogeneous and free from structural imperfections. In this case R^*, the critical size of the nuclei in a given system (or the corresponding critical free energy), can be calculated using an extension of the original theory of nucleation. This was derived for condensation from supersaturated vapours but has been corrected and extended to all types of phase changes. The theory relates R^* with ΔG_v, the difference of free energy between supersaturated vapour and bulk liquid:

$$R^* = \frac{-2\gamma}{\Delta G_v} \quad \text{or} \quad G_i^* = \frac{16\pi\gamma^3}{3\Delta G_v^2}$$

The derivation of these expressions assumes that the clusters are uniform and have the same properties of the bulk material and that the temperature of the system is below T_e (see Fig. 1.3a). T_e is the equilibrium temperature at which $\Delta G_v = 0$ and, therefore, the free energy of formation is infinite. This means that a phase change cannot take place unless there is some supersaturation to act as a driving force. The lower the temperature, the greater the supersaturation and hence the lower the value of R^*. This means that a larger number of nuclei will attain the critical size at lower temperatures.

The theory can also be used to predict J, the rate of nucleation, using a treatment similar to that of the transition state theory for homogeneous kinetics:

$$J = wa^*Ni^*$$

In this expression, Ni is the concentration of critical nuclei and w is the rate of impingement of atoms on the nuclei surface area, a^*.

Real systems always contain structural imperfections. The energy to generate a nucleus is generally less in these imperfections, which are high energy areas, and therefore "preferred" sites for nucleation. Hence, in heterogeneous nucleation, a geometric factor must be included in the equations to take into account the heterogeneity of the surface. In the case of a spherical cap nucleus, of spherical radius r and contact angle θ (see Fig. 1.3b), a factor, $f(\theta)$, has been defined, which is a measure of the "catalytic" potency of the substrate (14). The equation then becomes:

$$\Delta G_i^* = \frac{16\pi\gamma^3 f(\theta)}{3\Delta G_v^2}$$

In the expression, $f(\theta)$ is defined in such a way that when $\theta \to 0^o$ (that is, when the substrate is completely wetted), $f(\theta) \to 0$. Then $\Delta G_i^* \to 0$ and the nucleation will be rapid. If $\theta = 180^o$, $f(\theta) = 1$ and there will be only point contact with the surface. The equation will then become identical to that of the homogeneous nucleation. The value of the contact angle is determined by the relative values of the specific free energies of the vapour-substrate, vapour-condensate and condensate-substrate interfaces.

As shown in Fig. 1.3b) single atoms can join a critical nucleus either by direct addition from the gas phase or by surface diffusion after adsorption. The diffusion process is considered to predominate. At high temperatures the atomic mobility is high but, because of the large critical nucleus size, few nuclei are formed. At low temperatures the rate of nucleation is also low because, despite a small value of R^*, the atomic mobility is low. Hence, and particularly in the case of phase transformations in metals, the rate of nucleation should show a maximum at a temperature T_m (18).

Various theories have been proposed for crystal growth. Frank (19) postulated that crystals can grow satisfactorily from solutions of low supersaturation if the growth occurs at screw dislocations. This idea is capable of explaining the spiral growth patterns observed in some carbon-metal systems (20,21,22).

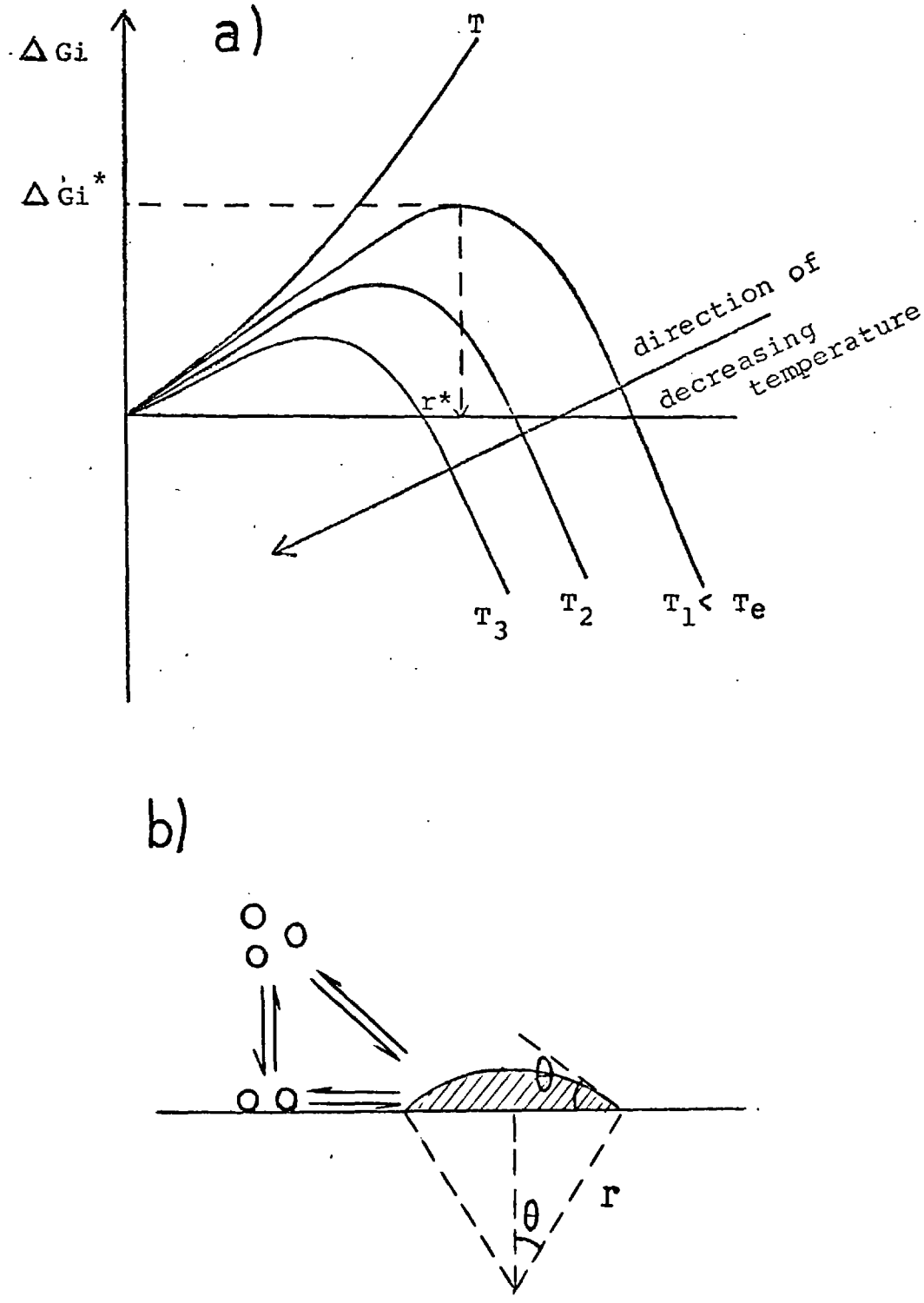

Fig. 1.3 Nucleation and Growth (Adapted from Reference 13):

a) Free energy of formation of a cluster

b) Formation of a cap-shaped nucleus in a vapour deposition process

1.2.3 The structure of carbon

Carbon can present a number of different structures ranging from near amorphous to highly crystalline. Graphite is the stable allotrope of carbon at normal conditions. Ideal graphite has an hexagonal structure (cell dimensions, a = 2.456 ^{o}A, b = 6.696 ^{o}A) with an interlayer stacking ABAB ... The interlayer spacing (d_c) is 3.353 ^{o}A at room temperature. A metastable rhomboedral form of graphite has also been observed with an arrangement of layers of the type, ABCABC... This form reverts to the hexagonal under mechanical treatment and both forms exist in association in natural graphite (13).

The "ideal" structure of graphite is rarely found, even in natural deposits. Crystallites of polycrystalline material (sometimes called "amorphous" carbon) consist of families of imperfect hexagonal planes, roughly parallel and equidistant, with a random orientation with respect to each other about the c-axis. This kind of stacking is called "turbostratic" (23). The material will be called "laminar" or "isotropic" depending on whether the c-axis of adjacent crystallites are nearly parallel or are randomly oriented, respectively.

The turbostratic stacking results in weaker bonds between the layers. The value of d_c increases proportionally and is 3.440 ^{o}A when the stacking sequence is completely random. In fact, a correlation between d_c and three dimensional order has been proposed (24):

$$d_c(^{o}A) = 3.440 - 0.086\ (1 - p^2)$$

where p represents the probability of adjacent layers being disoriented to each other. A similar correlation can also be formulated between the interlayer spacing and the degree of graphitization, defined as the probability of adjacent layers being ordered (13). Of all the parameters used to characterize carbons and graphite (d_c, crystallite diameter and height, density) the interlayer spacing is probably the most useful, as it is easily and accurately determined and is a good measure of the degree of structural order (25).

1.2.4 The formation and properties of carbon

Pyrolytic carbons are formed from carbon bearing gases at high temperatures, either homogeneously or heterogeneously. The two processes give two different types of carbon (gas phase and surface carbon). Gas phase carbon, also known as "carbon black", or "soot" is produced

in spherical particles formed by small crystallites, which tend to link together in chain-like structures. The mechanism of "soot" formation is still controversial, conflicting evidence having been advanced in favour of the different models proposed in the literature (26). Among these, the condensation theory seems to be quite successful in explaining most of the experimental facts in "soot" nucleation and the effect of the operation variables on the particles formed. According to this theory, the hydrocarbon is transformed by a gas phase reaction into macromolecules. The partial pressure of the macromolecules increases and eventually this induces the condensation into droplets, which are further pyrolysed to form a solid material. The type of carbon produced in this way seems to be independent of the structure of the parent hydrocarbon (27). In general, surface carbons have bigger crystallites, lower interlayer spacings and higher densities. They are obtained as films with well ordered crystallites deposited on solid substrates.

Typical properties and parameters of pyrolytic carbons are listed in Table 1.2.

In heterogeneous pyrolysis, the surface process appears to be the controlling factor in determining the crystallinity of the carbon. On some metallic substrates, highly crystalline deposits are formed at considerably low temperatures. Three dimensional order, together with considerable crystallite size, have been observed in many of these deposits. Similar degress of order could only be obtained in other surfaces if the temperature were substantially raised, sometimes more than 1000^{o}C (28). These substrates can thus be considered "catalytic" by comparison with "inert" surfaces, such as silica or porcelain. Nickel, cobalt and iron are highly effective catalytic substrates and have been the subject of many investigations (see Table 1.3). Some typical parameters of catalytic carbons are also included in Table 1.2.

Catalytic carbon deposits can be characterised according to their appearance and microstructure in three categories: laminar graphite, non-oriented graphite and fibrous carbon.

Laminar graphite has a structure close to that of ideal graphite, oriented with its basal plane parallel to the deposition surface to within a small angle (6,29). Complete films of this type of carbon have been described as featureless, except for a polygonal network of ridges that covers the whole surface. The ridges are believed to have been formed by compressive stresses set

Table 1.2 Typical properties of pyrolytic carbons

Type of Carbon	Temp (°C)	d spacing (°A)	Lc (°A)	La (°A)	C/H (atomic)	Density (g cm^{-3})
Gas phase	1000	3.61-3.70	12.2	42	8	—
Surface	1000	3.46-3.54	28	51	> 80	2.00
Catalytic	600	3.37	200	400	20	—
Graphite		3.35	∞	∞	∞	2.26

Abstracted from reference (7)

up in the film on cooling down (6,34). Laminar films can be obtained under conditions of relatively low hydrocarbon pressure and high substrate temperature (29-34). Derbyshire (34), produced these films pyrolysing light hydrocarbons over nickel and cobalt at 0.6 - 13 KN m^{-2} and 780-1100°C.

Non-oriented graphite, also described as "polycrystalline" or "floculent amorphous", is formed of small size crystallites, lacking orientation with the substrate. It is produced under conditions that favour high supersaturation of carbon in the metal (34). Usually, laminar graphite is also present in the deposits (31,33), and the nature of these two forms appears to be interchangeable. In fact, non-oriented graphite has been obtained from a laminar deposit by increasing the reactant pressure at fixed temperature, while a rise in temperature at fixed pressure results in the formation of laminar graphite from non-oriented films (33,34). Laminar graphite has also been formed from amorphous carbon films evaporated onto nickel and cobalt surfaces (34). Derbyshire et al. (35) found that there was a limit to the uptake of carbon on nickel substrates during the pyrolysis of methane and ethane. Total uptakes correlated well with the solubility of carbon in nickel from 800 to 1000°C, suggesting that a dissolution-precipitation mechanism plays an important role in the formation of laminar graphite.

Carbon fibres are usually long and thin (up to 7 μm long and 0.1 μm wide) and have an hollow core and a metal particle at the tip (36). The size of the particle correlates well with the fibre diameter (10, 22). Metal particles were also found along the fibre length (21, 46). The carbon is mainly turbostratic with the basal planes preferentially oriented parallel to the fibre axis (21,138). Filamentary carbon has been obtained on different metals (see table 1.3). On iron surfaces, filaments forming branched structures have been reported (22), while only single filaments were observed on nickel surfaces (36).

1.2.4.1 The influence of the metal substrate

The nature of the pyrolytic deposits depends on the catalytic activity of the substrate. This, in turn, depends on various factors, such as the homogeneity of the surface (6,37), the pretreatment of the sample (32,38-40) and the crystal faces presented to the gas phase (37,41-43).

Grenga and Lawless found that polycrystalline graphite nucleated at steps and kink sites on the surface, when decomposing carbon monoxide over nickel films (37). Presland et al. also observed preferential nucleation of graphite at kink sites in the surface during the pyrolysis of acetylene over platinum and nickel foils (6). Grain boundaries at their intersection with the surface, are zones of energetic heterogeneity and hence preferential sites for carbon nucleation (6).

Preannealing nickel foils under vacuum has been found to improve the rate of carbon formation and to lead to more crystalline deposits than those formed on untreated foils (32,38). Prereduction with hydrogen was also found to improve the crystallinity of the deposits. The hydrogen effect was attributed to the removal of the surface oxide (32). The rate of carbon formation over nickel was enhanced by preheating in air (39), while untreated foils and those prereduced in hydrogen gave similar rates of deposition (40). These apparently contradictory results can be reconciled. In fact, one of the more important effects of pretreatment is possibly to produce a particular crystalline rearrangement and this, in turn, may assist or retard the catalytic action of the metal (34).

In a series of papers, Leidheiser, Gwathmey and co-workers have shown that the catalytic activity for carbon formation of a metal depended on the crystal face exposed to the reacting gas (41-43). Rearrangement of the faces was observed during the decomposition of ethylene over nickel single crystal spheres (42). The order of descending activity for the deposition of graphitic carbon from carbon monoxide on single crystal spheres (41) was found to be: (111) > (110) > (100). However, in the case of ethylene, decomposition on the (111) face was less active than on the (110) face, and pretreatment with argon completely inhibited the deposition on both the (111) and the (100) faces (42).

Further evidence of the effect of crystal orientation was found in the pyrolysis of carbon bearing gases on nickel polycrystalline foils. After the reaction, certain grains were uncoated and the thickness of the carbon deposit varied from grain to grain (44).

1.2.5 The kinetics and mechanism of catalytic carbon formation from hydrocarbons

In recent years, a great number of publications (cf. Table 1.3), including some reviews (7,13), have dealt with the deposition of carbon from hydrocarbons on catalytic metals. Recently a detailed survey of the mechanisms proposed for the process of catalytic carbon formation has also been published (45). Table 1.3, updating references (7) and (13), summarises these publications.

Some important conclusions on the kinetics and the mechanism of carbon formation can be drawn from the literature survey presented in the table:

(a) Long periods of steady-state deposition have been observed in a large number of different systems (39,57,60,62).

(b) The carbon deposits contain metal particles (9,21,22,31,36,39,44, 46,60,68), often at the tip of carbon fibres (9,22,36,60,68). Different mechanisms of filament growth have been proposed (36,56,65). In the case of nickel (13,36), carbon deposited on the surface is taken into solution and diffuses through the nickel to active growth regions. Precipitation of carbon in these regions detaches particles from the surface or support. From then on, the particles will be carried on the top of the growing fibre. In the case of platinum-iron alloys a new mode of filament growth has been observed (65), involving extrusion of the filament from a catalyst particle which remains in contact with the support (see Fig. 1.4).

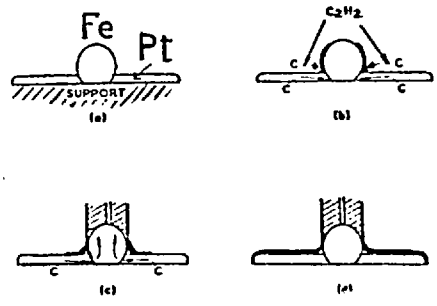

Fig. 1.4 Stages in the growth of filaments (65).

Table 1.3 Studies of catalytic carbon formation

AUTHOR		YEAR	PARENT GAS	CATALYST	TEMP (K)	COMMENTS
Cunningham	(42)	1957	C_2H_4	Ni	720	Effect of crystal face
Karu	(38)	1966	CH_4	Ni	1175-1375	Graphite growth
Lafitau	(48)	1967	CH_4	Ni	1270	C diffusion controls, E = 37 Kcal/mole
Escoubes	(47)	1967	CH_4,C_2H_2 C_2H_4,C_2H_6	Ni	460- 580	E = 22.5 Kcal/mole, C diffusion controls
Patrikiev	(49)	1968	C_2H_4	Ni	570- 820	Main gas products: C_2H_6 (700K), CH_4 (700-820K), H_2 (820K)
Tamai	(40)	1968	CH_4,C_2H_4 C_2H_6	Fe,Ni	1140-1300	Kinetic study
Tamai	(50)	1969	Idem	Fe,Ni	1170-1270	Effect of hydrogen: mechanism
Presland	(6)	1969	C_2H_2	Pt,Ni	1270	Mechanism proposed
Robertson	(29)	1969	CH_4	Fe,Co,Ni	920-1020	Growth of graphite
Robertson	(44)	1970	CH_4	Fe,Co,Ni	920-1020	Flake and polycrystalline carbon;metal found in carbon
Tesner	(51)	1970	C_2H_2	Ni-Cr	720- 970	Carbon fibres. Kinetics. Metal in carbon
Moayeri	(30)	1970	CH_4	Ni,Co	1070-1370	Growth of graphite Ni(111), Ni(110)
Presland	(32)	1970	C_2H_2	Ni	1270	Effect of crystal face on epitaxial growth
Blau	(33)	1970	C_2H_2	Ni	1070-1470	Effect of pressure and temperature on crystallinity
Lobo	(53)	1971	C_2H_2	Ni	670- 970	Complex temperature dependency. Gas phase above 870 K
Baird	(138)	1971	CH_4,C_3H_8	Ni	970	Structure of carbon fibres. Suggests atomic Ni in carbon
Tomita	(39)	1972	Benzene	Ni	870-1240	Flake and sooty carbon. Metal in carbon
Baker	(54)	1972	$CH_4/CO/CO_2$	Fe	725-1225	Mechanisms for amorphous C and graphite formation
Baker	(36)	1972	C_2H_2	Ni	870-1300	Mechanism for fibrous C formation. C diffusion in Ni

Table 1.3 (Continued)

Author		Year	Parent Gas	Catalyst	Temp (K)	Comments
Rostrup-Nielsen.	(10)	1972	CH_4,CO	Ni	720- 970	Equilibrium studies. Correlation with crystallite size
Robertson	(55)	1972	CH_4	Fe,Co,Ni	920-1020	Factors affecting flake or polycrystalline C formation
Lobo	(56)	1972	C_2H_2,C_2H_4, C_3H_6,C_4H_6 C_4H_8	Fe,Co,Ni Pd,Pt,Cu Ag,Au	570-1070	Pd,Pt,Cu,Ag,Au,inactive Mechanism: C diffusion in Ni, Ni crystallite transported
Lobo	(57)	1973	idem,plus C_3H_8 CH_4,C_2H_6,	Ni	670- 870	Autocatalytic deposition from olefins,very slow with paraffins. Effect of pretreatment
Baker	(22)	1973	C_2H_2	Fe,Co,Cr	785-1270	Mechanism of fibre growth: C diffusion in metal
Fryer	(58)	1973	C_6H_{12}	Pt	630	C fibres of graphitic nature
Lobo	(59)	1973	C_2H_4,C_4H_8	Ni	740- 820	Nucleation and growth models
Nishiyama	(60)	1974	Benzene	Ni/Cu	850-1170	Diffusion of C in metal
Moayeri	(61)	1974	C_3H_6	Ni	870	Graphite formed initially,then soot
Baird	(21)	1974	CH_4,C_3H_8 C_3H_6,C_4H_6	Fe,Ni	720- 970	Mechanism: surface diffusion of metal on carbon
Renaud	(11)	1974	CH_4,CO	Ni	720- 970	Correlation between particle size and excess free energy of formation of carbon
Figueiredo	(62)	1974	C_3H_6	Ni	670-1070	Effect of hydrogen. Mechanism of carbon formation discussed
Derbyshire	(35)	1975	CH_4,C_2H_4 C_2H_2,C_4H_6 benzene	Fe,Co,Ni	770-1370	Conditions of formation of laminar,non-oriented and fibrous carbon and metal carbides
Toei	(63)	1975	n-C_4H_{10}	Cr_2O_3/ γ-Al_2O_3	820	Dual active sites: dehydrogenation on cromia, coking on both cromia and alumina
Baker	(46)	1975	C_2H_2	Co	800-1150	Metal found in carbon fibres

Table 1.3 (Continued)

Author		Year	Parent gas	Catalyst	Temp (K)	Comments
Baker	(64)	1975	C_2H_4,C_6H_6 1,3-C_4H_6, C_3H_6	Co	1000K	Ratio: area filament wall/ area of filament, apparently correlates with the heat of formation of the hydrocarbon
Baker	(65)	1975	C_2H_2,C_2H_4	Pt-Fe	690-1175	Filaments extended from particles. Mechanism for extrusion growth proposed
Nishyama	(66)	1976	C_6H_6	Ni/Cu	840- 970	Effect of hydrogen: removal of chomisorbed species and of surface carbon
Wentreck	(67)	1976	CO	Ni	300- 723	Surface carbon from CO dissociation precursor to CH_4 formation
Keep	(68)	1977	C_3H_8	Ni	970	Carbon filaments formed from intermediate unsaturated hydrocarbons
Rostrup-Nielsen	(45)	1977		Ni		Review of the mechanisms of carbon formation on nickel
McCarty	(69)	1977	C_2H_4	Ni(110)	600	Dicarbon fragments formed on nickel surface

(c) The dependence on temperature of the rate of deposition is complex and a maximum between 500-650°C was observed by many researchers (7,13,34,51,66,70,71). Zero order kinetics (34,48,56,62) and apparent activation energies independent of the parent hydrocarbon, but dependent on the metal (22,36,56,62) were observed at lower temperatures. At higher temperatures the apparent activation energies decreases (34,53,62,66,71) and the orders of the reaction increase (7,62).

(d) Hydrogen has, in general, a positive effect on the rates of deposition (51,56,60) and, at high temperatures, plays an important role in preventing the deactivation of the metal (62,66).

(e) The diffusion of carbon through nickel has often been considered the rate controlling step at low temperatures (7,22,36,47,48,56,60, 68). The heat liberated in the decomposition of the hydrocarbon (which establishes a temperature gradient across the metal particles) was suggested to be the driving force for the diffusion of carbon (22,36,64). The basic difficulty with this approach is that the mechanism also explains the kinetics of carbon deposition, when the decomposition of the hydrocarbon is endothermic (7,45). A concentration driven dissolution-precipitation mechanism seems to be currently favoured (45). The upper and lower limits of the concentration gradient responsible for the diffusion are considered to be the solubility of carbon in nickel at the nickel gas interface and at the nickel graphite interface, respectively (see Fig. 1.5).

(f) As the temperature increases, the surface reaction becomes the rate determining step in some systems (45,53,62). The negative apparent activation energies observed in this temperature zone have been ascribed either to desorption effects (45,53,62), or to the formation of surface carbon films that deactivate the catalyst (34,66).

(g) At even higher temperatures the carbon forming reaction has been identified as the gas phase pyrolysis of the hydrocarbon (53, 72).

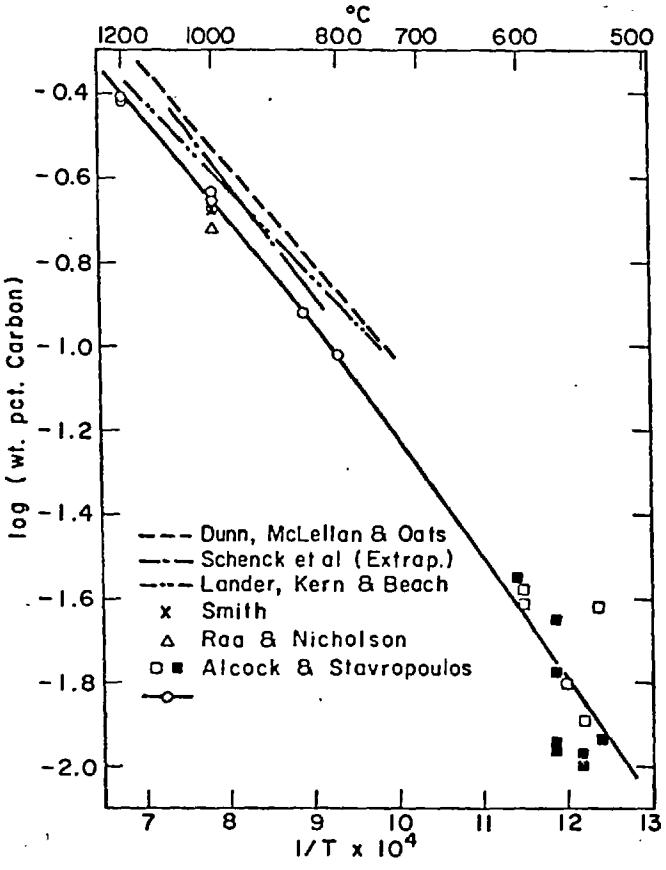

Fig. 1.5 Solubility of graphite in pure nickel (73)

——·——·—— Nickel-gas interface

———————— Nickel-graphite interface

1.3 THE GASIFICATION OF CARBON DEPOSITS

The gasification of carbon has been studied for many years and has been the subject of several reviews (74,75,76). Many of the earlier studies were concerned with oxygen gasification, mainly in the context of combustion processes. Interest in steam gasification has sprung from the necessity of preventing carbon deposition in the steam reforming of hydrocarbons (77). Carbon can also be gasified by carbon dioxide and by hydrogen.

Gasification, usually by steam and carbon dioxide, is the principal method used to modify the porosity of carbons and produce activated carbons. The properties of these carbons are dependent upon the existence of an extensive micropore structure, whose geometry is of prime importance in controlling the specificity of adsorption. The characterisation of this structure presents many difficulties since the determination of pore radius from adsorption measurements of BET surface areas and total pore volumes is not reliable in the case of microporous solids (79). Marsh and Rand (80,81) have used the Polanyi potential of adsorption to relate the distribution of the molar free energy of adsorption with the micropore volume. This is probably one of the best methods yet available to characterise the micropore structure it carbons. Recently a new isotherm equation that allows the determination of micropore volumes of carbon has been proposed (82). The volumes determined agree quite well with those obtained with the Dubinim equation (79).

The gasification by steam and carbon dioxide is not restricted by equilibrium limitations at high temperatures and atmospheric pressure, whereas these are important in the case of hydrogen (see Fig. 1.6). However, increasing the total pressure will favour gasification by hydrogen, and studies at temperatures as high as 1250^{o}C have been reported (78).

1.3.1 The catalysed gasification of carbon

The earlier studies of carbon gasification were, nolens volens, catalysed reactions, since the carbons used always contained a certain amount of impurities capable of catalytic action. The possibility of producing high purity carbons to which a controlled amount of catalyst could be added has enabled more detailed studies of the catalysed gasification. These studies have been the subject of an extensive

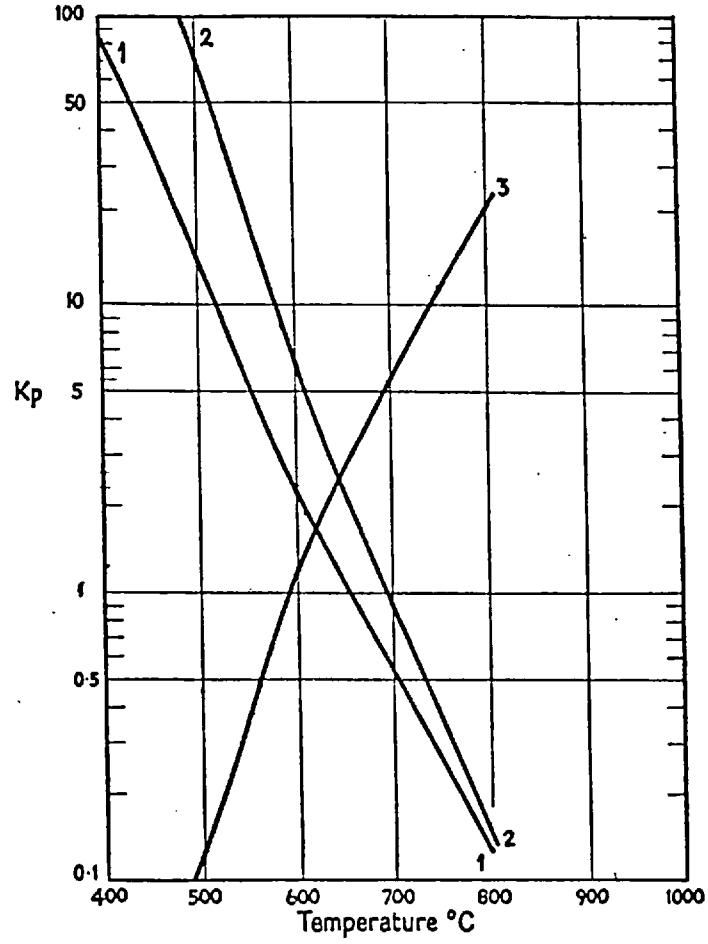

Fig. 1.6 Equilibrium constants for the carbon forming reactions: (From Reference 1)

$$(1)\quad CO+H_2 \leftrightharpoons C+H_2O \qquad K_p = \frac{P_{H_2O}}{P_{CO}P_{H_2}}$$

$$(2)\quad 2CO \leftrightharpoons C+CO_2 \qquad K_p = \frac{P_{CO_2}}{P_{CO}^2}$$

$$(3)\quad CH_4 \leftrightharpoons C+2H_2 \qquad K_p = \frac{P_{H_2}^2}{P_{CH_4}}$$

review by Walker et al. (76), which also reported their own results on gasification by carbon dioxide catalysed by transition metals. Two general mechanism of catalysis of the gasification were advanced by these authors: the oxygen-transfer and the electron transfer mechanisms.

The electron-transfer mechanism supposes that the unpaired electrons in the d-band of a transition metal will pair up with π electrons of the graphite in contact with the metal. As a result, the number of mobile π electrons in the graphite decreases. This, in turn, will weaken the average strength of the bonds between peripheral carbon atoms and carbon-oxygen complexes that are intermediates in the gasification process. Hence, the liberation of these to the gas phase will be facilitated and gasification enhanced.

This mechanism was not able to explain the observed experimental features of the carbon gasification catalysed by iron (83). The oxygen-transfer mechanism, originally advanced by Newman et al. (52), assumes that the catalyst undergoes a cycle between two oxidation states such as, metal and oxide or lower oxide and higher oxide. Walker et al. (76), extended the views of previous workers and proposed the following equation as representing the mechanism for the case of the $C-CO_2$ reaction:

$$xCO_2 + yFe = Fe_yO_x + xCO$$

$$Fe_yO_x + C = yFe + xCO$$

This mechanism implies catalyst-oxygen interaction and excludes interaction between carbon and catalyst. It was used to explain successfully the observed features of the carbon dioxide gasification, including the deactivation (by oxidation) of the catalyst (76). Experimental evidence was presented to support the view that the metal acts as a dissociation centre, producing active species that diffuse across the metal to react at the graphite-metal interface. Since the time Walker et al. published the aforementioned review much work has been published on catalytic gasification. Some of this work is listed in Table 1.4.

There exists disagreement amongst authors on the relative activities of transition metals as catalysts in gasification reactions. Walker et al. (76) reported the following order of reactivities for the gasification of carbon by carbon dioxide: Fe > Co > Ni (in the reduced state), whereas both Marsh et al. (91) and Tamai et al. (94) reported

Table 1.4 Studies of catalytic carbon gasification

Author		Year	Gas	Catalyst	Temp. (K)	Comments
Marsh	(84)	1971	CO_2	Ni,Fe	1120	Effect of metals on the development of microporosity during gasification
Tomita	(85)	1972	H_2	Various	300-1300	Order of reactivity: Rh ⩾ Ru ⩾ Ir > Pt > Ni >> Pd ⩾ Co ⩾ Fe
Gaidai	(86)	1974	H_2	Ni	570	Kinetics depending on the amount of carbon removed
Tomita	(87)	1974	H_2	Ni,Pt,Rh	700-1250	Two types of carbon present in the deposit gasifying at different temperatures
McKee	(88)	1974	Steam, H_2	Various	300-1300	Discussion of relative effects of the metals on the reactivity of graphite
Rewick	(89)	1974	Steam, H_2	Pt,Ru,Rh, Pd,Co,Ni	925-1175	Kinetics discussed, mechanism of gasification proposed
Marsh	(90)	1975	-	-	-	A mechanism is proposed for the catalysis of gasification by CO_2
Marsh	(91)	1975	CO_2,O_2	Ni,Co,Fe, Ag,Cu,Ca	770-1220	Porous and non-porous carbon studied. Gasification mechanism discussed
Figueiredo	(92)	1975	Steam, H_2	Ni, Ni/Al_2O_3	820-1020	Proposed rate determining steps: H_2-surface reaction, steam-diffusion of carbon through nickel
Nishiyama	(71)	1976	H_2	Ni	800-1170	Decrease of hydrogenation rate at high temperatures ascribed to equilibrium
Otto	(93)	1976	Steam	Ni,K	800-1100	Effect of addition of impurities
Tamai	(94)	1977	Steam, H_2,CO_2	Various	670-1220	Electron transfer mechanism used to explain the relative activities of the metals
Hahn	(95)	1977	Steam	Fe	1160-1270	Change of phase in iron influences catalytic activity
Marsh	(96)	1977	O_2	V,CR,Mn, Fe,Co	650-1000	Two different mechanisms possibly operative in the gasification

the order: Ni > Co > Fe. Disagreement is also found in the reported relative catalytic activities for steam and hydrogen gasification. The catalytic activity of nickel is considered to be greater than that of cobalt and iron by some authors (85,89,94) and smaller by others (88,97). These discrepancies are believed to be due to differences in the characteristics of the carbon (87,95) and to differences in the concentration and state of aggregation of the metal (91,96).

The concentration of the metal also influences the activation energy of the catalysed gasification. Marsh et al. (91) have observed that increasing the concentration of nickel in carbon decreased the activation energy for gasification by carbon dioxide (from 370 KJ $moles^{-1}$ for the pure graphite samples) to 190 KJ $moles^{-1}$. The authors explained this effect by suggesting that changes in concentration influence the size of the metal aggregates and this, in turn, determines their surface properties. A similar effect was observed in the oxygen gasification catalysed by cobalt (96). Otto et al. (93), studying the reaction between steam and carbon also observed a decrease in the activation energy (from 347 to 181 KJ $mole^{-1}$) when increasing concentrations of nickel were added to pure graphite. This effect, however, was explained by the occurrence of mass transfer limitations due to the enhancement of the gasification rate. Diffusion limitations have been detected in many systems (76,91,93,94), especially when steam was used as the gasifying agent (93,94).

The effect of the products of the $C-CO_2$ and $C-H_2O$ reactions on the gasification rate also depends upon the presence or the absence of a catalyst. In the uncatalysed reaction, CO and H_2 are inhibitors of the gasification (74), while in the catalysed gasification their presence can help to maintain the catalyst in the reduced (active) state. Tamai and co-workers (71,85,87) have studied the gasification of different types of carbon by hydrogen in the presence of various transition metals. In the case of metal-doped carbons, thermogravimetric studies (85) revealed the existence of two stages in the gasification. This was considered to depend on the structure of the carbon, amorphous carbon gasifying at lower temperatures and more crystalline carbon at higher temperatures. The metal in the deposits could account for the formation of crystalline carbon during the course of the reaction (87). In the gasification of carbon deposited from benzene on nickel foils (71), a maximum rate was observed at 630°C, above which the rate decreased rapidly. This was ascribed to the influence of the equilibrium

among carbon, hydrogen and methane at high temperatures. Carbon deposits formed in this way have shown a very high reactivity towards hydrogen and steam (71,92).

Various publications have dealt with the mechanism of catalytic gasification (89,90,91,94). A similar mechanism has been proposed for the metal catalysed gasification of carbon by hydrogen, oxygen and carbon dioxide (89,90,91). The mechanism supposes that the metal provides a site for the dissociation of the gas. Atomic species subsequently diffuse to the carbon-metal interface to form a metal-hydrogen-(oxygen)-carbon linkage leading directly to carbon gasification. This mechanism minimises the interaction between metal and carbon in the catalytic process. Recently, however, the electron-transfer mechanism has been used to explain successfully some of the features of the gasification of metal-doped carbon by carbon dioxide, steam and hydrogen (94). It appears that, at the moment, it is impossible to interpret all the gasification data by an unified mechanism. More work remains to be done before a detailed mechanism can be established.

1.4 THE DEPOSITION OF CARBON ON STEAM REFORMING CATALYSTS

The deposition of carbon on steam reforming catalysts has been the subject of a number of recent publications and reviews (98-104). In the steam reforming of hydrocarbons, carbon can be formed either by the direct decomposition of the hydrocarbon or by any of the gas-phase equilibria:

$$2CO \rightleftharpoons C + CO_2$$

$$CO + H_2 \rightleftharpoons C + H_2O$$

$$CH_4 \rightleftharpoons C + 2H_2$$

In commercial operations, coke originating from these reactions is usually prevented by using excess steam. This may lower the yield of the desired products of the reaction and hence a minimum steam-ratio is normally used. The steam-ratio, defined as the number of moles of water per carbon atom in the feed, is the lowest possible operating value before coking occurs. This value can be calculated thermodynamically and plotted as a function of temperature and pressure, as shown in Fig. 1.7. The influence of the operating conditions and feed composition on the value of the minimum steam-ratio have been extensively discussed by Bridger (99,103). He concluded that increasing

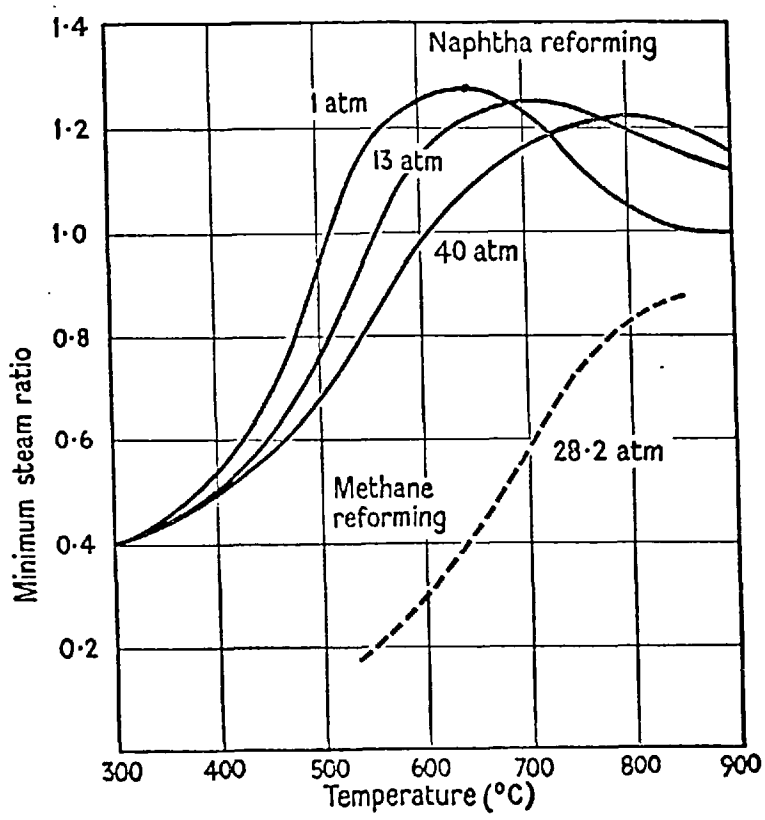

Fig. 1.7 Thermodynamic minimum steam ratios
(From Reference 1)

pressure and decreasing exit temperature decreases the minimum steam-ratio. The addition of carbon dioxide to the feed, particularly at high pressures, increases the minimum steam-ratio at temperatures up to 700°C and decreases it above 750°C.

Besides carbon, polymeric species have been detected on the catalysts (98,105). Macak et al. observed that these species can revert to carbon by a series of dehydrogenation reactions (98). The change brings about an increase in crystallinity and a decrease in the permeability of the coke layer to the reactants. This, in turn, reduces drastically the activity of the catalyst. At low temperatures (below 600°C) the layer is permeable and significant deactivation effects were not observed. This conflicts with results published by Bhatta and Dixon (105) who observed deactivation of the catalysts at temperatures between 400 and 500°C. They were able to identify high molecular weight hydrocarbons in the extract of the deactivated catalyst. Other researchers (100,101) have also detected deactivation of steam reforming catalysts at low temperatures.

Moseley et al. (100) have shown that increasing the molecular weight of the hydrocarbons in the feed increases carbon deposition on CRG catalysts. A similar effect was observed by Rostrup-Nielsen (101) in the steam reforming of aliphatic hydrocarbons. However, the deposition decreased when n-decane and n-dodecane were used. Ethylene (101) and aromatic hydrocarbons (100, 101) produced high coking rates. This was explained by the ease of formation of surface radicals favouring dimerization reactions (101). Rostrup-Nielsen (101) has also shown that the coking rate on nickel based catalysts at temperatures close to 500°C depends on the formulation of the catalyst. He noted that the ability of the catalyst for steam adsorption appeared to be important in depressing the formation of coke. At 500°C the coking was not accompanied by poisoning of the catalyst (possibly due to the presence of nickel particles in the carbon), unless blocking of the pore "mouths" caused diffusion restrictions.

It becomes apparent that the nature of coking in steam reforming depends on the temperature. At low temperature a significant deactivation of the catalyst occurs while coking is limited. Polymeric species could be responsible for the deactivation in these conditions (100,105). When the temperature is increased, the deactivation decreases and coking increases, a maximum rate being observed at circa 550°C (7,101). At

even higher temperatures (above 650°C) thermal pyrolysis and coking on the support material begins to be detected. Above 700°C cracking rates on the support depend on its acidic properties and the presence of alkali (or the use of magnesia) results in less coke. Andrew (106) also reported studies in this context, showing that the ease of carbon formation during naphtha reforming at 30 atmospheres and 750°C (exit temperature) depended on the acidity of the support. He suggested that olefins formed by hydrocarbon cracking could be the first stage of carbon formation.

A recent publication on steam cracking of hydrocarbons (104) advances different mechanisms for the formation of carbon at high temperatures (800-920°C). The mechanisms suppose a reaction in the gas phase as a first stage in the process. From then on carbonaceous deposits could be formed in different ways, depending on the nature of the initial hydrocarbon. With n-hexane, gaseous intermediate species are formed which further react on the substract to produce carbon. In the case of cyclohexane and toluene, high molecular weight hydrocarbons are formed in the gas phase which condense into droplets, striking the substrate on which they solidify.

The coking of steam reforming catalysts is a complex process and the different mechanisms proposed may reflect different operating conditions and catalyst formulations. However, a simplified scheme can be proposed that seems to conciliate most of the published results (7).

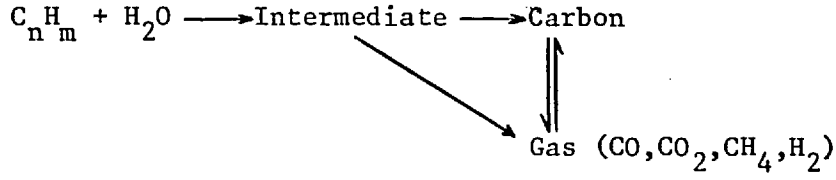

CHAPTER 2

EXPERIMENTAL

		Page
2.1	Introduction	30
2.2	Materials	30
2.3	The low pressure system	30
2.3.1	The vacuum line	30
2.3.1.1	The microbalance and reactor	35
2.3.1.2	The furnace	37
2.3.2	Procedure	39
2.4	Morphological and structural studies	41
2.4.1	Sample separation	41
2.4.2	The coating unit	41
2.4.3	Microstructure and composition determination	41
2.4.3.1	Microscopy	41
2.4.4	Procedure	42
2.5	The flow system	43
2.5.1	The flow reactor	43
2.5.2	The feed system	45
2.5.3	The analysis system	46
2.5.3.1	The katharometer chromatograph	46
2.5.3.2	The flameionisation chromatograph	46
2.5.3.3	Calibration of reactants and products	47
2.5.4	Procedure	49
2.6	Preparation of supported catalysts	51
2.6.1	Sample characterisation	51
2.7	Planning of experiments	54

CHAPTER 2

EXPERIMENTAL

2.1 INTRODUCTION

The system used in most of the experiments consisted of a microbalance associated with a vacuum line or with a flow reactor. Included in the system were means to measure pressure and temperature and to record the signals from the microbalance and the gas chromatograph detector. The kinetics of carbon deposition from light hydrocarbons were studied working either at low or atmospheric pressure. The gasification of carbon and the reaction of steam-reforming of n-hexane were studied at atmospheric pressure.

Morphological studies were carried out by observing the specimens used in the kinetic experiments under optical, stereoscan and transmission electron microscopes. Some samples were analysed by X-ray diffraction and electron probe. A vacuum coating unit was used to cover the samples with layers of homogeneous carbon of a known thickness for the dissolution-precipitation studies.

Supported catalysts were activated in a tubular reactor at a controlled temperature and fixed flows of hydrogen. A gravimetric system was used to determine the total and metallic surface areas of these catalysts.

2.2 MATERIALS

The type, purity, use and suppliers of all chemicals used throughout this work are listed in table 2.1. High purity transition metals used as catalysts are listed in table 2.2.

2.3 LOW PRESSURE SYSTEM

The kinetics of carbon deposition from acetylene on nickel as well as the dissolution and precipitation of carbon films in nickel were studied in this system.

2.3.1 The Vacuum Line

One of the vacuum lines used in the present studies is shown in Fig. 2.1 and represented diagrammatically in Fig. 2.2. The vacuum system consisted of an Edwards Speedivac rotary pump and a diffusion

Table 2.1 Purity, Purpose and Supplier of the Materials Used

CHEMICAL	PURITY (%)	USE	SUPPLIER
Nitrogen	> 99.9	Carrier, diluent	B.O.C.
Hydrogen	> 99.9	Carrier, reactant	B.O.C.
Air	-	Catalyst activation	B.O.C.
Methane	99.2	Identification, reactant	B.O.C.
Acetylene	99.5 - 99.8	Reactant	B.O.C.
Ethylene	99.85	Reactant	B.O.C.
Ethane	99.0	Reactant	B.O.C.
Propylene	99.8	Reactant	B.O.C.
1-Butene	99.0	Reactant	B.O.C.
Carbon monoxide	99.8	Identification	B.O.C.
Carbon dioxide	> 99.9	Reactant	B.O.C.
n-Hexane	> 99	Reactant	B.D.H.
Benzene	Analar	Reactant	B.D.H.
Toluene	Analar	Reactant	B.D.H.
p-Xylene	Analar	Reactant	B.D.H.
Naphtalene	Micro-analytical standard	Reactant	Hopkin & Williams, Ltd.
Silica Gel	-	Column packing	Phase Separations, Ltd.
3% OV-1 Chromosorb K	-	Column packing	Phase Separations, Ltd.
Poropak R	-	Column packing	Water Associates, Inc.
α - Alumina	99.3	Catalyst support	Norton
Nickel nitrate	Analar	Catalyst preparation	B.D.H.
Graphite single crystal	-	Deposition and gasification experiments	Union Carbide
MSC-Molecular Screening Carbon	-	Deposition and gasification experiments	Pittsburgh Activated Carbon Co.

Table 2.2 High Purity Metals Used

METAL	FORM	PURITY (%)	ORIGIN
Ni	Polycrystalline foil	99.9	Goodfellow Metals
Ni(111)	Oriented disk	> 99.9	*
Ni(110)	Oriented disk	> 99.9	**
Ni(100)	Oriented disk	> 99.9	**

* By courtesy of the British Gas Corporation, London Research Station

** By courtesy of Dr. Peter Williams, Imperial College

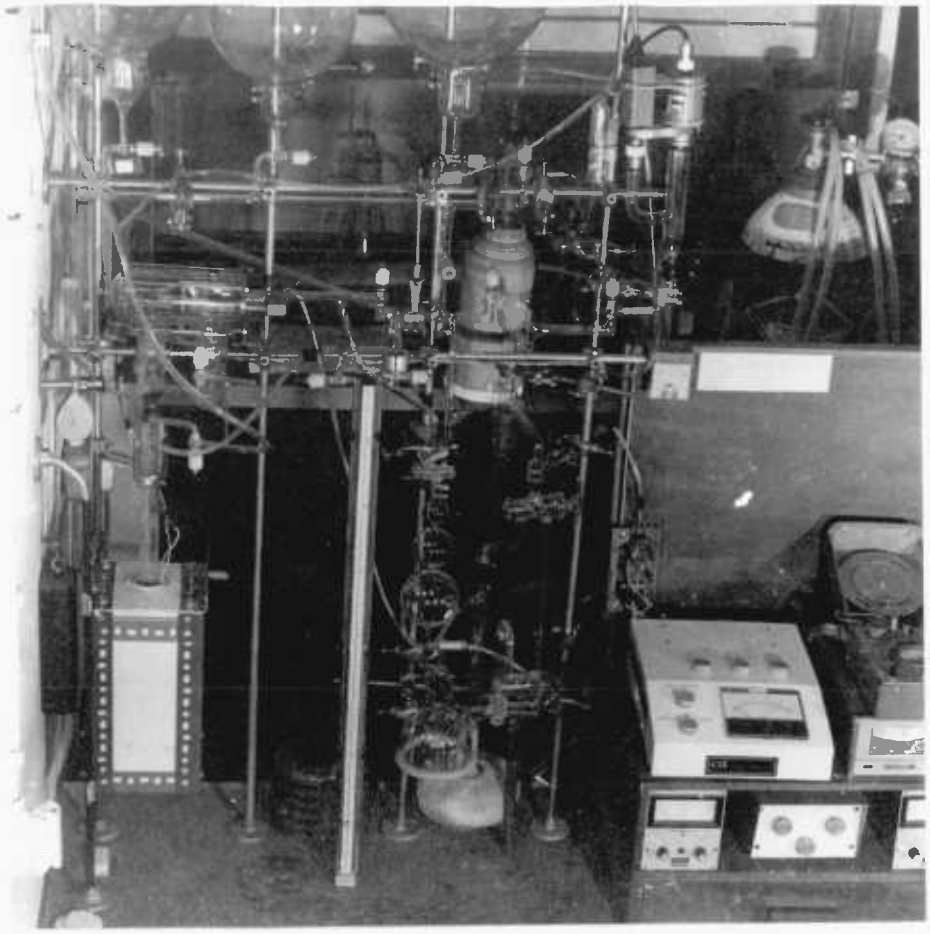

FIG. 2.1 THE VACUUM LINE

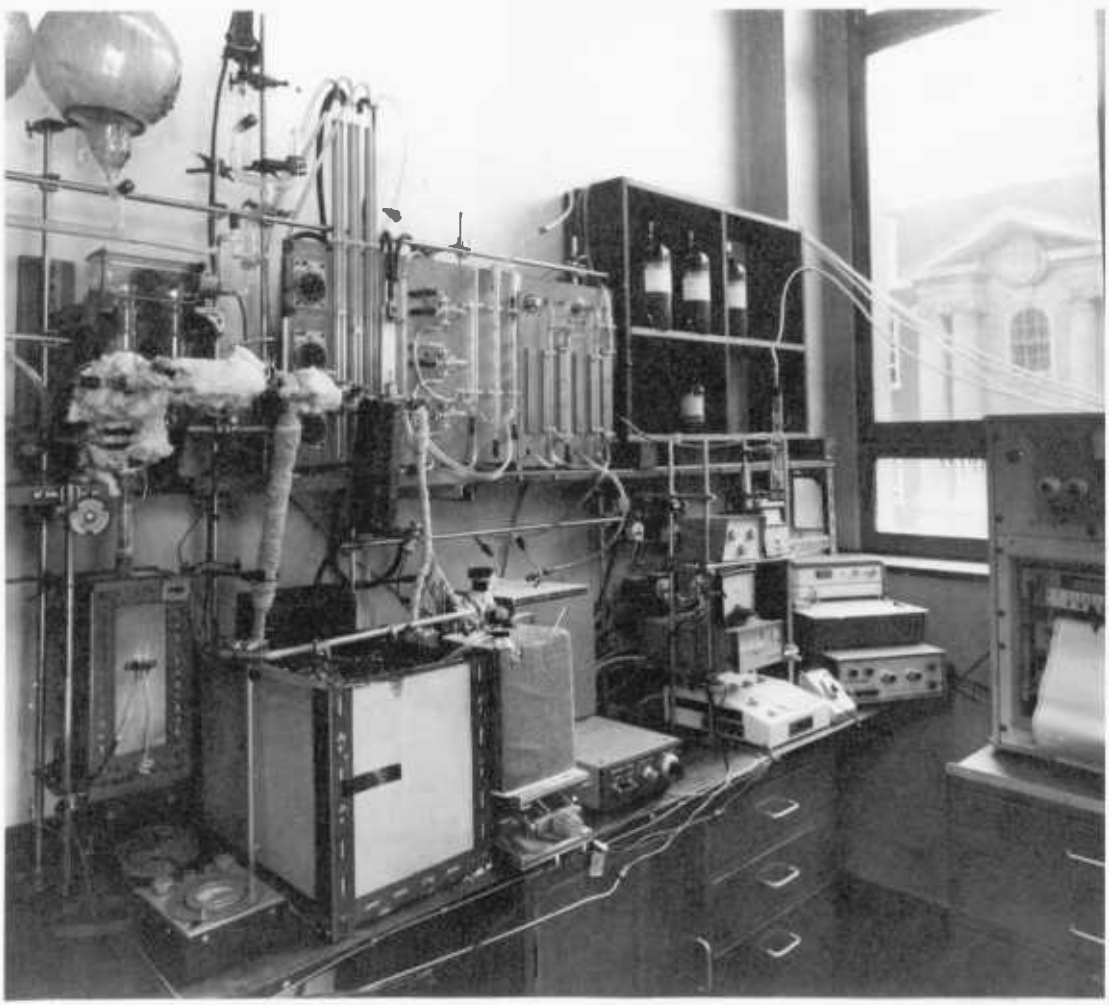

FIG. 2.5 THE FLOW SYSTEM

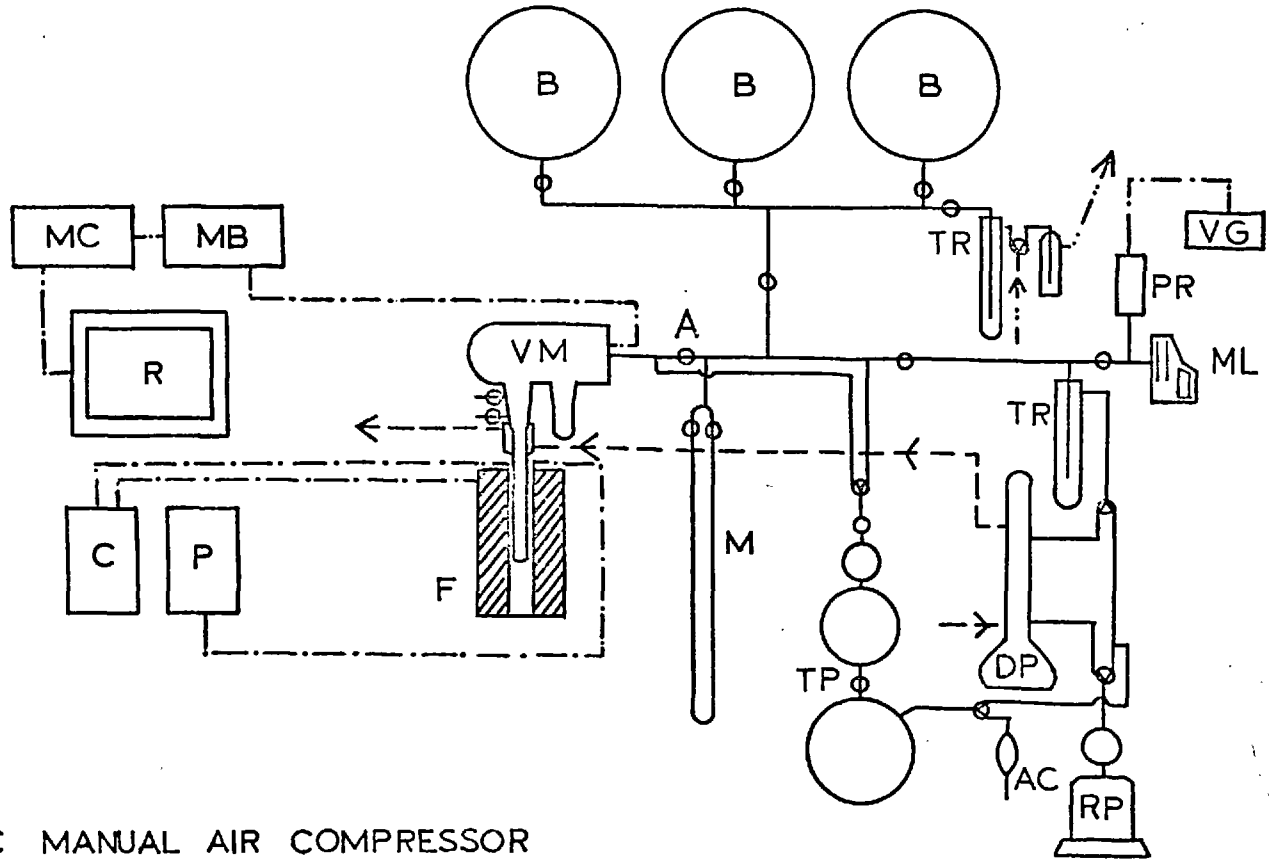

AC MANUAL AIR COMPRESSOR

B STORAGE BULBS

C PRT TEMPERATURE CONTROLLER

DP MERCURY DIFFUSION PUMP

F FURNACES

M MANOMETER

MB MATCHING BOX

MC MICROBALANCE CABINET

P POTENTIOMETER

PR PIRANI VACUUM HEAD

R RECORDER

RP ROTARY PUMP

ML MACLEOD GAUGE

TP TÖEPLER PUMP

TR TRAP

VG VACUUM GAUGE

VM VACUUM MICROBALANCE

—·— GAS LINES

--- WATER LINES

—·— ELECTRIC LINES

—o— SINGLE WAY TAPS

=o= DOUBLE WAY TAPS

Fig. 2.2 The vacuum system

mercury pump giving an ultimate vacuum of about 10^{-5} torr (1 torr = 0.1333 KNm^{-2}). Low pressures were measured by means of Edwards series 70 Pirani and Penning gauges and heads (Pirani 10, head G6B:3 to 10^{-3} torr, Penning 8, head 6:10^{-2} to 10^{-7} torr). The gauges were calibrated against a mercury Macleod gauge which, calibrated from its own geometrical dimensions, gives a reading independent of the nature of the gas. A Toeppler pump was included in the system, allowing the introduction of gases by increments of pressure of 10, 65 and 225 torr (1.33, 8.67 and 30.00 KNm^{-2}, respectively). Three storage bulbs of about 3.5 litres were used to store hydrogen, nitrogen and one hydrocarbon. The taps used in the system were either high vacuum pyrex glass stopcocks lubricated with silicone gresse (Edwards High Vacuum, Ltd.) or greaseless taps (O-ring taps, from J. Young).

2.3.1.1 The microbalance and reactor

A C.I. Electronics MK2B vacuum microbalance was included in the vacuum line. The microbalance head was fitted in a vacuum bottle with two B34 sockets and connected, via a special socket in a vacuum flange, to an electrical control cabinet. The connection to the vacuum line was made through the flange and sealed with wax.

The signal was conveyed via a matching unit, provided with damping and range expanding facilities, to a Honeywell recorder (-0.1 to 1.0 mV). The microbalance had the following characteristics:

Capacity: 1 gram sample, 1 gram counterweight;
Reproducibility: ± 0.5 μg;
Sensitivity: weight changes of 0.5% on indicating meter, even less on recorder;
Electrical tare: 9 mg;
Ranges: 5 ranges from 0 to 25 μg to 0 to 100 mg.

The reactor is represented in Fig. 2.3(a). The design, which is a modification of the "Universal Attachment" obtained from C.I. Electronics, allows a thermocouple to be inserted in an off-centre sheath to measure the temperature at the nearest possible position to the sample.

Below the lower connection, the reactor is made of silica (temperatures up to 1150°C). A water jacket was used to cool the connection, which was usually sealed with high vacuum silicone grease.

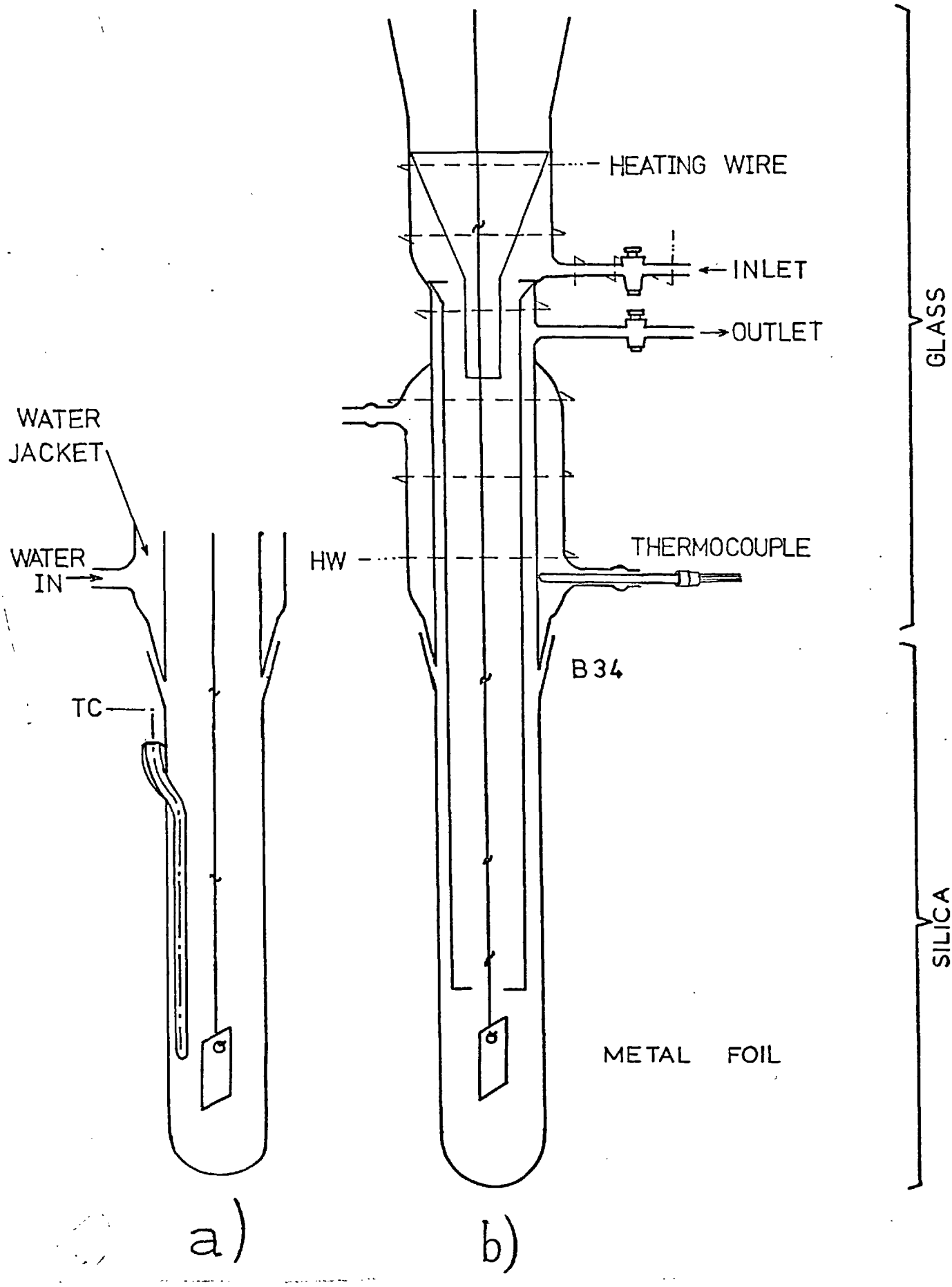

Fig. 2.3 The reactors: (a) vacuum system (b) flow system

This grease was chosen because it can stand temperatures of up to 200°C without serious deterioration.

The overall dead space of the microbalance head, counterweight flask, reactor and service line (up to point A in Fig. 2.2) was approximately 1120 cm^3 at STP conditions. This was measured using the Toeppler pump and applying the ideal gas law. The reaction zone itself had a volume of about 36 cm^3. The sample was suspended in that zone from the microbalance arm by means of a series of small glass and silica fibres (3 to 15 cm each) hooked together. These small fibres provided better dumping than larger ones and proved to be less prone to breakages. The counterweight, consisting of small glass spheres supported in a metallic boat, was also suspended by means of a glass fibre.

2.3.1.2 The furnace

The furnace was made by winding about 11 meters of nichrome wire (resistivity 2.77 Ω/metre) around a porcelain tube, 21 cm long and 4 cm I.D. The winding was made in such a way as to have the spirals closer to each other at both ends of the tube in order to insure an axial temperature profile as flat as possible. The spires were covered with alumina cement and the tube placed inside a box made of asbestos slabs in a Dexion frame. The interior space was filled with vermiculite. The furnace was capable of attaining temperatures up to 1100°C with a power of just below 1500 watts. The temperature was controlled to ± 0.5°C by a Eurotherm series 070 controller (PID mode) using a chromel-alumel thermocouple as a sensing probe. This thermocouple was placed in the furnace tube at the same depth as the suspended sample, and the temperature monitored by the thermocouple placed in the sheath in the reactor wall. This was connected to a potentiometer - Croydon Precision Instruments Type P6 - which gave a direct reading of the temperature, after correction for the cold junction. The readings of the two thermocouples coincided (within 2°C) throughout the working temperature range.

The temperature profiles along the axis of the furnace, for different temperature settings in the controller, are represented in Fig. 2.4. From the figure it can be seen that a constant temperature zone (± 2°C) existed over a length of 4 to 5 cm even at high temperatures. The centre of this zone was located at a distance of 16 cm from the furnace end. The samples were always suspended in this zone.

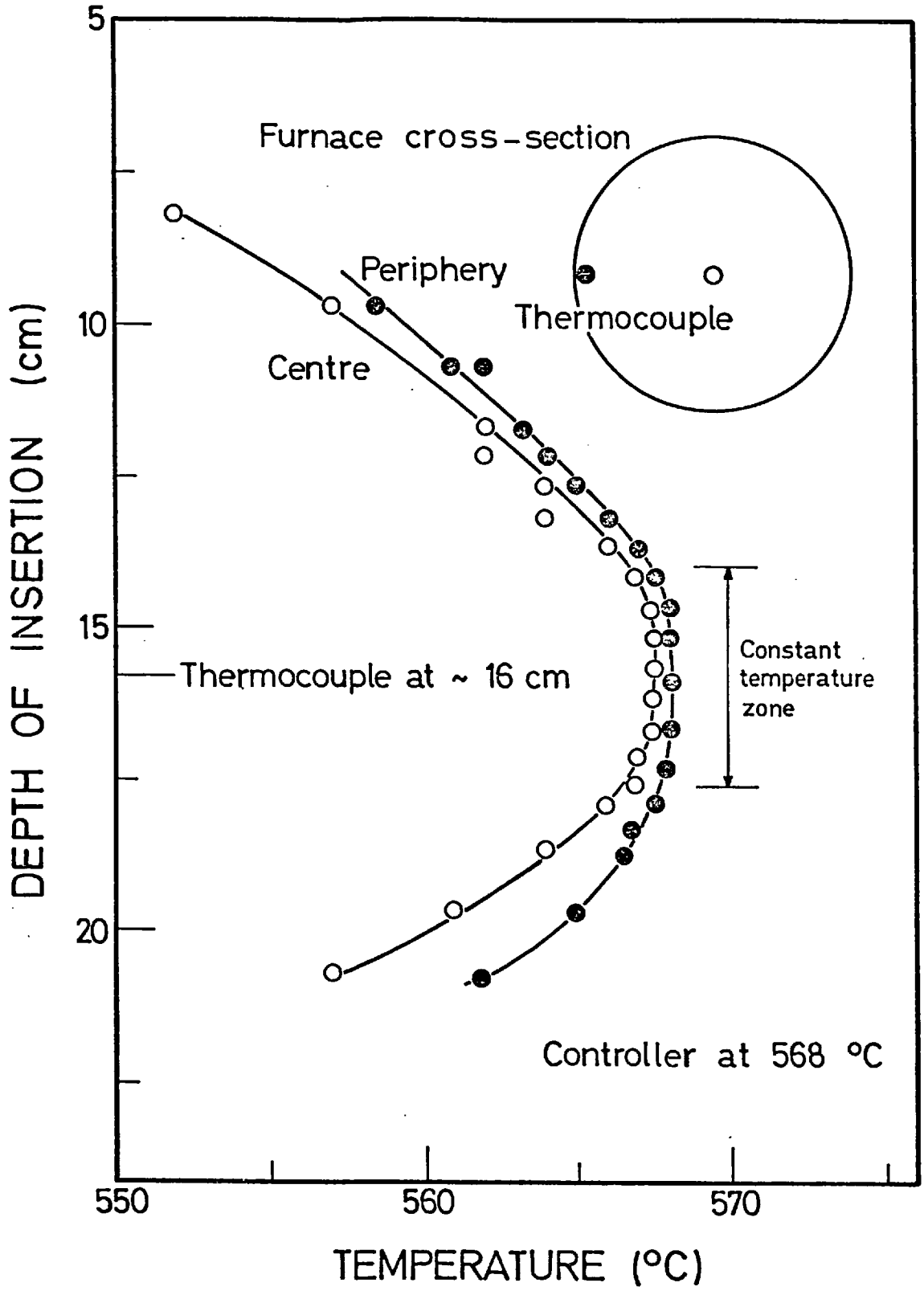

Fig. 2.4 Temperature profile of the reactor furnace

2.3.2 Procedure

In the experiments involving polycrystalline foils, the foil was cut to a convenient size, a hole was made in one extremity, and the exact area determined by weight. By means of the surface density of the parent metal foils (about 19 cm^2mg^{-1} for Ni foils 0.125 mm thick), the total area could be adjusted to a value of 3.00 ± 0.01 cm^2. The sample was then cleaned with acetone and suspended in the microbalance. Small metallic foils were placed in an anular silica ring that was hooked to the suspension fibres.

In the low pressure kinetic experiments, the system was degassed at room temperature and at reaction temperature for 0.5 and 1 hour, respectively. Pre-reduction with hydrogen at reaction temperature was carried out for one hour. The reactant gases were then admitted up to the working pressure from the storage bulbs and the reaction started.

Important instability problems could arise at this stage. These were mainly caused by the build up of electrostatic charges in the reactor walls that could attract the light silica suspensions. The build up was especially important when exhausting or admitting gases in the system. Increasing the weight of the suspensions would decrease this effect, but would increase the noise in the microbalance signal (which is roughly proportional to the suspended load). Eventually a compromise was reached by using an average suspension weight of 85 - 115 mg, and keeping the sample weight below 300 mg. The formation of electrostatic charges could be attenuated by wrapping a damp cloth around the lower connection of the reactor. Another cause of instability - the effect of the variable level of luminosity in the room on the photocells of the microbalance head - was eliminated by covering the head with sheets of Alcan aluminium foil.

Once the reaction started the amount of carbon deposited was recorded continuously as a function of time. One possible source of error of the recorded values were buoyancy effects due to the different geometries and temperatures of sample and counterweight. Experiments were performed to assess the importance of the buoyancy corrections. This was done by measuring the weight variations, Δw, when increasing pressures of an inert gas, p, were admitted into the reactor. From the values of Δw and p, the term $(V_c/T_c - V_s/T_s)$ in the expression:

$$\Delta w = (M/R)\ (V_c/T_c - V_s/T_s)\ .\ p,$$

where M - molecular weight of the gas

V_c, T_c - volume and temperature of counterweight

V_s, T_s - volume and temperature of sample

was determined. This term was found to be negligible for all the working temperatures used.

At the end of an experiment, a short evacuation was made and the reactor was allowed to cool down. Nitrogen was then admitted up to atmospheric pressure, the reactor tube disassembled and the specimen removed from the suspension.

In the batch experiments, whenever the overall conversion of the gas present in the reactor - as derived from the weight of carbon deposited - was below 6 to 10%, the deposition rates were obtained directly from the slopes of the recorded weight vs. time (w - t) lines. However, in most of the cases more than 100 mg of solid product was deposited. For an initial acetylene pressure of 133 KNm^2, for instance, this corresponds to a conversion greater than 75%. In these cases, the reactant depletion had to be taken into consideration in all the calculations made. Hence, pairs of w - t values obtained from the recorder chart were fed to an Hewlet-Packard 9820A computer with an on-line plotter and a continuous curve was derived using an Lagrange interpolation function of variable degree. This function was found to be the most convenient way of correcting the data for noise. The complexity of the w - t curves obtained in the chart (sometimes with two maxima) did not allow the fitting of a polynomial function, even of a high degree. The degree of the Lagrange function, n, was made higher (3 to 5) in the first part of the curve, and allowed to become lower in the later and smoother region:

$$w(t) = \sum_{j=0}^{n} w_j \prod_{i \neq j} \frac{(t - t_i)}{(t_j - t_i)}$$

Curves of the deposition rate vs.process time and vs. the fractional conversion of the hydrocarbon were then directly obtained from the computer.

2.4 MORPHOLOGICAL AND STRUCTURAL STUDIES

2.4.1 Sample Preparation

Nickel single crystals oriented in preferential directions were used in the experiments described in 3.2.1.2 and 3.2.1.5.3/4. The crystals were obtained from oriented flat disks of variable diameter and thickness. A crystal of appropriate dimensions (usually 5 x 4 mm) was sawed from the disk and the orientation checked by X-ray diffraction in an Unicam goniometer. The crystal was then preground to the required thickness (0.1mm). A Metaserv rotary pregrinder Model C200RP was used with 400 and 800 grit paper and Dialap diamond paste. The specimen was cleaned with alcohol and finally electropolished in a solution of 20% perchloric acid in ethanol at - 35°C. The faces were observed for smoothness in an optical microscope and the orientation checked again by X-ray diffraction.

Polycrystalline foils were cut to size (usually 15 x 10 mm) from pure metal sheets, 0.125 mm thick. They were cleaned with acetone (and sometimes electropolished) before being suspended in the micro-balance.

2.4.2 The Coating Unit

For the dissolution - precipitation experiments, the samples were covered with successive layers of amorphous carbon in a Nanotech vacuum evaporation unit. The carbon was evaporated by arcing between two spectroscopically pure graphite rods (Ringsdorff, grade RWO). The film thickness was estimated by the change to deep blue in the interference colour of an aluminium foil coated with gold, placed near the sample in the evaporation chamber.

2.4.3 Microstructure and Composition Determination

Electron probe microanalyses were carried out on the foils and deposits by the Imperial College Analytical Services Laboratories. Analysis of the structure was made by X-rays using a Philips PW 1310 Diffractometer. The samples were fixed to a slide with plasticine (carbon powders were simply pressed onto the slide) and placed on the stage. The powder method was used with carbon powders.

2.4.3.1 Microscopy

The deposits were observed under optical (OM), electron (TEM) and stereoscan electron microscopes. The optical microscope

(Olympus N-TR), was provided with facilities for dark field illumination. Phomicrographs were taken (using a camera attachment Olympus PM-6) on Kodak Microfilm film.

Extensive observations were made using a Cambridge MK IIA stereoscan electron microscope. For this, the samples were simply stuck to a specimen stub with a conductive glue and sometimes covered with a thin layer of evaporated gold to increase conductivity.

Carbon films were also observed in a JEOL JEM 7 high resolution electron microscope. Transmission electron micrographs as well as electron diffraction patterns could be obtained with the instrument. Before observation, the films had to be stripped from the foil. They were cut into squares with a scalpel and the metal dissolved in concentrated HCl, until the squares floated freely. After rinsing with distilled water they were mounted on copper grids. The measurements of the electron diffraction patterns were made by means of enlarged photographs. The A.S.T.M. Powder Diffraction File was used in the identification and interpretation of these patterns.

2.4.4 Procedure

In the dissolution-precipitation studies the samples were placed on the anular silica ring and suspended from the microbalance in the vacuum system. The use of the microbalance was not necessary in this work but the method was chosen because it provided an easy way to anneal the samples under vacuum in controlled conditions. The annealing was done at 1000°C and 1.33×10^{-2} Nm^{-2} until all the carbon was dissolved and the surface was clean. A thin carbon film was seen to precipitate on both faces when the temperature was lowered to (and maintained at) 900°C. Alternatively, clean samples were suspended in the microbalance and a weight of carbon corresponding to the saturation value at 950°C was deposited over them by carefully controlled pyrolysis of acetylene at 1000°C and 13.33 Nm^{-2}. The acetylene was pumped out and the dissolution-precipitation process executed as usual. In this case, the process was monitored by scratching the carbon from part of the foil prior to annealing and checking if the same film was formed on both faces on cooling down.

The films and deposits formed were examined by optical microscopy. The foils were then cut and half of the foil was stripped so that the carbon could be examined by transmission and diffraction

electron microscopy. The remaining foil was examined by scanning electron microscopy.

2.5 THE FLOW SYSTEM

The kinetics of carbon formation from different hydrocarbons, were determined in this system. The reactions of steam reforming of hexane and carbon gasification by hydrogen, steam and carbon dioxide were also studied.

The system, represented diagrammatically in Fig. 2.5 was built in such a way as to incorporate the microbalance, furnace and temperature controller described in 2.3. It included a feed system and an on-line chromatograph.

2.5.1 The Flow Reactor

The reactor, connected to the vacuum glass bottle of the microbalance by a conical glass connection, is represented in Fig. 2.3(b). The inner tube and funnel were used to prevent condensation of vapours in the microbalance head. By means of a flush gas (usually nitrogen) passing through the funnel, the reactants were forced to flow towards the sample. The funneling effect increased the linear velocity of the flush gas and prevented backflow of the reactants.

The water jacket could be used to cool down the lower cone connection. However, when working with condensable gases or when pre-heating was important, no water cooling could be used and, in fact, the reactor inlet had to be heated with heating wire. To maintain the temperature in the connection just below 200°C, careful control of the heating current was maintained with the aid of a small thermocouple inserted in the water inlet tube. In these conditions, for the flow rates used (usually below 4 cm^3(STP) sec^{-1}), the heat transfer in the counterflow path of incoming and outgoing gases was sufficient to heat up the reactants to near the reaction temperature.

The overall dead space of the system up to point A in Fig. 2.5 was approximately 1075 cm^3 at STP conditions, measured in the same way as in 2.3.1.1.

An off-centre silica sheath could not be built into the reactor because the inner tube did not allow enough space for it. Hence, the thermocouple used to monitor the temperature in the reaction zone had

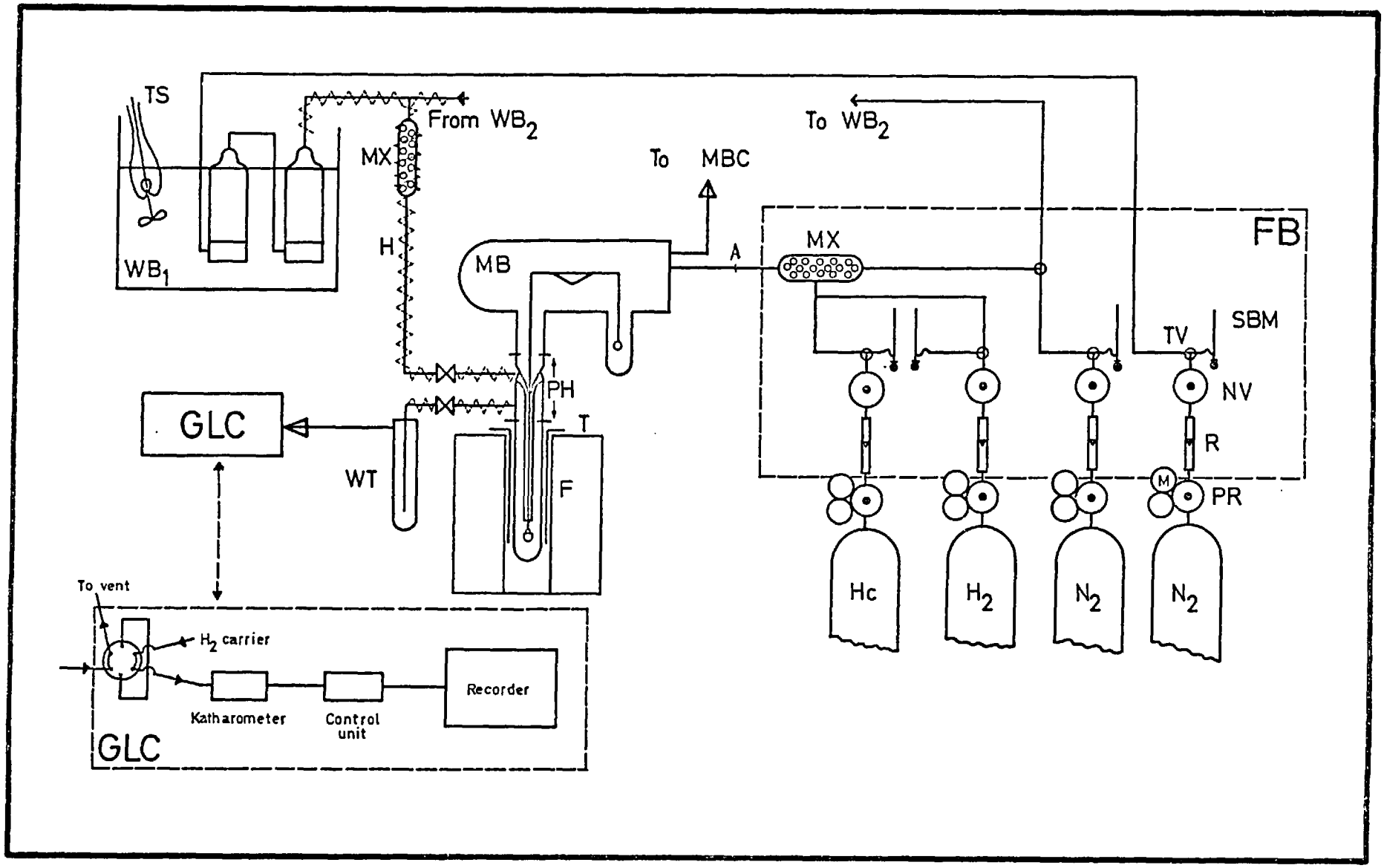

Fig. 2.5: The Flow system

Key: MB - microbalance; WB - water bath; F - furnace; HW - heating wire; WT - water trap; T - thermocouple; M - manometers; NV - needle valves; R - rotameters; PR - two stage pressure regulator; SBM - soap bubble meter; H - heated lines; PH - preheater; GLC - analysis system; MX - mixer; MBC - microbalance cabinet, matching box and recorder

to be placed outside the reactor wall. However, some calibration experiments were made without the tube and using the inner part of the reactor represented in Fig. 2.3(a). The temperature differences, ΔT, between the thermocouples in the sheath and outside the reactor wall, for various working temperatures and gas flows, are shown in Table 2.3. This calibration was used subsequently when using the outer thermocouple only.

2.5.2 The Feed System

The system is represented in part of Fig. 2.5. The gases were supplied from cylinders, through two-stage pressure regulators to a flow board. This consisted of a series of rotameters (calibrated for each individual gas against soap bubble meters), fine control needle valves (Edwards model LB2B and Hoke 1300 Series) and open-ended mercury manometers. The inlet pressure was always maintained at the same values (usually 200 mm above atmospheric) so that corrections of the rotameter readings were unnecessary.

Water and hydrocarbon vapours were produced in two parallel pick-up systems, consisting of 500 ml washbottles (SintA Glass) with flat sintered glass plates, immersed in water baths kept at constant temperature by means of thermostirrers (Gallenkamp 2 and Grant SU-5). These controlled the temperature, within $\pm$ 1°C, over the whole bath volume.

Nitrogen bubbling through the liquid in the bottles, picked up the vapours and carried them in heated lines to the reactor. The sintered disks in the bottles were covered with glass spheres, 5 mm in diameter, to minimise flow fluctuations. The relative amounts of water and hydrocarbon fed into the reactor could be controlled by varying either the flows of nitrogen or the temperature of the water baths. In the case of water and hexane, the exact concentrations were determined by gas chromatography. For hydrocarbons less widely used, saturation was assumed at the water bath temperature. The error involved in this assumption, as determined by condensation of the vapours delivered in a fixed time, was usually below 20% with nitrogen flows smaller than 1.7 $cm^3\ sec^{-1}$.

All the heated lines in the system were either in glass or in stainless steel. Asbestos paper was wrapped around the metal to isolate it from the nichrome wire. This wire was sheathed in a glass

cloth and electrically heated to a temperature of 130 - 140°C, by means of variacs.

2.5.3 The Analysis Systems

The analysis of reactants and products was made with the on-line gas chromatograph represented in Fig. 2.5. All the lines, the 6-port gas sampling valve and loop and the injection port were heated electrically.

In some cases samples were taken for analysis in a Flame Ionization chromatograph.

2.5.3.1 The katharometer chromatograph

The chromatograph consisted of a microkatharometer detector (Servomex MK 158) connected, in parallel, with two columns. The system was placed inside a Perkin-Elmer Precision air stirred oven, which controlled the temperature within ± 0.5°C. The columns were made of stainless steel tube, 3 mm OD. One, 15 cm long, was filled with silica gel (40 - 60 mesh) and acted as a reference. The other, 2 metres long, filled with poropak-R (80 - 100 mesh), was used to separate N_2,H_2O,n-C_6H_{14} (at 165°C) and N_2,CH_4,CO,CO_2 (at 56°C). Hydrogen was constantly passed through the columns at a flow rate of 0.5 cm^3(STP) sec^{-1}, as determined in the outlet with a soap bubble-meter. The katharometer was operated at 6 volts and the signal, amplified in a Servomex katharometer bridge control unit, was recorded on a Vitatron UR 402M linear integrating recorder.

2.5.3.2 The Flame Ionization chromatograph

A PYE Unicam GCD chromatograph using dual glass columns, 250 cm long and 2 mm ID, packed with activated alumina was used to separate light hydrocarbons. The best separation was obtained using an Helium carrier flow of 0.6 cm^3(STP) sec^{-1} (controlled with a PYE gas pressure and flow controller) and the following operating temperatures:

Injection port: 330°C;
Detector: 350°C;
Oven: 5 minutes at 30°C followed by linear heating (0.3°C sec^{-1}) to 330°C.

The mixtures were injected with an Hamilton 1 ml gas-tight syringe and the signals recorded in a UR 402M linear integrating recorder.

2.5.3.3 Calibration of Reactants and Products

Calibration of individual gases and liquids was carried out using 1 and 5 ml disposable Gillete gas-tight syringes and 1 µl, 5 µl SGE syringes respectively. Calibration curves for the katharometer were obtained plotting peak areas against number of moles injected. As in the range used all the curves were linear, calibration factors, f, could be obtained using the relationship:

$$f = \frac{n\ s}{uA}$$

where: n - moles of pure compound injected
s - synchronising factor for chart speed and dial setting in the integrator
u - number of counts in the integrator
A - atenuation factor.

It was found that these factors changed slightly with time in spite of working with constant conditions. Hence, up-dating of the calibration was needed from time to time and the values shown in Table 2.4 should be considered as an average.

The same procedure was used to calibrate the hydrocarbons analysed in the FID chromatograph. In this case, the calibration factors did not vary with time. Moreover, weight compositions calculated with them coincided, within 5%, with those calculated with correction factors (relative to benzene) obtained by the approximate method described in (107)

$$f_i = \frac{0.923\ M_i}{12 n_i} \qquad (f_{benzene} = 1)$$

where: M_i - molecular weight of substance i
n_i - number of carbon atoms in substance i.

The correction factors determined are listed in table 2.5.

Table 2.3 - Differences between inside and outside temperatures for various working conditions

Nitrogen Flow Rate ($cm^3(STP)sec^{-1}$)	Working Temperature (^oC)	$\Delta T = T_{outer} - T_{inner}$ (^oC)
1.7	400	0
6.7	400	1
3.3	560	3
1.7	725	3
6.7	725	4

Table 2.4 - Retention times and calibration factors for the katharometer chromatograph

Compound	Oven Temperature (^oC)	Retention times (sec)	Calibrating factors x 10^8 (moles $counts^{-1}$)
N_2	50	48	2.6
	156	43	2.1
CH_4	50	83	5.4
CO	156	54	4.5
CO_2	156	108	9.0
H_2O	156	156	18.7
$n-C_6H_{14}$	156	880	19.6

Table 2.5 - Retention times and correction factors for the FID chromatograph

Compound	Retention Times (sec)	Correction Factors
C_2H_4	380	1.077
C_2H_2	620	1.000
C_3H_6	690	1.077
$1-C_4H_8$	780	1.077

2.5.4 Procedure

The carbon deposition and carbon gasification experiments involved both polycrystalline nickel foils and supported nickel catalysts. The steam reforming experiments involved only supported catalysts.

Nickel foils were prepared in the same way as described in 2.3.2 and suspended in the microbalance. In the case of supported catalysts, a 400 mesh stainless steel basket was used to contain and suspend the catalyst. This basket allowed an easy access of the gases to the catalyst (thus decreasing the importance of mass transfer limitations) but could present some catalytic activity for carbon deposition. The effect was checked and found to be negligible when working with n-hexane. After suspending the sample, the microbalance was flushed with nitrogen and the furnace raised. The catalyst was then reduced with hydrogen at the reaction temperature for ½ hour (foils) or until no further weight loss was detected in the microbalance (supported catalysts). Nitrogen was again flushed through the microbalance, the reactants admitted and the reaction started. When working with condensable vapours, the technique used to admit the reactants was as follows:

The water baths were set at fixed temperatures and the line heating turned on. The carrier gas was then allowed to pass through the pick-up system at a fixed flow, and the mixture, short-circuiting the reactor, was discharged to the vent or analysed in the chromatograph. Nitrogen (and sometimes hydrogen) was passed through the microbalance head and its flow adjusted to keep the total flow rate constant. When the analysis showed a constant reactants concentration, the mixture was made to pass through the reactor.

In the gasification studies, coked catalysts from previous deposition runs were normally used. In between runs, the reactor was flushed with nitrogen and kept at the gasification temperature for ½ hour.

A direct record of the amount of carbon deposited (or gasified) was obtained as a function of time. From it, rates could be calculated by determining the slopes of the curves. Analyses of the effluent gases were made from time to time and the composition of the mixture determined with the aid of a computer program. A typical print out is presented in

G A S C O M P O S I T I O N

T (C) 575

HYDROGEN	NITROGEN	METHANE	ETHANE	ETHYLENE	PROPANE	PROPYLENE	BUTANE	1- BUTENE	ACETYLENE
		(HYDROCARBONS)							
		.08	.23	99.69	0	0	0	0	0

G A S C O M P O S I T I O N

T (C) 600

HYDROGEN	NITROGEN	METHANE	ETHANE	ETHYLENE	PROPANE	PROPYLENE	BUTANE	1- BUTENE	ACETYLENE
		(HYDROCARBONS)							
		.07	.41	99.51	0	0	0	0	0

G A S C O M P O S I T I O N

T (C) 625

HYDROGEN	NITROGEN	METHANE	ETHANE	ETHYLENE	PROPANE	PROPYLENE	BUTANE	1- BUTENE	ACETYLENE
		(HYDROCARBONS)							
		.06	.87	99.07	0	0	0	0	0

G A S C O M P O S I T I O N

T (C) 650

HYDROGEN	NITROGEN	METHANE	ETHANE	ETHYLENE	PROPANE	PROPYLENE	BUTANE	1- BUTENE	ACETYLENE
		(HYDROCARBONS)							
		.04	.51	97.55	0	1.89	0	0	0

G A S C O M P O S I T I O N

T (C) 700

HYDROGEN	NITROGEN	METHANE	ETHANE	ETHYLENE	PROPANE	PROPYLENE	BUTANE	1- BUTENE	ACETYLENE
		(HYDROCARBONS)							
		.60	4.04	90.36	0	5.00	0	0	0

Fig. 2.6 Typical print-out of the ANALI program: Concentrations of the reaction products in the outlet gas mixture versus temperature

Fig. 2.6. As the reactants conversion was usually below 10% the reactor could be treated as differential.

2.6 PREPARATION OF SUPPORTED CATALYSTS

CRG catalyst, a co-precipated nickel-alumina catalyst, was kindly supplied by The British Gas Corporation. Impregnated nickel - alumina catalysts were prepared using low surface area alumina support. A typical support analyses (weight %) is:

Al_2O_3	SiO_2	Fe_2O_3	T_iO_2	CaO	MgO	N_2O	K_2O
99.0	0.3	0.1	<0.01	0.1	0.1	0.1	<0.02

The support was crushed to BS 40 - 60 mesh (0.421 to 0.251 mm) and soaked in a 0.3 M $N_i(NO_3)_2 6H_2O$ solution. The excess solution was removed by drying in a water bath with constant stirring for about 6 hours followed by slow evaporation. The nitrate was decomposed to N_iO by calcining in nitrogen at 450°C for 2 hours. Metallic nickel was obtained by reducing, in hydrogen at 500°C for 3 hours. The activation was done in the apparatus described in (108) and represented in Fig. 2.7. Some properties of the reduced catalyst are shown in table 2.6.

2.6.1 Sample Characterisation

Surface areas were determined by the B.E.T. nitrogen adsorption procedure described in (79). The adsorption was followed using a gravimetric method in a vacuum microbalance system similar to the one described in 2.3.1.

A known amount of sample was placed in a glass boat and degassed at 300°C until no further weight loss was detected. Special care was taken at this stage to prevent the catalyst dropping from the boat by violent desorption. The sample was then isolated from the vacuum pump and cooled at 77 K. Nitrogen was admitted in the system at increasing pressures. For each value of pressure, the final adsorption equilibrium was attained in 5 to 10 minutes.

Pore size distributions were determined using the Pierce treatment (79). Total pore volume was calculated by applying the Gurvitsch rule. After the saturation pressure was reached, the desorption isotherm was obtained by careful partial evacuations of the system.

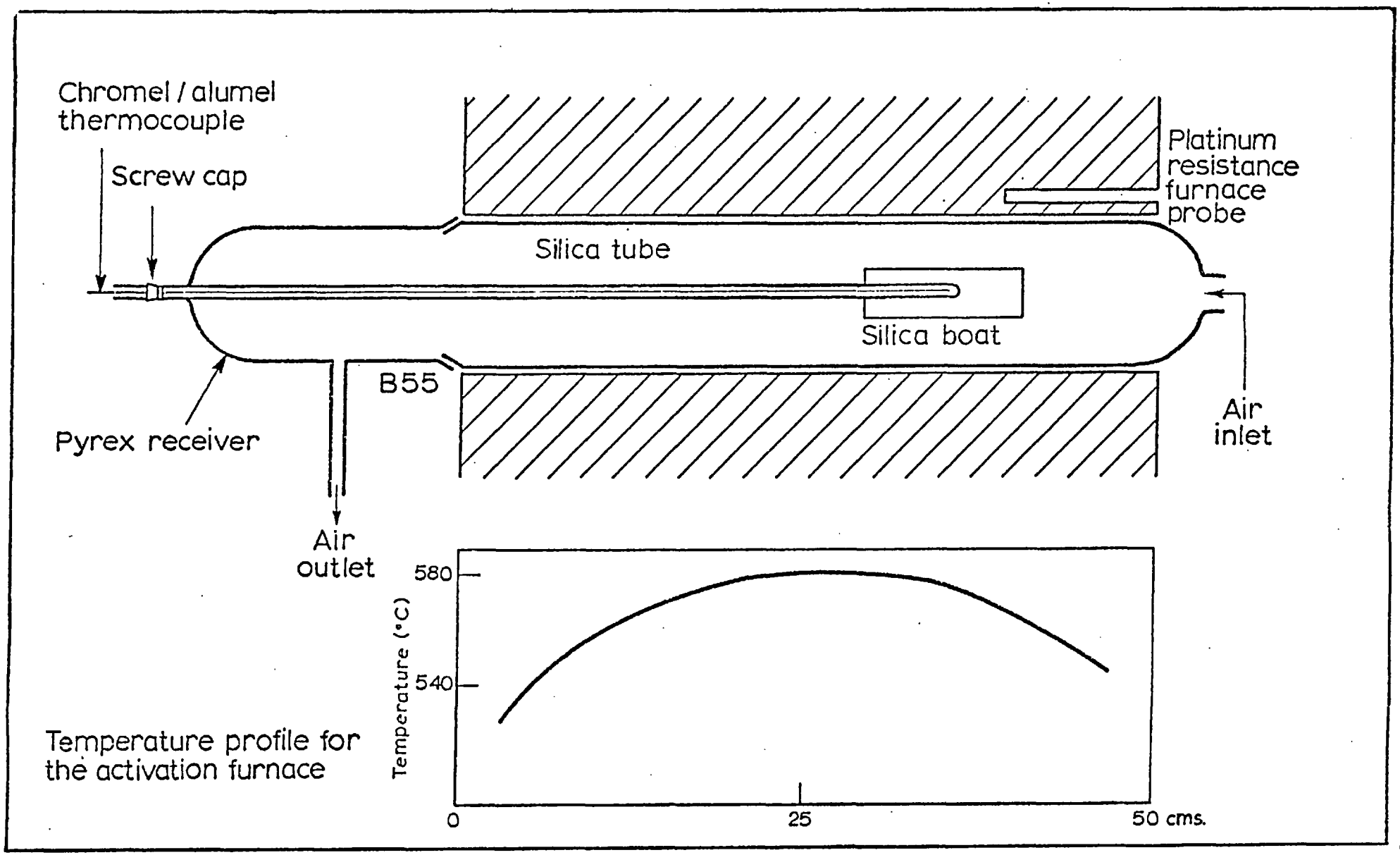

Fig. 2.1: Activation apparatus

Table 2.6

Catalyst	Composition (weight %) Ni	Al_2O_3	K	Total Surface Area (m^2/g)	Metallic Surface Area (m^2/g)	Acidity† (mg/g)
CRG	75*	24*	1*	93 ± 5	21.5 ± 2.5	-
Ni/Al_2O_3	18	82	-	8.5 ± 1.0	1.1 ± 0.2	.230

* Data from (109)

† Total pyridine uptake

Metallic surface areas were calculated by the same gravimetric method, using carbon monoxide adsorption at - 78°C. The effective molecular coverage area of CO in the nickel surface was assumed to be 13 $^{0}A^{2}$ (110).

Total acidity was obtained by pyridine adsorption using the method described in (111). Buoyancy effects were determined in the same way as in 2.3.2. When important they were incorporated in the calculations.

2.7 PLANNING OF EXPERIMENTS

In the carbon deposition and gasification experiments the observed rates were found to be dependent on the past "history" of the sample (preparation, pretreatment, etc.). So, whenever possible, kinetic parameters were obtained in single runs. This depended on the value of the rate observed. If this was too large, limitations were brought about by the range of the microbalance (deposition) and by the amount of deposit gasifiable in steady state conditions (gasification).

The temperature dependences were obtained by measuring the steady state rates when the temperature was varied stepwise at fixed reactants concentration. Orders of reaction were obtained, at fixed temperatures, by varying the partial pressures of the reactants. Alternatively, rates were measured in the same run (for different values of temperature and reactants concentration) and the kinetic parameters obtained by fitting to a theoretical model.

The coupling of a microbalance with an on-line chromatograph provides a means of relating a primary with a secondary reaction. For instance, in the reaction of steam reforming of hexane, the activity for methane production and the rate of carbon deposition on the catalyst could be measured at the same time. Also, the analysis of the effluent mixture provides a method of confirming the stabilisation of the operational conditions, which is important, for instance, in the determination of reaction orders.

Whenever it was necessary to use results from different runs in the same correlation, reproducibility problems arose and scattering increased. This was particularly the case of experiments made in batch conditions in the vacuum microbalance system.

CHAPTER 3

RESULTS

		Page
3.1	INTRODUCTION	57
3.2	CARBON FORMATION FROM HYDROCARBONS	57
3.2.1	Deposition on model catalysts	58
3.2.1.1	Acetylene on polycrystalline nickel foils	59
3.2.1.2	Acetylene on nickel single crystals	71
3.2.1.3	The negative dependence of the rate of deposition on temperature	76
3.2.1.4	Ethane and n-hexane on polycrystalline nickel foils	81
3.2.1.5	Morphological and structural studies	87
3.2.1.5.1	Kinetics and morphology	88
3.2.1.5.2	Analysis of the deposited nickel foils	88
3.2.1.5.3	Bulk diffusion of carbon in nickel	94
3.2.1.5.4	Dissolution-precipitation	98
3.2.2	Deposition on supported nickel catalysts	98
3.2.2.1	Deposition from ethane and hexane	98
3.2.2.2	The effect of hydrogen	104
3.2.2.3	Examination of the carbon deposits	105
3.2.2.4	Carbon deposition in the presence of steam	110
3.3	GASIFICATION OF CARBON DEPOSITS	117
3.3.1	Carbon gasification by carbon dioxide	117
3.3.1.1	Gasification from nickel foils	117
3.3.1.2	Gasification from supported nickel catalysts	123
3.3.1.2.1	General results	123
3.3.1.2.2	Reactivity and equilibrium	128
3.3.1.2.3	Changes in the structure of the deposits during gasification	131
3.3.1.2.4	Test for diffusion limitations	134
3.3.2	Carbon gasification by hydrogen from supported nickel catalysts	136
3.3.2.1	General results	136

3.3.2.2	Reactivity and equilibrium	143
3.3.3	Carbon gasification by steam from supported nickel catalysts	146
3.3.3.1	General results	146
3.3.2	Stoichiometry	151

CHAPTER 3

RESULTS

3.1 INTRODUCTION

The data presented in this chapter is divided into two main sections. The first section includes the results of experiments designed to study the formation of carbon from hydrocarbons on nickel catalysts. These experiments extend previous work to new systems and attempt to relate the kinetics observed with the structure and morphology of the deposits formed.

The second section deals with the nickel catalysed gasification of carbon. The gasifying agents are steam, hydrogen and carbon dioxide.

3.2 CARBON FORMATION FROM HYDROCARBONS

The results presented in the first part of this section complete previous work done on carbon deposition from unsaturated hydrocarbons on nickel foils (7 , 56) and extend it to aliphatic hydrocarbons (ethane and n-hexane). Deposition from acetylene over polycrystalline and single crystal nickel foils provided an insight into the role of grain boundaries in the reaction and on the importance of surface irregularities and crystal orientation. Although a certain amount of work has been published on the kinetics of carbon formation from olefins there are still some aspects open to question. One of these is the negative dependence of the rate on temperature. Previous work with propylene (7) was thus extended to other olefins and acetylene. The experiments with ethane and n-hexane were carried out to obtain a general pattern of the kinetics of the reaction of carbon formation from both unsaturated and saturated hydrocarbons.

The study of the structure and morphology of the carbon deposits formed completes the first part of this section. Section 3.2.2 deals with carbon deposition on supported nickel catalysts from saturated hydrocarbons in the absence and in the presence of steam. The study of carbon formation from ethane and n-hexane links the deposition on these catalysts with that on polycrystalline nickel foils. The negative dependence of the rate of deposition on the temperature, as well as the hydrogen effect, were also studied with

supported catalysts. In the majority of the experiments a steady state deposition develops after an initial transient stage. One of the problems affecting these studies was the irreproducibility of the steady state rate. This irreproducibility was found to depend on various factors, namely:

(i) Pretreatment of the catalyst - this factor was critical in the initial stages but less so once a steady state situation was attained.

(ii) Reusing the sample - partially burning-off the carbon deposit (usually with hydrogen) and reusing the sample in another deposition experiment in the same conditions, usually led to nearly identical steady state rates. If, however, burn-off was complete, an increase was observed in the value of the rate.

Even taking great care in the control of the experimental conditions, considerable scatter in the values of the rate was observed (relative standard variations ranging from 5 to 22%). Hence, whenever it was necessary to compare data from different runs (for instance to obtain activation energies or reaction orders) the technique of partially burning-off the carbon was used. Consecutive experiments of this kind were usually tabulated with the same numbers.

3.2.1 Deposition on model catalysts

Nickel polycrystalline foils and nickel single crystals were used in these studies. Carbon was deposited from acetylene, olefins and aliphatic hydrocarbons.

3.2.1.1 Acetylene on polycrystalline nickel foils

The formation of carbon from acetylene was studied in batch and flow conditions at temperatures between 400 and 600°C. Pure acetylene or mixtures with hydrogen and nitrogen were used.

The deposition rates, obtained by the method described in 2.3.2 as well as the conditions used are presented in Figures 3.1 to 3.7 and Tables 3.1 and 3.2.

Batch Experiments

Preliminary experiments were made to obtain some information on the conditions of the metal surface. Electron Spectroscopy for Chemical Analysis (ESCA) was used to check the presence of sulphur on

the surface before and after annealing in vacuum at high temperatures. After a general spectrum had been obtained, the instrument was set to scan the ranges of binding energies associated with sulphur 2s and 2p. No significant sulphur signals were detected in either case. As surface nickel oxides (evident in the spectra by the shape of the Ni(3s) and Ni(3p) peaks and the strong O(1s) peak) could be preventing the detection of sulphur, the sample was bombarded with argon ions (3KV, 40 μA) and the surface scanned again. Although only a small amount of oxide remained, there was no definitive evidence for the presence of sulphur, even in the expanded spectrum from 1265 to 1235 and 1335 to 1315 eV.

The importance of the surface finishing was also determined. Carbon was deposited over unpolished and electropolished polycrystalline nickel foils of the same area. On the latter, the rates measured for 100 torr (1 torr ≡ 133.3 N m^{-2}) acetylene at 475°C were 5 to 10 times smaller than on the unpolished samples. Further experiments using samples of different sizes, allowed the following conclusion: the rougher the surface and the smaller the sample the faster the deposition observed. The greater activity for carbon deposition found at the edges of the foil may explain the increase of the rate in the case of smaller samples.

It has been previously reported that acetylene forms carbon on nickel more readily than the olefins. This is clearly shown in the series of experiments at 500°C presented in Fig. 3.1. The deposition from acetylene is significantly faster. In the absence of hydrogen as a reactant, the deposition from acetylene is only slightly delayed, whereas in the case of 1-butene a very long induction period is observed.

The effect of acetylene pressure on the deposition at 500°C is shown in Fi. 3.2(a). The curves present various inflexions, and a representation of the rate of deposition rather than the deposited weight is more informative (Fig. 3.2.(b)). For brevity, only this representation will be used in the results to be presented next. The curves show, in general, two maxima, and the pressure of the hydrocarbon has a positive effect on the height of both of them up to 100 torr. At 200 torr, however, the deposition is rapidly inhibited at this temperature (Fig. 3.2(b)).

All the experiments lasted several hours. Only when conversion was complete did the reaction stop. Hydrogen was produced in the reactor but the total pressure did not change. This is in agreement with the assumption that the only important reaction taking place is:

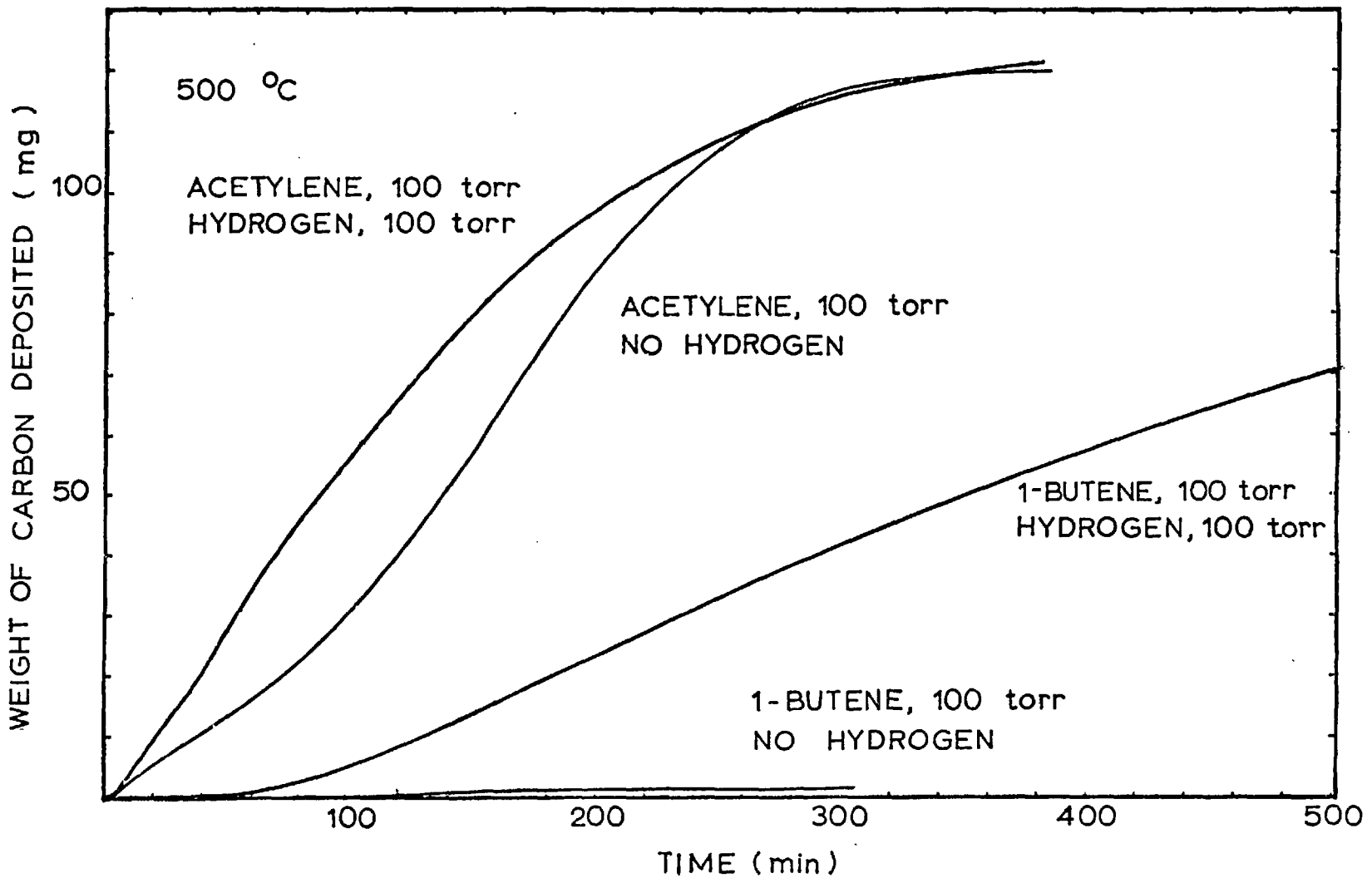

Fig. 3.1 Carbon deposition from acetylene and 1-butene on polycrystalline nickel foils

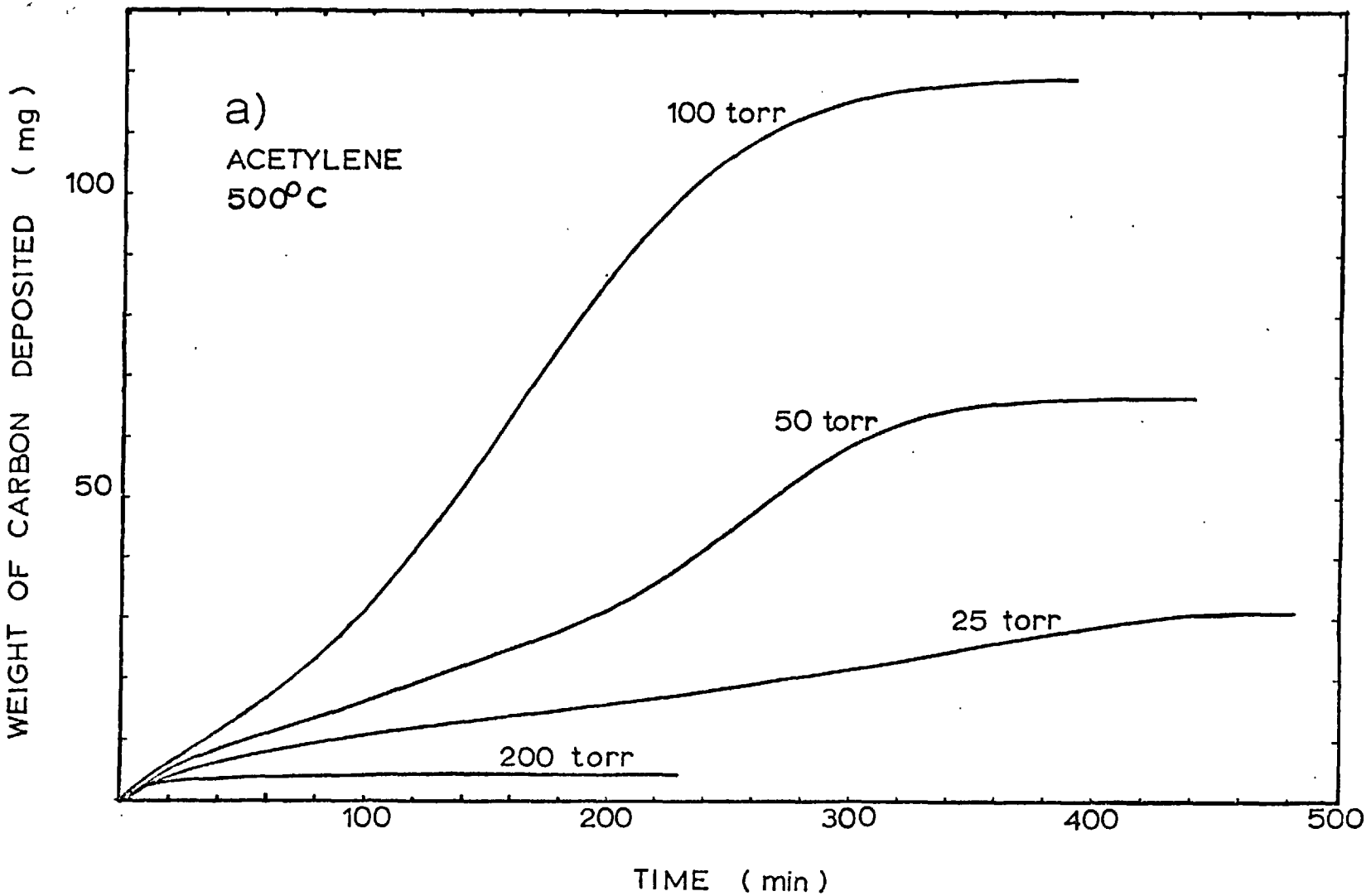

Fig. 3.2 Carbon deposition from acetylene at 500°C and different pressures (no hydrogen)
(a) Weight of carbon deposited vs. time of deposition

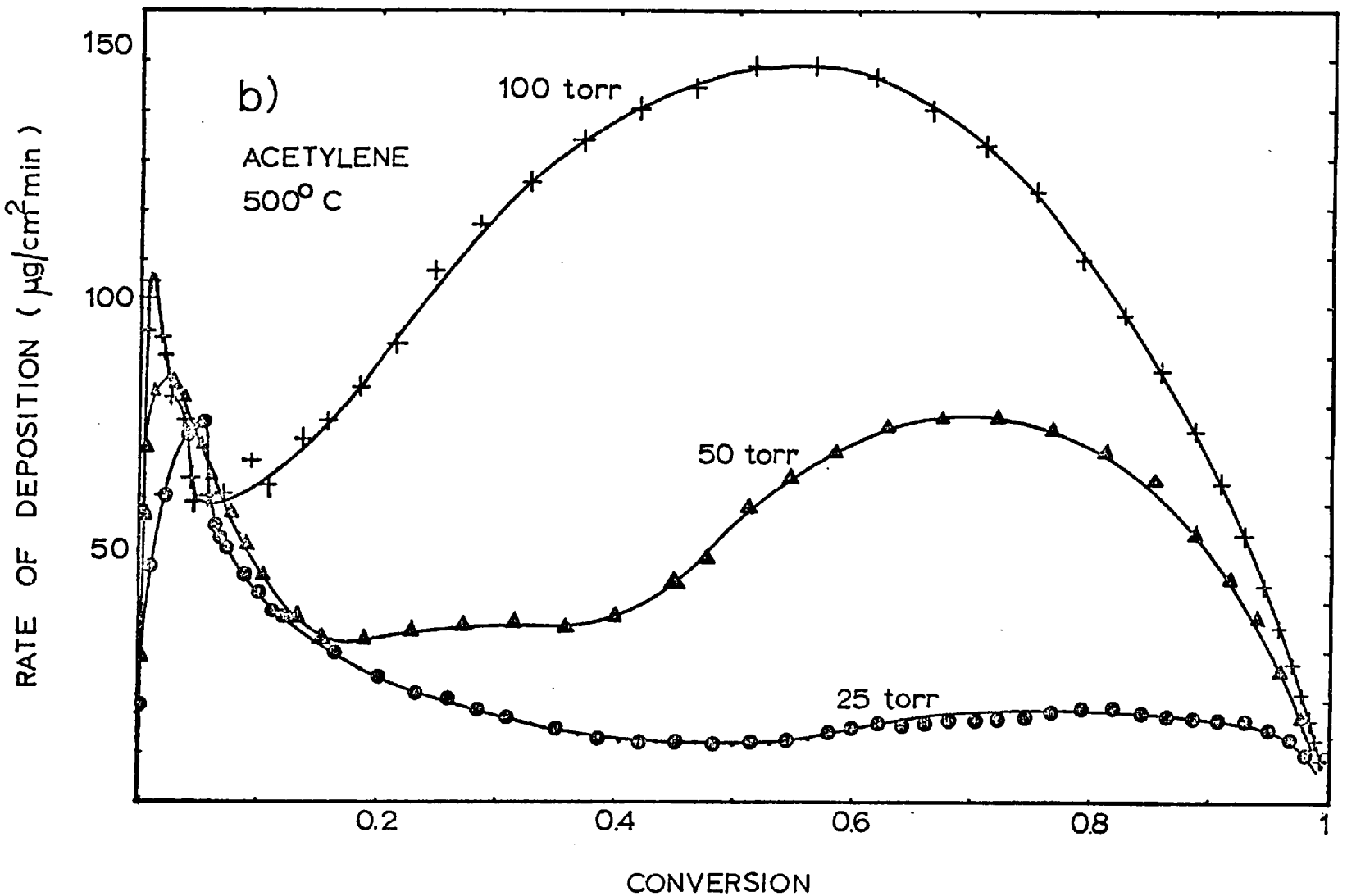

Fig. 3.2 Carbon deposition from acetylene at 500°C and different pressures (no hydrogen)
(b) Rate of deposition vs. conversion

$$C_2H_2 \rightarrow 2C + H_2$$

Thus the composition of the reactant gas can be determined at any stage. For example, in the rate vs. conversion curve for 50 torr shown in Fig. 3.2(b), the composition at the second maximum is 30% acetylene, 70% hydrogen. The partial pressures are 15 and 35 torr, respectively.

A more direct evaluation of the effect of hydrogen on the reaction was obtained in the series of experiments presented in Fig. 3.3. It can be seen that the first maximum increases at higher pressures, but the second decreases and is non-existent at 400 torr.

Two series of runs were also completed to study the effect of temperature on the reaction. In the first series, only acetylene (100 torr) was admitted to the system (Fig. 3.4). Both the first and second maxima increase with temperature up to 525°C. At 550°C the reaction is rapidly inhibited and only a very slow rate of deposition is observed after a few minutes. For the second series of runs regarding the effect of temperature, hydrogen (200 torr) together with acetylene (100 torr) were initially admitted to the reactor. The results are presented in Fig. 3.5(a) and (b). Again, the rate reaches a maximum at about 550°C. Very similar behaviour has been reported for carbon deposition from carbon monoxide-hydrogen mixtures on iron (112) and acetylene-hydrogen mixtures on nichrome (51). This confirms the general pattern observed with unsaturated hydrocarbons on nickel (56).

Flow experiments

The integral experiments in batch conditions reported above, offer a very convenient way of obtaining general information about the main kinetic features of the system. Some ideas have accrued about the influence of time of deposition, temperature and the pressures of hydrocarbon and hydrogen on the rate. However, the interaction of the different variables makes it difficult to obtain reliable values of orders of reaction and activation energies from the data presented so far.

Flow experiments present an easy way to obtain differential conditions. If a steady state can be observed after "development" of the reaction rate, conditions will exist which are particularly

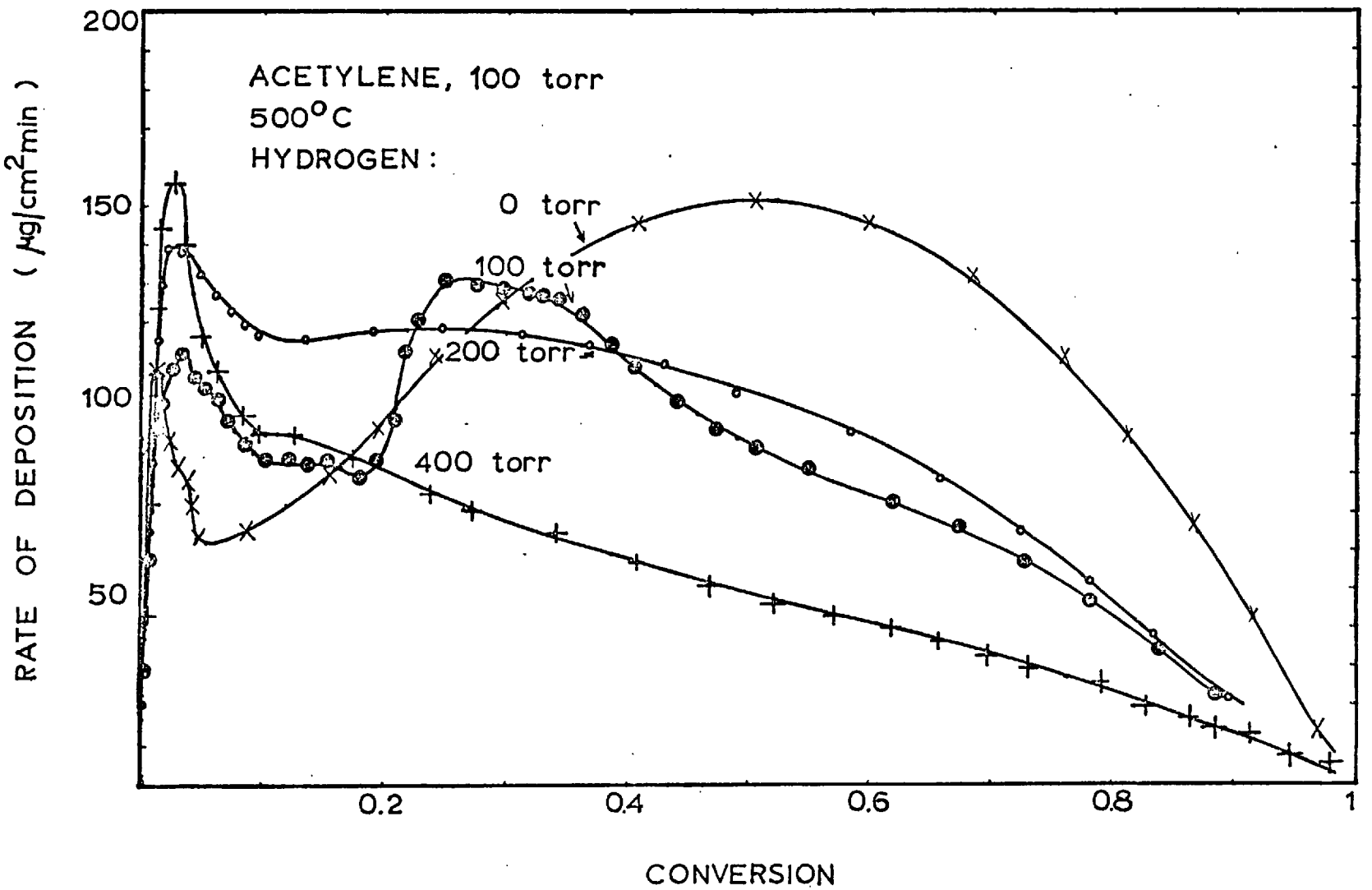

Fig. 3.3 Rate of deposition vs. conversion at 500°C and different hydrogen pressures

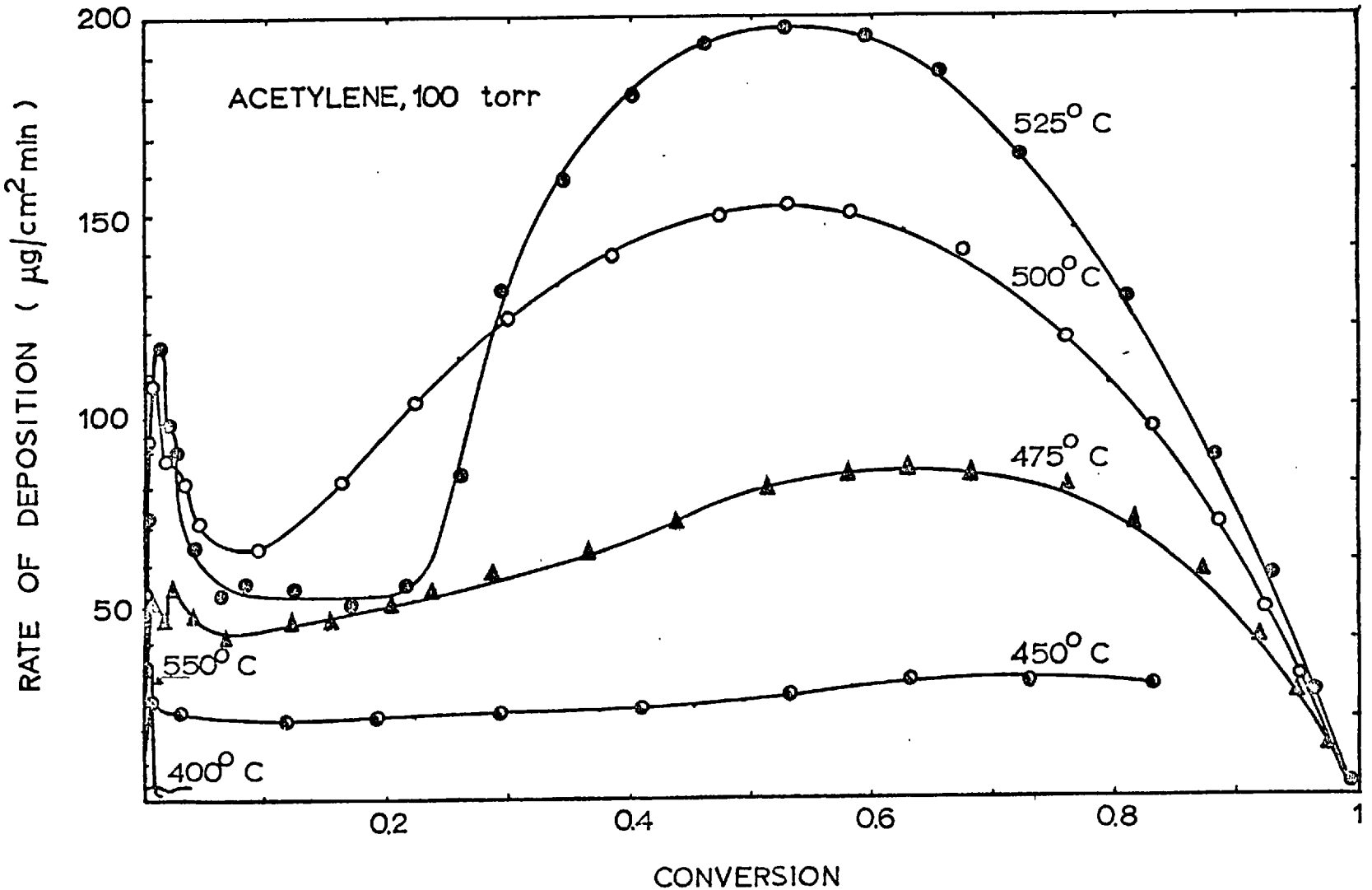

Fig. 3.4 Rate of deposition for 13.3 KN/m^2 (100 torr) at different temperatures (no hydrogen)

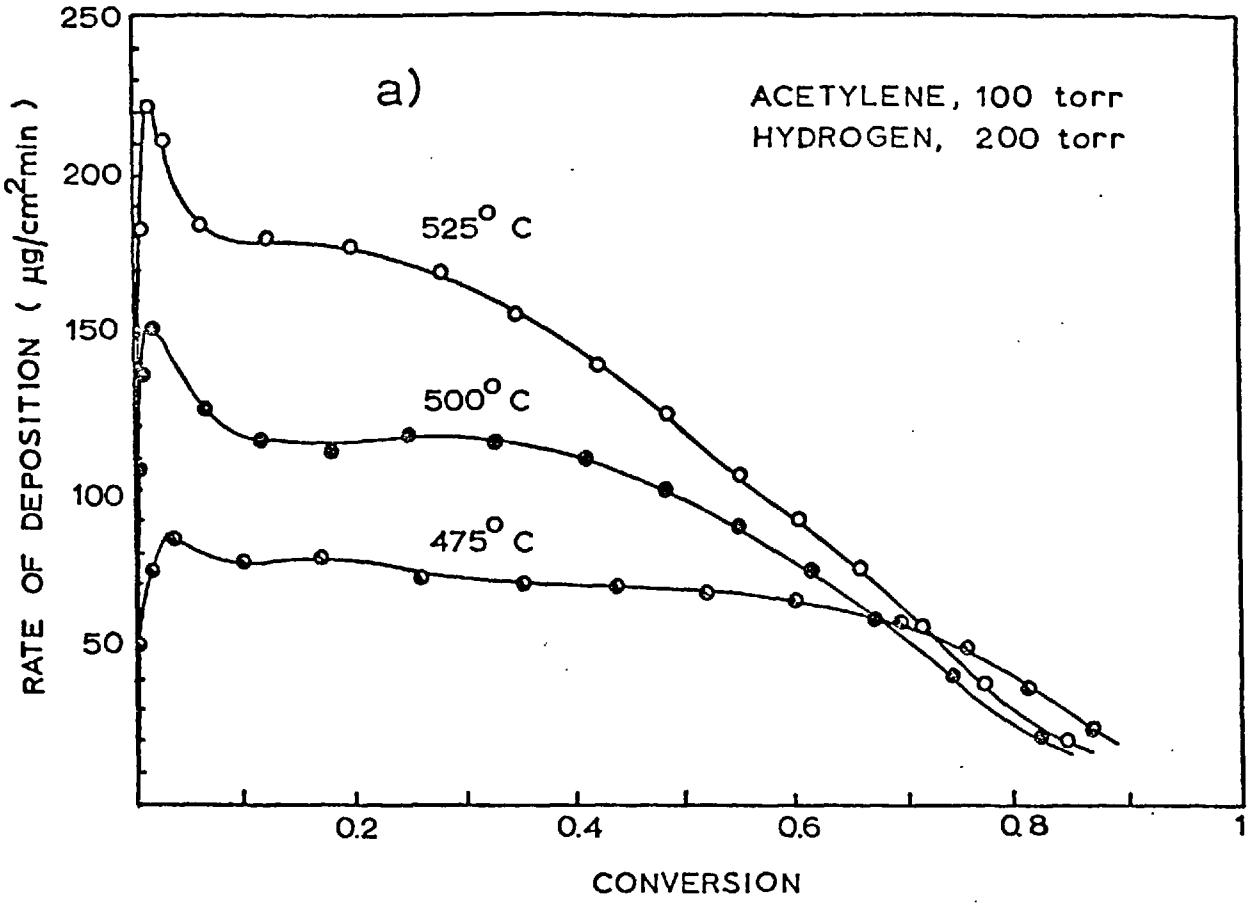

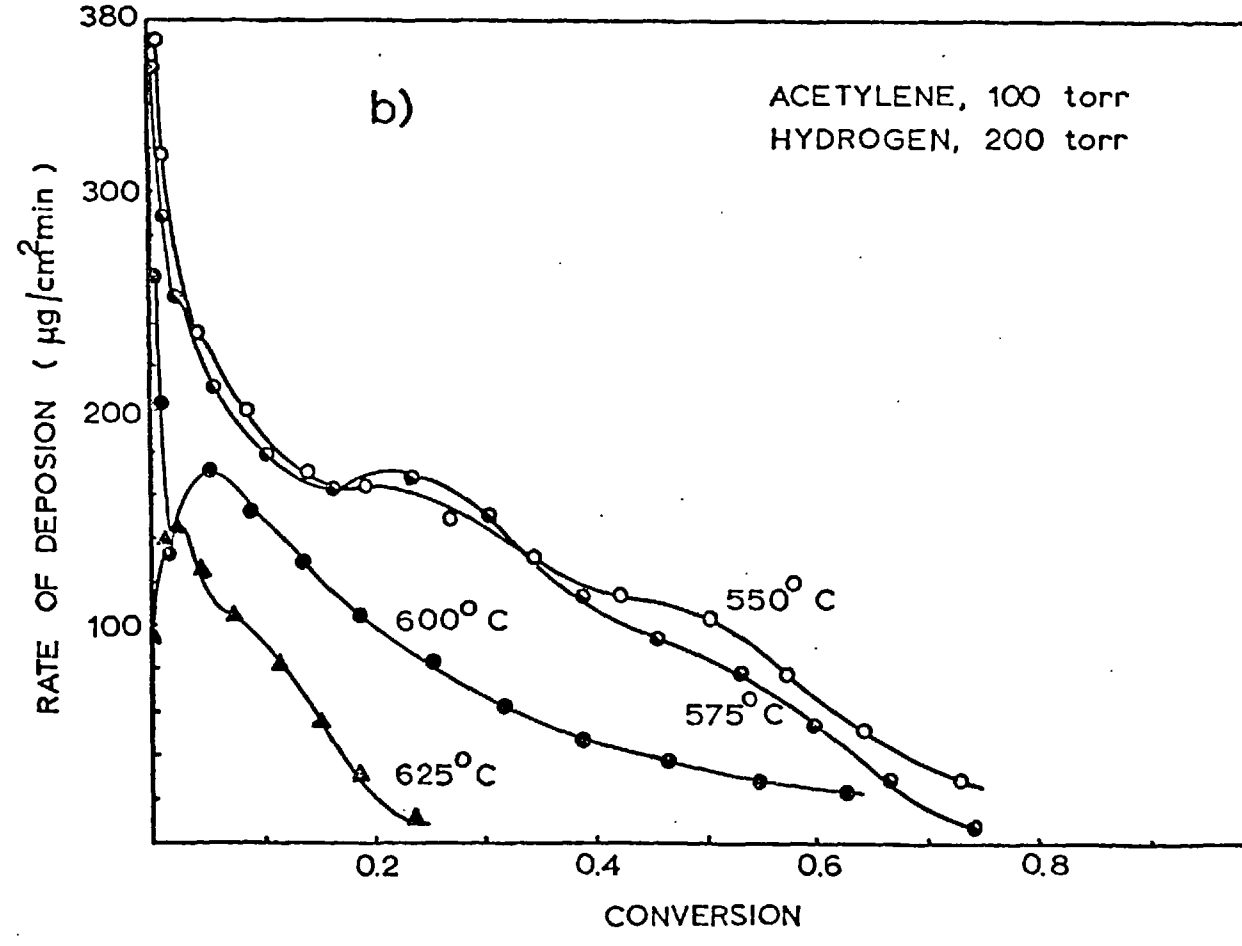

Fig. 3.5 Rate of deposition vs. conversion at different temperatures (with hydrogen)

favourable for further kinetic studies. This was found to be the case, as shown in Fig. 3.6. The comparison of the two runs depicted in the figure further shows that the second maximum in rate is due to the effect of hydrogen which accumulates in the system in batch conditions. It is also observed that if the pressure of acetylene is maintained (flow conditions) the reaction does not stop.

Various series of runs were performed to evaluate the activation energy of the reaction in the range of temperatures 400 - 500°C. These are presented in Table 3.1. If the hydrogen pressure is low (series A and B in the Table) a value of about 130 K J $mole^{-1}$ is obtained, within the range observed for other hydrocarbons (56). For higher hydrogen pressures, however, very high and disperse values are found (series C and D). This same "anomalous" behaviour was noted with ethylene and propylene (56).

It is appropriate to compare the values obtained with the ones that can be calculated using data from batch experiments. If the region of relatively stable rate following the first maximum (see Figs. 3.4 and 3.5) is used to change the temperature and evaluate activation energies, the values found are consistent with the ones obtained under flow conditions (series E and F). The activation energies estimated using the rate at the first or second maxima in Figs. 3.4 and 3.5 are also included in Table 3.1 (references G to J). It is obvious that the rate under these conditions is not only a function of the temperature but also of the "history", that is to say, of the mode of nucleation and growth of the carbon. The conclusion is that activation energies based on maximum rates (51 , 36) cannot usually have more than an empirical interest.

A comment must be made regarding the "anomalous" values observed for the higher hydrogen pressures. Possibly, a change of temperature in this case is accompanied by a change of the morphology, so that a "stable" steady state does not exist.

As referred to before, a maximum in the rate at a temperature (T_{max}) of 500 ± 50°C is observed, so that a negative apparent activation energy is measured above T_{max}. This was confirmed in four series of runs. The rates observed are shown in the Arrhenius-type plot presented in Fig. 3.7. Various conclusions can be drawn from the figure. The order is approximately zero at low temperatures and close to unity

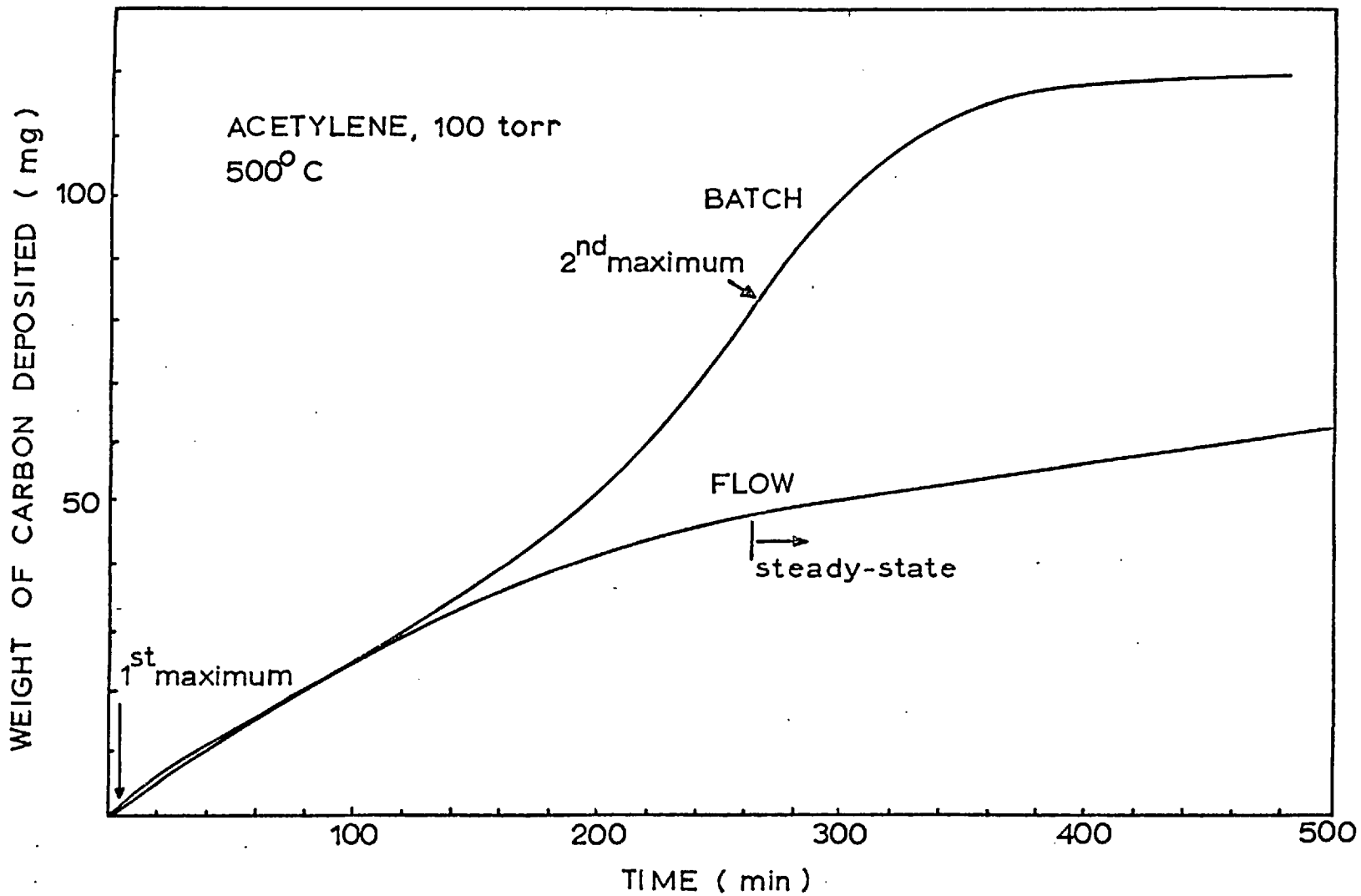

Fig. 3.6 Carbon deposition from 13.3 KN/m^2 (100 torr) acetylene at 500^{o}C in batch and flow conditions

Table 3.1 Comparison of observed activation energies for carbon deposition from acetylene on nickel under various experimental conditions.

REFERENCE	ACTIVATION ENERGIES ($KJ\ mole^{-1}$)	CONDITIONS	INITIAL PRESSURE ($KN\ m^{-2}$)		TEMP. RANGE (^{o}C)	OBSERVATION
			C_2H_2	H_2		
A	127.5 ± 6.5*	FLOW	13.3	-	415 - 465	STEADY - STATE
B	131.5 ± 6.5*		13.3	2.7	405 - 480	
C	265.5 ± 6.5		13.3	13.3	420 - 465	
D	200.5 ± 8.5		6.6	26.6	405 - 480	
E	130.0 ± 4.0*	BATCH	13.3	-	405 - 475	
F	130.0 ± 4.0		13.3	26.6	450 - 500	
G	138.0 ± 6.5		13.3	-	400 - 500	1st max.
H	148.5 ± 8.5		13.3	-	400 - 500	2nd max.
I	102.5 ± 6.5		13.3	26.6	475 - 550	1st max.
J	83.5 ± 4.0		13.3	26.6	475 - 525	2nd max.

* Values which more likely refer to a steady state.

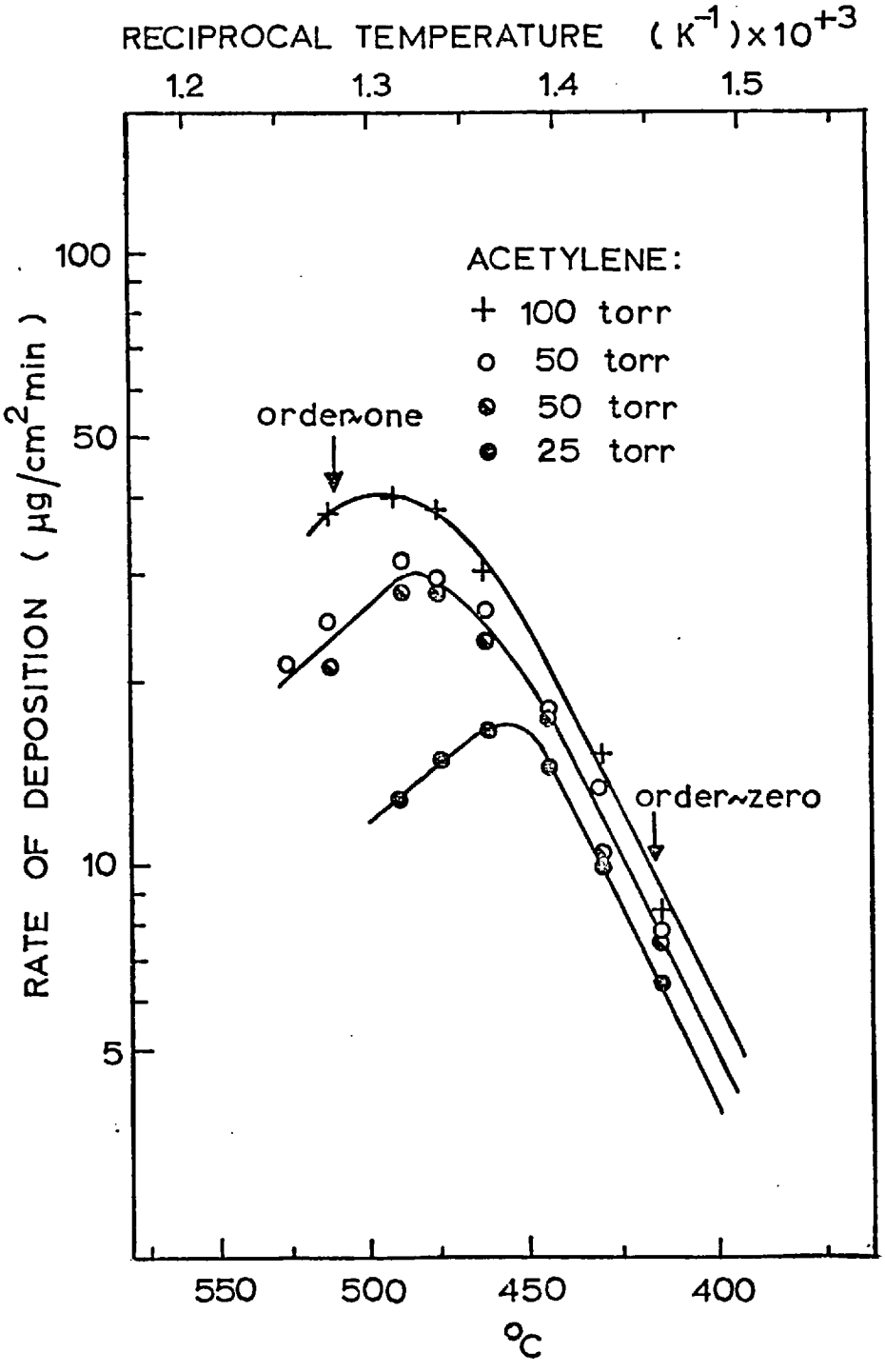

Fig. 3.7 Arrhenius-type plot of the deposition rate at different acetylene pressures

above T_{max}. The value of T_{max} increases with acetylene pressure. It can also be concluded, from comparision of Figs. 3.4 and 3.5, that T_{max} is further increased with increasing hydrogen pressure.

Finally, various series of runs were completed to obtain a direct evaluation of the orders of reaction. The temperatures of 430°C and 525°C were selected because they correspond to regions well below and well above T_{max} (cf. Fig. 3.7), so that the "transition region" was avoided. In fact, orders very close to zero at 430°C and very close to one at 525°C were observed with respect to both acetylene and hydrogen pressure, as listed in Table 3.2. This is again in agreement with values reported previously for various olefins (56).

3.2.1.2 Acetylene on nickel single crystals

Carbon was deposited in batch conditions on oriented nickel single crystals prepared in the way described in section 2.4.1. Acetylene was usually used at a total pressure of 13.3 K N m^{-2} (100 torr) and 475°C.

The rate of carbon formation over single crystal samples was always much smaller than over polycrystalline foils of the same size and finish (Fig. 3.8). Both curves present an immediate acceleration but the rate over the single crystal decreases drastically after the first few minutes. In this way, a true steady state was never observed. However, the deposition rate decreased very slowly, reaching a state in which it could be considered constant for limited periods of time.

Burning-off the carbon and reusing the single crystal showed always the behaviour represented in Fig. 3.8 with the exception that the initial deposition was greater. Microscopic observation of the surface after burn-off revealed a striking increase in roughening. Obviously, under these conditions random orientations are to be expected on the surface. To compare the effect of the different orientations the reaction was carried out over (111), (100) and (110) single crystals of the same size and finishing. The results are presented in Fig. 3.9.

Attempts were made to measure the apparent activation energy for the formation of carbon over the single crystals. Problems arose from the difficulty in attaining a steady state, but some reproducible results were obtained which are represented in Fig. 3.10.

Table 3.2 Orders to hydrogen and acetylene at different temperatures in flow conditions.

Temperature (^{o}C)	Pressures: ($KN\ m^{-2}$)	3.3	6.6	13.3	26.6	OBS.
430	ORDERS TO HYDROGEN	0.4	0.0	- 0.3		Acetylene pressure $6.6\ KN\ m^{-2}$
525		1.2	← 1.0 →			
430	ORDERS TO ACETYLENE	0.0	0.0	0.2		Hydrogen pressure $4.0\ KN\ m^{-2}$
525		1.0	1.2	0.6		

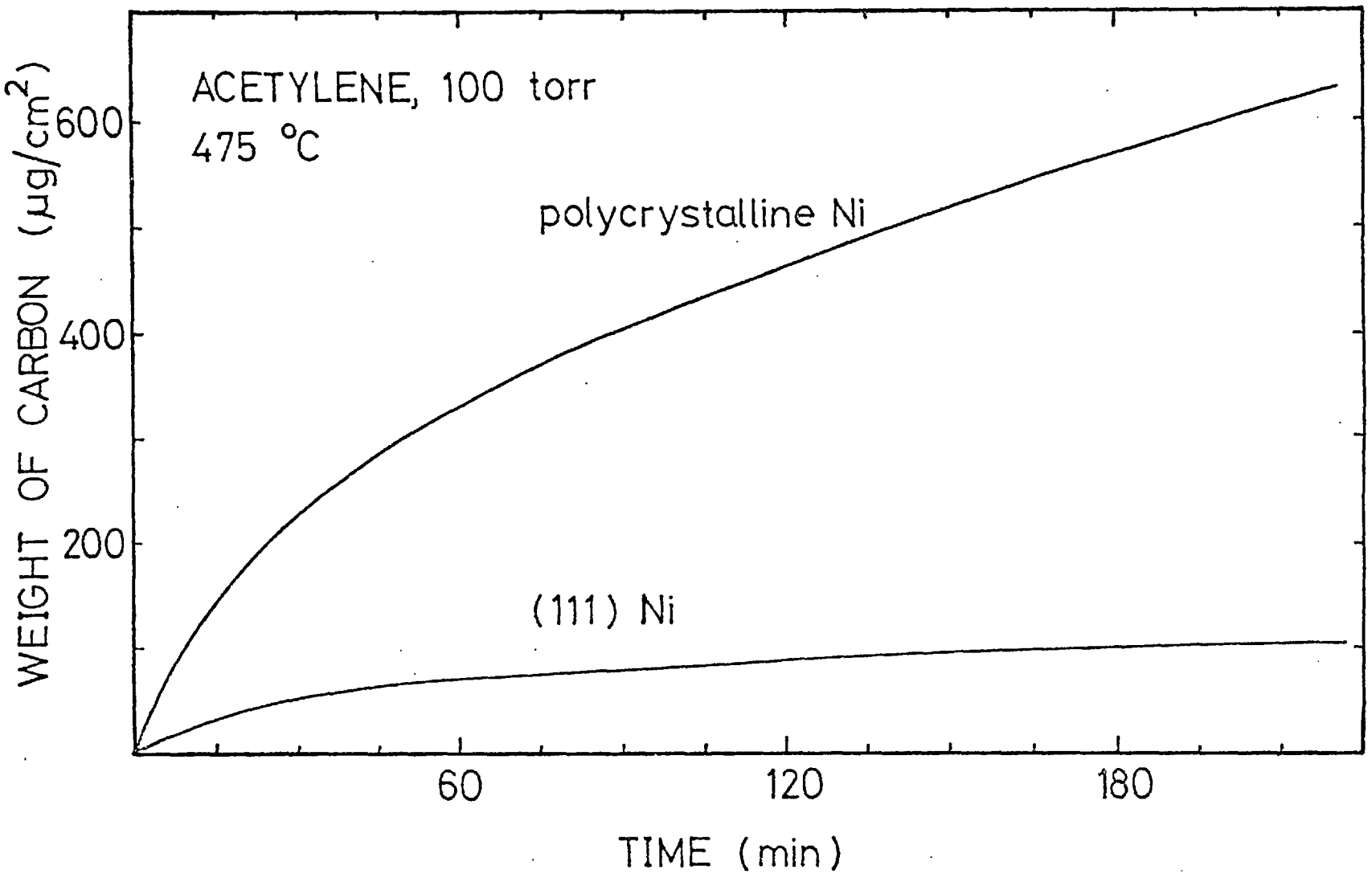

Fig. 3.8 Carbon formation from acetylene on electropolished polycrystalline and single crystal nickel foils

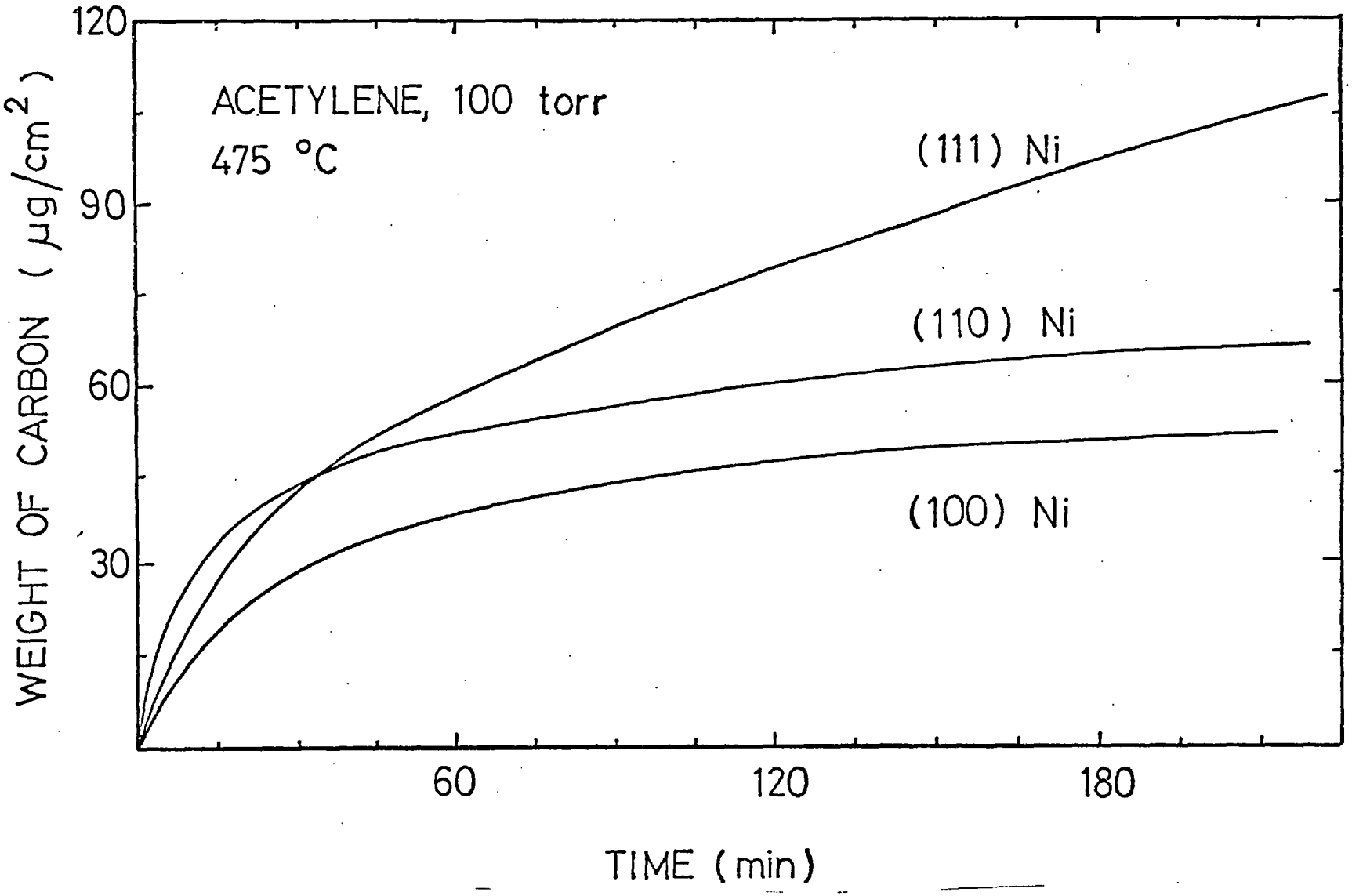

Fig. 3.9 Carbon formation on electropolished (111), (110) and (100) nickel single crystals

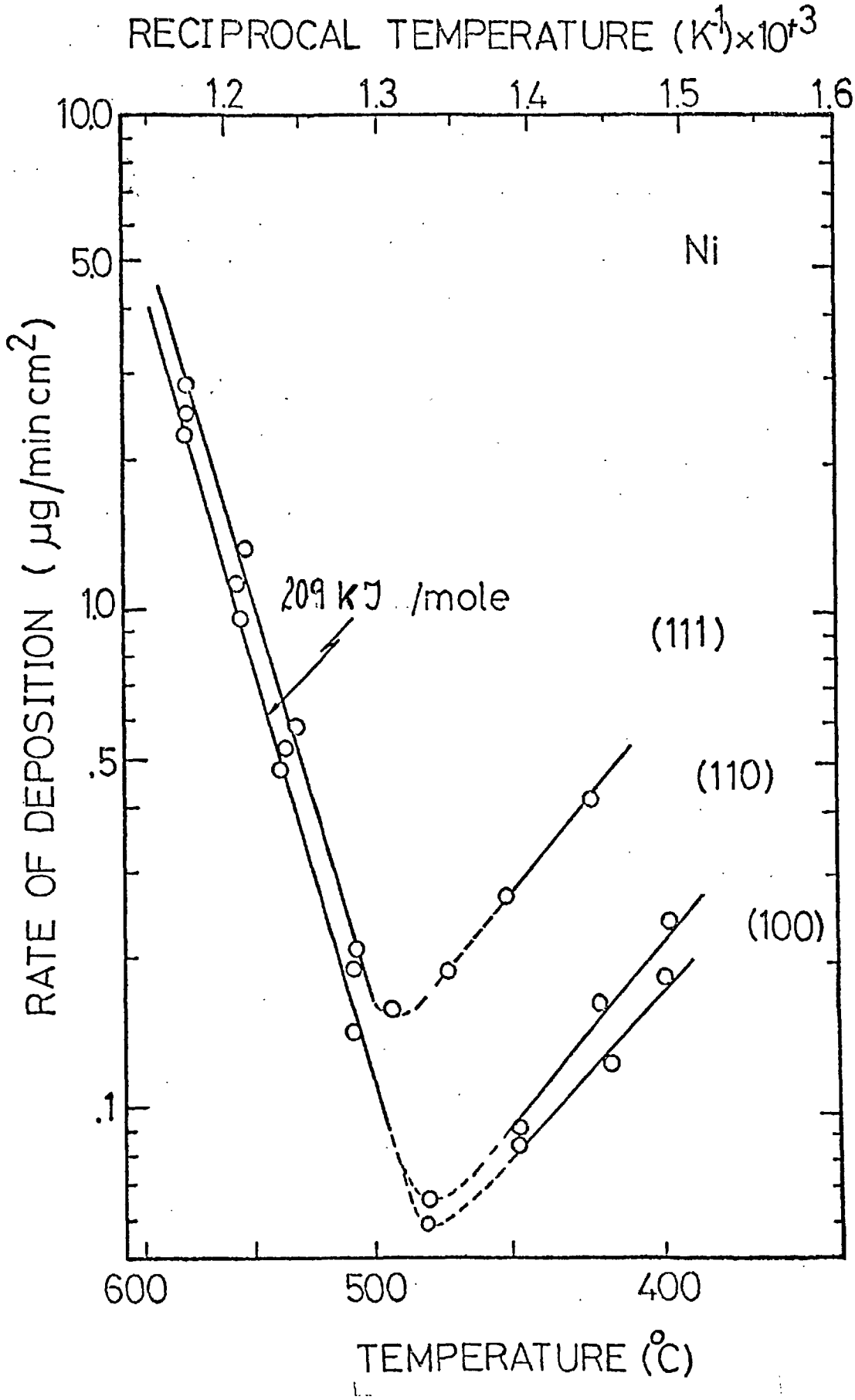

Fig. 3.10 Arrhenius-type plot of the rates of deposition from acetylene on (111), (110) and (100) nickel single crystals

The dependence of the rate is close to exponential at higher temperatures. Below 500°C the occurrence of a true steady state of the deposits is open to question. However, it is clear that the rates decrease with increasing temperature in this zone. Negative apparent activation energies are thus a common characteristic of the deposition from acetylene on both single crystals and polycrystalline nickel foils.

3.2.1.3 The negative dependence of the rate of deposition on temperature.

Although olefinic hydrocarbons have been investigated with some detail (7,56) one point is open to question. This is the negative dependence of the deposition rate on the temperature. With acetylene and the olefins on polycrystalline nickel foils, the rate decreases when temperature is increased from circa 550° to 675°C. Previous studies (7) proved that, in the presence of high partial pressures of hydrogen, no permanent deactivation of the catalyst occurs at these temperatures. The objective of the studies reported in this section is to investigate the kinetics of the reaction in this zone and to derive values for the true activation energy and the heats of adsorption of the reactants.

The hydrocarbons selected were acetylene, ethylene and 1-butene. Nickel polycrystalline foils of circa 3.0 cm^2 total area, prepared in the way described in 2.3.3, were used as catalyst. The results, as well as the conditions in which they were obtained, are presented in Tables 3.3 to 3.5

Preliminary experiments were carried out to check that homogeneous reactions did not interfere with the results. Two effects could be expected and these were checked in turn. In the first set of experiments, a silica "foil" of the same area as the nickel was used under the normal reaction conditions. No carbon uptake was observed at temperatures less than 675°C.

The second possible interference results from gas phase reactions which alter the nature or concentration of the gases in the reactor. The importance of this effect was assessed by analysis of the outlet gases over a range of temperatures. Typical results, obtained from an inlet gas mixture of C_2H_4 (0.43 $cm^3(STP)sec^{-1}$), hydrogen (0.85 cm^3sec^{-1}) and nitrogen (3.34 cm^3sec^{-1}), are shown in Fig. 3.11 and results for other gases are summarised in Table 3.3. Reported values of T_{lim} refer to temperatures below which the gas phase conversion, expressed as

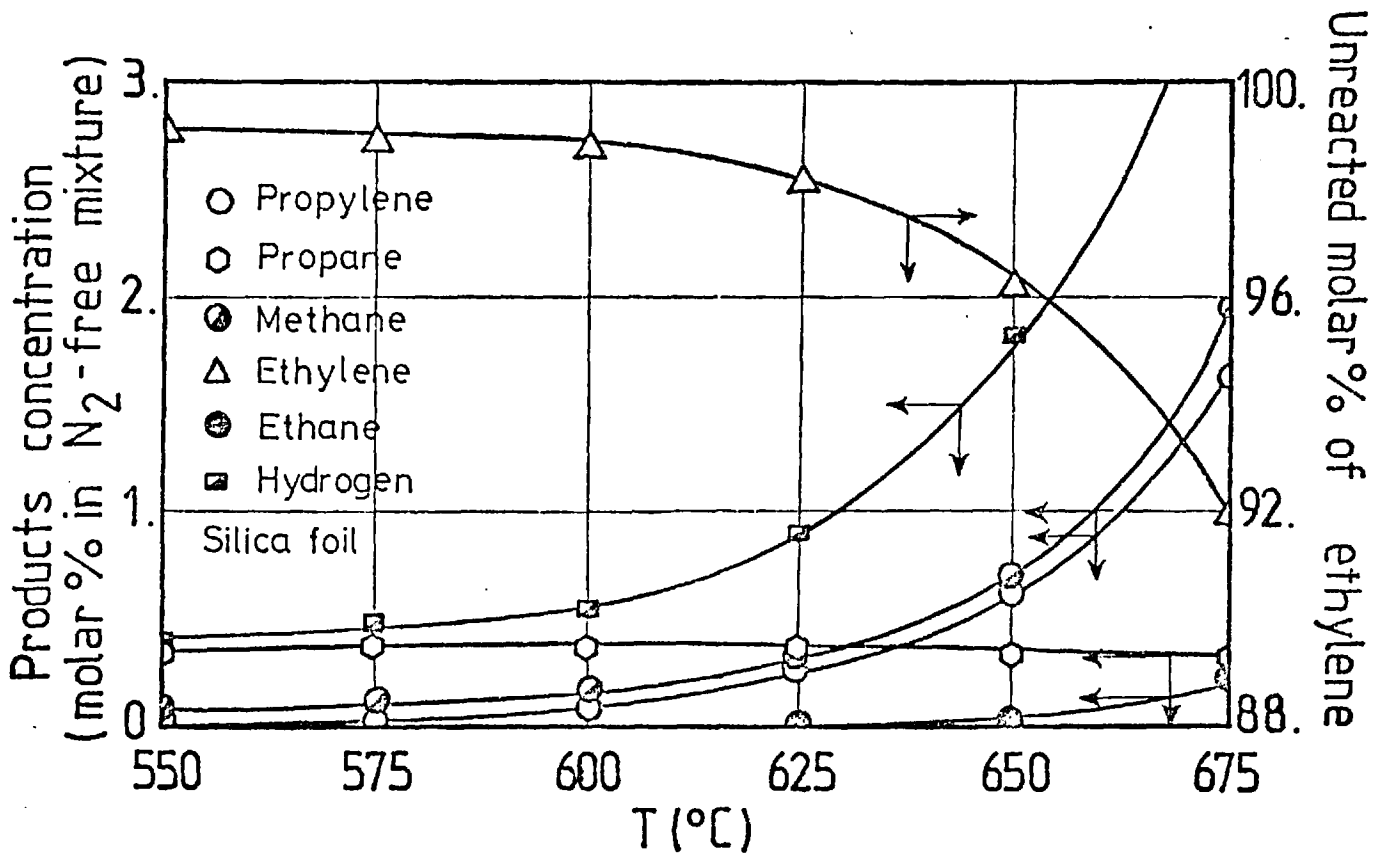

Fig. 3.11 Outlet composition vs. temperature
(feed: 4.6 $cm^3(STP)sec^{-1}$, $x_{C_2H_4} = 0.09$, $x_{H_2} = 0.18$)

Table 3.3 Analysis of the outlet gases at different temperatures.

Hydro-carbon	T_{lim} (°C)	Con-version (molar %)	Main product (excluding H_2)	Concentration (molar % in hydro-carbon mixture)
C_2H_2	625	9.10	C_2H_4	2.2
			C_3H_6	3.4
C_2H_4	675	8.1	CH_4	2.0
			C_3H_6	1.6
$1\text{-}C_4H_8$	650	9.28	C_2H_2	2.1
			CH_4	3.0

Table 3.4 Determination of the apparent activation energies (E_A). Conditions and Results.

Hydro-carbon (H_c)	Pressures (K N m^{-2})		Temperature Range scanned (°C)	E_A* (KJ $mole^{-1}$)
	H_c	H_2		
C_2H_2	11.0	46.5	573 - 627	- 222
C_2H_4	11.0	9.0	573 - 677	- 314
	12.5	58.0	575 - 676	- 213
$1\text{-}C_4H_8$	4.0	32.5	575 - 650	- 268
	62.5	39.0	550 - 625	+ 21

* Obtained by the least squares fit method. Standard deviation of E_A in each distribution below 10%.

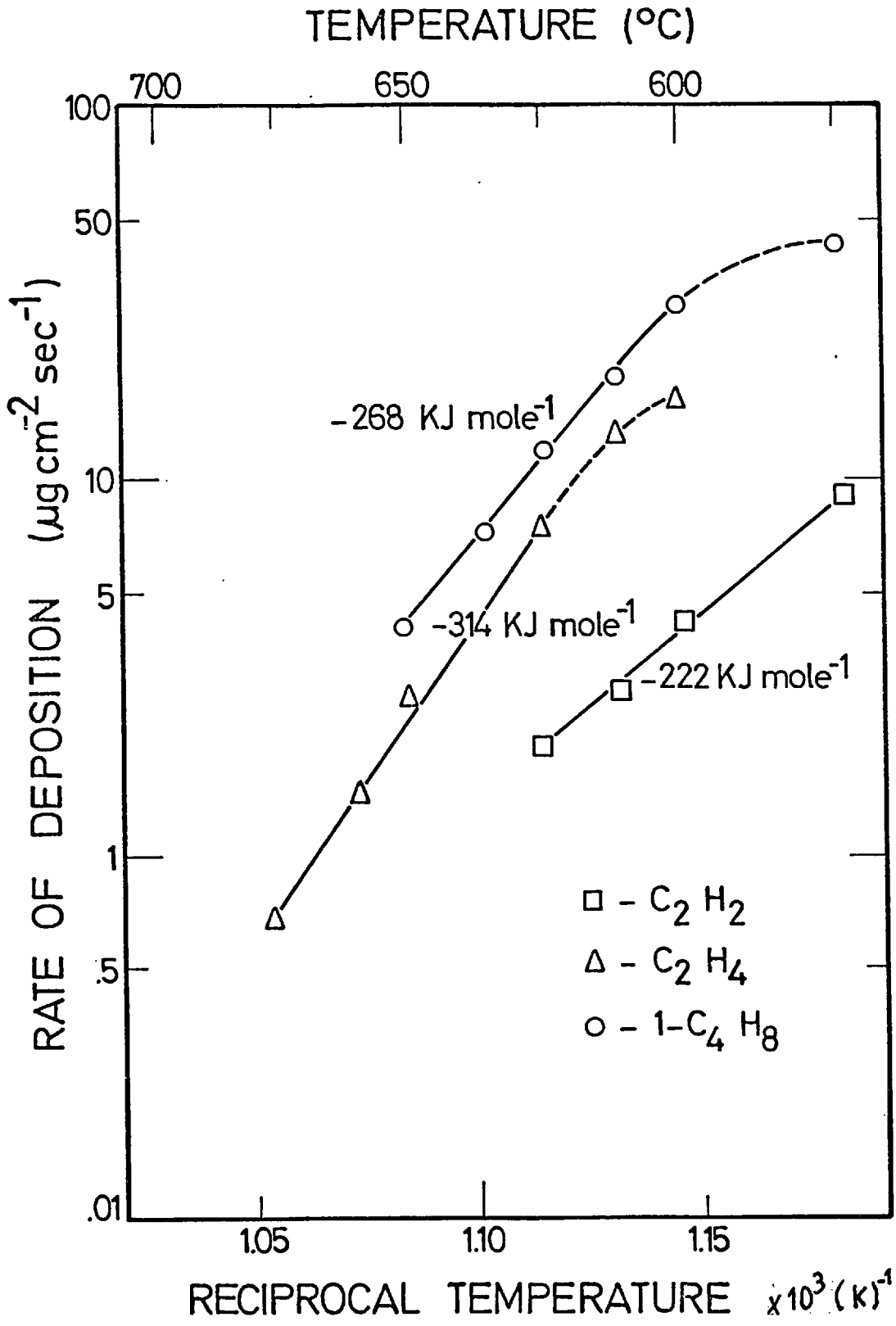

Fig. 3.12 Arrhenius-type plot of the rates of deposition from various unsaturated hydrocarbons.

(feed: 5.0 cm^3(STP)sec^{-1}; composition (mole %):

: C_2H_2 - 11%, H_2 - 46.5%; : C_2H_4 - 11%, H_2 - 9%;

: 1-C_4H_8 - 4.0%, H_2 - 32.5% ; N_2 as diluent)

Table 3.5 Dependence of the deposition rates on the partial pressure of hydrocarbon and hydrogen. Conditions and Results.

Hydrocarbon (H_c)	Temperature (^oC)	Pressures used ($K N m^{-2}$)		Orders measured	
		H_c	H_2	H_c	H_2
C_2H_2	600	3.5 to 12.0	50.0	1	-
		12.0	44.5 to 52.5	-	~ 0
C_2H_4	625	8.0 to 13.5	9.5	1	-
		13.0	9.0 to 14.0	-	1
		13.0	50.0 to 66.0	-	~ 0
$1\text{-}C_4H_8$	625	8.0	31.0 to 62.5	-	0
		4.0 to 25	32.5	1	-

a percentage of the initial composition, is within the reproducibility of the results. These were considered as upper limits of temperature in subsequent experiments with the nickel foil. Under reaction conditions, mass transfer effects were not rate limiting and hydrogen was found to be the major product.

In that the ratio of the hydrogen to hydrocarbon necessary to minimise deactivation has not been established in all cases, tests were devised to define it. These involved scanning the rate of carbon production over the temperature range concerned, with increasing and decreasing temperature. Reproducibility of the results has been shown to be a feature of lack of deactivation (7): this was ± 10% for a minimum hydrogen to hydrocarbon ratio of circa 0.5 and a hydrogen partial pressure greater than 8.0 $KN\,m^{-2}$.

Within these conditions, steady state rates of deposition were measured at different temperatures and various reactants compositions. They gave the basis for the determination of apparent activation energies, as shown in the Arrhenius-type plot presented in Fig. 3.12. A more comprehensive list of values, covering the whole range of the conditions used is presented in Table 3.4.

The orders with respect to hydrogen and the hydrocarbon were also determined at different temperatures. They are presented in Table 3.5.

Usually a total inlet flow of about 5.0 cm^3 (STP) sec^{-1} was used in this work. Varying the inlet flow at 600°C between 3.3 and 6.7 cm^3 (STP) sec^{-1} caused no apparent change in the steady state rate of carbon deposition.

3.2.1.4 Deposition from ethane and n-hexane on polycrystalline nickel foils.

The deposition of carbon from ethane and hexane was studied under flow conditions at temperatures between 450 and 800°C. The results obtained are presented in Table 3.6.

With ethane, deposition did not occur until circa 600°C, probably due to very long induction periods. However, once the deposition started, the temperature could be lowered until circa 450°C, without the reaction stopping. In fact, apparent steady states of deposition were observed in between those temperatures. These could be used to measure the activation energy and orders of the reaction with respect

Table 3.6 Carbon deposition from ethane and hexane on polycrystalline nickel foils. Conditions and Results.

Run	Hydro-carbon (H_c)	Foil area (cm^2)	Partial Pressure ($KN\,m^{-2}$)		Inlet Flow - cm^3(STP) sec^{-1}	Temp (^oC)	Rate x 10^4 (mg/sec cm^2)	Type of experi-ment
			H_c	H_2				
63	C_2H_6	2.70	75	25	3.3	450 to 600	0.56 to 13.8	E_A
64	C_2H_6	2.64	75	25		500 to 575	4.43 to 11.8	
65	C_2H_6	2.72	50	25	3.3	500	3.16	
			25	25			1.94	
			75	25			5.21	
			50	25			3.75	
			25	50			1.07	O
			25	75			0.27	
			75	25		600	12.9	
			50	25			9.10	
			25	25			5.72	
			25	50			9.18	
			25	75			3.62	
68	C_2H_6	2.68	75	25	3.3	600	13.2	
					4.3		14.2	F
					1.3		11.8	
98	C_2H_6	2.70	75	25	3.3	450 to 700	0.53 to 3.50(?)	
56	C_6H_{14}	2.70	13	25	3.3	450 to 800	1.18 to 16.0	E_A
57	C_6H_{14}	2.68	13	25	3.3	525 to 600	13.2 to 57.6	E_A
58	C_6H_{14}	2.70	13	25	3.3	600	53.4	S
59	C_6H_{14}	2.70	13	25	3.3	600	46.3	S
60	C_6H_{14}	2.66	4	25	3.3	475	1.27	
			8.5	25			2.74	
			10	25			3.05	
			13	25			3.90	O,E_A
			4	-			3.46	
			4	75			0.18	
			4	50			0.58	
			13	25		475 to 625	3.34(?) to 23.4	
61	C_6H_{14}	2.62	13	25	3.3	600	38.6	
			8.5	25			30.5	
			4	25			18.3	O
			8.5	50			32.3	
			8.5	75			23.2	
66-a	C_6H_{14}	2.70	13	25	3.3	600	55.2	B.O.
66-b	C_6H_{14}	2.70	13	25	3.3	600	67.2	B.O.
66-c	C_6H_{14}	2.70	13	25	3.3	600	69.1	B.O.

Table 3.6 (Continued)

LEGEND:

E_A - Determination of the apparent activation energy

O - Determination of the order of the reaction

F - Effect of the flow rate

S - Determination of the extent of the steady state

B.O. - Effect of carbon burn-off

to both hydrocarbon and hydrogen.

The Arrehnius-type plot in Fig. 3.13 shows different zones. Below 500°C a value of the apparent activation energy, E_A, of about 199 ± 11 KJ $mole^{-1}$ was measured. Between 525 and 600°C the rates increase slowly with temperature (Ea ≃ 70 kJ $mole^{-1}$). Above 600°C the existence of a true steady state is doubtful, the reaction rate decresing slowly with time at a fixed temperature. Above 650°C deactivation is almost complete.

The dependence of the rate of deposition on the partial pressure of ethane is shown in Fig. 3.14. Orders close to one at 500°C and 0.8 at 600°C were determined. Thus, here, in contrast to acetylene and the olefins (56), a change in the rate controlling step as the temperature increases is not accompanied by an increase in the value of the order with respect to the hydrocarbon.

The dependence of the rate on hydrogen (not shown in the figure) is somewhat complex. At lower temperatures, up to partial pressures of 50 $KN\,m^{-2}$, the order with respect to hydrogen is close to -1. At higher partial pressure the rate of deposition decreases drastically. At 600°C the pattern is the same, with the exception that a value of - 0.3 is measured at lower partial pressures.

Changing the flow from 1.33 to 4.32 cm (sec)sec^{-1} (partial pressures constant) at 600°C did not cause any apparent change in the steady state rate in run 68. This, together with the value of the orders with respect to hydrogen and ethane, indicates that the existence of a "film-diffusion controlled" process between 500 and 600°C is not likely.

Deposition from n-hexane was measured at temperatures above 400°C without significant induction periods being noticed. The pattern of deposition was very similar to that of acetylene under flow conditions (see Fig. 3.6). Usually a constant rate would be observed after 30 to 40 mg of carbon were deposited. This would last until the full scale deflection of the microbalance was reached (100 mg).

Rates measured in steady-state conditions are represented in the Arrhenius-type plot of Fig. 3.13.

As with ethane, different temperature zones can be observed in the graph. Up to 600°C the rate increases with temperature (Ea = 176 ± 12 KJ/mole and 116 ± 8 KJ/mole, respectively above and below

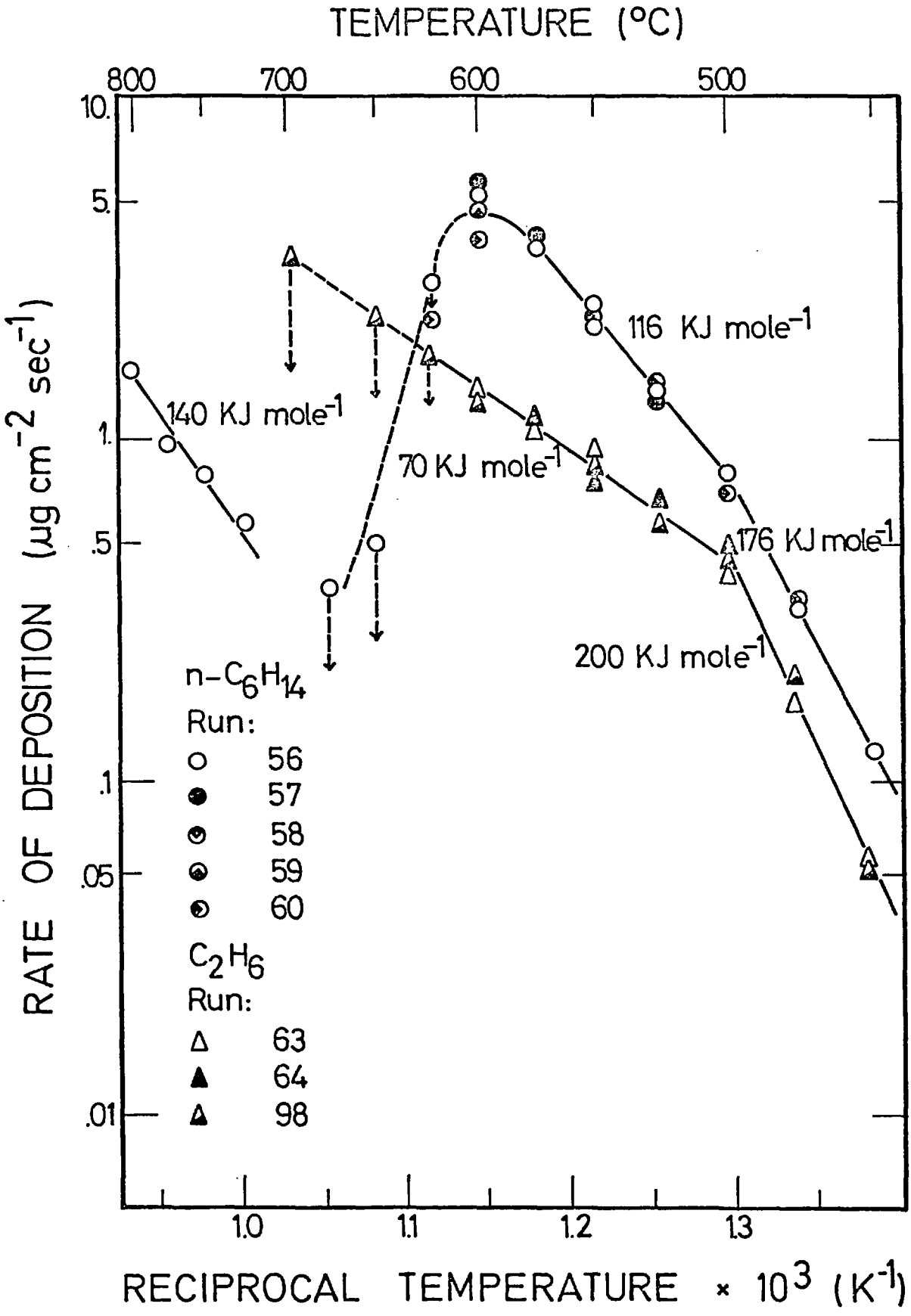

Fig. 3.13 Arrhenius-type plot of the rates of deposition from ethane and n-hexane on polycrystalline nickel foils. (Feed: 3.3 $cm^3(STP)sec^{-1}$; Ethane: $x_{C_2H_6} = 0.75$, $x_{H_2} = 0.25$; n-hexane: $x_{C_6H_{14}} = 0.13$, $x_{H_2} = 0.25$)

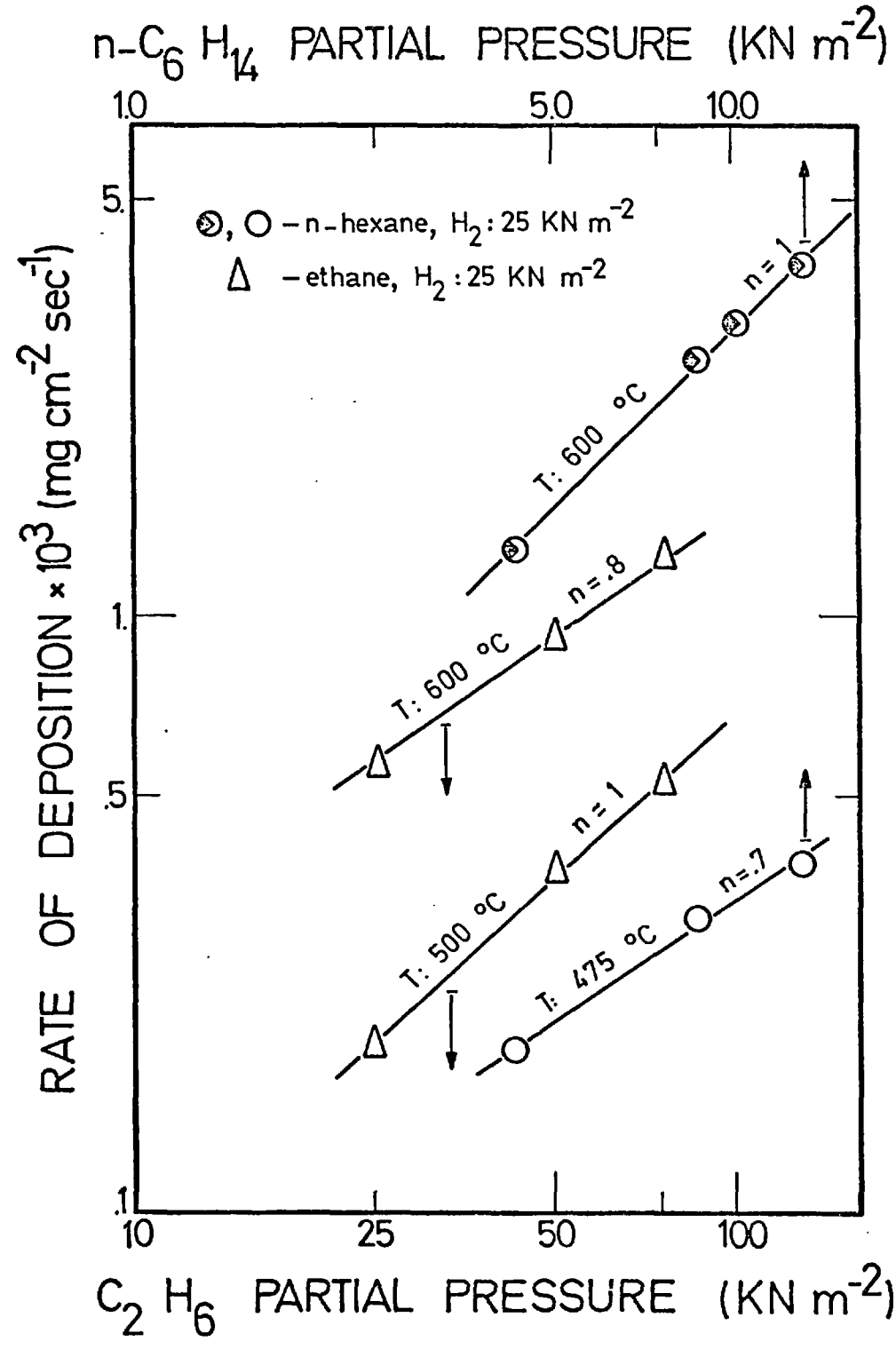

Fig. 3.14 Dependence of the rate of deposition on the partial pressure of n-hexane and ethane at different temperatures.

500°C). Between 600 and 700°C the rate decreases sharply with temperature. In fact, a true steady state is not observed in this zone, the rates decreasing slowly with time at a fixed temperature. This indicates that a strong deactivation process is taking place. Above 700°C the deposition accelerates again, probably due to the homogeneous reaction. An apparent activation energy of 140 ± 12 KJ $mole^{-1}$ was measured at these temperatures.

The dependence of the rate of deposition on the partial pressure of n-hexane, also represented in Fig. 3.14, is very similar to that of ethane. The order with respect to n-hexane is close to one at 475°C and about 0.7 at 600°C.

The dependence on hydrogen partial pressure, not shown in the figure, is also very similar to that of ethane for both the lower and the higher temperatures (- 1 and - 0.3, respectively). Burning-off completely the carbon with hydrogen and re-using the sample in another deposition experiment resulted in higher values of the steady state (cf. runs 66-a, 66-b, 66-c in Table 3.6). This is probably due to the increase in roughness of the foil (with the corresponding increase in the surface area) caused by the lifting-up of particles from the surface (56).

The kinetic parameters determined below 500°C for n-hexane and ethane present a major difference from those of acetylene and the olefins (56). Orders different from zero, and activation energies dependent on the nature of the parent hydrocarbon, indicate that a different process must be rate determing at low temperatures.

3.2.1.5 Morphological and structural studies.

A series of studies was carried out to:

(i) elucidate the relationship between the observed kinetics of carbon deposition and the morphology and microstructure of the deposit formed;

(ii) study the influence of grain boundaries and crystal orientation on the activity for carbon formation and on the processes of dissolution, diffusion and precipitation of carbon in/from nickel.

The experiments were mainly performed in the low pressure system described in section 2.3. The information obtained was complemented by analysis and microscopic observation of the foils and deposits.

A complete description of the experiments made is presented in Table 3.7.

3.2.1.5.1 Kinetics and morphology

Runs 1-a to 1-e refer to a series of experiments which were carried out to accomplish the first objective of this section. The experiments were stopped when the C_2H_2 conversion (x) corresponded to particular features of the curve for 13.3 $KN\,m^{-2}$ (100 torr) in Fig. 3.2-b. Reaction 1-a was stopped at x = 0.008, corresponding to the middle of the first "acceleration". Runs 1-b, c, d and e were stopped at x = 0.016, 0.05, 0.10 and 0.35, respectively, the first maximum, the minimum, the beginning of the new "acceleration" and the second maximum. The corresponding SEM micrographs are presented in Fig. 3.15 a-e). After an induction period the carbon nuclei started to grow (a) until, eventually, all the surface was covered by carbon (b). This brought about a decrease in the rate without any apparent changes in the morphology of the deposit (b, c). The fact that the reaction did not stop completely could be related with the appearence of a different type of carbon formation (d). The continuing deposition after this point is certainly due to the growth of this formation (e). The growth did not stop until the acetylene was virtually depleted. In the case of the flow experiment (Fig. 3.6), this formation should correspond to the steady state deposition.

3.2.1.5.2 Analysis of the deposited nickel foils

Experiments 3-a to 3-e were carried out under conditions similar to those of 1-a to 1-e. The deposited foils were sent for Electron Probe Micro Analysis (EPMA). The smaller deposits were difficult to analyse because the thickness of the carbon layer approached the resolution of the instrument (about 5 μm). This corresponds to a deposit of circa 3 mg for foils of 1.5 x 1.0 cm. Thus, virtually only the samples obtained in runs 3-c, d and e could be examined.

The analyses showed a significant amount of nickel particles in the carbon. Up to a given deposition (corresponding approximately to the appearence of the second formation in Fig. 3.15(d) the particles were mainly located in a layer at the outer surface of the carbon. This layer was roughly parallel to the nickel foil (see the Backscattered Electron Image and the X-ray photographs in Fig. 3.16). As the deposit increases, and its thickness exceeds 15 - 25 μm, the preferential

Table 3.7 Morphological and structural studies of carbon deposits formed on nickel.

Run	Catalyst	Experiment	Temp (°C)	Pressure		Analysis and observations
				C_2H_2 (K N m^{-2})	Degassing (N m^{-2})	
1-a to 1-e	Poly-crystalline foil	Deposition at low pressure (DLP)	500	13.3	-	SEM,XRD
3-a to 3-e	Poly-crystalline foil	DLP	500	13.3	-	EPMA,CA
4	Poly-crystalline foil	DLP	475	13.3	-	EPMA
6	(111) single crystal	DLP	475	13.3	-	EPMA
11 to 13	(111) single crystal	Coating in vacuum unit (CVU)+DLP	475	13.3	-	OM,XRD
14	(111) single crystal	CVU+anealling + DLP	900 475	- 13.3	1.33×10^{-2}	OM
15	Poly-crystalline foil	CVU + DLP	475	13.3	-	OM
16 to 18	(111) single crystal	CVU+dissolution and re-precipitation (DR)	1000 to 900	-	1.33×10^{-2}	EM,OM
19	(110) single crystal	CVU + DR	1000 to 900	-	1.33×10^{-2}	EM,XRD

LEGEND: SEM - scanning electron microscopy
EPMA - electron probe microanalysis
OM - Optical microscopy
XRD - X-ray diffraction
CA - chemical analysis
EM - electron microscopy, transmission and diffraction

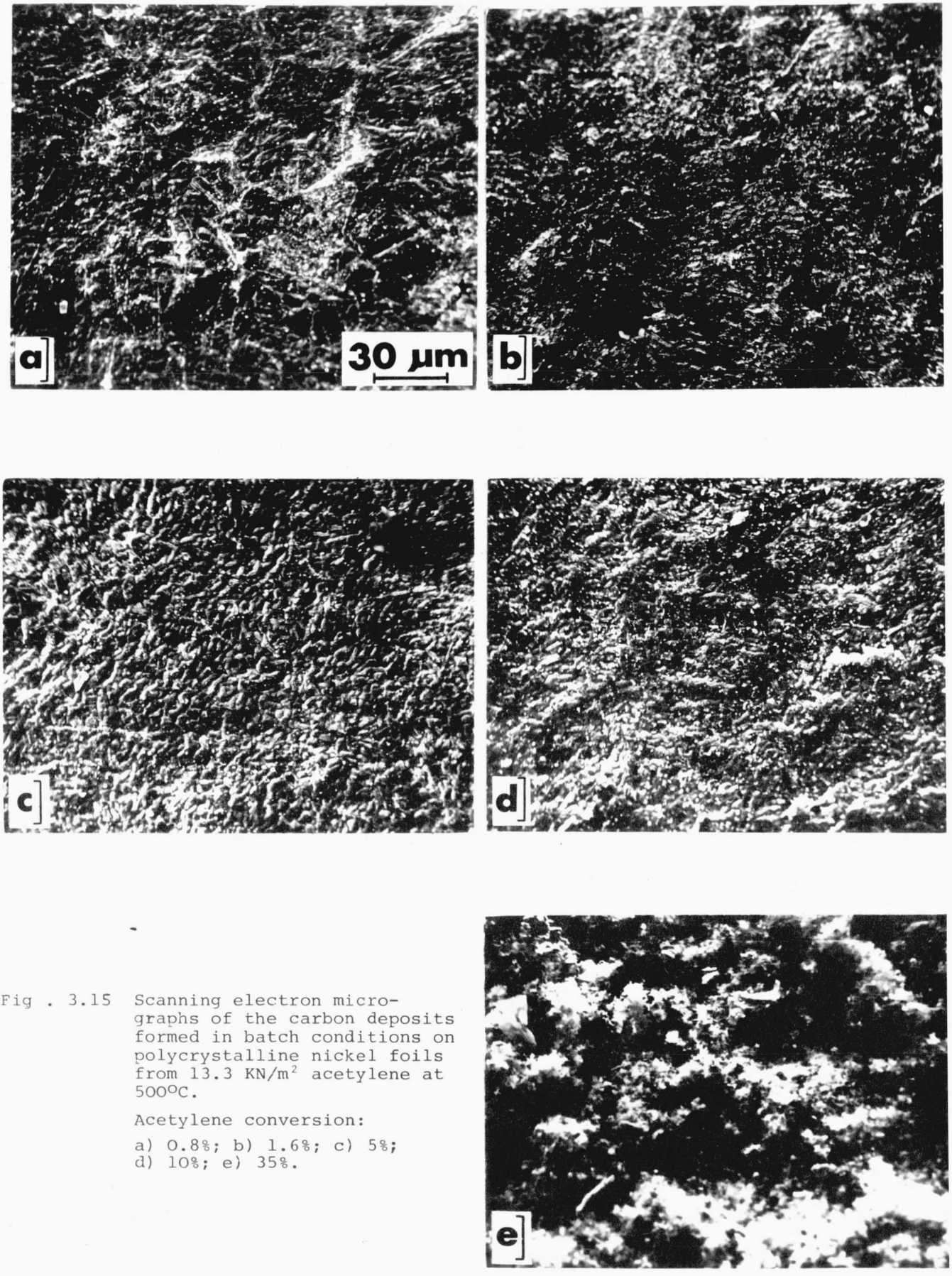

Fig . 3.15 Scanning electron micrographs of the carbon deposits formed in batch conditions on polycrystalline nickel foils from 13.3 KN/m^2 acetylene at 500°C.

Acetylene conversion:

a) 0.8%; b) 1.6%; c) 5%; d) 10%; e) 35%.

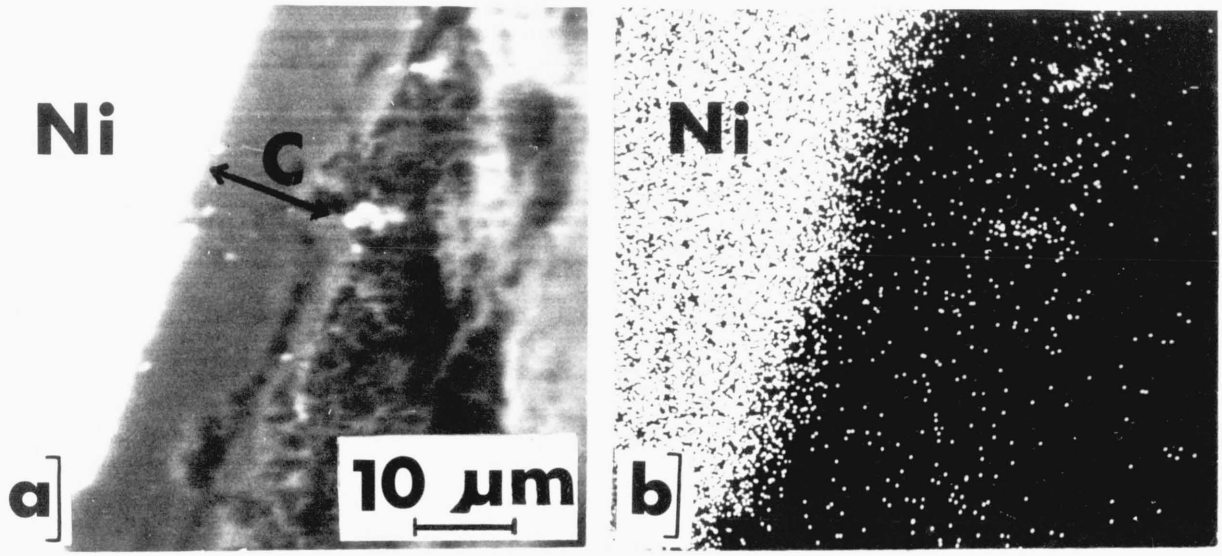

Fig. 3.16 Electron probe microanalysis: Backscattered electron image (a) and X-ray photograph (b) of the deposit formed on a polycrystalline nickel foil in Run 3-d.

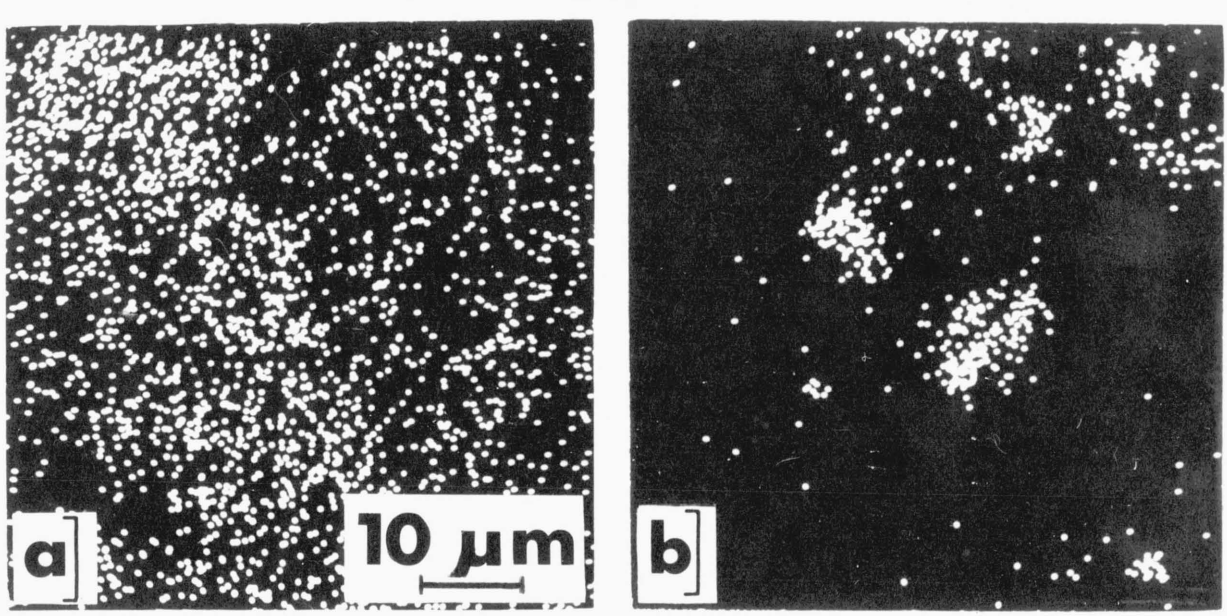

Fig. 3.26 Electron probe microanalysis: X-ray photographs of the deposited supported catalyst used in Run 67.

a) Nickel ; b) Aluminium

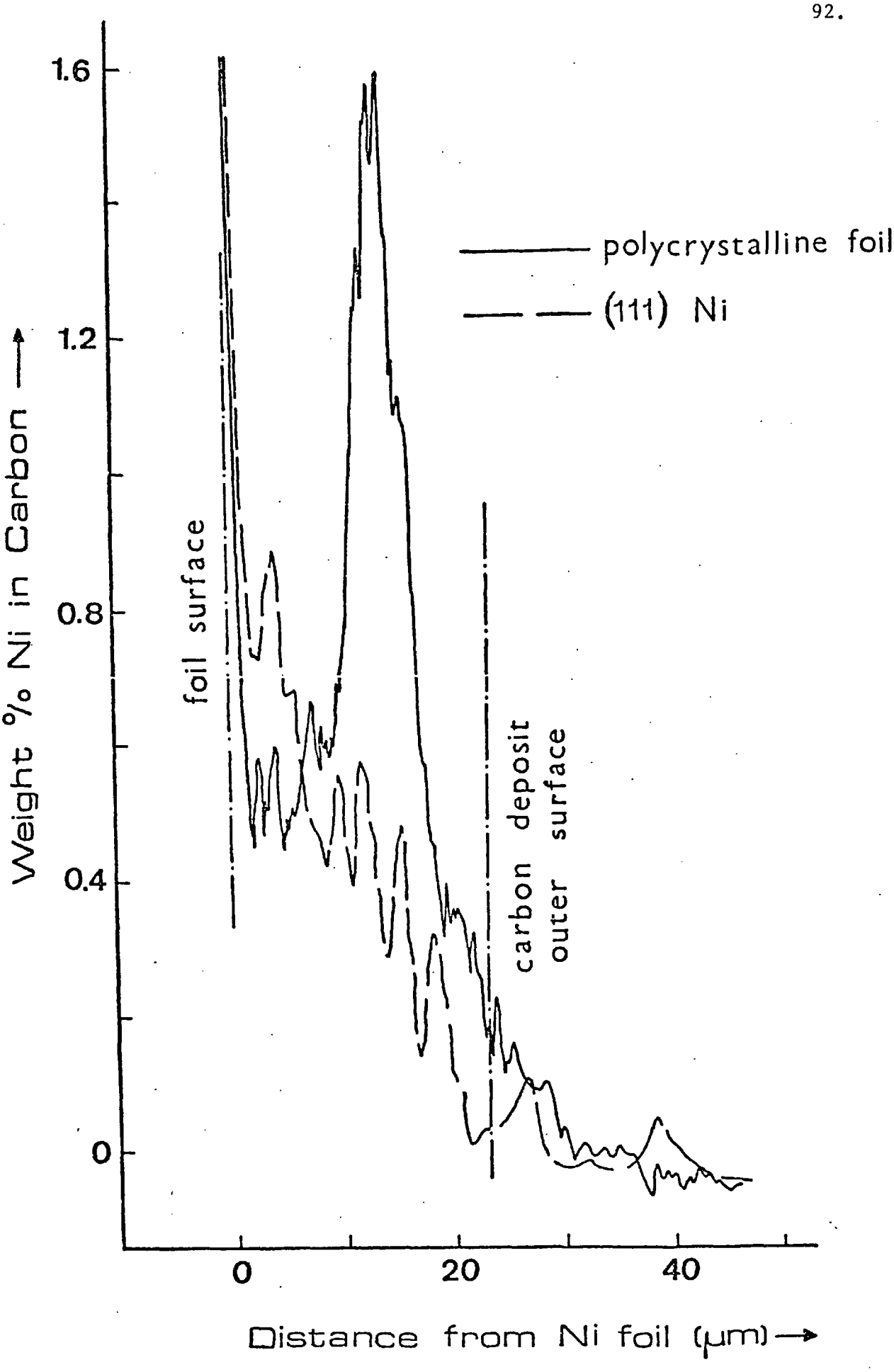

Fig. 3.17 Electron probe microanalysis of the deposits formed on polycrystalline and single crystal nickel foils from 13.3 KN/m^2 acetylene at 475°C.

Table 3.8 X-ray diffraction analyses: carbon and deposited nickel foils.

	d-spacings (^{o}A)	Relative Intensities
Carbon	3.373; 2.028; 1.760	VS; S; W
Deposited foil	3.378; 2.036; 1.763; 1.248	M: S; VS; MS
Graphite (ASTM 23-64)	3.36; 2.03; 1.678	100; 42; 21
Nickel (ASTM 4-850)	2.034; 1.762; 1.246	100; 50; 80

W - weak
MS - medium strong
S - strong
VS - very strong

orientation disappears: the X-ray photograph shows nickel evenly distributed across the carbon layer.

Carbon deposited on single nickel crystal foils, prepared in the usual way, were also examined by EPMA. Fig. 3.17 shows the X-ray spectrometer traces of one such foil (run 6). The result of the analysis of a 1.2 mg deposit (corresponding to a thickness of 15 to 20 μm) formed in run 4 on a polycrystalline foil of the same size (4 x 5 mm) and finishing is also included in the figure.

As the charts were calibrated by direct ratio to the 100% count rate (taken in the nickel foil), the concentration values in the figure can only be regarded as an approximation. However, it can be concluded that in the case of the single crystal, the nickel concentration decreases to near zero at a distance of about 20 μm from the surface.

By contrast, in the polycrystalline foil it reaches a maximum at the limit of the carbon deposit.

A direct evaluation of the nickel concentration in the carbon was made by wet chemical methods. For deposits of 6 and 85 mg respectively, it was found to be 1.50 and 1.20 ± 0.05% (w/w). Systematic analyses of deposits with increasing amounts of carbon showed no significant trend in the concentrations of nickel. If anything, the concentration seemed to decrease slightly with the extent of the deposition.

Carbon covered nickel foils were analysed by X-ray diffraction. The analyses showed the presence of graphite, the intensity of the diffraction peak being proportional to the weight of the deposit. The interlayer spacings measured varied between 3.36 and 3.41 Å. Some unidentified peaks were also found, possibly corresponding to nickel carbide.

Carbon was collected from the thicker deposits (cf. run 1-e) and analysed separately, showing in all cases the presence of nickel.

The results obtained are summarised in Table 3.8.

3.2.1.5.3 Bulk diffusion of carbon in nickel

Experiments 11 to 15 were performed to examine the role of bulk diffusion of carbon in the process of carbon formation on nickel:

Run 11. A single crystal nickel foil (4 x 6 x 0.1 mm) was hung in the

vacuum microbalance at a temperature of 475°C. Acetylene was admitted and carbon was quickly formed on the two faces of the foil.

Run 12. A similar foil was covered on both sides with a 400°A carbon layer in a vacuum coating unit. No catalytic deposition could be subsequently observed under the same conditions as in Run 11. The foil was poisoned by the carbon pre-coating.

Run 13. A foil was pre-coated as in Run 12, but on one face only (face 2). Under the same conditions as the previous runs, growth took place on the coated side. The uncoated face remained clean. Photographs of the two sides of the foil before and after deposition are shown in Fig. 3.18. Although more than 300 μg of carbon were deposited, equivalent to a layer of about 6 μm, almost no carbon is observed on face 1, except in localised areas near the edges (nucleation seems to be progressively spreading round the edges and over face 1). In this experiment side 2 (see Fig. 3.18) was poisoned, so the decomposition of C_2H_2 must have occurred on side 1. However, growth takes place on the opposite side. It seems that carbon migrates through the nickel crystal from face 1 to face 2 during the reaction.

Run 14. The foil was pre-coated on one side as in Run 13, followed by annealing at circa 900°C for five minutes. Under the reaction conditions referred to above, growth of carbon was observed on both sides of the foil.

The results of the above four runs are summarised in Fig. 3.19.

Run 15. A polycrystalline foil was polished and pre-coated on one face only as in Run 13. When reacting in the microbalance with acetylene at 475°C, carbon was again formed on both faces of the foil. It seems obvious that in Run 13 the pre-coating acts as seeding for carbon growth. The presence of carbon on face 2 prevents formation of nuclei on face 1, probably keeping carbon supersaturation in nickel sufficiently low from the beginning of the reaction.

In Run 14, dissolution and reprecipitation of carbon during annealing was enough to create nuclei on the opposite side. Growth was observed on both faces in this case, although the decomposition must have occurred on the clean areas in face 1, since face 2 was completely poisoned.

In Run 15, the presence of grain boundaries seems to make nucleation much easier. As can be seen in Fig. 3.8, grain boundaries have a marked influence on the activity for carbon formation on nickel. Apparently this is related with an easier nucleation process, because

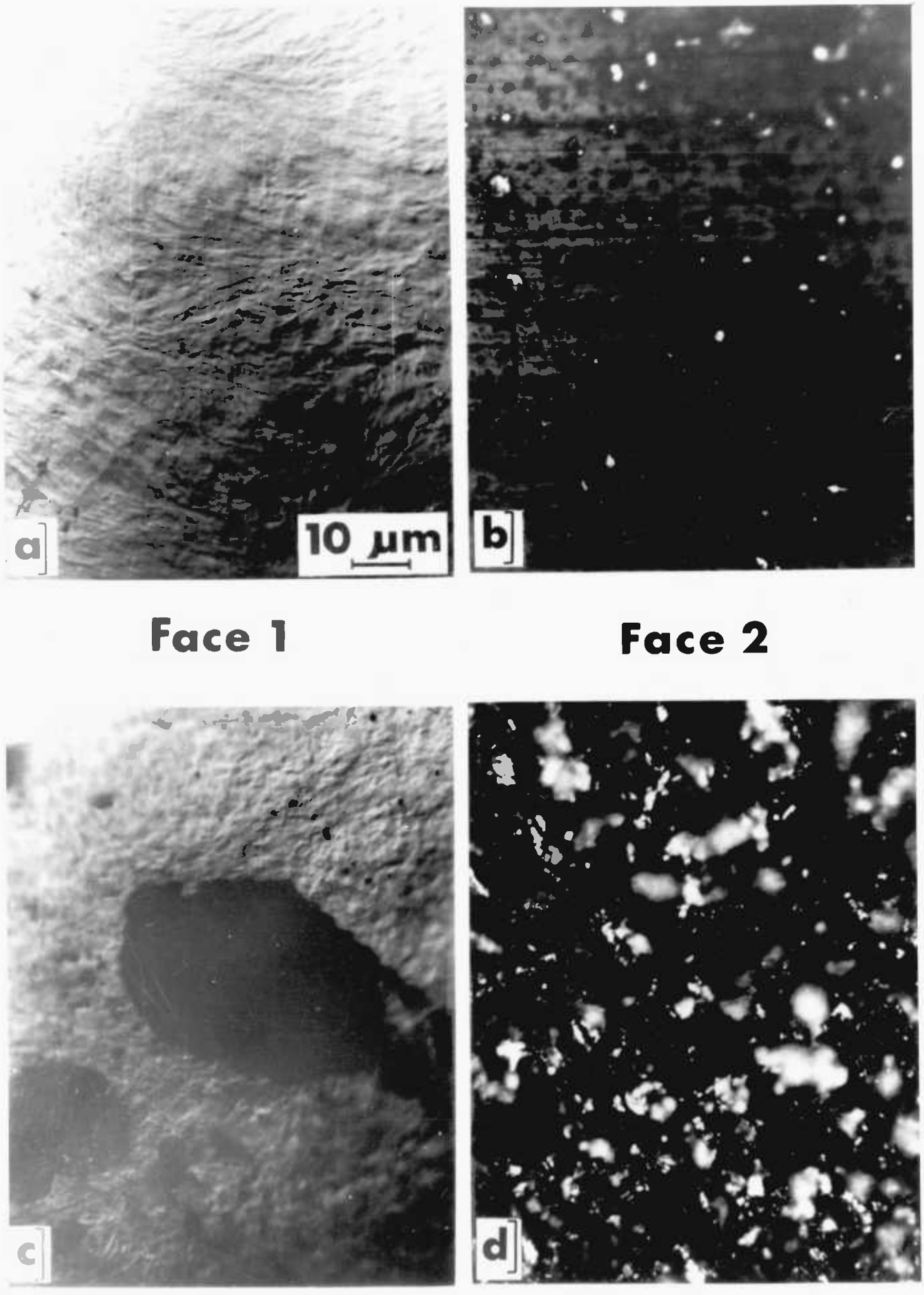

Fig. 3.18 Optical micrographs of the nickel single crystal used in Run 13.

a) and b) Uncoated and coated faces before reaction.
c) and d) Same faces after reaction.

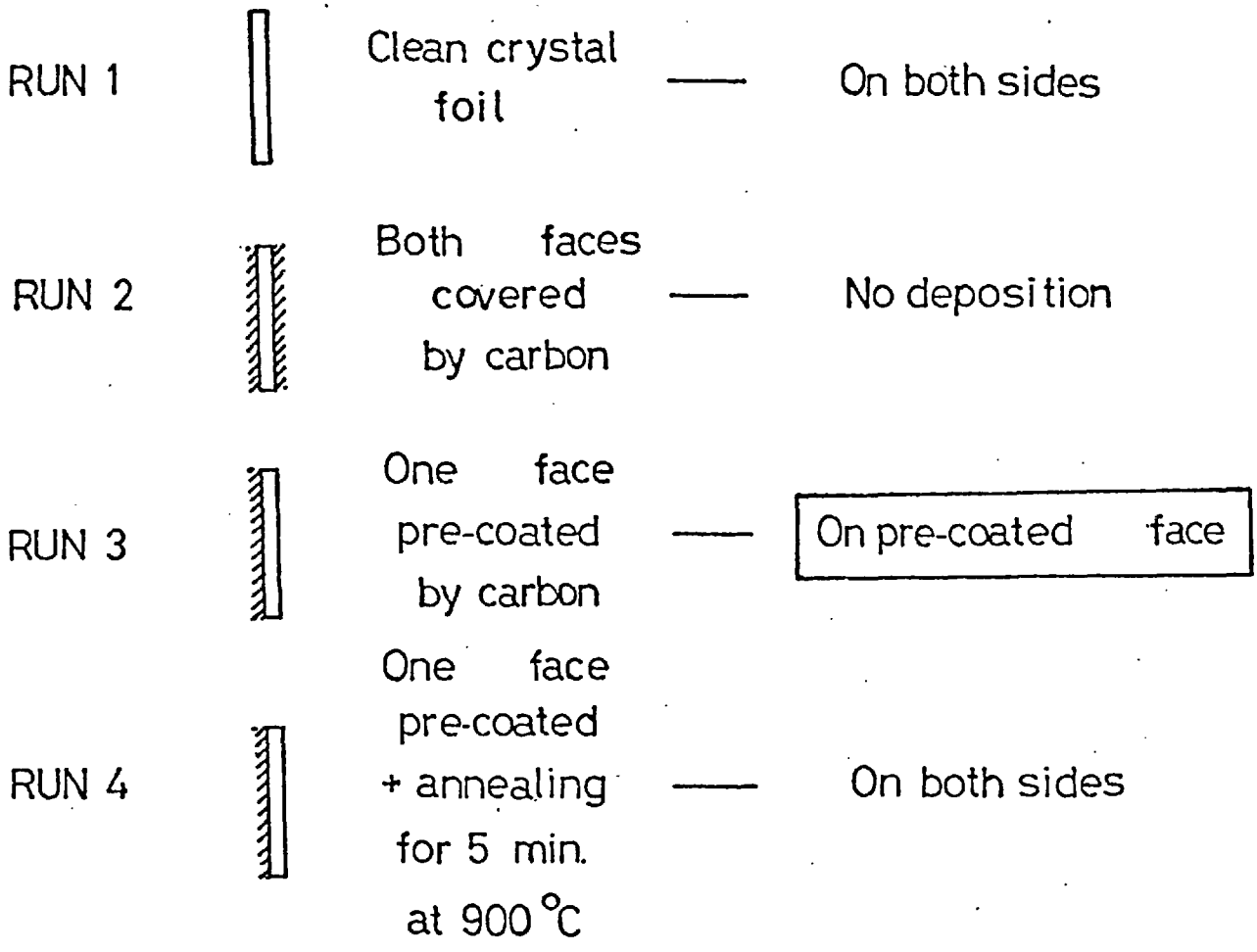

Fig. 3.19 Catalytic growth of carbon from acetylene on nickel single crystals under different precoating conditions (Deposition from 13.3 KN/m^2 acetylene at 475°C).

pre-seeding is not critical here.

3.2.1.5.4 Dissolution-reprecipitation

The films produced in Runs 16 to 19 by dissolution and reprecipitation of carbon in single crystals of nickel were examined by transmission and diffraction electron microscopy. The conditions used were described in section 2.4.4. On heating, the films behaved in a way similar to that described in (34). The amorphous carbon film, still complete at 550°C (Fig. 3.20a), dissolved into the nickel at 1000°C. On cooling, the crystal surface was rapidly covered by a thin film containing a network of lines (Fig. 3.20b).

Selected area diffraction patterns of the film formed on the (111) nickel face showed reflections corresponding to good single crystals with d_c spacings close to those of graphite (namely, corresponding to planes of the [0001] zone). These single crystals were found to be up to 10 μm wide (cf. Fig. 3.20c,d). On the (110) face, under the same conditions, the crystals were much smaller. A pattern of diffraction rings was usually observed.

3.2.2 Deposition on supported catalysts

3.2.2.1 Deposition from ethane and n-hexane

In contrast with nickel foils, carbon deposition from aliphatic hydrocarbons on supported nickel catalysts could readily be measured at temperatures of about 450°C. The catalyst, α-alumina impregnated with 18.0% (w/w) nickel, was prepared as described in section 2.6. The deposition rates, as well as the conditions used, are presented in Table 3.9.

Below 600°C carbon deposition from ethane was only significant in the presence of hydrogen. In fact, hydrogen was necessary for a steady rate to be observed at any temperature.

Fig. 3.21 shows the dependence of the steady state deposition rate on the temperature. As in the case of nickel foils, different temperature zones can be detected. The transition at circa 675°C, between the second and third zones, is not well defined but could be related to the onset of the homogeneous reaction. In fact, a gas-chromatographic analysis of the outlet gases at 650°C showed that the ethane conversion was minimal at this temperature. When the temperature was raised to 700°C, the gas phase conversion increased to about 6%. This is probably

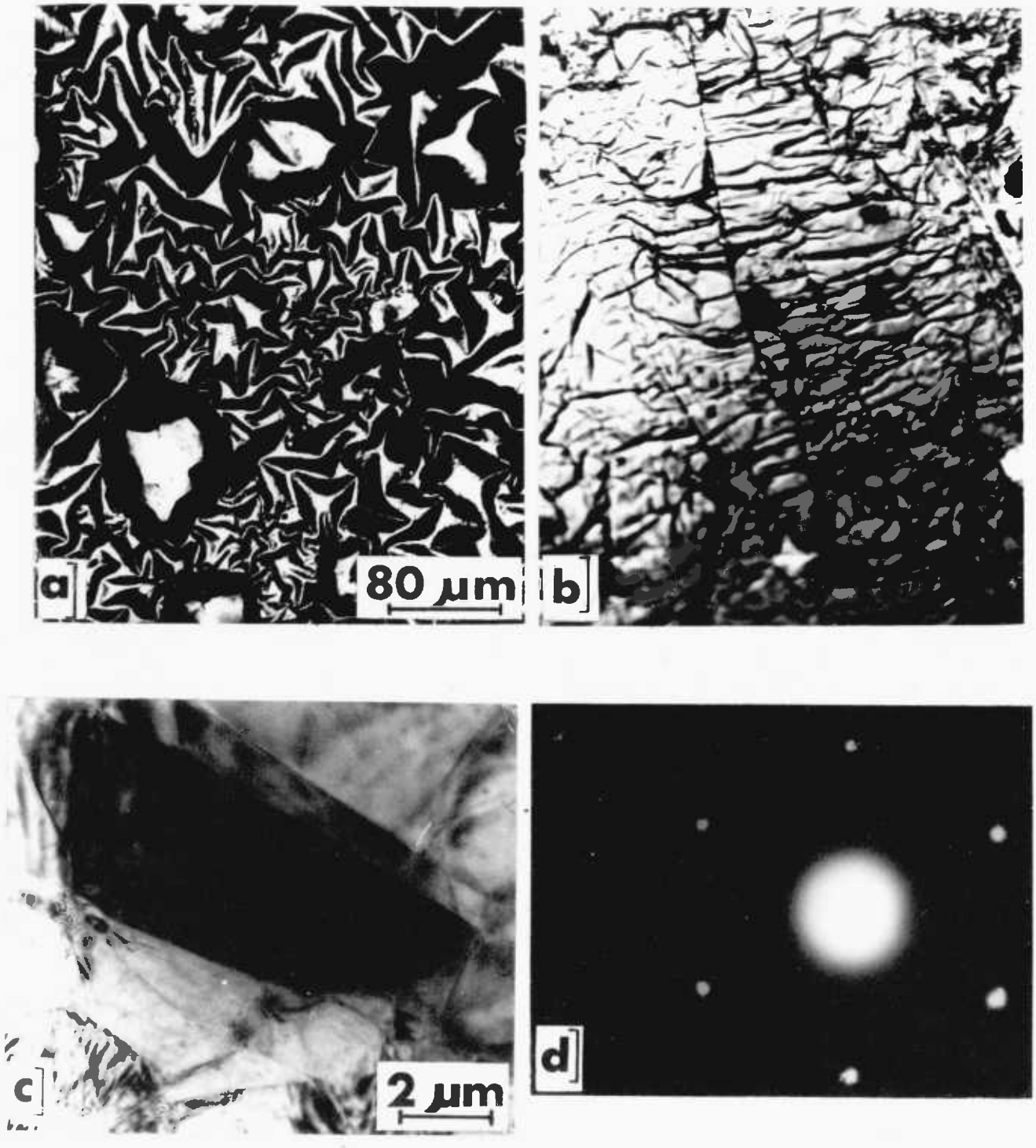

Fig. 3.20 Dissolution-reprecipitation of a carbon film in/from a(111) nickel single crystal (Run 16).

a) and b) Optical micrographs of the film before dissolution and after reprecipitation.

c) and d) Transmission electron micrograph and selected area diffraction pattern of the film after reprecipitation.

Table 3.9 Carbon deposition from ethane and n-hexane on supported nickel catalysts - Conditions and results.

Run	Gas	Catalyst (mg)	Partial Pressure ($KN\,m^{-2}$)		Inlet flow $-cm^3(STP)\,sec^{-1}-$	Temp (^oC)	Rate x 10^2 (mg/sec)	Type of experiment
			H_c	H_2				
16	C_2H_6	23.3	33	33	4.9	475 to 700	0.16 to 20.5	E_A
43	C_2H_6	20.6	25	25	3.3	550	0.32	
			50	25			0.68	O
			75	25			0.78	
44	C_2H_6	20.6	75	25	3.3	450 to 775	0.036 to 10.9	E_A,GLC
99	C_2H_6	23.8	75	25	3.3	475	0.18	
			50	25			0.11	
			25	25			0.050	
			25	50			0.028	O
			25	75			~0	
			25	75		550	0.35	
			25	50			0.19	
			25	25			0.045	
19	C_6H_{14}	23.6	9	50	3.9	450 to 800	0.25 to 3.60	E_A,GLC
20	C_6H_{14}	24.5	9	50	4.0	475 to 800	~0 to ~4.9	GLC
21	C_6H_{14}	NONE	9	50	4.0	600 to 800	—	GLC
67	C_6H_{14}	29.4	13	25	3.6	600	5.88	S,EPMA
76	C_6H_{14}	11.1	13	25	3.7	600	2.03	S
100	C_6H_{14}	23.8	4.5	12.5	3.4	500	0.59	
			9	12.5			1.10	
			15	12.5			1.21	
			4.5	25			0.45	
			4.5	75			0.31	O
			4.5	75		600	2.60	
			4.5	25			2.93	
			9	25			4.61	
			13	25			4.61	
101	C_6H_{14}	24.2	4.5	75	5.2	600	0.32	
					2.5		0.32	F
					1.7		0.22	

LEGEND:
- E_A - Determination of the apparent activation energy
- O - Determination of the order of the reaction
- GLC - Gas chromatographic analysis
- S - Determination of the extent of the steady state
- F - Effect of the flow rate
- EPMA - Electron Probe Microanalysis of the carbon deposits

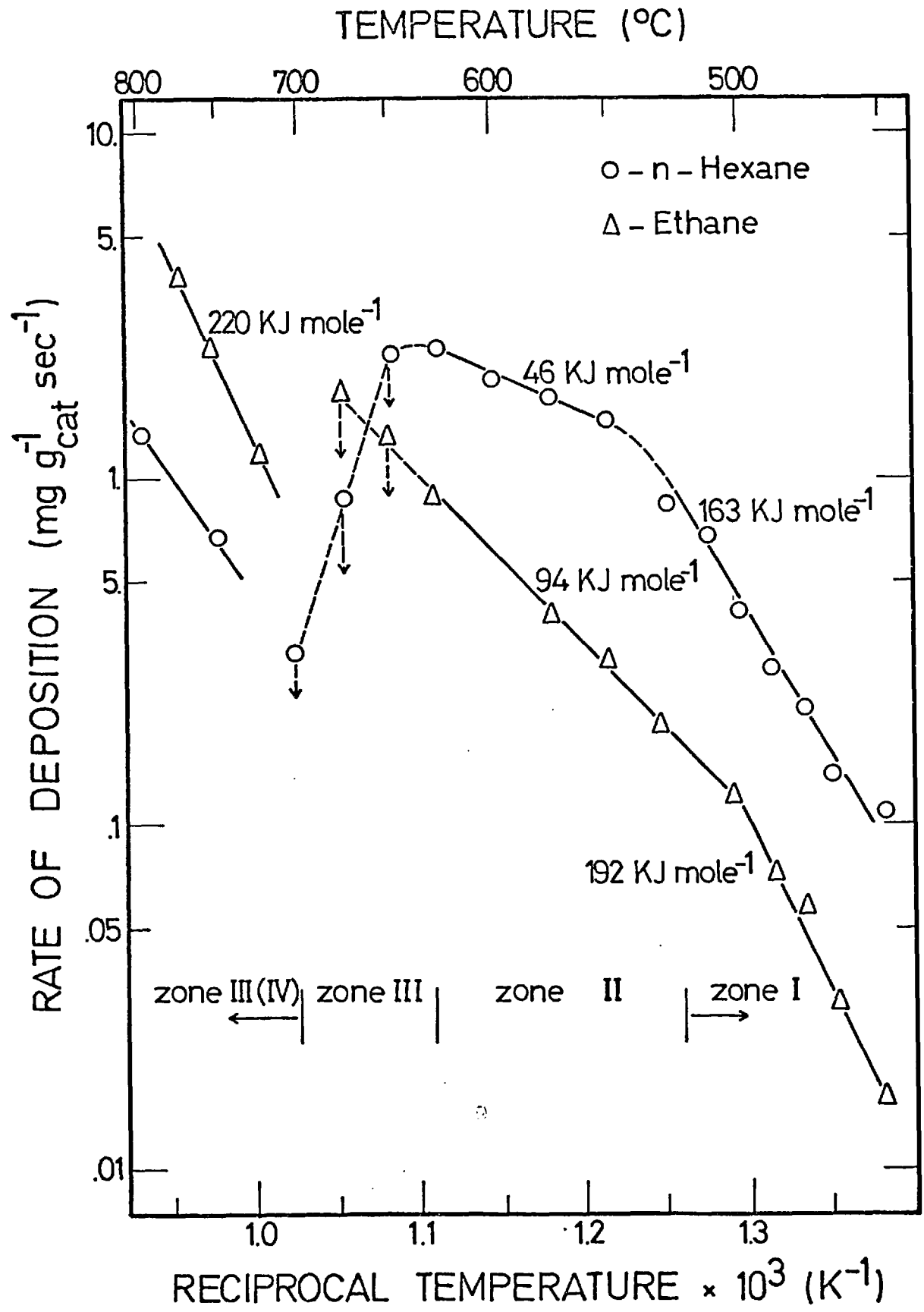

Fig. 3.21 Arrhenius-type plot of the rates of deposition of carbon from ethane and n-hexane on supported catalysts. (Feed: 3.6 cm^3 (STP) sec^{-1}; Ethane: $x_{C_2H_6} = 0.75$, $x_{H_2} = 0.25$; n-hexane: $x_{C_6H_{14}} = 0.09$, $x_{H_2} = 0.50$)

the temperature at which the homogeneous reaction starts to predominate. Above 675°C, however, the reaction rates decreased slowly with time and the temperature dependences measured are unreliable. Besides, the temperature of the catalyst surface (T_s) is also uncertain. With hexane the reaction is highly endothermic ($\Delta H_{873K} = 86.4$ K mole^{-1}). If the concentration gradient across the gas film begins to be important, the calculated value of the temperature drop indicates that T_s could be much smaller than the temperature of the bulk gas phase.

In the absence of hydrogen, the rate of deposition increased with temperature from 600 up to 700°C, but decreased with time at this temperature. When cooling down no speed-up of the reaction was observed, suggesting an irreversible deactivation at high temperatures.

All this evidence suggests a complex dependence of the rate on the pressure of both ethane and hydrogen (cf. Run 99 in Table 3.9). Between 475°C and 550°C the order with respect to hydrogen was close to - 1 up to hydrogen partial pressures of 50 KN m^{-2}. If the hydrogen pressure was increased even further, the reaction stopped. The order with respect to ethane was close to + 1 at 475°C and 550°C. At 550°C, however, the order decreased to about 0.4 when the partial pressure of ethane was increased above 50 KN m^{-2}.

Carbon formation from n-hexane is faster than that from ethane. Below 600°C no reaction was detected in the absence of hydrogen. Once hydrogen was present in the reactor the deposition could be measured at temperatures as low as 400°C. The dependence of the rate on temperature (Fig. 3.21) is similar to the case of nickel foils. The only exception is the lower value of the apparent activation energy (circa 46 KJ mole^{-1}) measured between 550 and 650°C.

The determination of the deposition rates presented in the Arrhenium-type plot was accompanied by a gas chromatographic analysis of the outlet mixture at different temperatures. The results are presented in Fig. 3.22. Above 650°C, the conversion of n-hexane in the gas phase increases with temperature. This is particularly important between 700 and 800°C. It can also be seen in the figure that the hydrocarbon conversion is practically the same, irrespective of the presence of the catalyst (Runs 20,21). This indicates that the increase in the rate of carbon deposition observed at these temperatures (see Fig. 3.21) should be related with the homogeneous reaction.

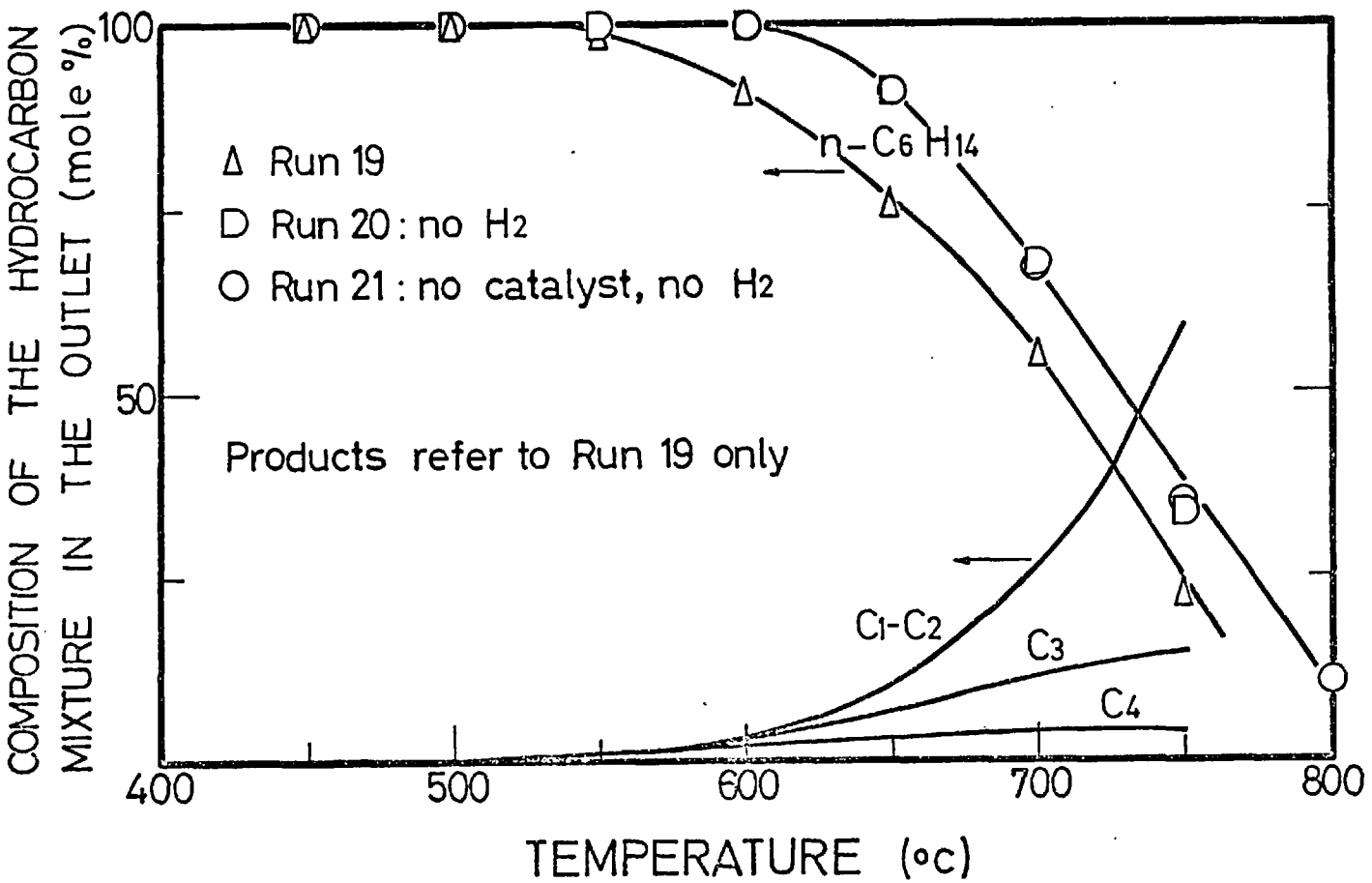

Fig. 3.22 Outlet composition vs. temperature.
(Feed: 3.9 $cm^3(STP)sec^{-1}$; $x_{C_6H_{14}} = 0.09$, $x_{H_2} = 0.50$ (Run 19))

As in the case of ethane, a complex dependence of the deposition rate on the pressure of the reactants was observed (cf. Run 100 in Table 3.9). At 500 and 600°C the order with respect to hydrogen was, respectively - 0.4 and zero. At both these temperatures, the order with respect to n-hexane was about +1 up to a partial pressure of 9 $KN\,m^{-2}$, decreasing to zero at higher pressures.

In run 101, the increase of inlet flow rate from 2.5 to 5.3 cm^3 $(STP)sec^{-1}$ (keeping the partial pressures constant: hexane - 5 $KN\,m^{-2}$, hydrogen - 75 $KN\,m^{-2}$) did not cause any apparent change in the steady state rate. When the flow rate was decreased to 1.7 $cm^3(STP)sec^{-1}$, the rate dropped slightly. The apparent activation energies and the orders of the reaction were obtained at an inlet flow of 3.3 $cm^3(STP)$ sec^{-1}. Hence, at 600°C, the results should not be significantly affected by film diffusion limitations.

3.2.2.2 The effect of hydrogen

Hydrogen plays a complex role in the process of carbon deposition from saturated hydrocarbons. Its presence is necessary for the deposition to be detected at lower temperatures (and also to prevent deactivation in most cases at higher temperatures). On the other hand, the rate of deposition decreases when the partial pressure of hydrogen is increased. In some cases (at partial pressures above 50 $KN\,m^{-2}$), this decrease is quite noticeable (cf. deposition on foils).

To investigate the hydrogen effect (namely its role in preventing deactivation), a systematic study was undertaken. The different temperature zones observed in Fig. 3.21 were studied separately. They were numbered (from lower to higher temperatures) I, II and III in the case of ethane, and I, II, III and IV in the case of n-hexane. Neither with ethane nor with n-hexane was deactivation detected in zone I. The term deactivation is used here as meaning an irreversible loss in activity, caused by the deposition of carbon. The majority of the experiments were carried out for zone II (II and III in the case of n-hexane). The reaction temperature was raised, in steps, up to 625 - 675°C and deposition rates were measured. This was followed by rapid cooling to 450 - 475°C and a second cycle of stepwise increases in temperature. The decrease in rate (expressed in % of the rate in the first cycle) at a given temperature indicates the loss of activity by deactivation.

A few experiments were made in the high temperature zone. The

temperature was again increased in steps up to 500 - 525°C and then increased rapidly, in a single step, to 775°C; the reaction was allowed to stabilise at this temperature. This was checked by determining the products distribution by gas chromatography. The temperature was rapidly dropped to 450 - 475°C and a second cycle of temperature increments performed as described above. The results for ethane are presented in Fig. 3.23. There was no deactivation in zone II. The only exception was Run 40, in which a decrease in the rate of about 20% was detected, possibly without significance. There was also no deactivation in zone III if the partial pressure of hydrogen was high. For low partial pressures, however, the reaction stops completely when cooling down.

The results for n-hexane are presented in Fig. 3.24. As with ethane, no deactivation was found in zone II, provided a minimum amount of hydrogen was present. In zone III, however, deactivation occurred in all cases, increasing with decreasing hydrogen partial pressures. When only a minute hydrogen concentration was present (below 5 $KN\,m^{-2}$), the reaction did not start again in the second cycle. In fact, the effect of very low hydrogen pressures is also felt in other ways (Run 46); (i) zone III apparently starts at much lower temperatures (525°C) and (ii) at 550°C the rate goes to zero after sometime; the reaction will not start again until the temperature is increased above 600°C. On cooling down, deactivation is complete.

In zone IV no evidence of deactivation was detected if a minimum hydrogen pressure was present. However, if the reaction was allowed to proceed at high temperatures for a long time, deactivation was observed on cooling down. At these temperatures (cf. Fig. 3.22), the gas phase conversion is important, and most of the carbon deposited should result from the homogeneous process. Apparently the deposition of this homogeneous carbon does not cause the kind of deactivation observed in zone III. Obviously this deactivation will be propagated from zone III to zone IV, if a continuous stepwise increase in temperature is made through zones I, II, III and IV.

Drastic deactivation is only observed in zone III, in which the rate of deposition decreases with temperature. Even using high partial pressures of hydrogen it is impossible to prevent deactivation completely. It is interesting to note that this behaviour was not observed with olefins and acetylene (3.2.1.3). It was decided to extend these

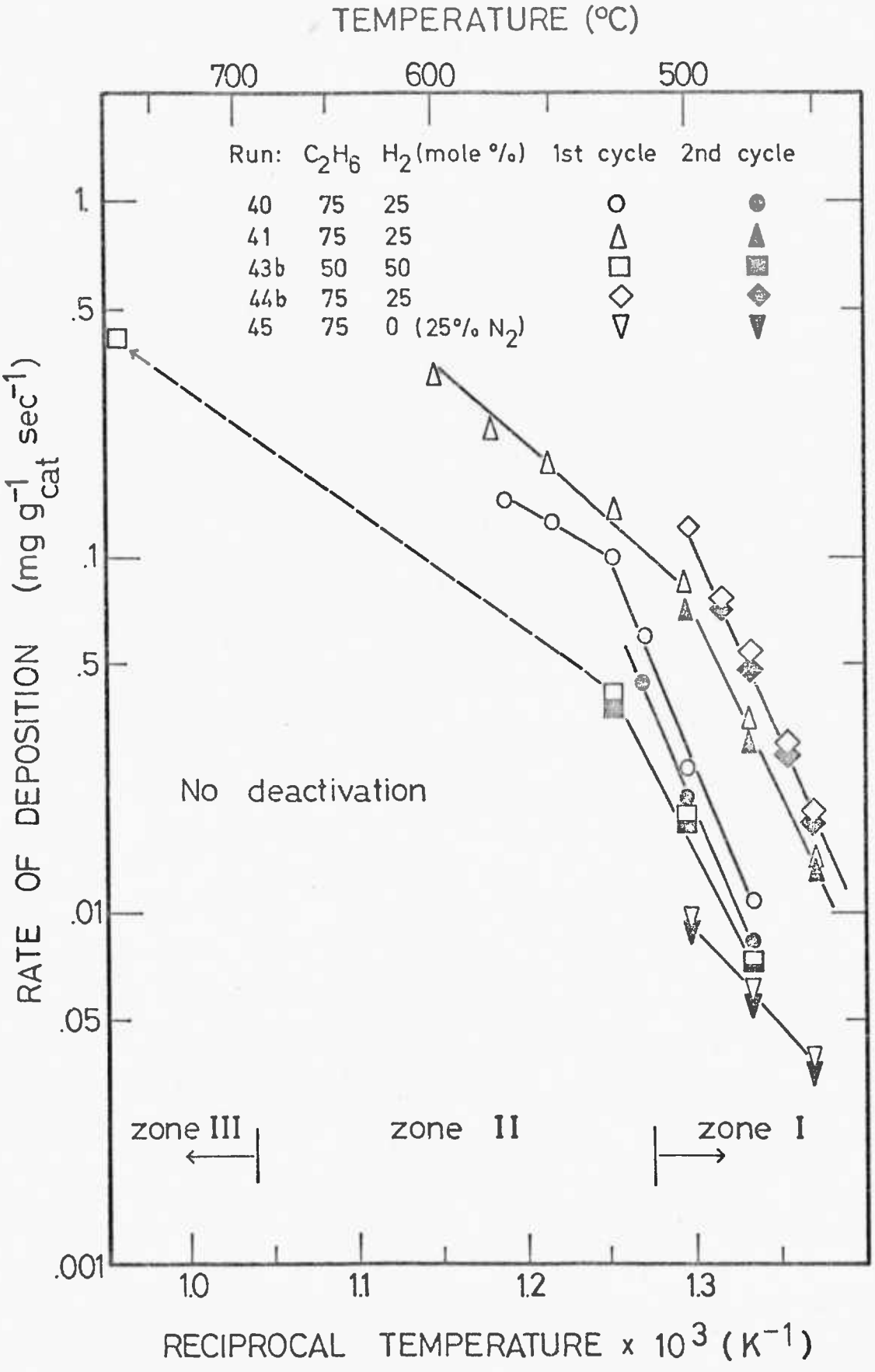

Fig. 3.23 Effect of hydrogen on the rate of carbon deposition from ethane (feed: 3.7 cm^3(STP)sec^{-1}).

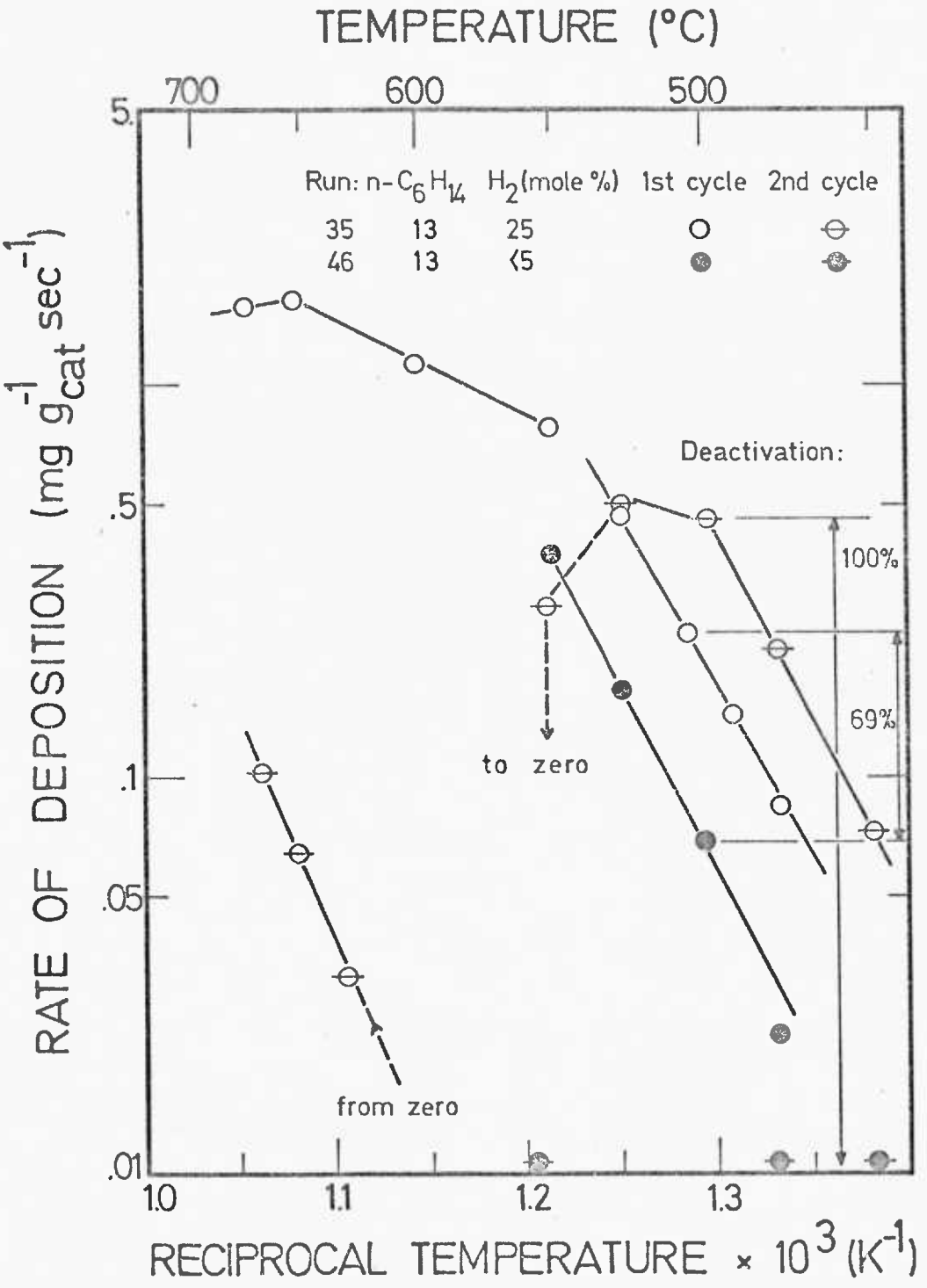

Fig. 3.24 Effect of hydrogen on the rate of carbon deposition from n-hexane (feed: 3.9 $cm^3(STP)sec^{-1}$).

studies to see if the same effect could be observed with aromatic hydrocarbons.

The overall Arrhenius-type plots for benzene and toluene are shown in Fig. 3.25. The apparent activation energy of benzene in zone I ($T < 575^{o}C$) was found to be 205 KJ $mole^{-1}$. The reaction order at $475^{o}C$ was -1 with respect to hydrogen and 0.4 with respect to benzene. In zone II, the rates were observed to decrease with time at fixed temperature and reactant partial pressure. In zone I, the apparent activation energy of toluene was 176 KJ $mole^{-1}$. At $500^{o}C$ the reaction orders with respect to hydrogen and toluene were -0.4 and 0, respectively. In contrast with previous results, with toluene the increase in rate observed above $700^{o}C$ (Zone III) was not accompanied by an increase in the gas phase conversion. In fact, this was not significant below $800^{o}C$.

Although not represented graphically, for both hydrocarbons the deactivation in zone I was minimal but was severe in zone II. For example, at $650^{o}C$ for a mixture of 25% hydrogen, 69% nitrogen and 6% benzene (V/V) a deactivation of more than 85% was measured on cooling down. The deactivation was particularly severe when the temperature was raised to $700^{o}C$.

Again, drastic deactivation seems to be associated with a negative temperature dependence of the deposition rate

3.2.2.3 Examination of the carbon deposits

The carbon deposits formed from n-hexane on supported catalysts were analysed by X-ray diffraction and EPMA.

The X-ray analysis showed that the intensity of the peak corresponding to the (0002) reflection of graphite increased from zone I to zone III. This indicates a greater degree of graphitization of the carbon produced in this zone. A similar trend was observed in deposits formed from benzene (71).

Previous EPMA examinations of fresh catalyst had shown that the metal (only metallic nickel was detected) was mostly concentrated on the outside layer of the alumina particles, but was still present near the centre.

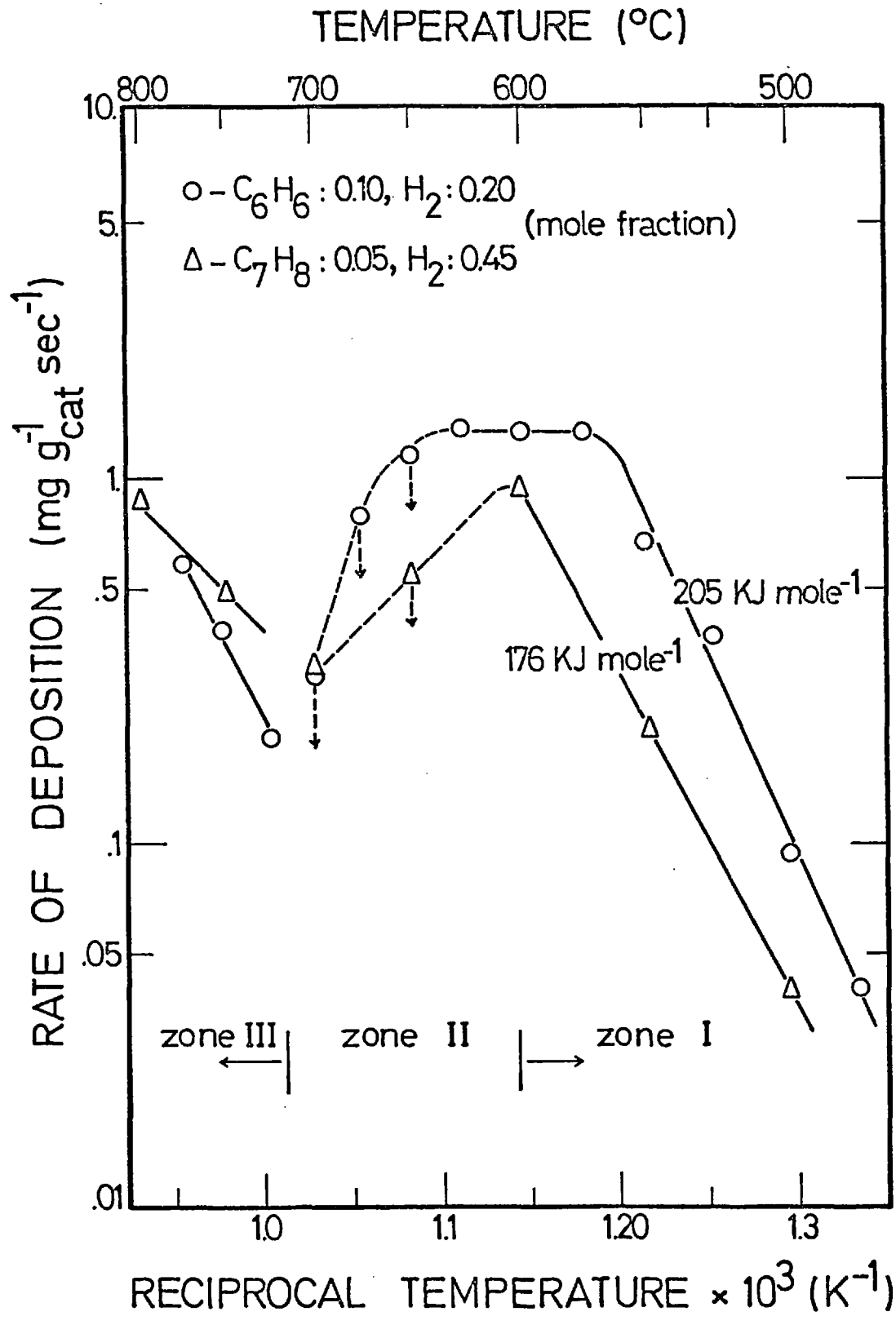

Fig. 3.25 Arrhenius-type plot of the rates of carbon deposition from benzene and toluene (Feed: 3.5 cm^3(STP)sec^{-1}).

After deposition, the EPMA of the carbon deposits showed the presence of alumina in patchy areas, well spaced and about 20 - 30 μm across. As they originally averaged 300 μm in diameter, most of the alumina particles were broken in the process of carbon formation. Nickel was found to be dispersed all over the deposit, bearing no apparent relationship with the original alumina particles (see Fig. 3.26 a,b). This fact may explain the activity observed when using carbon from previous experiments in a new deposition without catalyst.

3.2.2.4 Carbon deposition in the presence of steam

The formation of carbon during the steam reforming of n-hexane was studied using commercial and laboratory prepared catalysts. The reaction was carried out at atmospheric pressure and temperatures between 425 - 650°C in the system described in section 2.5. The British-Gas CRG catalyst (cf. section 2.6) was used initially. Before the reaction, the catalyst was hung in the microbalance and reduced in a steam of hydrogen at 500°C, until no loss in weight could be detected.

Some experiments were done to define the condition under which an appreciable rate of carbon formation would be observed:

(i) The steam to carbon ratio - moles of water per atom of carbon - in the feed was varied from 1.34 to 0.48 at 450 and 500°C (corresponding molar flows: steam, 5.8×10^{-5} moles sec^{-1}; hexane varying from 7.2×10^{-6} to 2.0×10^{-5}moles sec^{-1}). No deposition was detected even for values smaller than the thermodynamic minimum steam ratio (1) (below which carbon will be formed if the carbon forming reactions reach thermodynamic equilibrium).

(ii) p-Xylene was added to the feed in increasing concentrations (up to .35 moles per mole of hexane). It was thought that the addition of xylene would increase carbon deposition on the catalyst via: $p\text{-}C_8H_{10}$ → polymer → carbon. The "polymeric" route has been advanced before (105) to explain the deactivation of CRG catalyst between 400 - 500°C. At 450°C and with a steam to carbon ratio of about 0.8, an average deposition of 4.10^{-2} μg sec^{-1} was detected. The more sensitive ranges of the microbalance had to be used to detect such small depositions. Hence, the measurements were strongly affected by noise (and fluctuations caused by the flow of the gases) and could not offer the basis of a reliable kinetic study.

Normal catalyst loads varied between 190 and 200 mg. Increasing the catalyst load did not produce a marked increase in the deposition and was, anyway, limited by the capacity of the microbalance.

The reason why only minimal carbon deposition was detected with this catalyst is not clear. It may be related with the potassium present in the catalyst (see section 2.6), which is believed to promote the gasification of carbonaceous deposits by steam (101). However, it is known that carbon or high molecular weight hydrocarbons are deposited on this catalyst in industrial conditions (100). This indicates that the conclusions obtained from studies with microbalances at atmospheric pressure, are not applicable to fixed bed reactors working at 15 atmospheres and above.

The reaction was also studied using the unpromoted nickel/alumina catalyst prepared by the impregnation method described in section 2.6. After an induction period, whose duration decreased with increasing temperature, the deposition started and a steady state was rapidly attained. The presence of hydrogen was found to be necessary to maintain this steady state. The results obtained using an inlet flow of n-hexane of 7.1×10^{-6} moles sec^{-1} and a steam to carbon ratio of 1.4 are presented in Fig. 3.27. For comparison, the results obtained, under the same conditions, with the CRG catalyst are also included in the figure. The decrease in weight sometimes observed with this catalyst is probably due to further reduction under reaction conditions. A similar behaviour has been reported for a nickel-γ alumina coprecipitated catalyst (113). This was explained by the formation of a nickel aluminate phase (whose reduction is less energetically feasible than that of the nickel oxide) that could be reduced by some of the products of the reaction.

Preliminary experiments were carried out to establish the influence of the metal concentration and the catalyst particle size on the steady state deposition rate. The results presented in Table 3.10 show that the rate increasedif the nickel concentration increased and did not depend on the particle size. The differences observed were well within the irreproducibility of the measurements (standard deviation of the rate in 4 experiments, in the same conditions, was 19%). As catalysts with smaller particle size were likely to be less affected by diffusion limitations, catalyst 3 was selected for the remaining experiments.

The deposition rates were not significantly affected by the inlet flow rates as can be seen in Table 3.11. Hence, at this temperature, no film-diffusion limitations were likely to affect the rates in the

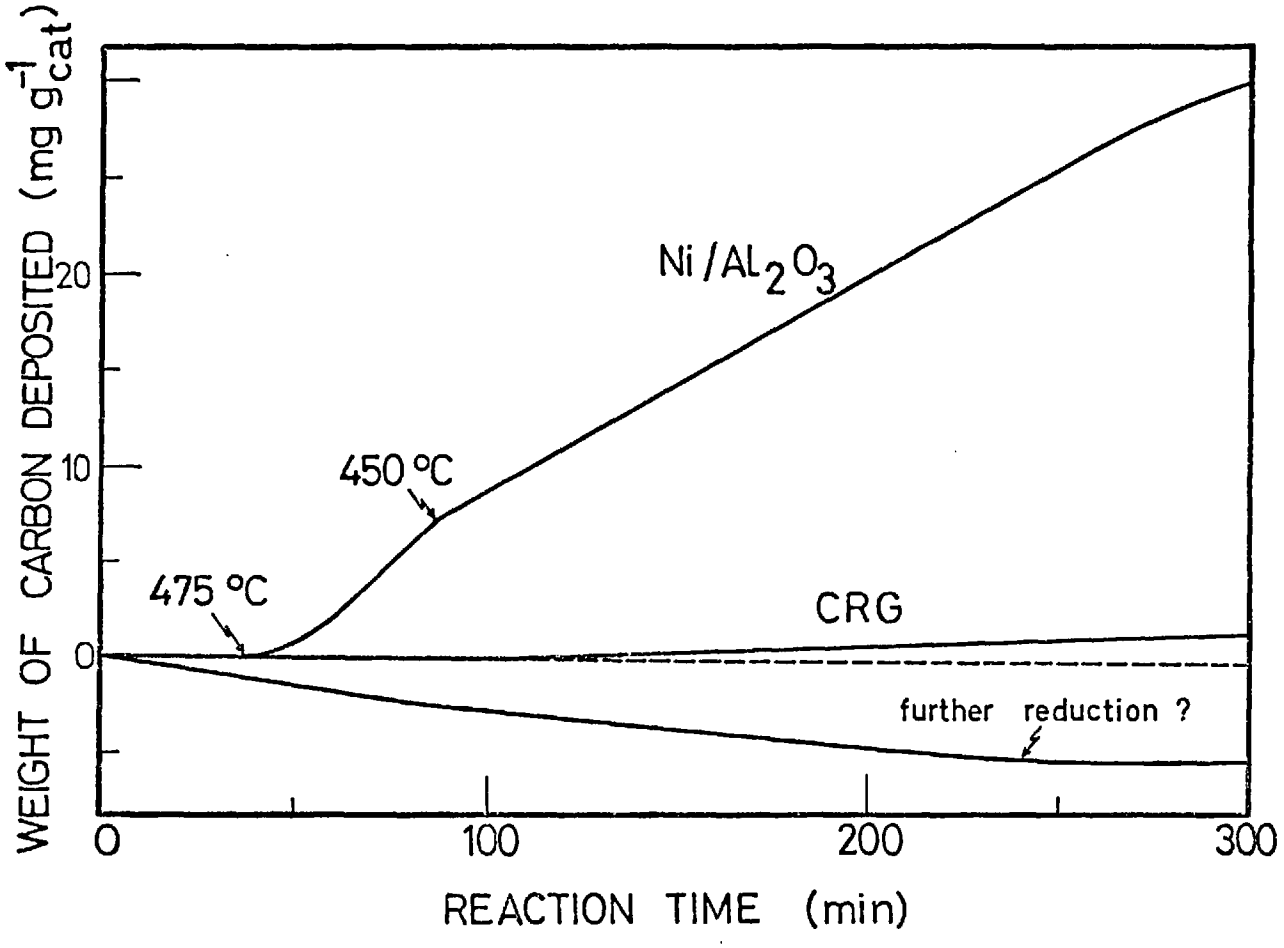

Fig. 3.27 Deposition of carbon from n-hexane in the presence of steam on supported nickel catalysts.
(100 mg of catalyst; H_2O/C: 1.4; n-hexane inlet flow: 7.1×10^{-6} moles sec^{-1}).

Table 3.10 Carbon deposition for different supported nickel catalysts at 450°C (Feed: total molar flow - 2.27×10^{-4} moles sec^{-1}; partial pressures (K N m^{-2}): H_2O - 25, C_6H_{14} - 3.1, H_2 - 15; steam/C = 1.3).

Catalyst	Average particle size (mm)	Weight % Ni*	Steady-state rate (μg sec^{-1} $gcat^{-1}$)
1	0.702	11	1.4
2	0.702	18	2.1
3	0.316	18	1.9

* Reduced state

Table 3.11 Effect of the inlet flow rate in the deposition of carbon on supported nickel catalysts at 450°C (Feed conditions, other than inlet molar flow, as in Table 3.10).

Inlet flow rates $\times 10^4$ (moles sec^{-1})	Catalyst load (mg)	Steady-state rate (μg sec^{-1} $gcat^{-1}$)
1.62	110	1.65
2.84	190	2.02
5.41	365	2.02

Table 3.12 Dependence of the deposition rate on the partial pressure of n-hexane and steam at 450 and 625°C (total molar flow: 2.32×10^{-4} moles sec^{-1}; H_2 partial pressure: 15 K N m^{-2}).

Flow $\times 10^6$ (moles sec^{-1})		Rate of deposition (μg $sec^{-1} gcat^{-1}$)	
n-hexane	steam	450°C	625°C
7.2	58	1.56	9.10
15	58	2.10	19.2
15	92	2.02	13.3

usual experimental conditions (catalyst - 100 mg, flow 2.3×10^{-4} moles sec^{-1}). The temperature dependence of the deposition rate is presented, in Fig. 3.28. Below 550°C an apparent activation energy of 119 ± 17 KJ $mole^{-1}$ was determined. Above 550°C the rate decreased as the temperature increased. A similar effect was observed before for the steam reforming of propylene (7).

Gas chromatographic analyses of the effluent gases have shown that the major products of the reaction were hydrogen, carbon dioxide and methane (only traces of carbon monoxide were detected). Typical values of the products distribution were (mole %) : Hydrogen - 71, carbon dioxide - 27, methane - 2. The attempts to determine the orders of the reaction with respect to the hydrocarbon and steam were limited by the difficulty in changing the partial pressure and keeping the steam to carbon ratio above the thermodynamic minimum. The results presented in Table 3.12 show that, at 450°C, the rate increased with the partial pressure of the hydrocarbon ($n \simeq 0.5$) and was almost independent of the partial pressure of steam. The fact that the gasification of carbon by steam is enhanced as the temperature increases (see section 3.33), may explain the negative orders ($n \simeq -0.8$) observed at 625°C. At this temperature the order with respect to the hydrocarbon was close to one. Experiments were made to check the existence of polynuclear aromatics in the deposits formed at low temperatures (105). Chloroform extracts obtained from the used CRG and the used impregnated catalyst were analysed by gas-liquid chromatography. The catalysts were also sent to be analysed in a VARIAN 311A mass spectrometer at the London Research Station of the British Gas Corporation.

The chromatographic analysis of the catalysts used in experiments with a normal hexane feed proved inconclusive. The analysis of the extracts from the CRG catalyst, used in the experiment where p-xylene was added to the feed, showed the presence of aromatic hydrocarbons with one to three rings and possibly with alkyl side chains.

The mass spectrometer analysis proved more conclusive, as can be observed in the electron impact and field ionisation spectra shown in Fig. 3.29(a) and (b). From the m/e values observed it can be concluded that paraffins, cycloparaffins, alkylbenzenes and traces of aromatics are present in the extracts (3.29(a)). Higher hydrocarbon, with carbon numbers ranging from 9-14 to 19-30, were also detected (3.29(b)). As the number of rings increases, the material becomes, for all practical

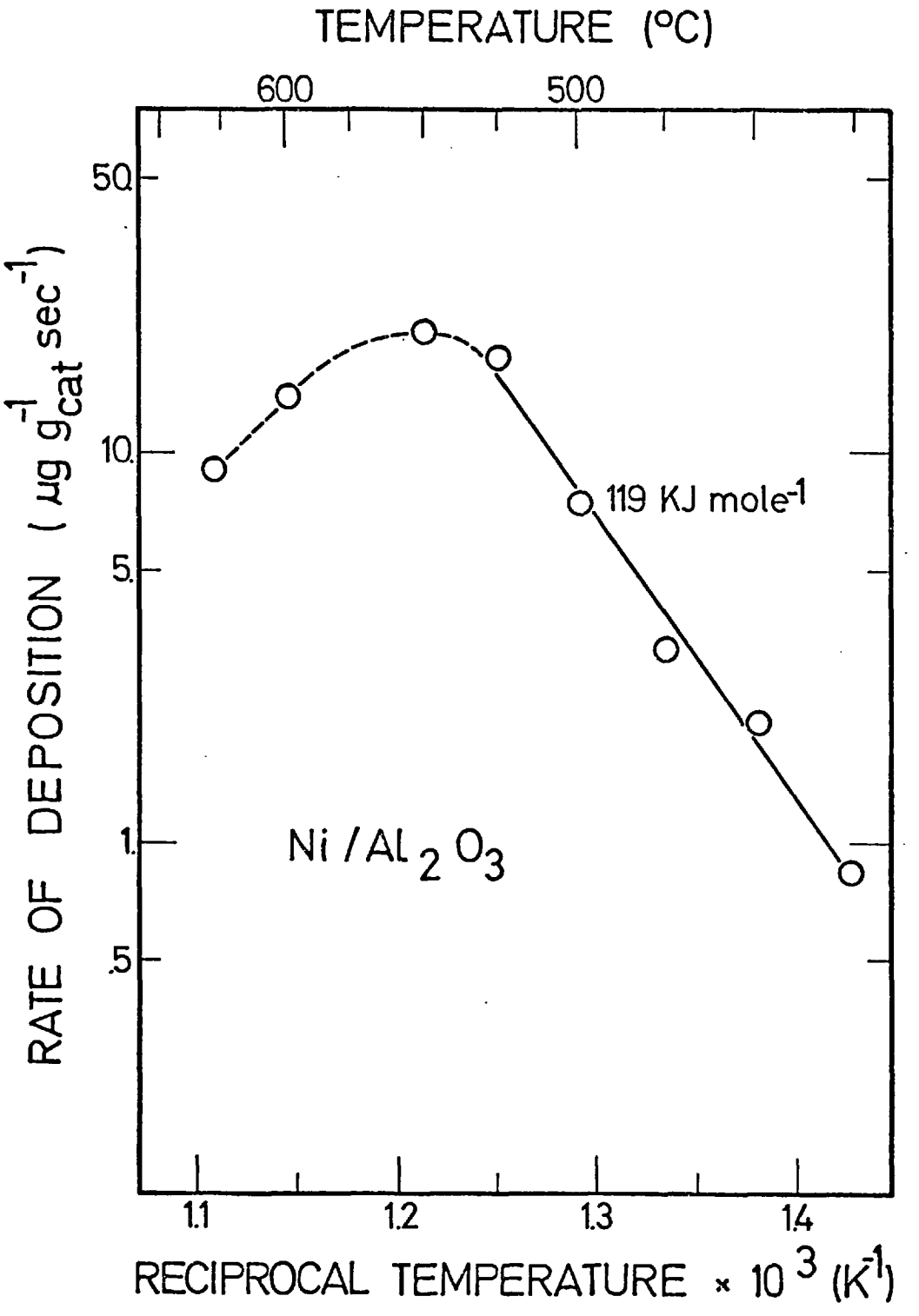

Fig. 3.28 Arrhenius-type plot for the deposition from n-hexane in the presence of steam on supported catalysts.

(Feed: H_2O/C = 1.4, n-hexane inlet flow: 7.1×10^{-6} moles sec^{-1})

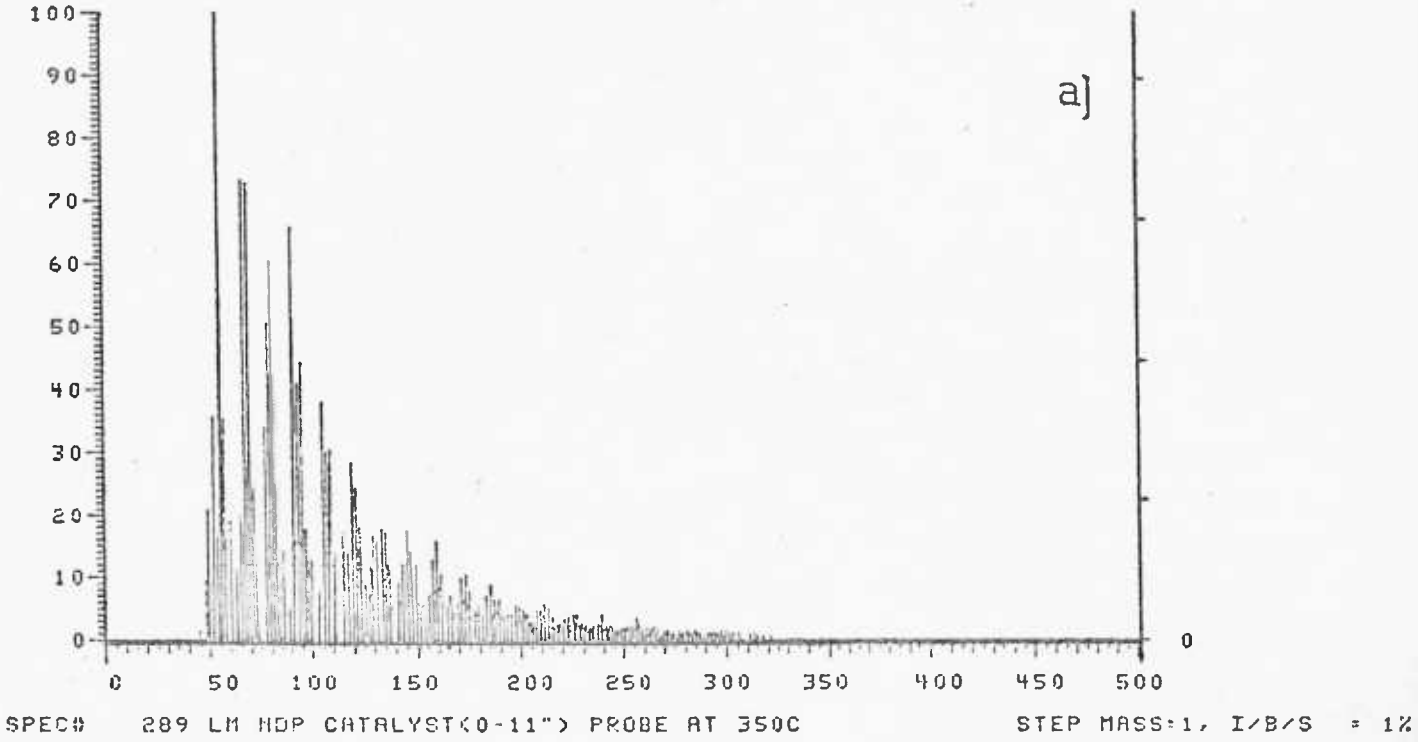

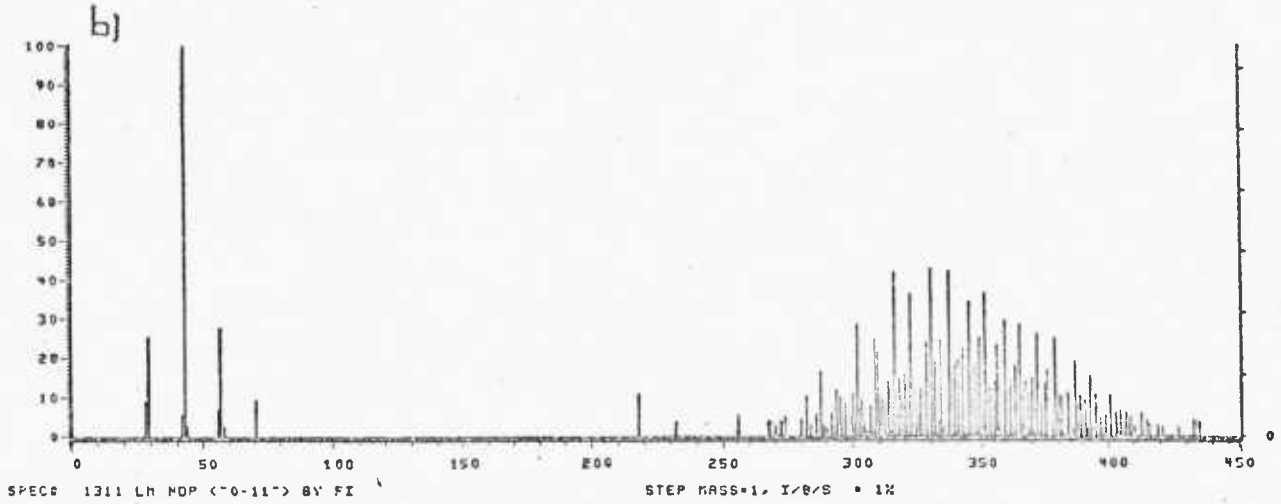

Fig. 3.29 Mass spectrometer analysis of the extracts of deposited catalysts.
(a) Electron impact (b) Field ionisation

purposes, nearly identical to carbon. This analysis proves that a large variety of hydrocarbons are formed in the CRG catalyst at low temperatures.

The fact that the deposition of these substances was not detected by the microbalance is certainly due to the small amounts deposited. The use of an high pressure microbalance system,with higher capacity, may prove to be successful to study the deposition in CRG-type catalysts.

3.3 GASIFICATION OF CARBON DEPOSITS

Carbon deposits formed from n-hexane on foils and supported nickel catalysts were gasified by carbon dioxide, hydrogen and steam. In most cases it was possible to define a range of burn-off (usually 15 to 65% of the initial deposit) where the rate of gasification was constant. Such "steady state" rates were usually reproducible and could be used to determine kinetic parameters. The results of these gasification studies are presented in the next three sections.

3.3.1 Carbon gasification by carbon dioxide

3.3.1.1 Gasification from nickel foils

The gasification by carbon dioxide of carbon deposits formed on nickel foils was studied at temperatures between 475 and 775°C. Pure carbon dioxide or mixtures of nitrogen and carbon dioxide were used.

The carbon deposits were obtained at 600°C, from a mixture of n-hexane (13.5%), hydrogen (25%) and nitrogen (61.5%) - molar % - at a flow rate of 3.3 $cm^3(STP)sec^{-1}$. The gasification rates measured, as well as the conditions in which they were obtained, are presented in Table 3.13.

The rates were minimal below 475°C and increased with increasing temperature thereafter. In most of the cases, the gasification runs were characterised by a small induction period (temperature dependent), followed by a period of constant rate that lasted between 15 and 75% of burn off. From that point onwards it gradually dropped to zero. Thus, for most of the gasification, the rate could be considered as being of zero order with respect to the amount of carbon present in the system. For different runs, however, the rates were roughly proportional to the initial amount of carbon deposit up to a given value and nearly independent thereafter.

Table 3.13 Carbon dioxide gasification of carbon deposits formed on nickel foils - conditions and results.

Run	Foil area (cm^2)	Initial carbon deposit (mg)	Flow rate ($cm^3(STP)sec^{-1}$)		Temp (^oC)	Rate x 10^2* (mg/sec)	Type of experiment
			CO_2	N_2			
56	2.70	58	3.3	-	775 to 725	5.39 to 3.93	E_A
57	2.70	49	3.3	-	700 to 625	2.11 to .792	E_A
59	2.69	110	3.3	-	775 to 475	6.33 to 0.018	E_A
61	2.73	125	0.77	-	675	2.04	
			1.7			2.38	F
			3.3			2.42	
62	2.60	30	3.2	-	625 to 475	0.903 to 7.6×10^{-3}	E_A
63	2.82	31	0.77		575	0.238	
			1.6			0.254	
			2.4			0.276	F
			3.3			0.282	
			2.5	0.76	575	0.262	
			1.7	1.7		0.211	O
			0.77	2.5		0.133	
63-b	2.82	55	3.3	-	775	4.02	
			2.5			3.91	F
			1.7			2.62	
			0.79			2.76	
64	2.85	22	3.3	-	625	0.682	C
65	2.85	42	3.3	-	625	1.08	C
66	2.85	78	3.3	-	625	1.60	C
67	2.85	105	3.3	-	625	1.61	C
77	6.06	65	3.3	-	625	1.58	A
77-b	6.06	70	3.3	-	725	6.15	
			1.7	1.7		3.29	O
			0.83	2.5		1.67	
77-d	6.06	102	3.3	-	625	2.33	C,A
78	2.77	52	3.3	-	625	0.155	C
79	2.77	109	1.7	1.7	700 to 550	1.54 to 5.7×10^{-2}	E_A

* Rates tabled refer to gasification in steady state conditions

LEGEND: E_A - Determination of the apparent activation energy

O - Determination of the order with respect to carbon dioxide

F - Effect of the flow rate

C - Effect of the initial amount of carbon

A - Effect of the area of the foil

Similarly to the results reported by Walker (76), no deactivation was noticed for intermediate values of burn-off. Also, a treatment in hydrogen after interrupting the carbon dioxide gasification (at 650°C), did not cause any significant effect on the rates observed when the gasification was resumed. This result differs from that reported in a recent publication (91). The dependence of the steady state rates of gasification on the initial amount of the deposit is presented in Fig. 3.30. It can be seen in the figure that above 50 mg of deposit, the rates are nearly independent of the initial amount of carbon. This raises the problem of comparing rates obtained in different experiments, with different initial amounts of carbon. One way around this problem would be to use always the same initial amount of carbon. This procedure, however, would limit the range of deposits that could be gasified.

It was decided to normalise the rate by dividing by w, such as:

$w = w_c$; if the weight of carbon deposited (w_c) is < 50 mg
$w = 50$ mg; if the weight of carbon deposited is $\geq$ 50 mg

The Arrhenius-type plot of the gasification rates normalised in this way is presented in Fig. 3.31. Two distinct regions can be seen in the figure. In both of them the observed rates were reproducible, as detected by changing the temperature in discrete steps upwards and downwards. At low temperature (below 650°C) the apparent activation energy is 163 ± 13 KJ $mole^{-1}$ and above 650°C, 71 ± 9 KJ $mole^{-1}$. These values agree reasonably well with values reported in the literature for the gasification of porous carbon doped with nickel (91). It can be seen in Fig. 3.31 that when the partial pressure of carbon dioxide was halved (Run 79) there was a significant decrease in the rate of gasification. No evidence of a zero order reaction with respect to carbon dioxide was found throughout the entire temperature range. It is also evident from the figure that the reproducibility of the rates was poor at high temperatures.

Fig. 3.32 shows the dependence of the gasification rate on carbon dioxide pressure. This dependence was examined by mixing carbon dioxide with oxygen free nitrogen (and occasionally argon) and keeping the total pressure at one atmosphere. There was no effect in the rates when argon replaced nitrogen as a diluent, keeping the carbon dioxide partial pressure constant.

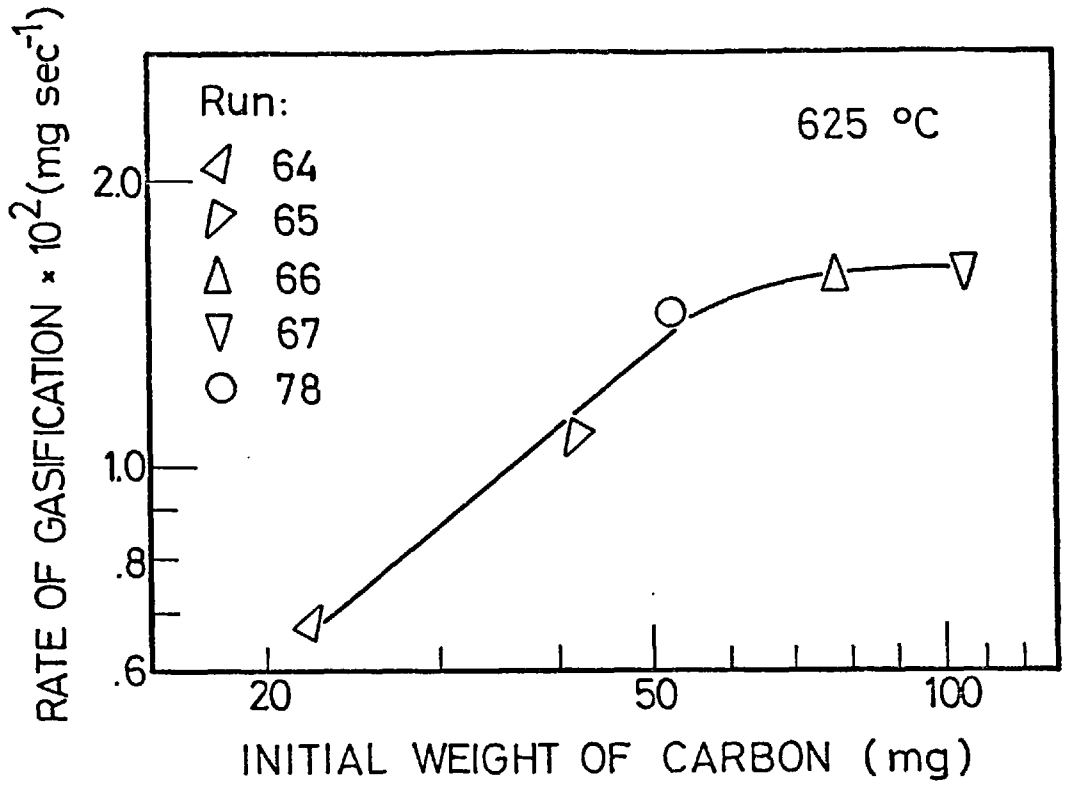

Fig. 3.30 Dependence of the steady-state gasification rate on the initial weight of the carbon deposit.

(Carbon dioxide flow rate: 3.3 $cm^3(STP)sec^{-1}$)

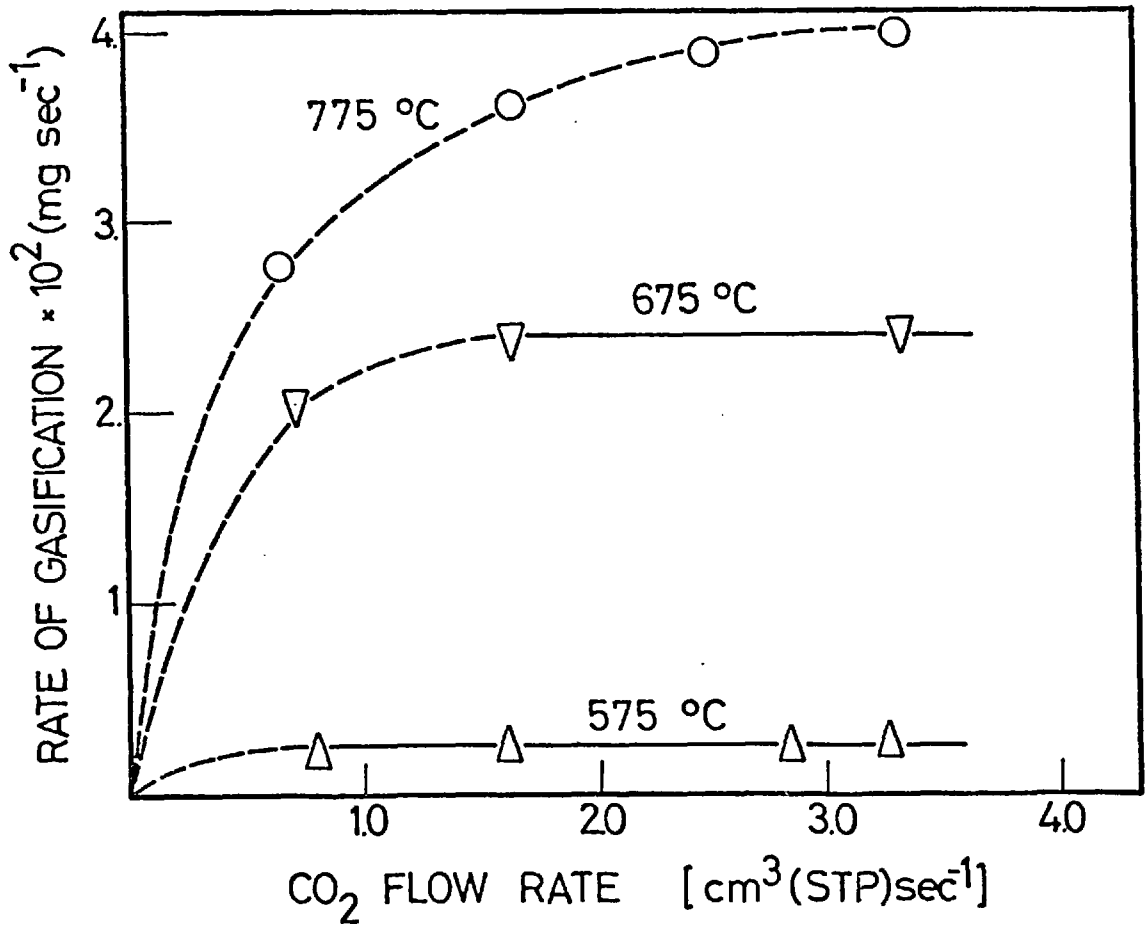

Fig. 3.33 Effect of carbon dioxide flow rate on the rate of gasification at different temperatures.

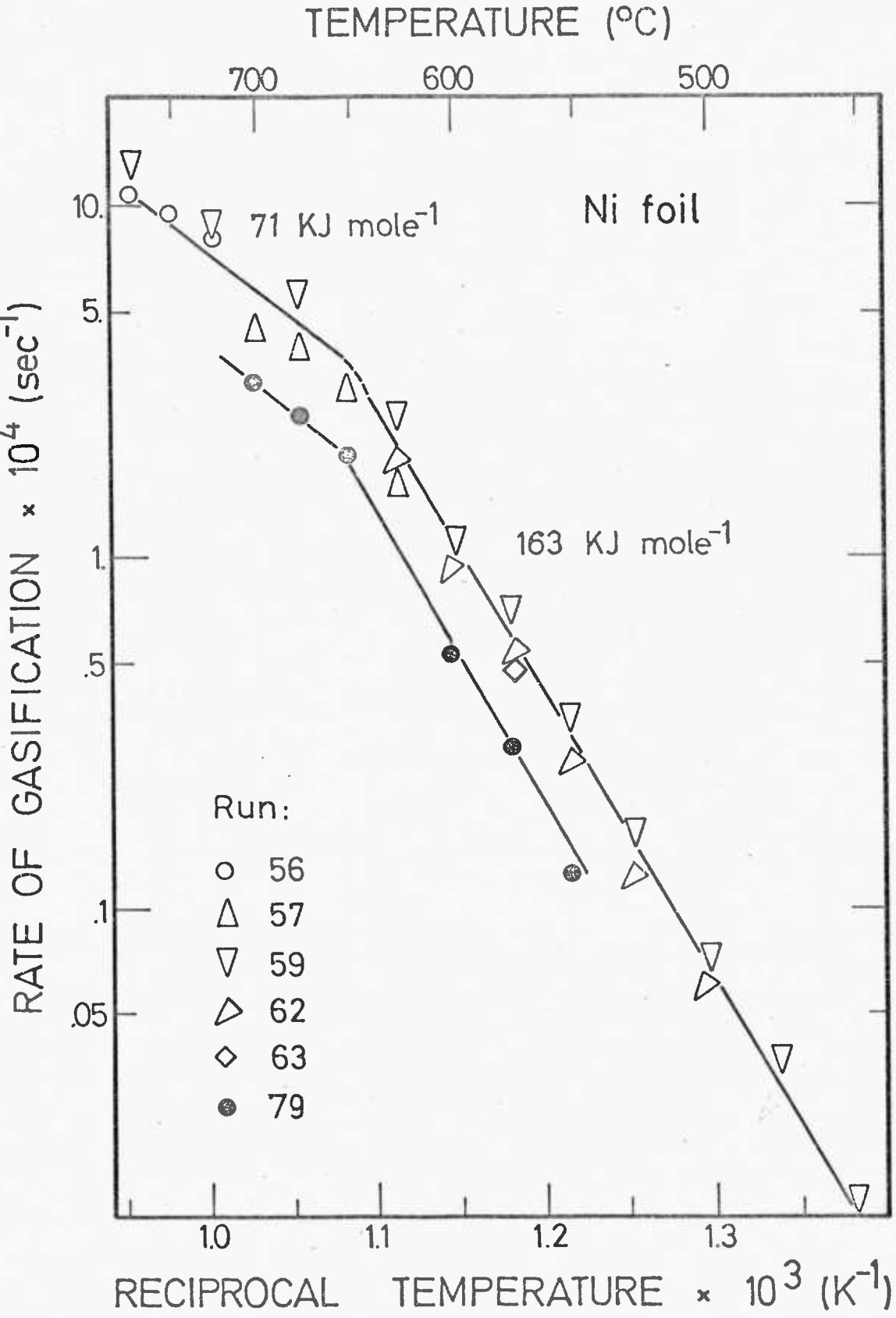

Fig. 3.31 Arrhenius-type plot of the gasification rates at a constant CO_2 flow rate (3.3 cm^3(STP)sec^{-1}) and atmospheric pressure

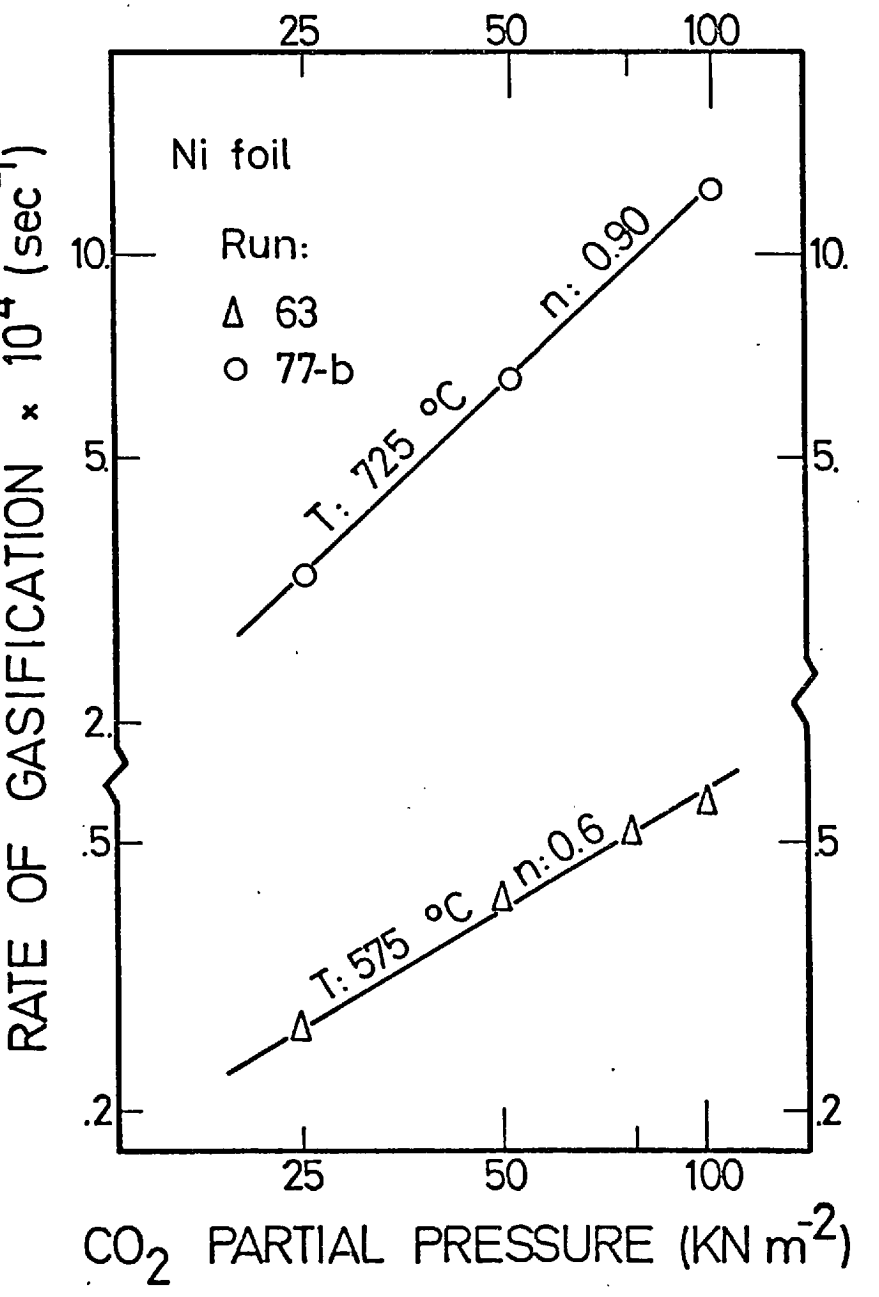

Fig. 3.32 Dependence of the gasification rate on carbon dioxide partial pressure at different temperatures.

The order with respect to carbon dioxide at temperatures below 675°C is somewhat complex (see also the results for supported catalysts), but it is evidently a fractional number. The order increases to values close to one at temperatures of 725°C and above.

The effect of the flow rate is shown in Fig. 3.33. Increasing carbon dioxide flow rate resulted in the increase of the gasification rate. Above a given value of flow rate, however, the gasification rates levelled off. This value increased with temperature andwas circa 3.3 $cm^3(STP)sec^{-1}$ at 675°C. Considering the geometrical arrangement of the reactor, this corresponds to a linear velocity at the point of contact with the sample of about 6.1 cm sec^{-1} (at the reaction temperature). The figure shows that the gasification rate increased with increasing flow rates over the entire temperature range, but there was a tendency to level off at higher flow rates as the temperature increased.

Gas chromatographic analysis of the effluent gases showed that the only detectable product of the reaction was carbon monoxide. In Run 58, at 625°C and with a flow of pure carbon dioxide of 3.3 $cm^3(STP)sec^{-1}$, the carbon monoxide concentration corresponded to circa 9% of the value calculated on the assumptions that the whole gas phase was in equilibrium with the solid carbon and that carbon was in the form of graphite. Carbon monoxide concentrations become closer to the equilibrium values when the temperature was increased and the flow rates decreased. Some experiments were made to obtain an idea of the effect of the area of the nickel foil on the steady gasification rate. As can be seen in Table 3.13 (Runs 77, 66 and 67), there was no significant difference in the rate (for the same temperature and carbon dioxide flow rate) when the area of the nickel foil was doubled. However, comparing run 77 with run 77-d it can be seen that the gasification rate depended on the initial carbon deposit up to 100 mg, contrary to what happened in the case of the experiments represented in Fig. 3.30.

3.3.1.2 Gasification from supported nickel catalysts

3.3.1.2.1 General

Gasification by carbon dioxide of carbon deposits formed on supported nickel catalysts was studied at atmospheric pressure and temperatures between 500 and 850°C. The carbon was deposited in the same conditions described in section 3.3.1.1. Pure carbon dioxide or mixures of carbon dioxide and nitrogen or carbon dioxide and carbon monoxide were used.

Table 3.14 Carbon dioxide gasification of carbon deposits formed on supported nickel catalysts - Conditions and Results.

Run	Catalyst* (mg)	Initial carbon deposit (mg)	Flow rate (cm^3 (STP) sec^{-1})			Temp (°C)	Rate x $10^{2\dagger}$ (mg/sec)	Type of experiment
			CO_2	N_2	CO			
31	21.7	55	0.83	-	-	650	1.08	
			1.7	-	-		1.39	F
			3.3	-	-	650	1.29	
						to	to	E_A,W
						500	3.0×10^{-2}	
32	41.0	63	0.83	2.5	-	650	0.74	
			1.7	1.7	-		1.06	O,W
			2.5	0.83	-		1.16	
			3.3	-	-	650	1.50	
						to	to	E_A
						550	0.208	
34	31.6	100	3.3	-	-	750	5.28	
						to	to	E_A,GLC
						500	4.1×10^{-2}	
36	31.6	100	3.3	-	-	725	3.56	
			0.83	-	-		2.40	F
			1.7	-	-		3.02	
			4.8	-	-		3.40	
38	31.6	103	3.3	-	-	675	2.22	F
			4.8	-	-		2.32	
39	31.6	53	2.6	0.83	-	775	3.75	
						to	to	E_A
						525	0.835	
40	20.4	20	3.3	-	-	675	1.83	C
41	20.4	49	3.3	-	-	675	2.46	C
42	20.4	8	3.3	-	-	675	1.00	C
43	20.4	64	3.3	-	-	675	2.49	C
44	20.4	107	3.3	-	-	675	2.50	C,W
						650	1.45	
74	11.1	35	3.1	-	-	550	0.147	
			2.5	0.83	-		0.134	
			1.7	1.7	-		0.129	O,W
			0.83	2.5	-		0.109	
			3.3	-	-	650	1.20	
75	11.1	93	3.5	-	-	725	4.04	
			1.8	1.7	-		2.82	
			0.83	2.5	-		2.00	O
			0.50	2.8	-		1.46	
76	11.1	107	3.3	-	-	850	7.98	
						to	to	E_A
						750	4.65	
80	33	90	1.7	1.7	-	775	2.66	
			0.83	2.5	-		1.26	O
			2.5	0.83	-		3.90	
			3.3	-	-		5.41	
82	26.8	93	2.8	-	0.50	725	3.50	
						650	1.35	
						575	0.130	Eq
			3.3	-	-	575	0.340	

Continued...

Table 3.14 Continued

Run	Catalyst* (mg)	Initial carbon deposit (mg)	Flow rate ($cm^3(STP)sec^{-1}$)			Temp (^oC)	Rate x 10^2† (mg/sec)	Type of experiment
			CO_2	N_2	CO			
						650	1.40	
						725	3.35	
83	26.8	97	2.8	-	0.50	725	3.51	
						650	1.30	
						575	0.150	
			3.1	-	-	575	0.350	
						650	1.45	Eq
						725	3.20	
			2.9	-	0.50	725	3.40	
						650	1.38	
						575	1.42	
84	31.1	40	3.3	-	-	650	1.29	
		35					1.29	SA
		24					1.27	
		16					1.05	
85	31.1	80	3.3	-	-	625	0.980	SA
		41					0.980	

* 18% Ni/Al_2O_3 , 40 - 60 mesh BSS

† Rates tabled refer to gasification in steady state conditions

LEGEND: GLC - Gas Chromatographic analysis

W - Effect of the catalyst load

Eq - Effect of carbon monoxide addition to the feed

SA - Determination of surface area, pore volume and pore size distribution

Other symbols - As in Table 3.13

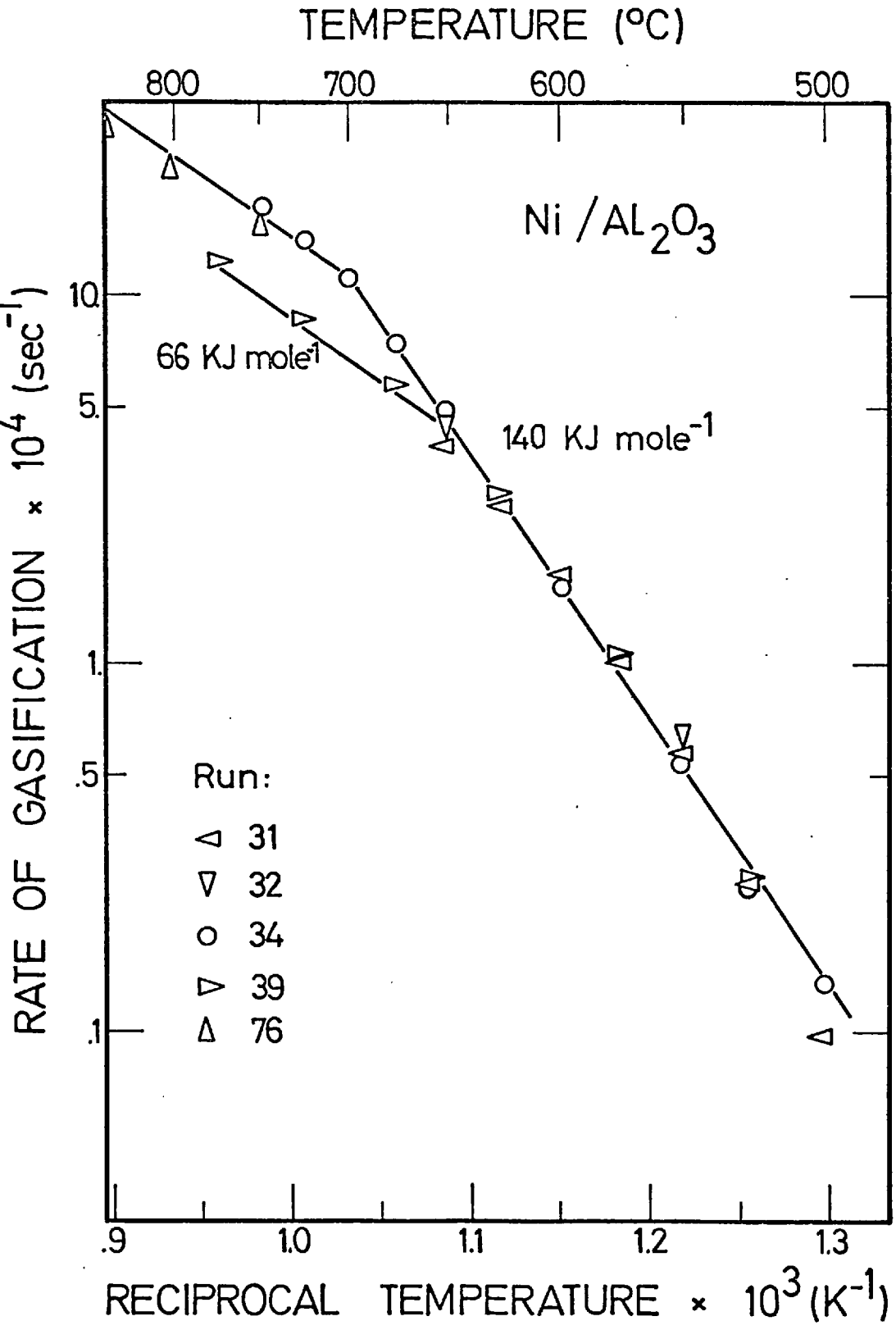

Fig. 3.34 Arrhenius-type plot of the gasification rates at a constant CO_2 flow rate (3.3 cm^3(STP)sec^{-1}) and atmospheric pressure

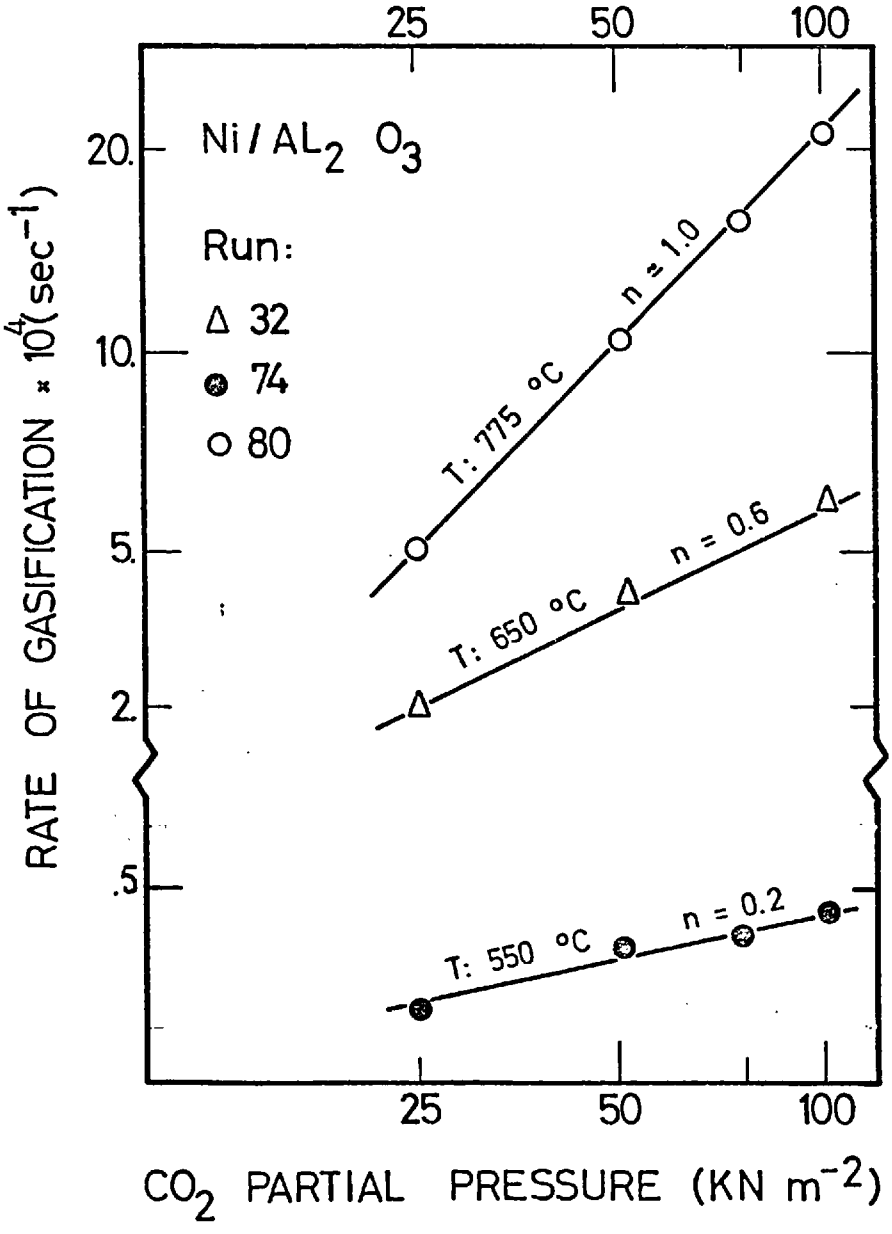

Fig. 3.35 Dependence of gasification on the partial pressure of carbon dioxide at different temperatures.

The gasification conditions as well as the rates measured are presented in Table 3.14. As in the case of nickel foils, the gasification experiments were characterised by a short induction period followed by an acceleratory period and a period of constant gasification rate. This usually lasted between 10 and 65% burn-off. Again, no deactivation was detected for intermediate values of burn-off.

As can be seen in Table 3.14 by comparing Runs 40, 41, 42, 43 and 44, the gasification rates appear to depend on the initial amount of carbon deposit up to circa 30 mg.

Fig. 3.34 shows the Arrhenius-type plot of the gasification rates normalised in the same way as in the case of foils ($w = w_c$ if $w_c < 30$ mg; $w = 30$ mg, if $w_c \geq 30$ mg). Again two regions can be observed in the figure: the apparent activation energy is 66 ± 8 KJ mole^{-1} and 140 ± 8 KJ mole^{-1}, respectively above and below 675°C. It can also be seen in the figure (Run 39) that decreasing the partial pressure of carbon dioxide from 1 to 0.75 does not have an appreciable effect below 650°C, whilst above this temperature an order with respect to carbon dioxide of about 1.2 can be obtained from Runs 39, 34 and 76.

This is confirmed by the results presented in Fig. 3.35. The order with respect to carbon dioxide increases from values close to zero at 550°C to one in the upper temperature region. Some experiments were performed to determine the influence of carbon dioxide flow rate on the gasification rates (Runs 31, 36 and 38). As in the case of nickel foils, the rates increased with increasing flow rate, more noticeably, at 725°C. It can also be seen in the table, comparing Runs 31, 32 and 44, that the gasification rates do not depend appreciably on the catalyst load.

3.3.1.2.2 Activity and equilibrium

Gas chromatographic analyses of the effluent gases showed that the only significant product of the reaction was carbon monoxide. A simple calculation proves that the reaction is proceeding according to the stoicheiometry:

$$CO_2 + C \rightarrow 2CO \qquad (1)$$

For instance, for Run 34 at 700°C:

CO_2 flow rate in feed : 1.39×10^{-4} mole sec^{-1}

Effluent gases flow rate: 1.42×10^{-4} mole sec^{-1}

Composition of effluent mixture (molar fraction)

Carbon dioxide: 9.61×10^{-1}

Carbon monoxide: 3.9×10^{-2}

Rate of carbon gasification:

$R_c = 3.5 \times 10^{-2}$ mg sec^{-1} or

2.9×10^{-6} moles sec^{-1}

In agreement with eqn.(1): $R_{CO} \simeq 2 \times R_c$

Fig. 3.36 shows the results of the GLC analysis in Run 34 for the complete range of temperatures. The results are representative of all the other analyses made. The ordinates in the figure represent the carbon dioxide conversion - mole of carbon dioxide reacted per mole of carbon dioxide in the feed - calculated according to the stoicheiometry referred to above (Curve c). Also represented in the figure are the conversions that would be attained, assuming that the whole gas phase was in equilibrium with carbon in the form of graphite (using data from reference (1)). It can be seen from the data that the outlet concentration varied between 2.5 and 15.4% of the equilibrium value when the temperature increased from 550 to 750°C. When carbon dioxide flow rates were decreased from 3.3 to 0.42 cm^3(STP) sec^{-1} at 750°C, 48% of the equilibrium value was attained.

The effect in the gasification rates of the addition of carbon monoxide to the feed is also shown in figure 3.36. Curve (a) was obtained from Runs 31, 32, 34 and 76a represented in Fig. 3.34. In a series of experiments, 15% (V/V) of carbon monoxide was diluted in the feed and gasification rates measured at different temperatures. The carbon monoxide dilution was stopped and the rates measured again at the same temperatures. In the figure, the circles represent the average rates measured in three experiments in these conditions. It is seen that the dilution does not affect the rates at high temperatures but has an inhibiting effect at 575°C. At this temperature, minimal amounts of carbon monoxide would be enough to keep the nickel in the metallic state (76). At 575°C, the equilibrium concentration of carbon

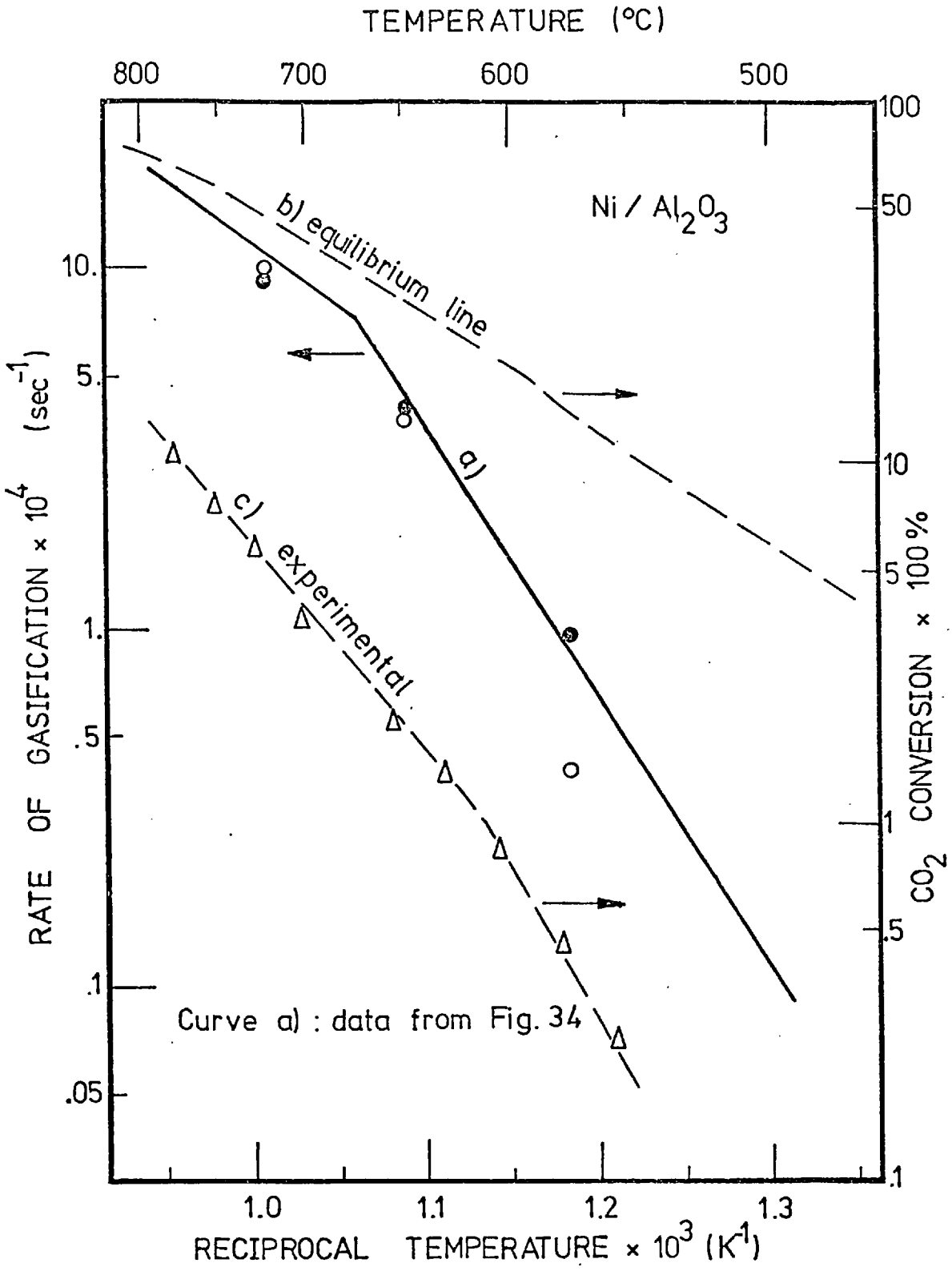

Fig. 3.36 Effect of the addition of CO to the feed on the gasification rate (curve a). A comparison between CO_2 conversion in equilibrium (obtained from data in reference 1) and the gas conversion determined in Run 34 is also presented (curves b and c).

(Feed composition (molar fraction): O O-CO-0.15, CO_2-0.815
● ●-CO-0.0 , CO_2-1.00

Flow at inlet: 3.3 cm^3(STP)sec^{-1})

monoxide in the gas phase is 24% (V/V) and, due to the reaction, about 0.9% were present. Admission of 15% carbon monoxide in the feed could thus have a significant effect in reversing equation (1). Alternatively, competitive adsorption of carbon monoxide could be responsible for the decrease in the reaction rate.

3.3.1.2.3 Changes in the structure of the deposits during the gasification.

Surface areas of carbon deposits at various percentages of burn-off were determined by nitrogen adsorption at 77 K. The corresponding isotherms are represented in Fig. 3.37. From them, values of the surface area and total pore volume of the carbon were calculated. These are represented in Fig. 3.38, expressed per unit weight of carbon at the corresponding % burn-off and per unit weight of the initial carbon deposit.

During the gasification, the external volume of the deposit remained apparently unchanged until circa 60% burn-off. The apparent densities were determined taking 1.95 as the density of the pore walls (Table 1 in reference (81)):

% burn-off	0	12	38	61	91
Apparent density (d_a)	1.61	1.59	1.50	1.37	1.09
Porosity ($\theta = 1-\frac{d_a}{d}$)	0.17	0.18	0.23	0.30	0.44

It is evident from the data that the increase in the total pore volume is accompanied by a corresponding increase in the surface area. This means that, as the % burn-off increases, a certain amount of small pores are either formed or becoming accesible to the adsorbate in the adsoprtion experiments.

The pore size distribution, determined by the method described in (79), remained nearly the same up to 50% burn-off. The radius of the majority of the pores corresponded to the beginning of the transitional pore zone.

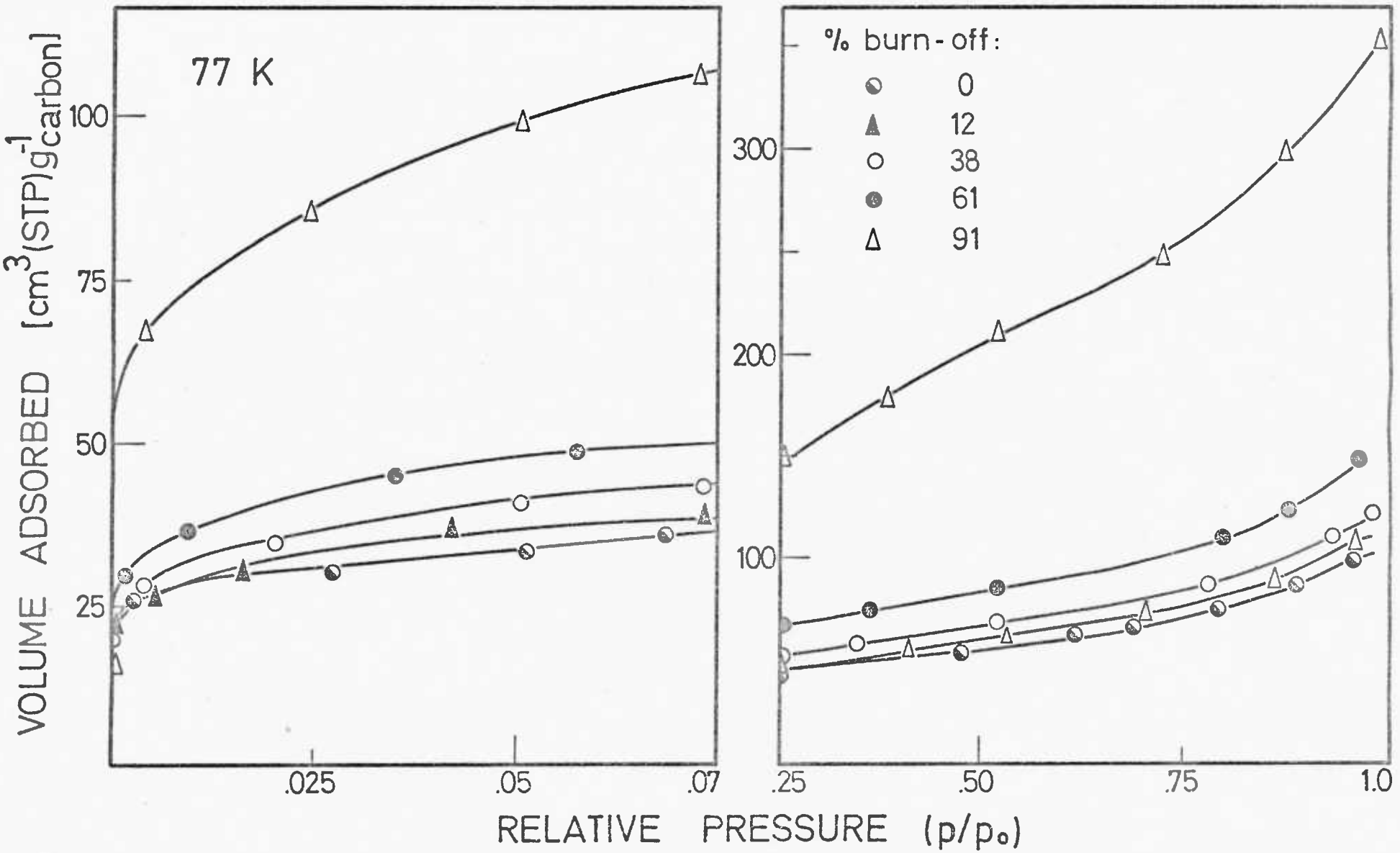

Fig. 3.37 Adsorption of N_2 at 77 K on carbon at different % burn-off. (Gasification by CO_2 at 650°C)

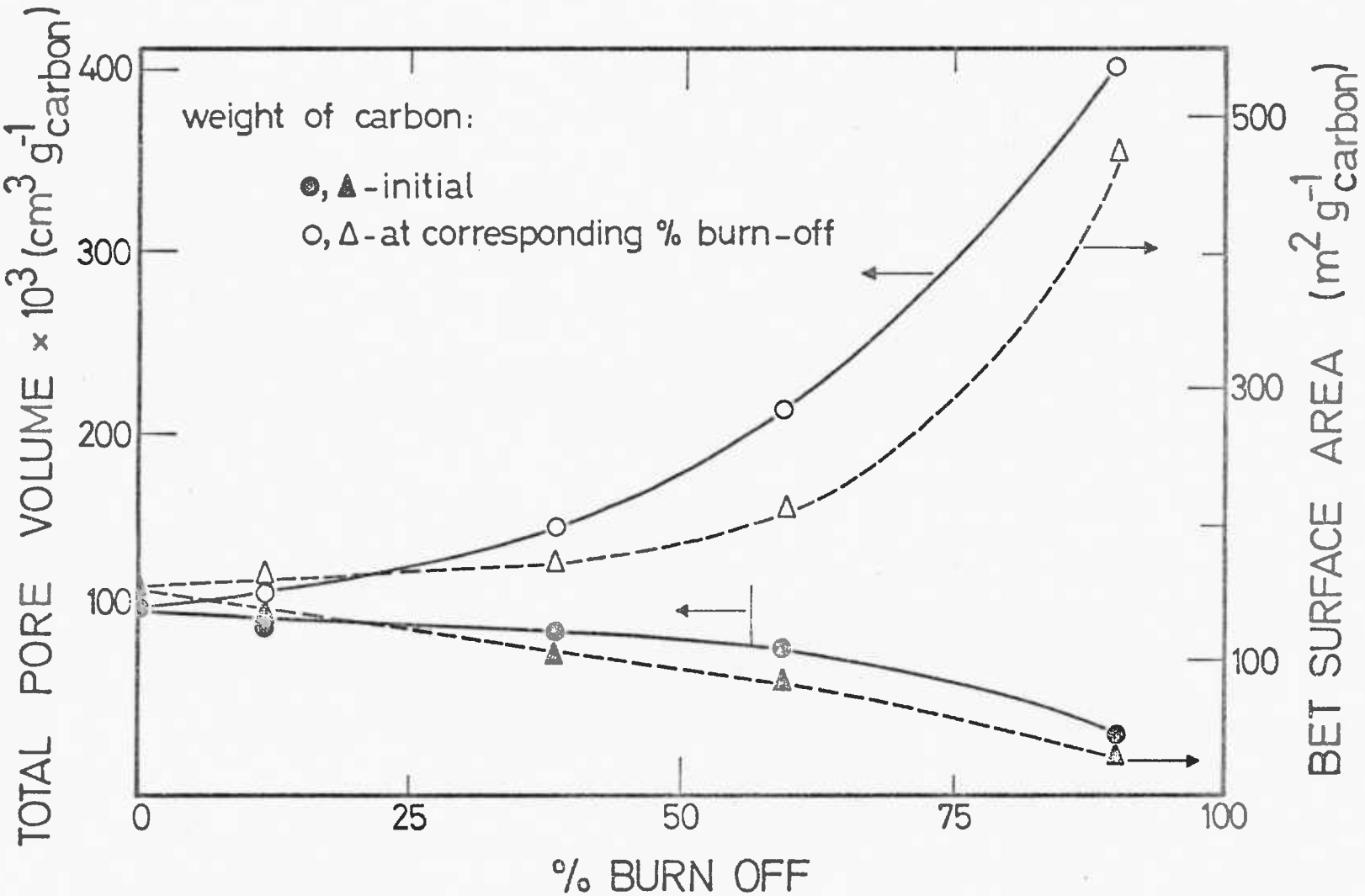

Fig. 3.38 Pore volumes and BET surface areas of the carbon deposits at different % burn-off. (Gasification by CO_2 at 650°C and atmospheric pressure)

3.3.1.2.4 A test for diffusion limitations

Above 675°C, in both nickel foils and supported nickel catalysts, gasification by carbon dioxide of carbon deposits is similar. In both cases, the apparent activation energy is about one half of that of the previous zone and the orders are seen to move towards one. In order to test for limitations by diffusion in the pores, the treatment of Roberts and Satterfield (4) was applied.

This treatment is based in the determination of an effectiveness factor, η, as a function of a modulus, ψ, for different values of KP_{CO_2}. ψ and K are defined as:

$$\psi = (L_c^2 RT/D_e P_{CO_2}) R_{CO_2}$$

and

$$K P_{CO_2} = \frac{k_1/k_2 - 1.6\ k_1'/k_2}{1 + 1.6\ k_1'/k_2} P_{CO_2}$$

where:

P_{CO_2} - partial pressure of CO_2 outside the carbon

L_c - characteristic dimension of the carbon particle in cm (L_c = R/3 in the case of spheres)

D_e - effective diffusivity of CO_2 into the pores in $cm^2 . sec^{-1}$

R_{CO_2} - rate of the reaction in moles cm^{-3} sec^{-1}

k_1, k_1' and k_2 - direct and reverse specific rates for the oxygen exchange between the gas phase and the carbon surface and the specific rate for the carbon gasification step, respectively.

Assuming that the rate equation in the chemical reaction controlled zone is of the type:

$$\text{Rate} = \frac{kP_{CO_2}}{(1 + b_{CO_2} P_{CO_2} + \varepsilon_i b_i P_i)} ,$$

The value of η can be obtained directly from Fig. 3.39.

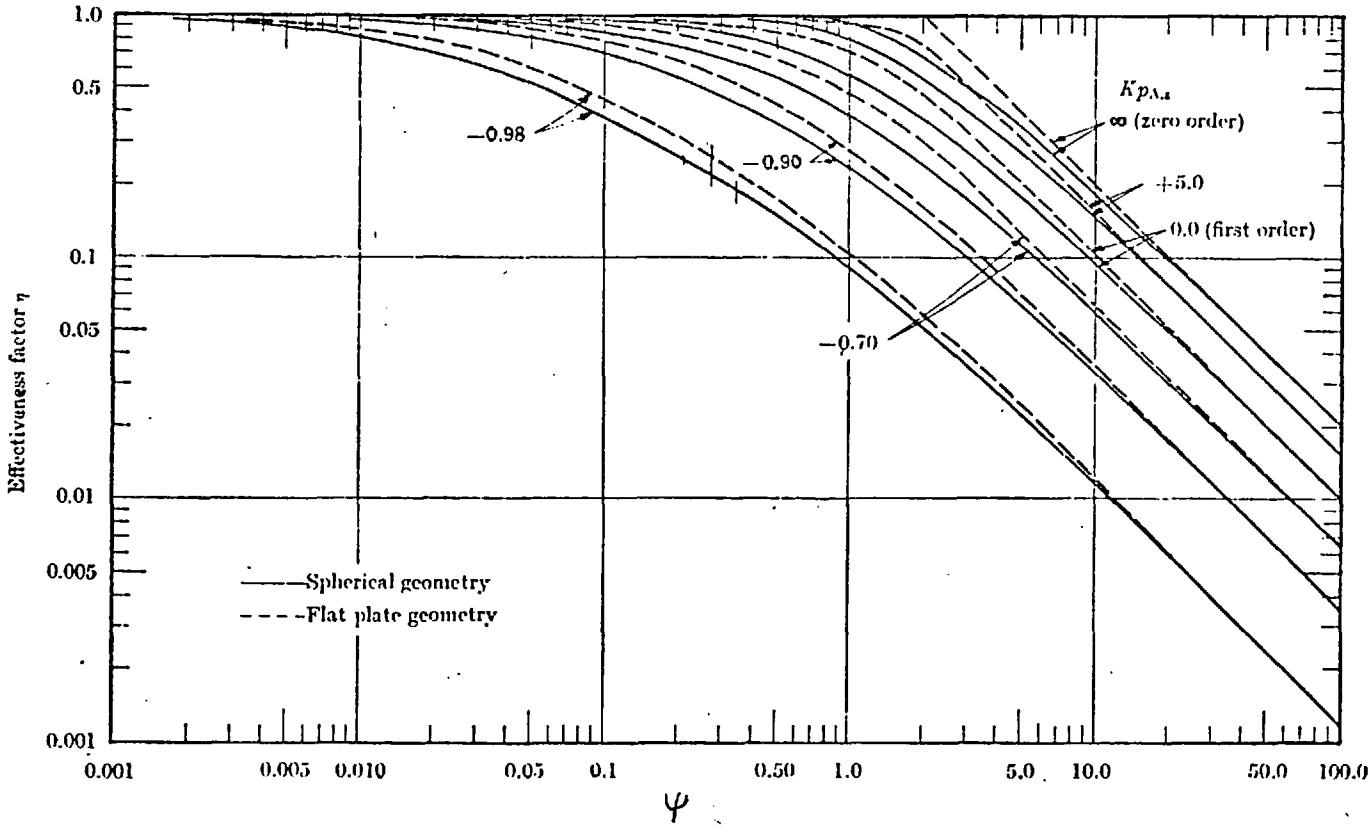

Fig. 3.39 Effectiveness factor, η, as a function of the Thiele modulus, ψ, for spherical and flat plate geometry (from Ref. (4)).

In the case of supported catalysts the deposits were formed by roughly spherical carbon particles whose diameter was estimated (by microscope observation) to be 0.1 cm in average. The effective diffusivity, D_e, was estimated (from the data presented in (4) for carbon dioxide diffusivity in a graphite electrode) to be 4.3×10^{-2} $cm^2 sec^{-1}$ at 725°C and $P_{CO_2} = 1$ atm.

For run 34 at 725°C, the rate is 1.4×10^{-3} mg sec^{-1} mg^{-1}. Taking the apparent density of the carbon particles to be 1.43 g cm^{-3} at an average burn-off of 50%, $R_{CO_2} = 1.7 \times 10^{-4}$ moles sec^{-1} cm^{-3}.

Thus:

$$\psi \simeq 0.090$$

K was obtained from Table III in reference (114).

At 725°C, K = - 0.99.

From Fig. 3.39, $\eta \simeq 0.4$.

The intrinsic rate would be $R^i_{CO_2} = R_{CO_2}/\eta \simeq 4.25 \times 10^{-4}$ moles sec^{-1} cm^{-3}. Although a calculation of this type can only be taken as a rough approximation, it seems evident that pore diffusion limitations are affecting the rates observed at 725°C.

3.3.2 Carbon gasification by hydrogen from supported nickel catalysts

3.3.2.1 General results

Gasification by hydrogen of carbon deposits formed on supported nickel catalysts was studied at atmospheric pressure and temperatures between 475 and 850°C. The deposits were again formed at 600°C from a mixture of n-hexane, hydrogen and nitrogen (molar fractions: 0.135, 0.25 and 0.615, respectively) flowing at 3.75 cm^3(STP)sec^{-1}.

As in the case of carbon dioxide, three distinct periods were observed. A short induction period, an acceleratory period and a long period of constant gasification rate that lasted until circa 70% of the carbon deposit was burned-off. Thus, the rates were independent of the amount of carbon present in each run for a large extent of the gasification. Steady state rates, together with the gasification conditions are presented in Table 3.15.

Table 3.15 Hydrogen gasification of carbon deposits formed on supported nickel catalysts - conditions and results.

Run	Catalyst* (mg)	Initial carbon deposit (mg)	Flow rate (cm^3(STP)sec^{-1})			Temp (^oC)	Rate** x 10^2 (mg sec^{-1})	Type of experiment
			H_2	N_2	CH_4			
46	39.4	54	3.3	-	-	675	2.43	B,C
48	39.4	81	3.3	-	-	775 to 625	1.01 to 2.21	E_A,GLC
49	39.4	122	3.3	-	-	675 750 to 475	2.38 1.44 to 5×10^{-3}	C,E_A,W
50	19.3	98	3.3	-	-	675	2.35	
			3.3	-	-	700	1.88	
			2.5	0.83	-		1.10	
			1.7	1.7	-		0.521	C,O,W
			0.83	2.5	-		0.150	
			3.3	-	-	625	2.29	
			2.5	0.83	-		1.51	
			1.7	1.7			0.833	
			0.83	2.5			0.310	
51	19.3	101	5.0 to 0.88	-	-	725	1.25 to 0.583	F,GLC
			5.0 to 0.83	- - -	- - -	625	1.79 to 1.17	
53	20.2	100	3.3 to 0.85	-	-	550	0.295 to 0.280	F
54	-	92.6***	3.3	-	-	625	0	N
68	34.5	43	3.3	-	-	550	0.289	
			2.5	0.83	-		0.222	O
			1.7	1.7	-		0.177	
			0.83	2.5	-		0.092	
69	34.5	48	3.3	-	-	600 to 500	1.28 to 0.192	E_A
70	34.5	109	3.3	-	-	850 to 550	0.611 to 0.267	E_A
71	39.5	40	3.3	-	-	625 675	1.82 2.42	C
72	39.5	21	3.3	-	-	625 675	1.01 1.30	C
73	9.8	34	3.3	-	-	550	0.126	
			2.5	0.83	-		0.114	O,W
			1.7	1.7	-		0.092	
			0.83	2.5	-		0.048	
81	26.8	95	3.0	-	0.5	700 650 600 550	$\sim$ 0 6×10^{-2} 0.150 0.145	

Table 3.15 (Continued)

Run	Catalyst* (mg)	Initial carbon deposit (mg)	Flow Rate (cm (STP)sec^{-1})			Temp (^{o}C)	Rate** x 10^2 (mg sec^{-1})	Type of experiment
			H_2	N_2	CH_4			
			3.4	-	0.18	550	0.180	A
						600	0.66	
						650	1.36	
						700	1.22	
						725	0.58	
			3.2		0.33	750	-	E_q
86	24	99	3.3	-	-	750	1.36	
			-	-	-		0.063****	F,CH_4
			3.3	-	-		0.222	

* 18% Ni/Al_2O_3, 40 - 60 mesh BSS

** Rates tabled refer to steady state conditions

*** Carbon molecular sieve, 40 - 60 mesh BSS

**** Batch conditions; 1 atmosphere of hydrogen, rate measured after gasification of 10 mg of carbon.

LEGEND: B - Effect of the % of burn-off

A - Effect of the addition of methane to the feed in the gasification rate

Eq - Determination of the equilibrium concentrations

N - Catalytic nature of the gasification

Other symbols - As in Tables 3.13 and 3.14.

At low and intermediate temperatures, the reactivity of the carbon deposits towards hydrogen was not very different from the reactivity towards carbon dioxide. However, the relative reactivities changed with the temperature and above 700°C carbon dioxide gasification become progressively more important. As the relative reactivities could also depend on the total pressure at a given temperature (see discussion in section 4.25), general statements like "$C-H_2$ reaction is 1000 times slower than $C-CO_2$ reaction" should be considered with great care (1,p.75).

It is interesting to note that the rates shown in Table 3.15 are similar to those reported by Nishiyama et al. (71) for hydrogen gasification of carbon deposits formed in nickel foils from benzene. This may indicate that the present results can be generalised to the gasification of carbons formed on various nickel catalysts from a large number of hydrocarbons. The dependence of the steady state rates of gasification on the initial amount of the deposit can be obtained from Table 3.15 (Runs 46, 49, 71 and 72). At 675°C the gasification rates appear to be roughly proportional to the initial amount of carbon up to circa 35 mg of deposit and nearly independent thereafter. Also in Table 3.15, runs 49 and 50 show that gasification rates do not apparently depend on the load of catalyst used. However, when this is reduced below 10 mg the steady state rate decreases (Runs 68 and 73). As more than 19 mg of catalyst were used in all but two experiments, the rates were normalised in the same way as in the previous sections.

Fig. 3.40 shows the Arrhenius-type plot of the normalised steady state gasification rates. Three distinct zones can be seen in the plot. The apparent activation energy is 265 ± 17 KJ $mole^{-1}$ below 550°C, 180 ± 9 KJ $mole^{-1}$ between 550 and 625°C and -82 ± 5 KJ $mole^{-1}$ above 700°C. The decrease of the gasification rate with temperature in the last zone is thought to be related with the reverse reaction:

$$CH_4 \rightarrow C + 2H_2$$

which becomes progressively more important at high temperatures (see 3.3.2.2). In any of the three zones, the rates were found to be reversible with temperature when this was changed upwards and downwards in discrete jumps.

The effect of hydrogen flow rate is shown in Fig. 3.41. The gasification rate increased with the flow rate but there was a tendency to

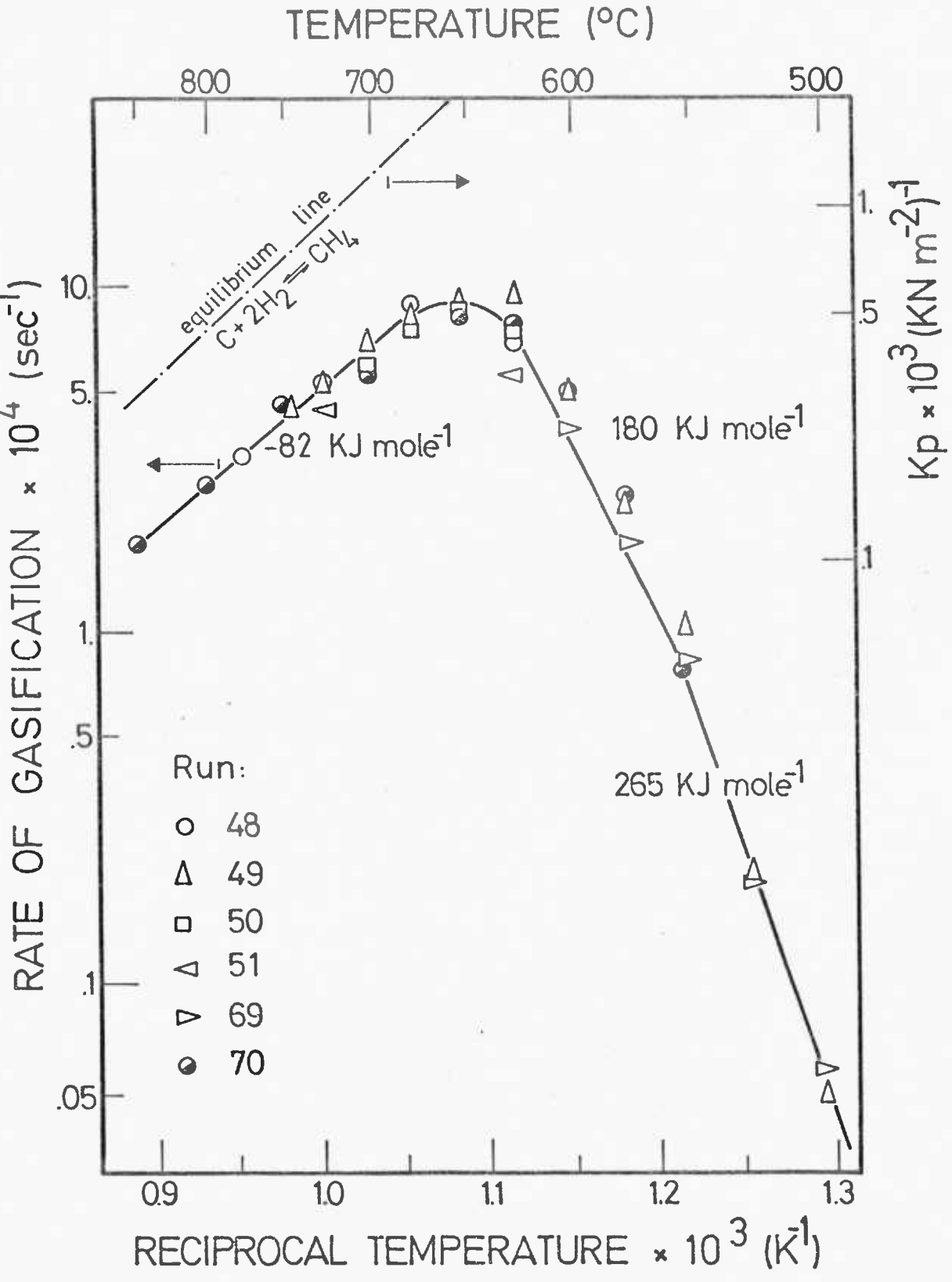

Fig. 3.40 Arrhenius-type plot of the gasification rate at an hydrogen inlet flow rate of 3.3 $cm^3(STP)sec^{-1}$ and atmospheric pressure.

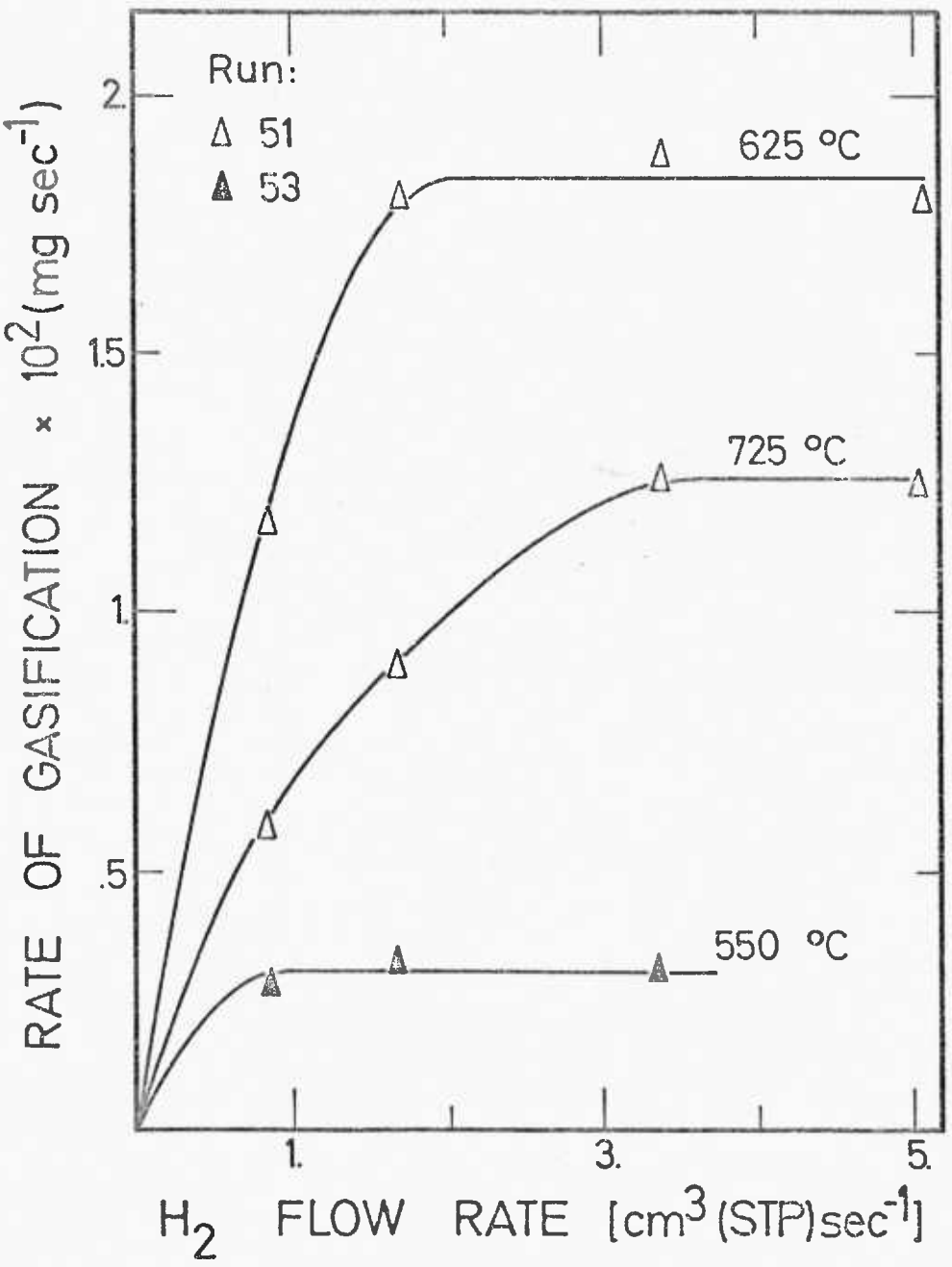

Fig. 3.41 Dependence of the gasification rate on hydrogen flow rate at different temperatures.

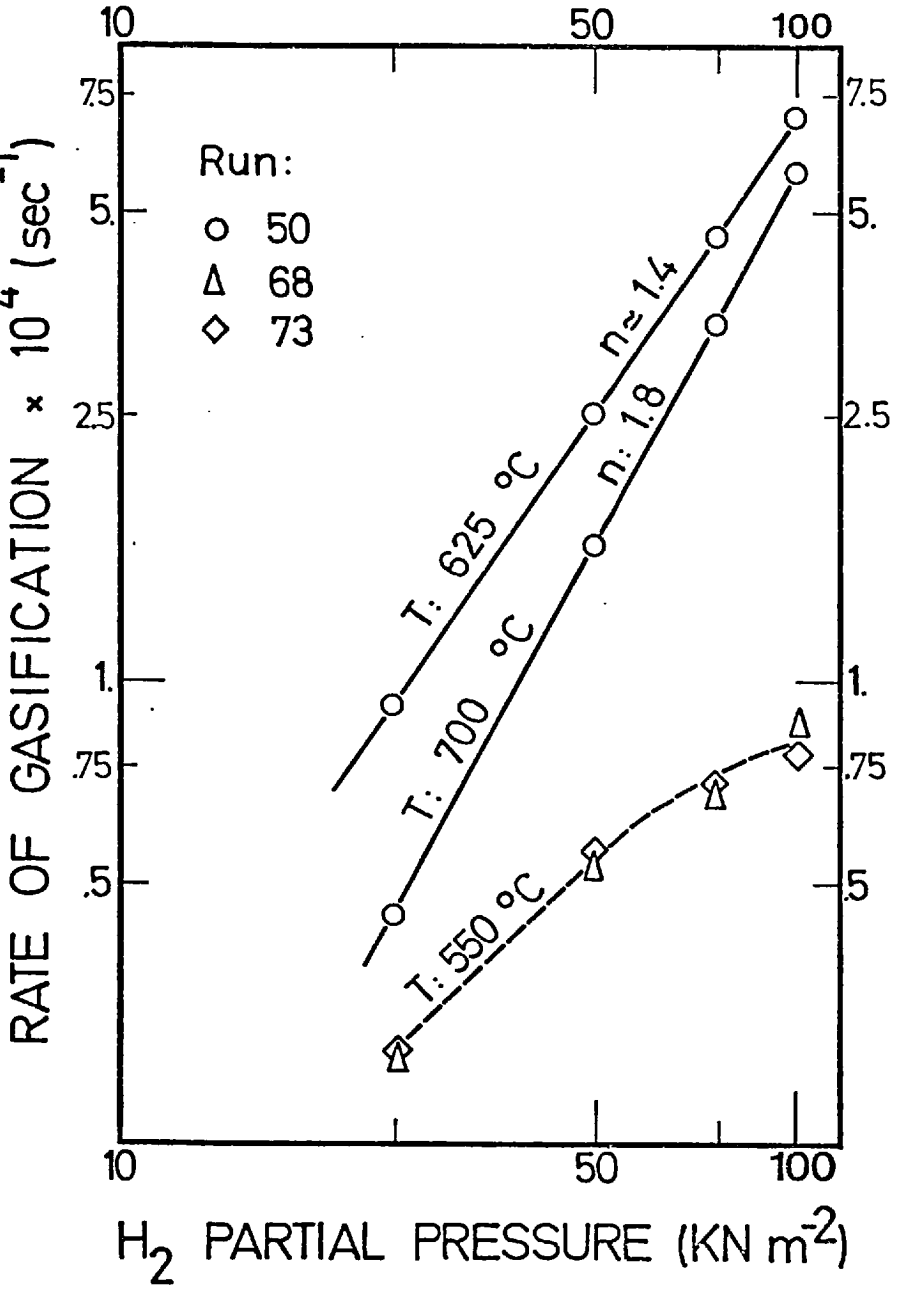

Fig. 3.42 Dependence of the gasification rate on hydrogen partial pressure at different temperatures and a constant inlet flow rate (3.3 cm^3(STP)sec^{-1}).

(In Run 73 the rates were corrected taking into account the reduction of the catalyst load).

level off above 3 $cm^3(STP)sec^{-1}$. The dependence of the gasification rates on the partial pressure of hydrogen was examined by diluting the feed with oxygen-free nitrogen (and sometimes argon), keeping the total pressure atmopheric. The results are shown in Fig. 3.42. No difference was detected when the nature of the diluent was changed keeping the partial pressure of hydrogen constant.

At 550°C the order with respect to hydrogen is apparently changing from values close to 1 to values close to 0.3 as the partial pressure increases. As the temperature increases, the order rises to 1.4 (end of second zone) and 1.8 (third zone).

An experiment was made to ascertain the catalytic nature of the gasification reaction. Molecular-sieve carbon, of the same particle size as the catalyst normally used, was kept for 3 hours in the microbalance at 625°C and an hydrogen flow rate of 3.33 $cm^3(STP)sec^{-1}$ (Run 54, Table 3.15). No gasification was detected during that period (the sensitivity of the balance was better than 25 μg).

3.3.2.2 Reactivity and equilibrium

Gas chromatographic analysis of the effluent gases have shown that the major product of the reaction was methane. Only traces of higher hydrocarbons (C_2) were found.

The analysis also showed that, for the whole range of temperatures, the reaction was proceeding according to:

$$C + 2H_2 \rightarrow CH_4$$

As an example, a mass balance is presented using the results of Run 48 at 625°C:

Effluent gas flow rate	1.44×10^{-4} moles sec^{-1}
Composition of effluent gas (molar fraction)	
CH_4	1.3×10^{-2}
H_2	9.87×10^{-1}
Rate of gasification	2.21×10^{-2} mg sec^{-1}

Carbon balance:

Reacted (moles sec^{-1})	outlet (moles sec^{-1})
1.84×10^{-6}	$1.44 \times 10^{-4}(1.3 \times 10^{-2}) = 1.87 \times 10^{-6}$

The concentration of methane in the effluent gas was shown to be dependent on the hydrogen flow rate. For instance, in Run 51 at 625°C, the methane concentration increased from 3.9% to 18% of the equilibrium value when the flow rate changed from 5.0 to 0.83 cm^3/sec. At 725°C these values were 7.2 and 33%, respectively.

Thus, at temperatures of 700°C and above, the concentration of methane near the reaction sites is probably affecting the gasification rates measured. To verify this assumption an experiment was made, where methane was added to the feed in various concentrations and the gasification rates measured at different temperatures (Run 81). The results obtained are presented in Fig. 3.43. Also represented in the figure are the equilibrium line obtained from reference (9) and the Arrhenius type plot corresponding to a feed of pure hydrogen, derived from the data in Fig. 3.40. As the methane concentration increases from 5 to 14% (moles of methane per mole of hydrogen in the feed), the gasification rate decreases, more noticeably at high temperatures. For 14% methane, no gasification was detected above 675°C. In fact, at 750°C an increase in weight was detected. When the methane concentration was decreased (in discrete steps) to zero, the gasification started again. The concentration was again increased and the process repeated. The equilibrium methane concentration determined in this way was circa 9.5% (V/V). Furthermore, the previous results were obtained with a total flow rate of circa 3.5 $cm^3(STP)sec^{-1}$. The lower the flow rate, the nearer to the equilibrium values will the methane concentration be and hence the greater the importance of the reverse reaction. At the limit, if the reaction were carried out under batch conditions, the equilibrium would be reached even starting with pure hydrogen. In Run 86 at 750°C, the hydrogen flow was stopped. The gasification rate was seen to decrease progressively towards zero. After the gasification of approximately 10 mg of carbon, the reaction almost stopped. When flow conditions were restored, an immediate increase in the gasification rate was observed.

From the present results it is evident that steady gasification rates are only measured above 700°C because methane is constantly being removed from the reaction sites and thus the system is kept away from equilibrium. Another interesting feature can be observed in Fig. 3.43. The apparent activation energy measured above 700°C, -82 ± 5 KJ $mole^{-1}$, is very close to the average heat of the reaction between 600 and 800°C, -87 KJ $mole^{-1}$ (determined from data in reference (9)).

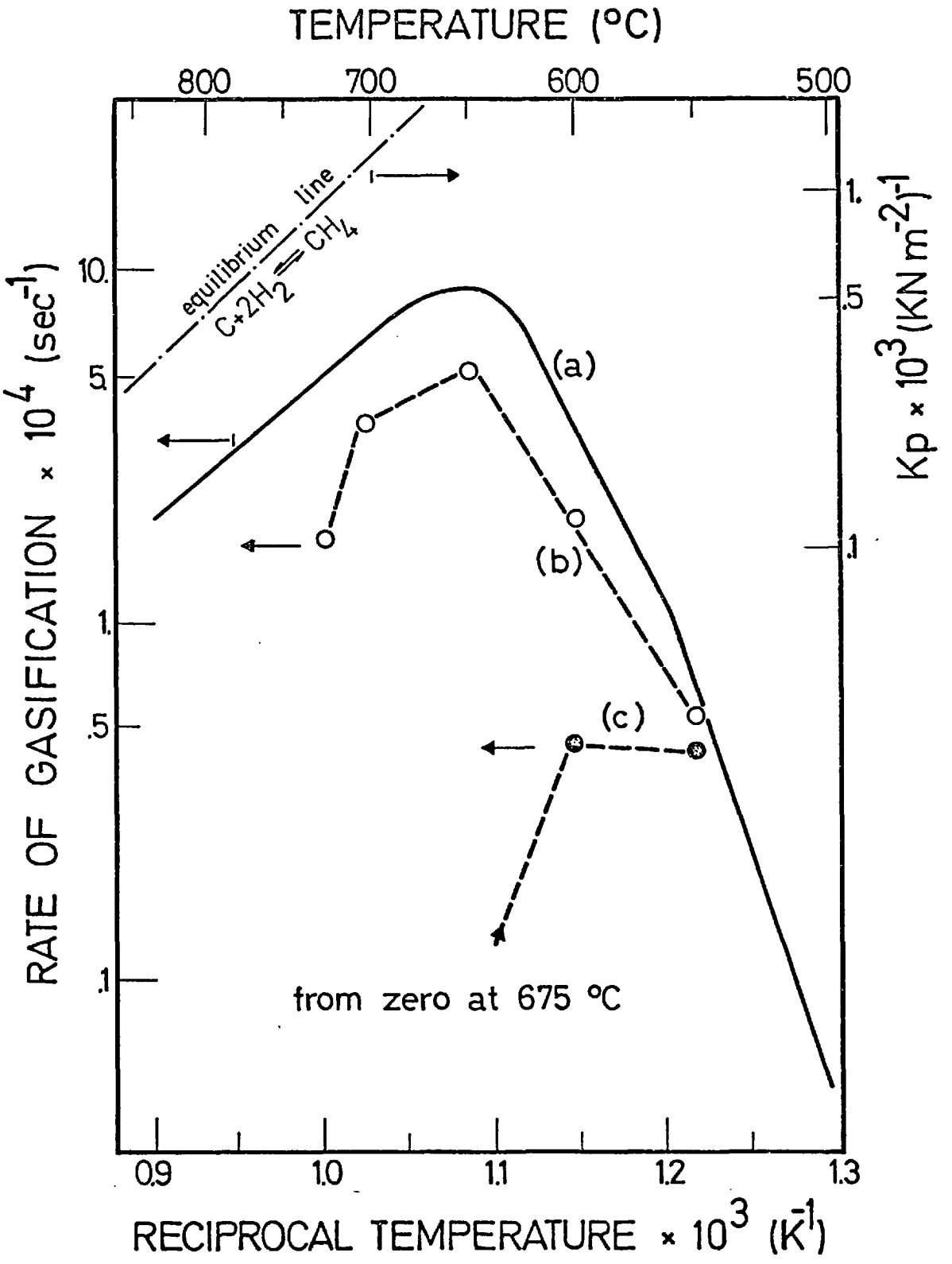

Fig. 3.43 Dependence of the gasification rate on the methane concentration in the feed. Equilibrium line from reference (9).
Inlet composition: a) H_2 - 100% (from Fig. 3.40)
b) H_2 - 95%, CH_4 - 5% (molar %)
c) H_2 - 86%, CH_4 - 14% (molar %)
Inlet flow rate: 3.3 cm^3(STP)sec^{-1}.

This point will be discussed in section 4.2.3.

3.3.3 Carbon gasification by steam from supported nickel catalysts

3.3.3.1 General Results

Steam gasification of carbon deposits was studied at atmospheric pressure (steam partial pressures from 7 to 30 KN m^{-2}) and temperatures between 500 and 825°C. The carbon was formed by decomposition of n-hexane over supported nickel catalysts in conditions identical to those described in 3.3.1. Similarly to carbon dioxide and hydrogen, the gasification did not depend on the amount of carbon present in a single run. The long steady state periods observed were used to measure the rates listed in Table 3.16. As can be seen, comparing Runs 91-a, b and 92-a, b in the table, the rates are apparently independent of the initial amount of the deposit above 35 mg weight.

The gasification started to be significant between 475 and 500°C and increased markedly with temperature thereafter. This is shown in the Arrhenius-type plot of Fig.3.44 for two different partial pressures of steam. The rates in the figure were normalised in the usual way, by dividing by w_c (35 mg in this case).

Up to circa 700°C, the general features of the plot are similar to those of Fig. 3.34. Two different zones are observed: at lower temperatures the apparent activation energy is 164 ± 9 KJ/mole, decreasing to 61 ± 4 KJ/mole between 600 and 700°C. Above this temperature, however, the rate does not increase significantly with temperature. As the steam partial pressure increases from 13.6 to 25.8 KN m^{-2}, the transition between the zones moves towards higher temperatures. This is consistent with the values of the orders with respect to steam shown in Fig. 3.45. The order changes from 0.6 at lower temperatures to 0.75 at 650°C (second zone) and circa 1 at 750°C (third zone). As the rate in this zone increases more markedly with steam pressure, its onset occurs at progressively higher temperatures.

Assuming the orders to remain constant up to atmospheric pressure, the rates can be extrapolated as shown in the ——·—— line in Fig. 3.44. It is now evident that the third zone would not be observed below 800°C if steam alone were present in the reactor. From the values of the orders and the temperature dependences, it appears that diffusion limitations are affecting the measured rates at intermediate and high temperatures (most probably pore diffusion and film diffusion limitations,

Table 3.16 Steam gasification of carbon deposits formed on supported nickel catalysts - conditions and results.

Run	Catalyst* (mg)	Initial Carbon deposit (mg)	Steam partial pressure ($KN\,m^{-2}$)	Temp (^{o}C)	Rate x 10^{2}† (mg/sec)	Type of experiment
89-a	24.2	78	13.6	700	1.47	
				750	1.74	E_A
				800	1.75	
89-b	24.2	71	13.6	625	1.06	E_A
				600	0.84	
89-c	24.2	79	13.6	600	0.66	
				650	1.18	E_A
				700	1.75	
				750	1.65	
89-d	24.2	86	13.6	625	0.84	
				675	1.34	
				725	1.54	E_A
				775	1.55	
				825	1.53	
89-e	24.2	85	13.6	750	1.69	
			16.5		1.93	O
			7.4		0.72	
			11.4		1.15	
90-a	20.3	31	13.6	600	0.55	
				575	0.44	E_A
				550	0.23	
				525	0.10	
90-b	20.3	34	13.6	550	0.22	
			16.3		0.24	O
			7.8		0.17	
			10.1		0.19	
91-a	20.3	38	13.6	625	0.84	C
91-b	20.3	69	13.6	625	0.77	C,GLC
92-a	24.5	95	13.6	625	0.94	C,GLC
92-b	24.5	33	13.6	625	0.92	C
93	24.8	33	13.6	550	0.24	
			25.8	550	0.36	O,E_A
				575	0.64	
				525	0.16	
				500	0.06	
94	24.8	58	25.8	750	3.28	
				700	2.89	O,E_A
				800	3.18	
95-a	24.2	95	13.6	750	0.86 to 2.10	F; total inlet flow changed from 0.6×10^{-5} to 2.6×10^{-4} moles sec^{-1}.
95-b	24.2	33	13.6	550	0.19 to 0.22	F; total inlet flow changed from 0.6×10^{-5} to 1.5×10^{-4} moles sec^{-1}.
96	24.5	67	25.8	650	1.85	
				625	1.53	E_A,O
				675	2.18	
97	24.5	47	13.6	625	0.82	GLC

Table 3.16 (continued)

* 18% Ni/Al_2O_3, 40 – 60 mesh BSS

† Rates tabled refer to steady state conditions

LEGEND: GLC – Gas chromatographic analysis

Other symbols – as in Tables 3.13 to 3.15

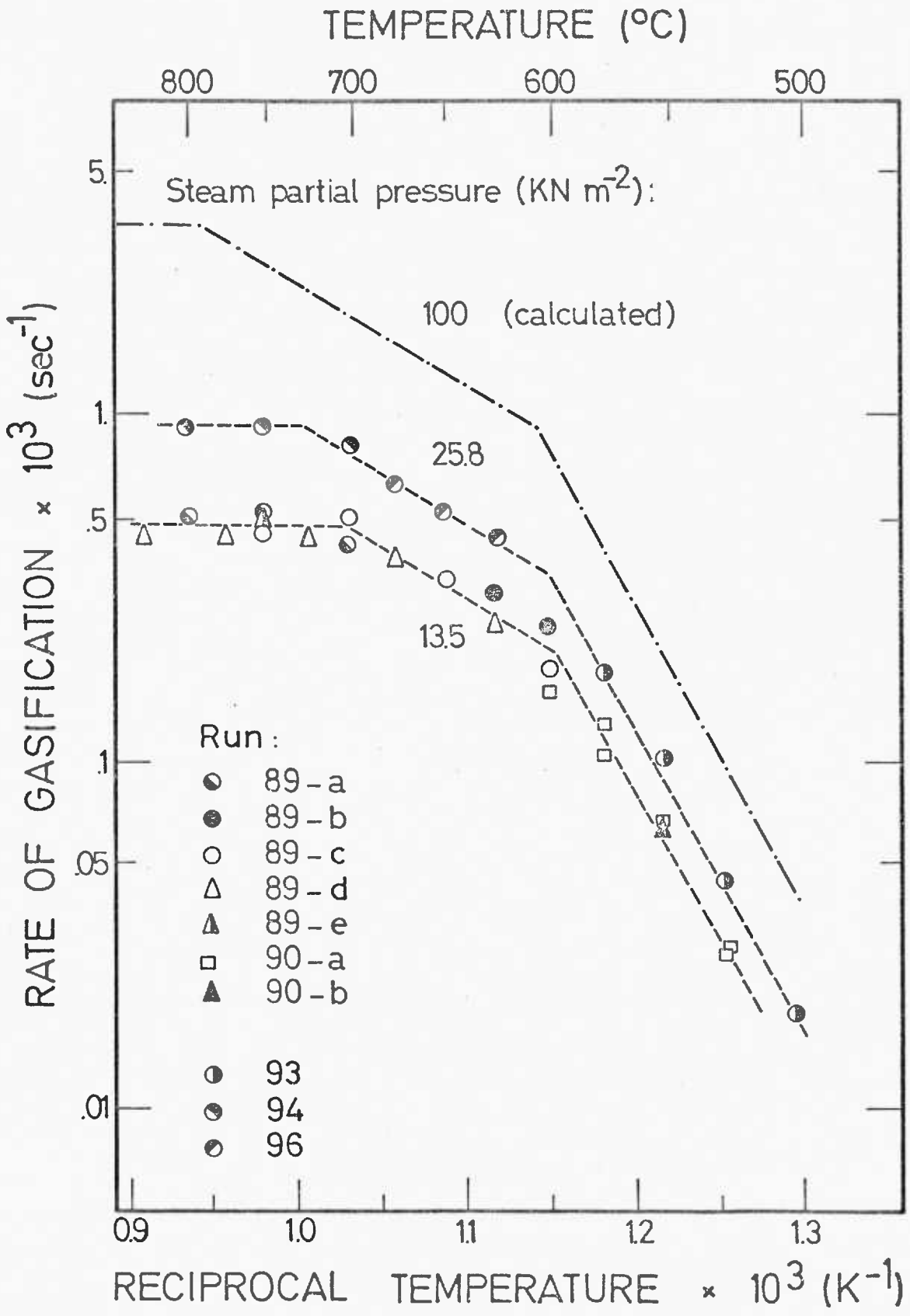

Fig. 3.44 Arrhenius-type plot of gasification rates at different steam partial pressures.

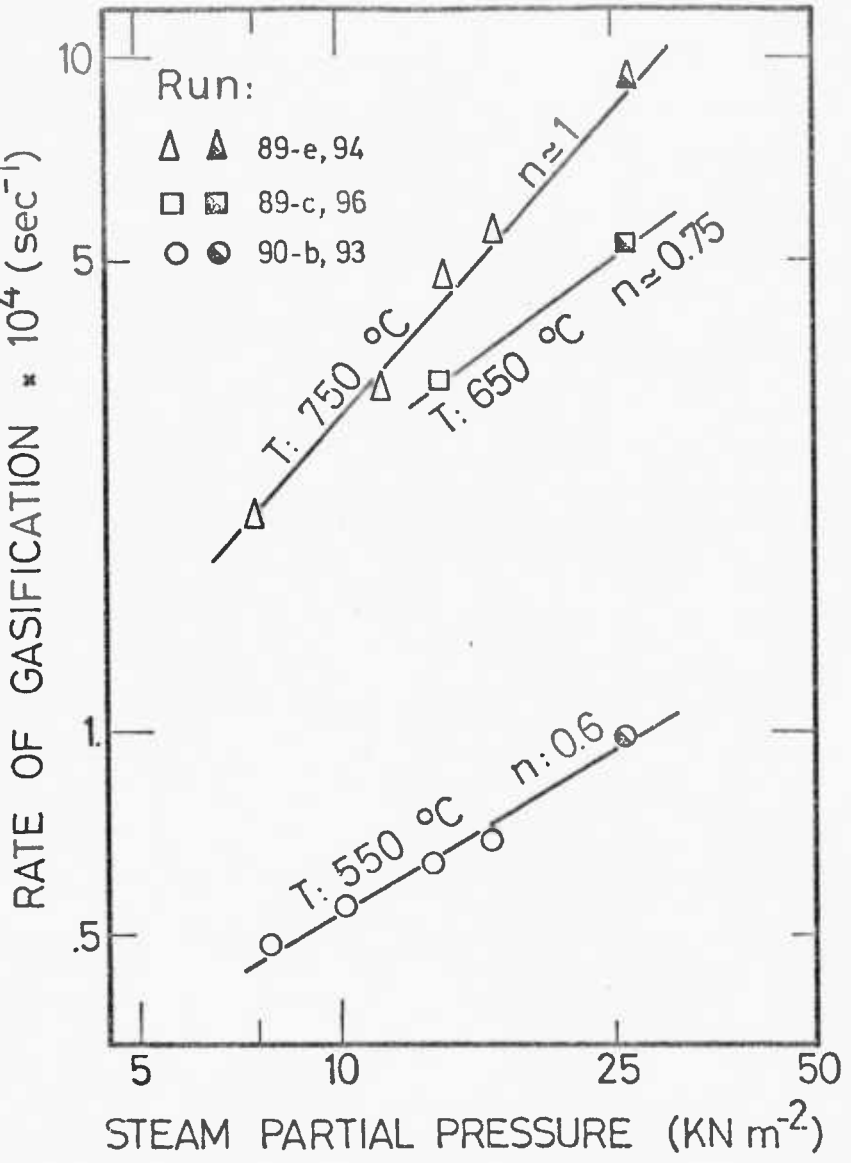

Fig. 3.45 Dependence of the gasification rate on the partial pressure of steam at different temperatures.

Fig. 3.46 Effect of the inlet flow rate on the rate of gasification at different temperatures.

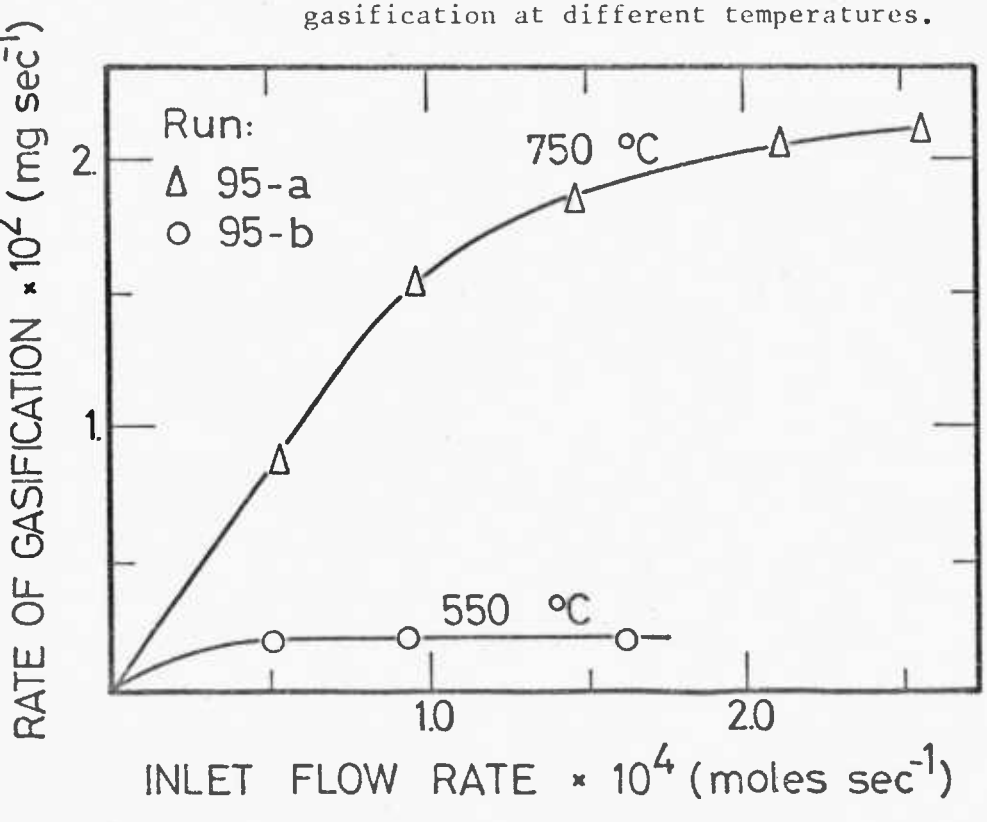

respectively). Thus, it is not surprising to observe that the gasification rate becomes closer to that of carbon dioxide as the temperature increases. The experiments represented in Fig. 3.46 were executed to obtain further evidence for the existence of film diffusion limitations at high temperatures. At 750°C the gasification rates were dependent on the total inlet flow rate up to values of 2.3×10^{-4} moles sec^{-1}. Attempts to increase the flow rate even further were hindered by growing instabilities in the microbalance head, probably due to the back-flow of steam. In fact, it was found that the best stability conditions were obtained with flow rates between 7.6×10^{-5} and 1.1×10^{-4} moles sec^{-1}. Hence, whenever possible, the inlet flow rate was maintained at 7.6×10^{-5} moles sec^{-1} throughout this work.

3.3.3.2 Stoichiometry

The effluent gases (after condensation of the steam) were analysed by gas chromatography using argon as carrier. A typical result obtained in Run 91-b, at 625°C with an outlet gas flow rate of 1.7 $cm^3(STP)sec^{-1}$:

GAS	MOLAR FRACTION
Carbon dioxide	0.0061
Carbon monoxide	-
Hydrogen	0.0127
Nitrogen	0.9812

Although theoretically possible, the presence of carbon monoxide in the gaseous mixture was not detected. This could be due to the closeness of the retention times of carbon monoxide and nitrogen (the major component of the mixture), in the conditions and with the column used.

Based on the above analysis, the reaction was assumed to proceed according to the following stoichiometry

$$C + 2H_2O \rightarrow CO_2 + 2H_2 \qquad (1)$$

Thus, per mole of carbon dioxide formed, one mole of carbon should be consumed. Moles of carbon dioxide formed:

$$\frac{1.71 \times 10^{-3} \cdot 6.1 \times 10^{-3}}{273 \times 0.082} = 4.56 \times 10^{-7} \text{ moles } sec^{-1}$$

The steady state rate of carbon gasification, as measured in the microbalance, was: 7.65×10^{-3} mg sec^{-1} or 6.38×10^{-7} moles sec^{-1}.

The difference, circa 28%, questions the validity of the stoichiometry assumed.

Two sets of chromatographic analysis were done in Run 92-a at 625°C with an outlet flow rate (after drying) of 1.72 $cm^3(STP)sec^{-1}$. The first, when the gasification was at steady state and the second at later stages, when the rate had already diminished significantly.

Gas	Composition (molar fraction)	Rate (moles sec^{-1})
Carbon dioxide	0.0079	
Carbon monoxide	-	
Hydrogen	0.0175	7.83×10^{-7}
Nitrogen	0.9746	
Carbon dioxide	0.0037	
Carbon monoxide	-	
Hydrogen	0.0084	4.01×10^{-7}
Nitrogen	0.9879	

In these conditions, the rate of carbon dioxide formation was 6.10×10^{-7} moles sec^{-1} and 2.86×10^{-7} moles sec^{-1}, respectively. Again, differences of 22 and 28% from the values that would be obtained from equation (1) were calculated.

In Run 97, the dried outlet gases flowing at 1.77 $cm^3(STP)sec^{-1}$, were analysed by injecting the mixture in a different gas chromatograph. This could separate efficiently carbon monoxide in the presence of a large excess of nitrogen.

Gas	Composition (molar fraction)
Carbon dioxide	0.0063
Carbon monoxide	0.0018
Hydrogen	0.0143
Nitrogen	0.9776

The steady state rate of carbon gasification, as measured in the microbalance, was: 6.87×10^{-7} moles sec^{-1}.

A new reaction scheme was considered assuming that, besides equation (1), the gasification was also occurring in accordance with:

$$C + H_2O \rightarrow CO + H_2 \qquad (2)$$

Furthermore, it was assumed that per each gram atom of carbon gasified through reaction (1), 0.3 gram atoms reacted to form carbon monoxide, or:

$$1.3\ C + 2.3\ H_2O \rightarrow\ CO_2 + 0.3\ CO + 2.3\ H_2 \qquad (3)$$

This scheme respected the ratio: moles of carbon dioxide/moles of carbon monoxide/moles of hydrogen, determined in the analysis.

Hence, a new relationship was formulated: per mole of carbon dioxide formed, 1.3 moles of carbon are gasified.

$$\text{Moles of } CO_2 \text{ formed} = \frac{1.77 \times 10^{-3} \times 6.3 \times 10^{-3}}{273 \times 8.2 \times 10^{-2}} = 4.98 \times 10^{-7} \text{moles sec}^{-1}$$

$$\text{moles of carbon gasified: } 1.3 = 5.28 \times 10^{-7} \text{ moles sec}^{-1}$$

The difference, 5.7%, is now within the error of the method used. The results of the analyses of Runs 91-b and 92-a should now be adjusted for the presence of carbon monoxide. Considering a molar ratio 1 : 0.3 (carbon monoxide to carbon dioxide) and dividing the rates of carbon gasification by 1.3, the previous calculations will be correct within 7%. It could be argued that, at 625°C, the carbon monoxide concentration in the gas phase should be negligible due to the water-gas shift reaction:

$$CO + H_2O \rightleftharpoons CO_2 + H_2 \qquad (4)$$

In fact, at 625°C, the equilibrium constant of reaction (4) is Kp = 2.199 (1). In all the experiments considered the partial pressure of steam in the inlet gas mixture was 13.5 $KN\,m^{-2}$. Taking into consideration the water consumption (equation (3)), the composition of the reactional mixture can be calculated. For Run 97:

Gas	Molar fraction
Steam	0.1214
Carbon dioxide	0.0055
Carbon monoxide	0.0016
Hydrogen	0.0126
Nitrogen	0.8589

Thus,

$$K = \frac{[CO_2]\ [H_2]}{[CO]\ [H_2O]} = 0.357 < Kp$$

This means that the mixture in the gas phase has not reached equilibrium with respect to equation (4).

CHAPTER 4

DISCUSSION

		Page
4.1	CARBON FORMATION ON NICKEL CATALYSTS	156
4.1.1	General	156
4.1.2	The role of the metal surface	158
4.1.3	The kinetics of acetylene decomposition	160
4.1.4	The mechanism of carbon formation	165
4.1.5	The deposition from aliphatics and aromatics	170
4.1.6	The negative dependence of the rate of deposition on temperature	174
4.2	GASIFICATION OF CARBON DEPOSITS	185
4.2.1	General	186
4.2.2	Gasification by carbon dioxide	187
4.2.3	Gasification by hydrogen	192
4.2.4	Gasification by steam	195
4.2.5	Comparison of the carbon gasification rates	197
4.3	CARBON DEPOSITION IN THE PRESENCE OF STEAM	199

CHAPTER 4

DISCUSSION

4.1 CARBON FORMATION ON NICKEL CATALYSTS

4.1.1 General

The deposition of carbon from hydrocarbons on nickel has been the subject of several previous investigations (Chapter 1). It is useful to review here, albeit briefly, the state of knowledge at the start of this study and to show how the various topics investigated fit the overall picture.

Carbon formation occurs when unsaturated hydrocarbons are passed over nickel at temperatures greater than 375 - 400°C. Three kinetic regions have been identified: low temperatures (below 500°C), where the reaction is essentially zero order and has an apparent activation energy (E_A) of circa 144 KJ/mole, intermediate temperatures (500 - 650°C), where the apparent activation energy is negative and the orders of the reaction are positive, and high temperatures (< ∿ 675°C), where E_A is again positive and the orders are generally positive.

Whenever deposition occurred, the general pattern would be the same, provided "deactivation effects" were absent. After an induction period of variable duration, an acceleratory period would follow leading to a steady state rate of carbon deposition. The steady deposition was sometimes maintained until the limit of the largest range of the microbalance. The duration of the induction period, and the lowest temperature at which deposition could be observed, was dependent on the hydrocarbon, the type of catalyst used and on the presence or absence of hydrogen in the system.

Deactivation could be observed, in some instances, as a loss of catalytic activity with the deposition of carbon. No direct correlation exists between weight of carbon and deactivation. This has been explained in terms of deposition of two different types of carbon, one of which deactivates the nickel and one of which does not.

The present studies have been concerned with different aspects of the problem. Initially attempts were made to identify a common mechanism for the production of carbon from all hydrocarbons at low temperatures (3.2.1.1, 3.2.1.4 and 3.2.2.1). These were unsuccessful.

The kinetics of the deposition from acetylene showed the common features already mentioned (zero orders and a similar value of E_A), but with aliphatic and aromatic hydrocarbons, the apparent activation energies observed were dependent on the nature of the hydrocarbon. A different mechanism must be operative in these cases.

The rates of carbon deposition from the various hydrocarbons were compared at low temperatures, showing the following order of reactivity.

acetylene $\geqslant$ olefins > one ring aromatics $\sim$ C_6-aliphatics > C_2-aliphatics

The carbon formed at low temperatures is mainly turbostratic in nature and does not apparently cause deactivation (3.2.2.1). Nickel is always found in the deposits, its concentration being approximately independent of the amount of carbon.

The present work also shows that, above 500°C, the increasing importance of a different type of carbon formation may cause deactivation of the catalyst by encapsulating the nickel particles. The role of hydrogen is paramount in preventing the formation of this type of carbon. In the case of aliphatic and aromatic hydrocarbons some deactivation is always present (3.2.2.2), whereas with acetylene and olefins it can be completely prevented. In this case , the negative values of E_A observed are explained using a model based on the effect of the heats of adsorption of the reactants on the rate expressions (3.2.1.3).

In terms of the mechanism for carbon formation previously proposed (see discussion in next section), it was expected that grain boundaries, as well as the condition of the metal surface, would play an important role in the process of deposition. This was confirmed in experiments with polycrystalline and single crystal nickel foils (3.2.1.1 and 3.2.1.2). Single crystals were further used to prove that carbon diffusion through nickel is involved in the process (3.2.1.5.3).

The particular aspects of the different systems studied will now be discussed in detail.

4.1.2 The role of the metal surface

The common kinetic features described in 4.1.1 for the deposition of carbon from acetylene and the olefins on nickel were explained in terms of a general mechanism (56). The mechanism suggested that nickel particles, separated from the bulk of the metal, can act as centres for further carbon growth. Carbon dissolves in, diffuses through and precipitates from the particles, leaving a free surface for the decomposition of the hydrocarbon.

In such a mechanism the process of breakaway of nickel particles is of paramount importance. Several factors play a part in this process. Thus, it is necessary for carbon to nucleate on the surface, to dissolve in the nickel and to precipitate, this precipitation leading to breakaway. It could be expected that the smoothness of the surface or the possible different activity of distinct crystal planes would affect the nucleation rate. Dissolution of carbon in nickel should be dependent on the type of carbon deposited and on the amount of carbon already in solution. Precipitation, particularly at a favoured site such as a grain boundary, could well lead to dislodgement of the metal particle above the boundary. In addition, mechanical breakaway of projections on the surface could occur.

In the light of these ideas it was expected that carbon deposition on electropolished nickel single crystals would show significantly longer induction periods than on polycrystalline foils of the same size and finishing. As can be seen in Fig. 3.8 this was not the case, although the initial rate in the latter was much higher. Microscopic observation of both samples at early stages of deposition showed that the growth of carbon is more limited and localised on the single crystal. On the polycrystalline foil carbon seems to grow all over the surface. It is probable that the defects still present on the surface of the single crystal provide enough sites for a rapid nucleation. However, because the number of nucleation sites is smaller, the initial deposition rate will also be proportionally smaller.

One interesting feature emerging from the deposition on single crystals is the relative rates of carbon formation on the (111), (110) and (100) faces of nickel presented in Fig. 3.9. The orders of reactivity reported by Presland et al. (6) and Grenga and Lawless (37) - (111) > (110) > (100) - are only correct above a certain weight

of deposit. At earlier stages of deposition, the rate of carbon formation on the (110) face is greater than on the (111) face. Since, at this stage of the reaction, carbon is deposited on clean nickel, geometrical arguments (like the close fit of the (002) faces of graphite over the (111) faces of nickel [6]) must be rejected. However, the orientation of the crystal may affect the crystallinity of the deposit, as shown in 3.2.1.5.4.

At later stages of the reaction, where the rate is greater on the (111) face, carbon is probably also being deposited on nickel particles which are removed from the crystal face. Under these circumstances, the rate of deposition should depend on the number of nickel particles in the carbon deposits. The relative reactivity of the three faces at this stage could thus be a consequence of the relative ease with which the particles are removed from them. This could depend more on the presence of topographical imperfections on the surface and on the size of the sample than on the crystal orientation. The reversal of reactivity of the (110) and (111) faces at later stages of deposition further indicates that the break-away of particles is not connected in a straightforward way with the ease of nucleation on the surface.

The importance of the surface imperfections was also demonstrated by comparing the deposition on polycrystalline foils of the same size but different finishing: the initial rate of carbon formation is much smaller on an electropolished foil than on an unprepared one.

An argument similarly based on the energetic heterogeneity of the surface can be used to explain the enhanced carbon deposition observed in the present work near the edges of the foils. In fact, the edges are zones where the crystal lattice has been severely disrupted and should thus provide preferential sites for nucleation and growth of carbon. This also explains why smaller samples showed consistently higher specific activity. Considering that the ratio perimeter-area increases when the size of the foil decreases, the smaller the sample the greater the rate of deposition per unit area.

In the work reported in 3.2.2.1 and 3.2.2.2 pre-reduction of the samples in hydrogen was found to increase moderately the rate of carbon formation once the reaction started. This could be due to different reasons. The obvious one was the removal of surface oxide.

However, it has been observed that sulphur impurities, present in minor concentrations in the bulk of the nickel, can at the reaction temperature, be segregated to the surface forming a two-dimensional sulphide (115). Thus, the reduction of this sulphide could also explain the increase in the rate. With our samples, the Electron Spectroscopy For Chemical Analysis (ESCA) described in 3.2.1.2 failed to detect the presence of sulphur on the surface. As the ESCA evidence for the presence of nickel oxide on the surface of the annealed samples is undeniable, the hydrogen effect should be mainly explained by the reduction of the oxide. Hydrogen could also cause grain boundary delineation, making it easier for particles to break away.

4.1.3 The kinetics of acetylene deposition

The steady state kinetics reported in 3.2.1.1 for the deposition on polycrystalline foils under batch conditions are in general agreement with the mechanism reviewed in the last two sections. From the data in Tables 3.1 and 3.2 it can be seen that both the orders and the activation energies have the value that should be expected (56).

Orders vary from zero at low temperatures (< 475°C) to one at high temperatures and, at the same time, the activation energy changes from a positive to an apparent negative value. The change of rate determining step from carbon diffusion in the metal (below 475°C) to a pressure dependent surface reaction also explains the increase of T_{max} with the acetylene pressure observed in Fig. 3.7.

The curves of rate vs. conversion shown in 3.2.1.1 present in general two maxima. The first maximum may be due to the combined effect of nucleation and self-poisoning, while the second should be related to the positive effect on the rate of reaction of the hydrogen being produced (autocatalysis). The discussion of these effects will be facilitated considering a schematic representation of the various steps involved in the process, as shown in Fig. 4.1.

The process of carbon formation on a catalytic surface involves:

(a) Decomposition of the gas on the surface;
(b) Diffusion of the species formed;
(c) Growth of carbon.

Before growth can start, nucleation has to take place. If the

MECHANISM:

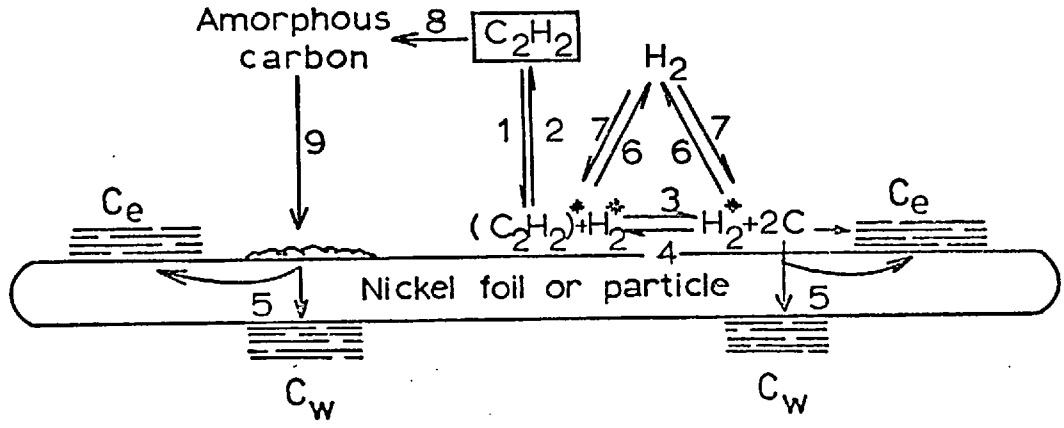

Fig. 4.1 The mechanism of carbon formation.

Steps:
1) Adsorption of acetylene;
2) Desorption of acetylene;
3) Surface decomposition;
4) Surface reformation;
5) Carbon diffusion through nickel;
6) Hydrogen desorption;
7) Hydrogen adsorption;
8) Homogeneous pyrolysis;
9) Diffusion to the surface.

*The nature of adsorbed species is not stated.
C_e - "encapsulating" carbon; C_w - filamentous carbon.

growth process is the rate controlling step, a continuous acceleration should be observed, as the size and number of nuclei increase. This must be the case in the early stages of the deposition. If the surface reaction is controlling, a continuous decline in rate would be expected, as the area available for the gas reaction is progressively reduced by the growth of carbon on it. Now, when the carbon diffusion step is the slower and controlling one, the rate will be a function of the size and number of both the uncovered metal surface (source of carbon atoms) and the nuclei formed (sink of carbon atoms). So, an acceleration is to be initially expected, as the nuclei are formed and grow, but at the same time the metal area is being reduced and this will eventually lead to a decline of the observed rate. This is thought to be the cause of the occurrence of the first peak in the rate curves.

If a steady state situation is not reached at some stage, with certain areas being available for the decomposition and other areas being active for growth, the process of self-poisoning may be total and the reaction stops. This is probably what happens in some systems. In the case of the deposition from acetylene on polycrystalline nickel foils however, a steady state seems to be reached. This is evident from the flow experiments data (cf. Fig. 3.6). Whether a maximum in the rate is observed or not depends on when the steady state is established: early in the acceleratory period or later after some deceleration has already taken place. This could explain the different curves obtained from olefins in previous work (56) and those presented in 3.2.1.1.

The effect of hydrogen in the reaction is complex. In Figs. 3.3 and 3.2-b it is seen that the first peak increases with increasing hydrogen pressure, as it does with acetylene pressure. However, the degree of self-poisoning seems to be more drastic for higher hydrogen pressures, as observed in Fig. 3.3. It is interesting to note here that a similarly ambiguous effect of hydrogen addition was reported by Walker et al. (112) for the carbon deposition from carbon monoxide on iron catalysts.

The effect of hydrogen in the later stages of the deposition is more clear. Assuming that at 10% conversion the process of growth is stablised, and that the orders to acetylene pressure (P_A) and to hydrogen pressure (P_H) are 1, the rate is given by:

$$r = k\, P_A\, P_H = k\, P_{Ao}\, (1 - x)\, (P_{Ho} + P_{Ao} x) \qquad (1)$$

where x is the fractional conversion of acetylene and P_{Ao} and P_{Ho} are the initial pressures. This equation expresses the autocatalytic effect of hydrogen on the reaction. Application of the above equation with appropriate k values to the upper and lower curves showed in Fig. 3.4 (0 torr and 400 torr of hydrogen, respectively) gives the good fitting presented in Fig. 4.2. The fitting for the intermediate curves (100 torr and 200 torr) is not good, suggesting that the growth has not stabilised, that is to say, self-poisoning is not confined to the early stages of the deposition. Radical changes in the structure of the deposit possible go on for a much longer time.

The non zero orders sometimes observed for hydrogen at low temperatures are somewhat anomalous. In fact, all the evidence points to a carbon diffusion controlled mechanism at these temperatures. The slight effect of hydrogen could possible be attributed to a rearrangement of the morphology rather than to a purely kinetic effect. An increase in hydrogen pressure may not accelerate the rate of the surface reaction but can have an effect on the stability of the metal particles or other solid phases involved, so that the area available for reaction can be increased or reduced. This is consistent with the somewhat ambiguous effect of hydrogen in Fig. 3.3.

The extension of this discussion to the deposition of carbon from acetylene on nickel single crystals is limited by the absence of a true steady state in this case. In fact, at low temperatures the results should be affected by deactivation (see 4.1.6). However, as this is slow, the deposition rate is reasonably repreducible for limited periods of time. Some comparison between the two systems can thus be made. Consider, for instance, the Arrhenius-type plot presented in Fig. 3.10, which refers to the deposition on three faces of nickel. Below 500°C the deposition rate decreases when temperature increases. The same happened with polycrystalline foils above T_{max}. At higher temperatures, the activation energy obtained is + 207 KJ $mole^{-1}$, in accordance with that of the thermal decomposition of acetylene (72).

The temperature at which the homogeneous process begins to be detected is circa 50°C lower than that for the polycrystalline foil in batch conditions (53). This can be understood by considering that the homogeneous and heterogeneous reactions are competitive parallel

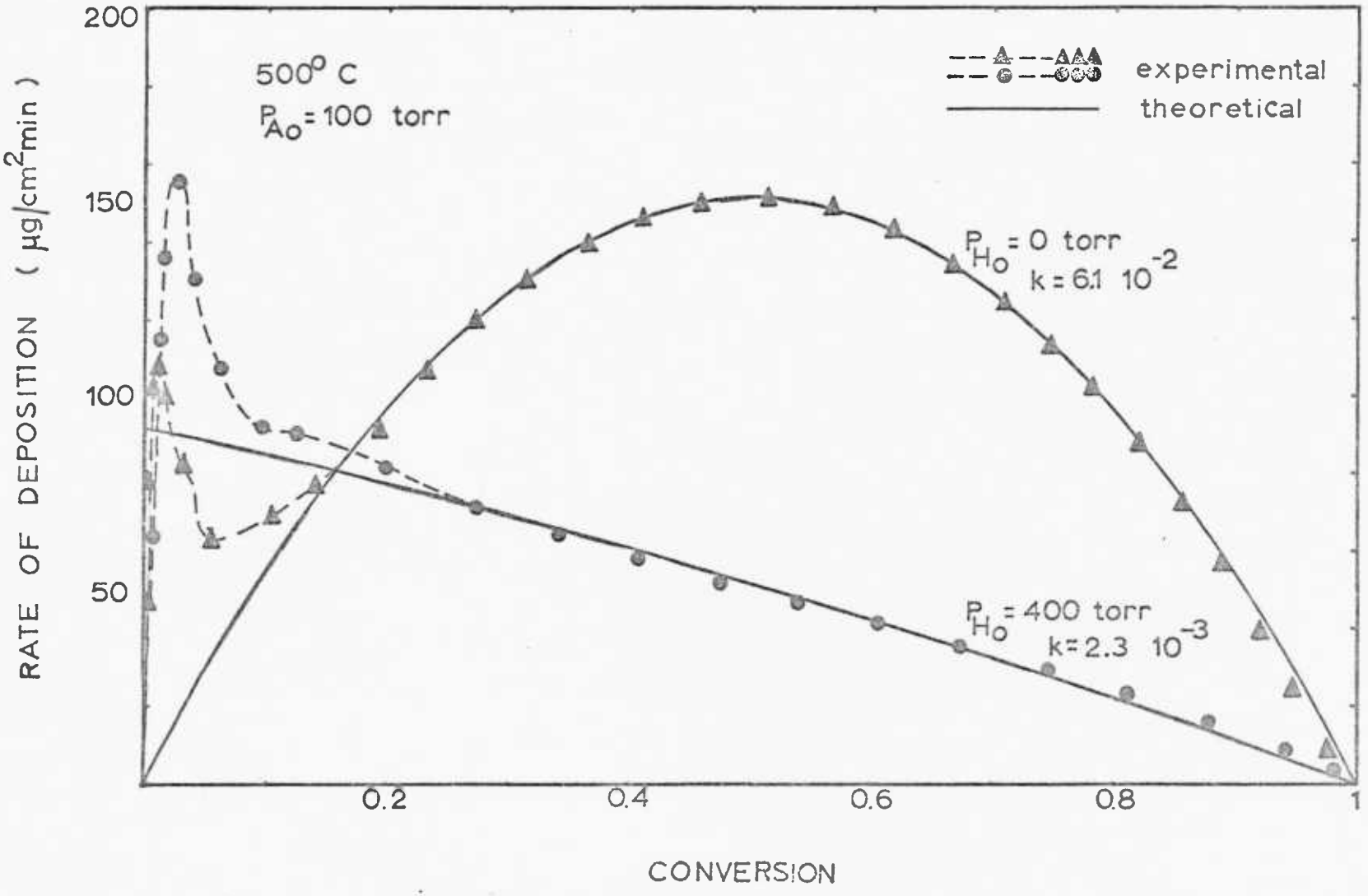

Fig. 4.2 Experimental rates of carbon deposition compared with a theoretical autocatalytic model (Equation (1)).

processes (e.g. Routes C and A on page 184). In the case of the single crystal, the heterogeneous process is much less important at these temperatures due to the limited amount of active sites on the surface. Hence, if the homogeneous process is independent of the metallic surface (see discussion in section 4.1.6), the change in rate controlling step will occur at lower temperature.

As the main features of the deposition from acetylene agree with those observed with olefins (existence of an extended steady state of deposition, similar values of the rate) (56), a common mechanism should be operative with all these hydrocarbons. Furthermore, as the kinetics determined at lower temperatures are also common, (zero order kinetics, same activation energy), the rate controlling step should be the same at these temperatures.

The common mechanism will now be discussed in detail.

4.1.4 The mechanism of carbon formation

The points to be answered in this section are:

- To what extent does the morphology and the nickel distribution of/in the carbon deposits fit the mechanism proposed on kinetic grounds?
- In what way do grain boundaries influence the deposition both at initial and later stages?
- Can the bulk diffusion of carbon in nickel justify the kinetics observed at lower temperatures?

Morphology and composition of the carbon deposits

The results shown in Figs. 3.15a-e) throw some light on the morphology of the carbon formed on the surface during the catalytic cracking of acetylene under batch conditions. Comparing these results with Fig. 3.2b), for instance, it seems clear that the process of growth of carbon nuclei brings about the self-poisoning of the surface and causes the decrease in the rate (cf. Figs. 3.15 a to d). The fact that the reaction does not stop and would eventually reach a steady state implies a constant amount of available metal area thereafter. The process of whisker growth, already mentioned, could justify this constant area via the nickel particles carried at top of the carbon fibres. It is possible that the second type of formation seen in Figs. 3.15 d,e) represents the development of this process. After the

initial competition for the available surface between the different types of carbon (platelet, filamentous (36)) whisker growth becomes predominant. It is interesting to note that the EPM analysis of the deposits in the conditions of Fig. 3.15d) shows a definite increase in the concentration of nickel in the outer layers (cf. Figs. 3.16 and 3.17). However, after some time the growth of a given fibre stops when the nickel particle at the top is encapsulated by carbon. The termination process is well documented, the average length of a whisker being of the order of 0.5-1.0 μm (36). New fibres are formed, probably due to the surface diffusion of new nickel particles from the surface to the region of carbon growth (116). The breakage of a nickel particle on top of a fibre originating new fibres has also been observed (36). In the deposit shown in Fig. 3.15e), the thickness of the carbon layer is greater than 35 μm. Hence a large number of fibres should have contributed to its formation. By then, a significant amount of nickel must be trapped inside the deposit. This explains why no preferential orientation in the nickel distribution was detected in the EPMA of thicker deposits. All these factors should determine the concentration of nickel inside the carbon. If the deposts were formed by a single set of carbon fibres with a nickel particle at the top, the curve of nickel concentration vs. extent of deposition should be similar to the broken line (- - -) in the figure:

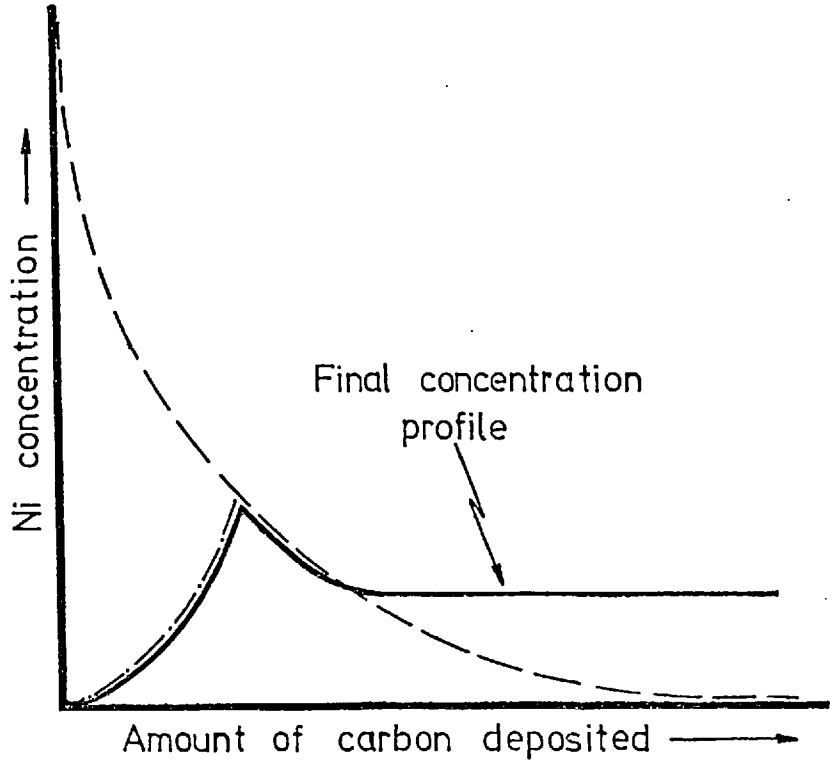

However, such an hypothesis is an extreme simplification. In the initial stages of deposition, other types of carbon are preferentially formed, probably without involving removal of nickel from the surface. Eventually, as discussed above, they will become unimportant. The concentration profile should thus be corrected accordingly (-•-).

Furthermore, a sequence of nickel fibres rather than a single set are involved in the formation of the deposits. Apparently the number of fibres being terminated and initiated is constant (or rather the total available area of the nickel particles at their top is constant), because a steady state rate is observed. The final concentration profile should then be represented by the continuous line in the figure.

These ideas are in line with the fact that the nickel concentrations determined in the carbon deposits are almost independent of the extent of the deposition (from 6 to 85 mg of deposit).

It is interesting to compare the curve obtained with those in Fig. 3.2-b. If it were not for the presence of the hydrogen autocatalytic effect, the shape of the curves would be almost the same. It is possible that there is a correlation between the nickel concentration in the carbon deposits and the rates observed. For instance, as discussed in 4.1.3 the decrease in rate after the first maximum can be explained by the decrease in the nickel area available. It is also interesting to note that the analysis of the deposit formed on a nickel single crystal shows almost all the nickel inside the carbon layers (cf. Fig. 3.16) When the growth of carbon nuclei stops due to self poisoning, no more nickel particles are carried away from the surface. Some fibres may have been formed but were terminated without being replaced by new ones. Here, again, the link between grain boundaries and the predominance of a whisker-like type of carbon (after the initial stages) appears to be evident. It is not surprising to observe that the deposition rate was minimal under the conditions where the deposit analysed was obtained.

The role of carbon diffusion through nickel in the deposition process

A considerable amount of experimental evidence supports the view that carbon diffusion through the bulk metal plays an important role in the process of carbon formation on nickel at low temperatures (cf. Fig. 4.1). The arguments for this view have already been presented in the

Introduction and will not be repeated here. However, it is important to discuss to what extent the present results are in accordance with them. In 3.2.1.5.3 it was shown that, for acetylene below 475°C, bulk diffusion was involved in the process. In no other way, as pointed out for Run 13, could carbon grow in the poisoned face while the uncoated one remained almost undeposited. The results also show that the absence or presence of grain boundaries determines to what extent nucleation and growth of carbon can occur without diffusion into the bulk metal. If diffusion is also absent at later stages of deposition no steady state will be detected, as observed in 3.2.1.2. Apparently grain boundaries make the existence of a driving force for bulk diffusion possible. The nature of this driving force needs some further explanation.

It has been suggested that the driving force could be due to a temperature gradient developed across the metal particle (by the exothermic decomposition of the reacting hydrocarbon) (36). As pointed out by Figueiredo (7), this argument should be dismissed since the mechanism must be operative for all olefins, and some of the reactions are endothermic. It has been argued recently (68) that in the case of the endothermic decomposition, the gas-phase reaction can produce intermediates that form carbon exothermically over the catalyst. This argument cannot be accepted for some of the endothermic carbon formation reactions in which the mechanism was shown to be applicable (56). In fact, the gas-phase conversion should be minimal under the experimental conditions used.

The concentration driven diffusion mechanism postulated by Lobo et al. (56) appears to be more likely. Two problems arise when considering this mechanism. First, the existence of a concentration gradient across the metal particle requires the definition of the limits of concentration on the decomposition side and on the growth side. So if carbon diffusion were rate controlling, the change of carbon solubility with temperature ($\Delta H_S \simeq 42$ KJ/mole (117)) should be reflected in the activation energies measured. However, the value obtained in the present work for acetylene, 128-132 KJ/mole, coincides "per se" with the activation energies reported in the literature for diffusion of carbon through nickel, 128-145 KJ $mole^{-1}$ (118-121).

In fact, this contradiction seems to derive from incorrect data. The literature values are based on experiments performed at much higher

temperatures (800-1200°C) than those reported here. A more recent study in the temperature range 350-700°C gives a much lower value for the activation energy of carbon through nickel, 84 ± 8 KJ $mole^{-1}$ (122). The two values are probably related to two different modes of carbon diffusion: an interstitial mechanism at low temperatures and a vacancy mechanism at higher temperatures. A similar shift of mechanism is known to occur in the C-α Fe system (122).

The calculation of the apparent activation energy for the process must be based on the lower temperature value, 84 KJ $mole^{-1}$. The result, 84 + 42 = 126 KJ $mole^{-1}$ is now in good agreement with the observed values.

The second problem with this mechanism is that it involves diffusion of carbon from a side of the particle in contact with carbon bearing gases (source) to other in contact with carbon deposits (sink). Apparently the direction of the process should be the reverse. At the sink side, preferential nucleation on energetically favourable sites can facilitate the growth of carbon. Considering the grain boundaries to be one of such sites, the results in the present work support the view that the growth can occur without a significant supersaturation of the metal by carbon. It remains to be explained how it is possible to have on the source side a concentration of carbon above the saturation without precipitation of carbon. The best explanation has possible been presented by Rostrup-Nielsen and Trimm (45). They considered that the activity of carbon in a mixed gas can be far higher than unity and that as a consequence, the solubility of carbon in nickel in the source side can be much higher than that observed in the nickel graphite system. Using their ideas it is possible to discuss the experimental evidence available. Baker et al. (36) reported that carbon filaments with "pear shaped", 30 nm wide, nickel particles at their ends, grew with a rate of circa 75 nm sec^{-1} at 600°C. They also observed a dense external wall in the filaments and a more loose core, including a central hole channel. In this case, a calculation of the diffusion controlled rate of growth can be attempted. Knowing the exact geometry of the system the probable size of the diffusion path can be estimated. Hence an approximate law (56):

$$\text{Rate} = \frac{D\Delta C}{\ell}$$

can be used and the result compared with the observed rate of growth of an individual whisker.

For particles such as these, the distance the carbon atoms have to diffuse to feed the wall growth is probably not more than a few nanometers (say 2 nm). At 600°C, the diffusivity coefficient of carbon in nickel is estimated to be 3.4×10^{-10} $cm^2 sec^{-1}$ (117). ΔC will be the difference between the solubility of carbon in a nickel gas system and in a nickel-graphite system, circa 1.8×10^{-3} g cm^{-3} (73). This gives:

$$\text{Rate} \simeq 3.1 \ \mu g \ sec^{-1} \ cm^{-2}$$

Assuming the density of partially graphitised carbon to be approximately 2, the linear rate of growth will be circa 15 nm sec^{-1}. This is well within the order of magnitude of the value experimentally observed. The diffusion of carbon into the inner regions of the filament should be much slower, as the distance to be crossed is of 10 nm or more. So the process is at least 5 times slower, and the rate at which the core is filled does not keep pace with the faster wall growth. Accordingly, the density of the core is lower and an hollow channel is observed in the less accessible central region.

It should be noticed however, that calculations of this type are of limited value when the actual geometry of the system is not known. Due to the extent of the uncertainties involved, they should not be used to justify a supposed mechanism.

4.1.5 The deposition from aliphatics and aromatics

Aliphatic hydrocarbons

The kinetics of carbon deposition from aliphatic and aromatic hydrocarbons on nickel catalysts were determined in an attempt to generalise the mechanism previously described to these systems. Below 500-525°C the apparent activation energies (E_A) measured changed with the hydrocarbon but were not significantly influenced by the type of catalyst. (200 ± 10 and 176 ± 12 KJ $mole^{-1}$ for ethane and n-hexane, respectively). With both aliphatics, first order with respect to the hydrocarbon and negative orders with respect to hydrogen (greater in absolute value in the case of ethane) were measured. As the temperature increased above 500-525°C the former decreased slightly and the latter became closer to zero. E_A decreased but still main-

tained a positive value.

At low temperatures the values of E_A are dependent on the nature of the parent hydrocarbon and the reaction orders measured are different from zero. Hence carbon diffusion through nickel cannot be considered to be the rate controlling step. This is a major difference from acetylene and the olefins. The nature of this step will depend on the relative rates of the different steps on the surface (or in the bulk) of the metal considered in the mechanism:

(i) surface reaction leading to carbon species that dissolve in the metal
(ii) bulk diffusion of carbon
(iii) precipitation of carbon leading to whisker growth.

For olefins and acetylene, step (i) is fast and step (ii) is rate controlling. If step (i) were slow it would limit the rates observed. This could be the case of aliphatics, as can be inferred from the relative rates of carbon deposition shown in table 4.1.

Table 4.1 Comparison of the steady state rate of carbon deposition from different hydrocarbons on nickel foils (Conditions: 500°C; 25 KN m^{-2} H_2; 13 KN m^{-2} hydrocarbon, rate calculated when necessary)

Hydrocarbon	Rate (μg sec^{-1} cm^{-2})*	Comment
acetylene	2.0	batch
propylene	2.5	from ref (7)
ethane	1.0×10^{-1}	-
n-hexane	7.2×10^{-1}	N_2 diluent
benzene	≃ 1.0	from ref (71)

* referred to the initial area of the foil

The calculation at the end of section 4.1.4 can be repeated at 500°C to give a rough estimation of the limiting rate at which carbon diffusion in nickel becomes important. This gives a value of about 1 μg sec^{-1} cm^{-2}, referred to the unit metal area.

The deposition rates of the aliphatics are below the limiting value (more so in the case of ethane) at low temperatures. Hence, the surface reaction could be controlling the rate.

Above 500-525°C the surface reaction could also be rate controlling. This situation occurs with unsaturated hydrocarbons at these temperatures (cf. 4.1.6). The observed decrease in E_A would then be explained by the enhanced desorption of the reactants (because the negative heats of adsorption are becoming increasingly important in the rate expressions). If this were the case, an increase in the reaction orders would be expected as the temperature increases above 525°C. The orders with respect to both ethane and n-hexane decreased, albeit slightly. As the decrease is small, this is possibly without significance. The orders with respect to hydrogen did increase from negative to near zero values. This may indicate strong hydrogen adsorption on the surface (competing with the hydrocarbon for the same sites) at low temperatures, progressively becoming less important as temperature increases.

Different apparent activation energies were measured above 525°C for the deposition from n-hexane on foils and supported catalysts (46 and 116 KJ $mole^{-1}$, respectively). If the surface reaction were rate controlling in both cases, E_A should be approximately the same considering the closeness of the partial pressures of the reactants.

One alternative explanation is that, with supported catalysts, diffusion of the reactants is limiting the rate at these temperatures. This explanation is also consistent with the values of the orders observed. In fact, the hydrogen molecule can be expected to have an easier access to the active reaction sites than the much larger n-hexane molecule. Hence, the reaction rate will be nearly independent of hydrogen pressure (order zero) and will depend on the pressure of n-hexane (order 1).

More probably, a clear cut situation does not occur and the rates of deposition from n-hexane in this temperature zone are determined simultaneously by the surface reaction and the diffusion process. The importance of the latter would be proportionally greater with supported catalysts. Contrary to the case of unsaturated hydrocarbons, no carbon deposition was detected at low temperature in the absence of hydrogen. This could be due to the lower reactivity of the aliphatics already mentioned. The process of carbon formation involves the sur-

face dehydrogenation of the hydrocarbon to form an adsorbed carbon species (see discussion in next section). If the absorbed hydrocarbon is sufficiently reactive, the reaction can proceed without hydrogen. When the reactivity is low hydrogen is necessary to produce the carbon species, probably via an hydrogenolysis process (56).

Increasing hydrogen pressures have a negative effect on the deposition rate. This could be due to:

(a) the aforementioned competitive adsorption of hydrogen and hydrocarbon and

(b) the reverse reaction of surface hydrogenation becoming important, once the surface concentration of the carbon species is significant.

The removal to the gas phase (as methane) of this species by hydrogen gasification should not be considered, because the rate of hydrogen gasification is negligible below 500°C (cf. 3.3.2).

As the temperature increases above 600-625°C, the deposition rate decreases. Time deactivation effects are detected in almost all cases. These effects can be explained by the strong adsorption on the catalyst surface of polynuclear aromatic species formed by aromatisation and polymerization, either on the surface or in the gas phase. A more detailed discussion is presented in the next section.

At even higher temperatures, the rate of carbon formation is certainly determined by thermal pyrolysis, leading to the direct formation in the gas phase of homogeneous carbon (soot). This can occur without direct involvement of the metal surface. In the case of ethane, for instance, the value of E_A measured in Fig. 3.21 above 700°C (circa 220 KJ mole^{-1}) is similar to that reported in the literature for the thermal decomposition, 242 KJ mole^{-1} (123).

Aromatic hydrocarbons

Some common characteristics can be found at low temperatures (below circa 575°C) between the deposition of aromatic and aliphatic hydrocarbons. As seen in Fig. 3.25 the apparent activation energy depended on the nature of the parent hydrocarbon and the orders determined were different from zero. Thus, carbon diffusion through nickel cannot be the rate limiting step at these temperatures.
It should be noticed, however, that in a previous work on carbon deposition from benzene on nickel foils, this step was in fact considered

rate determining in this zone (71). Values of the order were not reported. The determination of the true nature of this step must remain tentative until results are gathered for more aromatics, especially values of apparent activation energies and orders of reaction.

Above 600°C E_A decreased, becoming negative in the case of toluene. The data obtained were not enough to allow the identification, even tentatively, of the rate determining step. Above 650°C there is undeniable evidence of time deactivation effects, especially important in the case of benzene.

Above 700°C the deposition rate increased again with temperature. With toluene the gas phase conversion was not significant until 750-775°C (no determination was made with benzene). The reason for this apparent anomaly would appear to be the possibility of homogeneous reactions initiated on a surface (26). If a metal is present, it could provide the intermediates necessary to start the gas phase reaction at lower temperatures than those necessary in the absence of metal. Polynuclear aromatic species could thus be formed in small quantities in the gas phase and adsorb and grow on the surface of the solid.

4.1.6 The negative dependence of the rate of deposition on temperature

In the mechanism for carbon formation described previously for acetylene and the olefins, the surface reaction was supposed to be the rate controlling step at temperatures between circa 550 and 675°C. The increasing importance of the desorption of the reactants from the metal surface was used to explain the decrease in rate with rising temperatures. In the case of propylene, it has been shown (7) that high partial pressures of hydrogen were able to prevent deactivation of the catalyst in this temperature zone. However, no attempt has been made to verify the assumption on the nature of the rate controlling step and to extend the determination of the kinetics to other hydrocarbon systems.

The results presented in 3.2.1.3 show that hydrogen can indeed prevent deactivation in the case of acetylene and various olefins. Keeping the hydrogen pressure above an experimental minimum, the kinetics of the deposition can be determined and the results used to fit the experimental rate with theoretical models based on the control by the surface reaction. Several models were considered, and rate equations were generated. The most relevant of these are summarised in table 4.2. Since the experimental evidence shows that both hydrocarbon and

hydrogen affected the rate, the rate equations were suitably adjusted.

The experimental results were tested against these models using a computer program (see Appendix A), a model being considered acceptable when the "standard deviation" (σ) was of the order of the experimental error (without systematic deviations). σ was defined as:

$$\sigma = \sqrt{\frac{\sum (E_R)^2}{(N - n)}}$$

Where E_R - relative error = $\frac{\text{calculated rate} - \text{measured rate}}{\text{measured rate}} \times 100$

N - number of experimental points (rates measured)

n - number of parameters of the model.

The rate equation selected for a given hydrocarbon was the one with smaller σ for the smaller number of parameters. Table 4.3 summarises the mechanisms selected. It is apparent from this table that a Langmuir-Hinshelwood type mechanism may be operating in all cases. The fitting allows the determination of specific rates, k, and of the adsorption equilibrium constants, b_H and b_C. These are also presented in the table, as well as the range of experimental conditions in which the models were applicable.

An analysis of the rate expressions shows that the experimental "apparent activation energy" must depend on the value of the reactants pressure at which it was determined. By plotting rates (calculated with the best values of the parameters) as a function of the partial pressure of one reactant and keeping the pressure of the other constant, the range of conditions where the rate expression can be reduced to a power law is easily determined. Fig. 4.3, refers to one such plot for 1-butene at 625°C. It can be concluded from the figure that for very low and very high partial pressures of hydrogen, the rate expression can be simplified and written as the product of a pressure and a temperature dependent factor. The temperature dependent factors and their applicability are listed in Table 4.4 for the three hydrocarbons.

Some idea of the validity of the values in table 4.3 may be obtained from the dependence of b_H on temperature. Over a short temperature range, the heat of adsorption of hydrogen may be calculated directly from the Van't Hoff equation. This leads to a value of - 83 KJ/mole (600-625°C), which is quite different from the initial heat of adsorption of hydrogen on nickel reported in the literature, -130 KJ/mole (124). As desorption is favoured at high temperatures such as these, the results

Table 4.2 Kinetic Expressions Tested.

Mechanism (bimolecular reaction)		Rate equation
Langmuir-Hinshelwood (Adsorbed A reacts with adsorbed B)	Competitive (1)	$\frac{kb_H P_H b_c P_c}{(1+b_H P_H+b_c P_c)^2}$
	Non-competitive (2)	$\frac{kb_H P_H b_c P_c}{(1+b_H P_H)(1+b_c P_c)}$
Rideal - Eley (Adsorbed A reacts with gaseous B)	Hydrocarbon adsorbed (3)	$\frac{kb_c P_c P_H}{(1+b_c P_c)}$
	Hydrogen adsorbed (4)	$\frac{kb_H P_H P_c}{(1+b_H P_H)}$

Table 4.3 Selected mechanism and parameters obtained.

Hydrocarbon (H_c)	Temp (^oC)	Partial Pressures ($KN\,m^{-2}$)		Selected Mechanism	σ (%)	$kx10^{-1}$	$b_c x10^3$	$b_H x10^2$
		H_c	H_2					
C_2H_2	600	3-51	11-67	1	10.0	1.3	9.3	2.2
C_2H_4	625	6-51	8-89	2	11.1	11.5	7.3	1.6
$1\text{-}C_4H_8$	625	3-51	14-74	2	9.5	4.2	0.45	1.5

σ - standard deviation

k - specific rate (µg of carbon deposited/sec cm^2)

b_H - adsorption equilibrium constant for hydrogen $[(KN\,m^{-2})^{-1}]$

b_c - adsorption equilibrium constant for the hydrocarbon $[(KN\,m^{-2})^{-1}]$

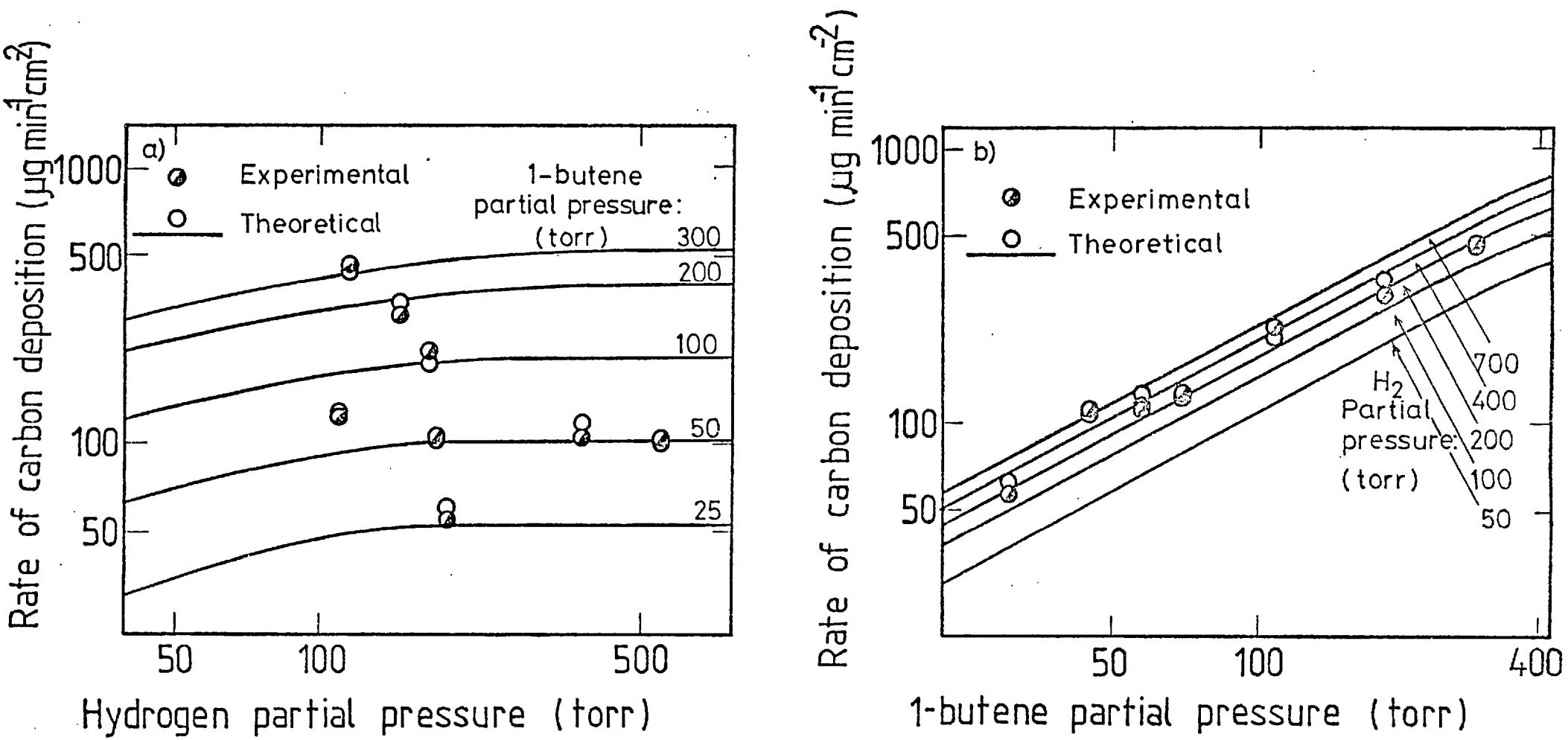

Fig. 4.3 Experimental rates of carbon deposition compared with a theoretical model.

Table 4.4 The temperature dependent factors of the kinetic expressions.

Hydrocarbon (H_c)	Temperature dependent factor	Conditions	Applicability: Pressure (KN/m)	
			H_c	H_2
C_2H_2	$kb_H\ b_{C_2H_2}$	Sparsely covered surface	<12	<7(?)
	$kb_{C_2H_2}$	Maximum in rate	<12	46-50
C_2H_4	$kb_H\ b_{C_2H_4}$	Sparsely covered surface	<14	>13
	$k\ b_{C_2H_4}$	Strong hydrogen adsorption	<14	>50
$1\text{-}C_4H_8$	$kb_H\ b_{1\text{-}C_4H_8}$	Sparsely covered surface	<25	<14(?)
	$k\ b_{1\text{-}C_4H_8}$	Strong hydrogen adsorption	<25	>27
	k	Reactants strongly adsorbed	>55(?)	>27

would be expected to be closer. However, more recent sources (125) have cited that, at 273 K, the differential heat of adsorption of hydrogen on polycrystalline nickel films decreases from - 67 to - 21 KJ/mole (when the surface coverage varies from 10 to 90% of the complete monolayer). This is much closer to the present value. The temperature dependent factors are consistent with the orders with respect to hydrogen and hydrocarbon shown in Table 3.5. In fact, they could easily be derived from the kinetic expressions, taking into consideration the simplifications implied by the orders shown in the table. One debatable point, however, is the temperature dependent factor corresponding to the maximum in rate for acetylene, $kb_{C_2H_2}$.

The discussion of maxima of this type is well documented in the literature (126,127). However, a different formulation can be presented in order to make the concepts involved more clear. Equation 1 in Table 4.2 (which does not consider the reverse reaction and the adsorption of products or poisons and includes all the assumptions of the Langmuir-Hinshelwood mechanism) can be written as

$$\text{Rate} = k\,\theta_H\,\theta_{H_c} \qquad (2)$$

where θ_H, θ_{H_c} are the fractions of the surface covered by hydrogen and hydrocarbon, respectively. Defining θ_0, the uncovered surface, as $1-\theta_H-\theta_{H_c}$, the relation between the θ_i can be obtained directly from the Langmuir isotherms:

$$\frac{\theta_0}{1} = \frac{\theta_H}{b_H P_H} = \frac{\theta_{H_c}}{b_{H_c} P_{H_c}} = \frac{1}{1+b_H P_H + b_{H_c} P_{H_c}} \qquad (3)$$

or

$$\theta_H = \theta_0 b_H P_H \quad , \quad \theta_{H_c} = \theta_0 b_{H_c} P_{H_c} \qquad (4)$$

Relation (3) clearly shows that $b_H P_H$ and $b_{H_c} P_{H_c}$ are, in fact, a measure of the surface covered by hydrogen and the hydrocarbon not in terms of the total surface but <u>in terms of the uncovered surface</u>.

If the pressure of the hydrocarbon is kept constant at a given temperature, the product $b_{H_c} P_{H_c}$ will be constant and hence there will be a constant proportionality between θ_{H_c} and θ_0 for any θ_H (cf. eqn (4)). Thus (as $1-\theta_H = \theta_0 + \theta_{H_c}$):

$$\theta_O + \theta_{H_c} = \left(\frac{1}{b_{H_c} P_{H_c}}\right) \theta_{H_c} = \left(\frac{1 + b_{H_c} P_{H_c}}{b_{H_c} P_{H_c}}\right) \theta_{H_c} = f\,\theta_{H_c} = 1 - \theta_H \qquad (5)$$

and

$$\theta_{H_c} = \frac{1}{f}(1 - \theta_H) \qquad (6)$$

where f stands for the constant factor $\left(\frac{1+b_{H_c} P_{H_c}}{b_{H_c} P_{H_c}}\right)$. This shows that, at fixed pressure and temperature, the hydrocarbon occupies a constant fraction of the surface not covered by hydrogen.

Now equation (2) can be rewritten as:

$$\text{Rate} = \frac{k}{f} \theta_H (1 - \theta_H) \qquad (7)$$

The maximum rate is given by:

$$\frac{dr}{d\theta_H} = 0 = \frac{k}{f}(1 - 2\theta_H) \qquad (8)$$

or
$$(\theta_H)_{max} = 0.5 \qquad (9)$$

and

$$(\theta_O + \theta_{H_c})_{max} = 0.5 \qquad (9a)$$

The value of $(\theta_{H_c})_{max}$ may now be found using equation (5):

$$(\theta_{H_c})_{max} = 0.5 \cdot \frac{b_{H_c} P_{H_c}}{1 + b_{H_c} P_{H_c}} \qquad (9b)$$

It can be concluded that the rate is maximum when the coverage of the variable pressure reactant is 50% of the complete monolayer and the remaining 50% are available for the other reactant to be adsorbed according to its own adsorption equilibrium.

Combining eqn.(9,9b) with eqn. (3) the relation between the pressures of the reactants in the conditions of maximum rate can be obtained:

$$b_H P_H = 1 + b_{H_c} P_{H_c} \qquad (10)$$

(and not $b_H P_H = b_{H_c} P_{H_c}$ as sometimes stated).

If the process of varying P_H (keeping the partial pressure of the hydrocarbon (P_{H_c}) constant) is repeated for different fixed values of P_{H_c}, the condition of the maximum rate will always be obtained for a value of $\theta_H = 50\%$. However, the pressure at which this coverage is attained will increase with increasing values of P_{H_c} (cf. eqn. 10). Hence, if mechanism (1) is used to explain the kinetics observed for acetylene, an experimental dependence of the type

$$\text{Rate} = k b_{H_c} P_{H_c} \qquad (11)$$

can only be justified if $b_{H_c} P_{H_c} < 1$. In fact, in this case the partial pressure of hydrogen $(P_H)_{max}$ corresponding to $(\theta_H)_{max}$ will be approximately constant for all the values of P_{H_c} and, for a narrow range of pressures around $(P_H)_{max}$, the rate can be expressed as in eqn. (11).

The values of the heats of adsorption and of the true activation energy obtained from these results can now be summarised as in Table 4.5. The value $\Delta H_H = -91$ KJ mole^{-1} obtained directly from the apparent activation energies should be more reliable than the value calculated from the Van't Hoff equation. It is again within the range of values obtained from the literature for the initial heat of adsorption of hydrogen (- 130 and - 67 KJ mole^{-1} (124,125)). In the case of 1-butene, when high reactant pressures were used, it was possible to measure the true activation energy for the reaction and to derive the heat of adsorption of the hydrocarbon, $\Delta H_{1\text{-}C_4H_8}$. Although the value of the temperature dependence may be affected by the fact that the measured rates are not completely independent of the hydrocarbon adsorption (as can be seen in Figure 4.3), the value of $\Delta H_{1\text{-}C_4H_8}$ obtained (- 289 KJ mole^{-1}) is similar to the reported values for other hydrocarbons. In the case of acetylene and ethylene, initial heats of adsorption on nickel have been reported (- 281 KJ mole^{-1} and - 253 KJ mole^{-1} (124) respectively). This allows the direct estimation of the true activation energies given in Table 4.5.

As a consequence of the results discussed in this section it has been possible to establish tentatively the role of the surface reaction as the rate determining step (and also the values of the true activation energies) in the process of carbon formation from acetylene and some

Table 4.5 Summary of the values of the heats of adsorption and true activation energies (calculated).

Hydrocarbon (H_c)	Temperature dependences	"E_a" measured (KJ mole^{-1})	ΔH_H calc. (KJ mole^{-1})	ΔH_{H_c} calc. (KJ mole^{-1})	E calc. (KJ mole^{-1})
C_2H_2	$E+\Delta H_{C_2H_2}$	-222	-	-	59
C_2H_4	$E+\Delta H_H+ H_{C_2H_4}$	-309	- 91	-	35
	$E+\Delta H_{C_2H_4}$	-218			
$1\text{-}C_4H_8$	$E+\Delta H_{1\text{-}C_4H_8}$	-268	-	-289	21
	E	+ 21			

ΔH_H, ΔH_{H_c} - Heats of adsorption of hydrogen and the hydrocarbon

E - True activation energy of the reaction.

olefins on nickel between 550 and 675°C. It should be noticed that the type of treatment used in the discussion has well known limitations (128). In spite of this, the Langmuir-Hinshelwood-type expressions used will still lead to rate functions that are qualitatively correct (129).

Attempts were made to determine the nature of the rate determining step above 600°C in the case of aliphalic and aromatic hydrocarbons. This is described next, together with a general discussion of the different mechanisms that may be responsible for the negative values of E_A determined at these temperatures.

The fundamental finding that allowed the realisation of the work described in 3.2.1.3 could not be observed with n-hexane, benzene and toluene: a permanent loss of activity was always detected when the temperature was increased above T_{max}, even for very high partial pressures of hydrogen. The obvious explanation for this irreversible loss of activity is the formation on the surface of a different type of carbon deposit (encapsulating carbon) as suggested in 4.1.1. A different explanation for the decrease of the rate of carbon deposition with temperature has been advanced (26). At temperatures above T_m, polymers or aromatic intermediates are formed in the gas phase. If these intermediates can adsorb strongly on the metal sites they will act as a surface poison. As the concentration of the gas phase intermediates increases with temperature (130), this will lead to a progressive poisoning of the surface and a decrease in the reaction rate. Consideration of Figs. 3.21 and 3.22 shows that, in the case of n-hexane, this explanation could be true. In the case of olefins and acetylene, however, negative temperature dependences were measured over a temperature range where the gas phase conversion of the parent hydrocarbon was negligible. For instance, for ethylene from 600 to 650°C the gas phase conversion was smaller than 5% (see Figs. 3.11 and 3.12). All the different arguments about the cause of the negative apparent activation energies observed above 550-600°C can be discussed on the basis of the following scheme:

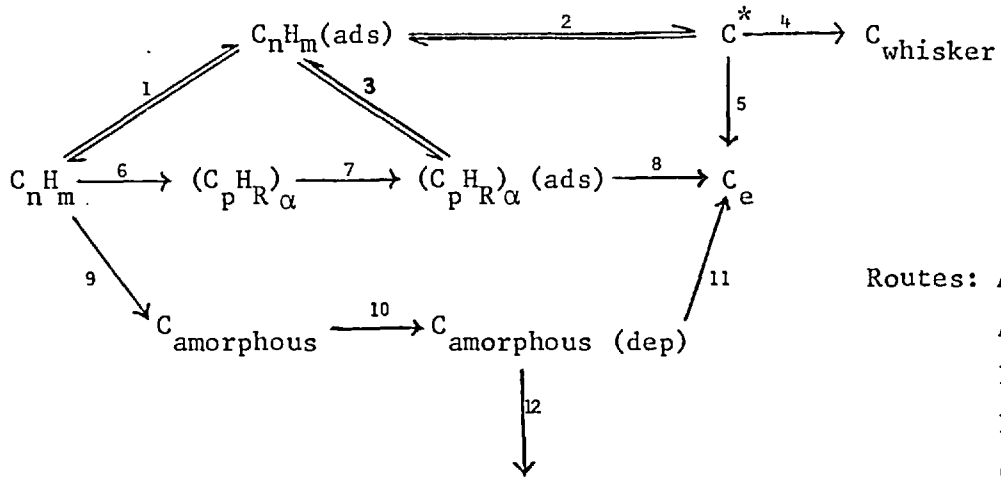

Routes: A - 1,2,4
A' - 1,2,5
B - 6,7,8
B' - 1,3,8
C - 9,10,11

where:

1 - reversible adsorption of the hydrocarbon; 2 - dehydrogenation and hydrogenation reactions on the surface; 3 - aromatisation and polymerisation on the surface; C^* - adsorbed carbon species capable of dissolving and diffusing in nickel (4) to form fibrous type of carbon ($C_{whisker}$), or to nucleate and grow on the surface (5) to form encapsulating carbon (C_e); 6,7 - gas phase conversion of the hydrocarbon to form a polynuclear aromatic species, irreversibly adsorbed on metallic sites of the surface; 8 - surface rearrangement leading to encapsulating carbon; 9,10 - formation of amorphous carbon ($C_{amorphous}$) in the gas phase, physically deposited on the surface; 11 - dissolution and reprecipitation leading to encapsulating carbon; 12 - gasification by hydrogen.

The various routes in the previous scheme can be used to explain the negative temperature dependences observed in different systems. In route A (steps 1,2 and 4) the surface reaction is rate determining and negative E_A are observed due to enhanced desorption (acetylene and olefins with high partial pressures of hydrogen). As can be concluded from the values of the order with respect to hydrogen in Tables 3.2, 3.5 and the rate expressions in Tables 4.2, 4.3, hydrogen is directly involved in the reaction, probably in an hydrogenolysis process (56).

Via Route A', negative E_A will be observed if step 5, competing with 4, becomes more important as temperature increases. The formation of encapsulating carbon would lead to the decrease in the rate. As the increase in temperature would favour simultaneously steps 4 and 5, both Routes A and A' should be responsible for the negative apparent

energies observed with some systems. This is probably the case of unsaturated hydrocarbons at low hydrogen partial pressures. In the deposition from acetylene on nickel single crystals, carbon nucleates mainly on the surface (as the absence of grain boundaries do not favour the bulk diffusion process, cf. 3.2.1.5.3). Route A' possibly predominates in this case.

The reason why the partial pressure of hydrogen can determine the type of carbon formed needs some further explanation. The formation of fibrous carbon via step 4 will depend on the nucleation of carbon somewhere inside the metal in zones of favourable interfacial energy, such as grain boundaries (cf. Run 15 in 3.2.1.5.3). Nuclei growth will eventually push the metal particles out of the surface. Route A depends on this process as the available metal area must remain constant. However, if carbon can also nucleate and grow on the surface without diffusing into the bulk metal (setp 5 in the scheme), encapsulating carbon will be formed. It has been suggested that hydrogen dissolved in nickel may loosen the grain boundaries of the metal (66). This would facilitate the detachment of particles from the surface. Increasing the partial pressure would increase the concentration of dissolved hydrogen, and thus favour Route A.

Either enhanced formation of polynuclear aromatic species in the gas phase (Route B, steps 6,7) or enhanced dehydrogenation and polymerization of the adsorbed hydrocarbon (Route B', steps 1,3) could explain the decrease in rate as temperature increases. Further rearrangement on the surface (step 8) could produce polynuclear aromatics of very large molecular weight that, for all partial purposes could be considered as encapsulating carbon (see Fig. 3.29b).

Obviously all these processes will be competing against each other. Increasing the partial pressure of hydrogen would favour Route A vs. Routes B,B' through the reverse path of reaction 3, i.e. the hydrocracking of the polynuclear aromatic species. The smaller fragments will then dehydrogenate via step 2. The nature of the parent hydrocarbon will also influence the relative importance of the processes. Obviously Routes B and B' will be more important with aromatics than with light olefins because setps 3 and 7, leading to the formation of polynuclear rings, would be facilitated. Apparently this is also the case for some aliphatics. With n-hexane, the irreversible deactivation detected between circa 625 and 700°C was accompanied by an appreciable

conversion in the gas phase. In this case, Route B should be responsible for the decrease in rate with increasing temperature.

Route C, involving the formation in the gas-phase of amorphous carbon, will become important as temperature increases. Contrary to the polynuclear aromatic species in Route B' (step 7), the deposition of this amorphous carbon on the catalyst (step 10) does not depend on the available metallic surface. Hence, after an initial decrease due to encapsulation of the surface, this route will eventually lead to an increase in the rate of carbon uptake (e.g. Zone IV in Fig. 3.21). At this stage the rates measured will mainly correspond to the thermal cracking of the hydrocarbon. The fact that no permanent deactivation was detected when the system was kept at high temperature for short periods of time (cf. section 3.2.2.2.) may be due to the gasification of the homogeneous carbon by hydrogen once the temperature is decreased. The increase in crystallinity of the carbon on the surface (step 11 in the scheme, probably a dissolution-precipitation process similar to the one described in 3.2.1.5.4) can be responsible for the deactivation observed when the system was kept at high temperatures for a long time. A more crystalline carbon will be more difficult to remove by hydrogen (87).

4.2 GASIFICATION OF CARBON DEPOSITS

4.2.1 General

In a number of important industrial reactions, such as steam reforming and steam cracking, carbon is simultaneously produced and gasified. In fact, beside being a reactant, steam can gasify carbonaceous deposits that would otherwise deactivate the catalyst:

$$2H_2O + C \rightleftharpoons CO_2 + 2H_2 \qquad (1)$$

Both carbon dioxide and hydrogen can also gasify carbon:

$$CO_2 + C \rightleftharpoons 2CO \qquad (2)$$

$$2H_2 + C \rightleftharpoons CH_4 \qquad (3)$$

Over the years there has been great interest in these reactions (77 , 94), although not many publications have dealt with the type of carbon formed on the catalysts used in the present work (71 , 131). In the present studies, carbon deposits formed on foils and supported nickel catalyst were gasified by carbon dioxide, hydrogen and steam.

Common characteristics were observed in the gasification by each of the three gases:

(1) Steady state rates independent of the amount of carbon deposit in a given experiment (from 15 to 65% burn-off).

(2) Steady state rates dependent on the initial amount of deposit in different experiments up to a value (saturation weight) but independent thereafter.

(3) Steady state rates in different experiments independent of the area of the foil (or the load of the supported catalyst) but the saturation weight increasing proportionally with it.

(4) Saturation weights consistently higher on foils than on supported catalysts.

These findings are discussed in section 4.2.2, together with the results of the carbon dioxide gasification, in the light of a proposed mechanism for the process. The kinetics of hydrogen gasification are discussed in section 4.2.3. The equilibrium observed at high temperatures allows the calculation of the excess free energy of the carbon formed.

Finally, in sections 4.2.4 and 4.2.5 the kinetics of steam gasification is discussed and the relative reactivities of the three gases compared.

4.2.2 Gasification by carbon dioxide

The results presented in 3.3.1 for the gasification on foils and supported nickel catalysts indicate that the presence of the support does not affect the reaction significantly.

One obvious question with this system is that the presence of carbon dioxide may lead to the formation of nickel oxide:

$$CO_2 + Ni \rightleftharpoons NiO + CO \qquad (4)$$

The oxidation of the metal is responsible for the deactivation effects observed in some catalysed gasifications (76). With both foils and supported nickel catalyst no deactivation was observed at intermediate values of burn-off. The amount of carbon monoxide produced by the gasification of carbon is enough to shift to the left the above equilibrium, thus keeping the nickel in the reduced state.

From the equilibrium constant of reaction (4), the concentration of carbon monoxide in equilibrium with nickel oxide can be estimated at different temperatures. This is presented in Table 4.4 together with the actual gas phase concentration of carbon monoxide determined in Run 34:

Table 4.6 Comparison of carbon monoxide concentrations

Temperature (^{o}C)	CO concentration (molar %)	
	Equilibrium*	Produced by carbon gasification (Run 34)
775	0.468	19.2
727	0.359	11.0
650	0.240	3.73
550	0.102	0.383

* From data in Reference (76)

As can be seen in the table, the gas phase carbon monoxide concentrations are much higher than the equilibrium ones. The probability that mostly metallic nickel is present is further reinforced by the fact that no increase in the gasification rate was detected when resuming the reaction after a treatment in hydrogen.

These results differ from those of Marsh et al. on the gasification of nickel-doped (PFA) carbon (91). Probably oxide was present in their case. The existence of oxide will depend on the carbon monoxide concentration. This is turn will depend on the reactivity of the gasification reaction. Accordingly, the gasification rates reported (91) are circa one order of magnitude smaller than those of the present work.

The kinetics of the gasification under steady-state conditions can be summarised as follows:

Catalyst	E_A (KJ mole^{-1})		Order w.r.t. CO_2	
	T < 650°C	T > 675°C	T < 650°C	T > 675°C
Polycrystalline foil	163 ± 13	71 ± 9	0.5 (1 to 0?)	∿ 1
Supported catalyst	140 ± 8	66 ± 8	0.2	∿ 1

The order of the gasification reaction changes from a fractional number to unity as the temperature increases from the first to the second zone. At the same time the apparent activation energy is nearly halved. At low temperatures and espcially with nickel foils, there is the suggestion of a change in the order from a positive to a near zero value as the carbon dioxide partial pressure increases. This result seems to indicate that chemical reaction is rate controlling below 650°C and mass transfer effects are important above 675°C. A similar effect has been noted for the uncatalysed gasification (132), the transition temperature being circa 1100°C. The greater reactivity of the present carbon-metal system probably brings about an earlier transition of the controlling step. A satisfactory explanation of the kinetics observed at lower temperatures can be obtained by analogy with a model proposed for the uncatalysed gasification (114):

Carbon dioxide adsorbs and dissociates in the metal giving atomic oxygen (oxygen-transfer mechanism). Eventually the oxygen will form a metal - oxygen-carbon linkage and carbon monoxide will desorb to the gas phase:

$$CO_2 \rightleftharpoons CO + (O)_M \qquad (5)$$

$$(O)_M + C \longrightarrow (CO)_M \qquad (6)$$

$$(CO)_M \rightleftharpoons CO \qquad (7)$$

If the forward reaction in step 7 is assumed to be rate controlling, the overall kinetic expression obtained would be similar to that of the uncatalysed reaction:

$$\text{Rate} = \frac{k\, P_{CO_2}}{k_1 + k_2 P_{CO_2}}$$

The derivation assumes that the amount of carbon monoxide in the gas phase do not affect the overall rate via the reverse reaction in step (7). The trend observed in the order can now be understood, as the increasing importance of the term P_{CO_2} in the rate expression will eventually bring about a zero order with respect to carbon dioxide.

The presence of pore diffusion limitations at 725°C was shown in the calculation presented in 3.3.1.2.4. The fact that similar kinetics are observed above 675°C for both foils and supported nickel catalysts confirms the assumption underlying the calculation: that the diffusion limitations should occur in the pores of the carbon. In these conditions carbon monoxide, the main product of the gasification, accumulates within the porous structure of the carbon. Even if the gas phase is composed mainly by carbon dioxide, the reaction inside the pores is akin to the gasification by carbon dioxide-carbon monoxide mixtures.

The mechanism of carbon dioxide gasification will be further clarified if the discussion is extended to cover the role of the nickel dispersed in the carbon deposits.

The presence of metal aggregates in the deposits influences not only their reactivity for gasification but also the activation energies observed (76). The efficiency of the metal action depends on its concentration and state of dispersion. In the present work nickel was finely dispersed (cf. Fig. 3.26a) in a carbon deposit of high internal surface area (cf. 3.3.1.2.3) at a concentration of about 1.5% (W/W). As mentioned before, the rates observed were much higher than those reported by Marsh et al. (91). This is thought to depend on the mode of formation of our deposits. In section 4.1, nucleation of carbon previously dissolved in the metal, was considered to be the cause of breakaway of nickel particles. In this way, at the initial stages of the gasification, some carbon is already dissolved in the nickel. A process inverse of that of the deposition (cf. 4.1.4) can thus be envisaged: carbon is consumed in the bare face of the particle; in the parts in contact with the deposit more carbon dissolves and diffuses through the bulk to feed the reaction areas (131). This common mechanism would explain the similarities observed between the deposition and gasification of carbon: short induction periods, followed by acceleratory periods leading to long steady-states. It would also explain the high reactivity of the present system. In fact, step 6 in the proposed reaction scheme (the linkage of the metal-oxygen species

to a carbon atom) should be facilitated if the carbon is precipitated from the bulk of the metal.

The main features of the gasification described in section 4.2.1 can now be discussed in the light of these ideas.

If the reaction occurs mainly on the metallic sites, the constancy of the rate in a given run means that the number of the active nickel particles in the deposit (or rather the available nickel area) remains constant throughout the gasification.

Now there is a point which is not clear. In the case of foils the nickel concentration is approximately independent of the extent of deposition. Hence, in different experiments, the steady state rates should always be proportional to the initial amount of carbon. The fact that a saturation weight is observed can only mean that, above a certain extent of deposition, a fraction of the deposit is no longer active for carbon dioxide gasification. In the case of supported catalysts the reason for this is easy to understand. In the process of deposition the alumina particles are broken by the growing carbon and eventually all of the nickel available will be dispersed in the carbon (cf. Fig. 3.26a,b). So, in different experiments with the same initial amount of catalyst there will be a stage after which the total amount of nickel in the deposit will remain constant. However, foils can act as a virtual infinite source of nickel particles. In this case the reason for the saturation weight should be found in the structure of the deposit itself. Probably, in spite of the porosity, thicker deposits can only partially be reached by the gasifying gas. This would explain why higher saturation weights were observed with foils with larger areas (since, in this case, the same amount of carbon corresponds to a proportionally thinner deposit).

The unavailability of a fraction of the deposit has already been postulated for carbon dioxide gasification of low porosity metal-doped carbons (96). The importance of the effect will obviously depend on the porosity of the carbon deposits. The results reported in 3.3.1.2.3 show that, as burn-off increases, the pore volume and the surface area of the remaining carbon also increase. Hahn et al. reported a similar result for the steam gasification of iron-doped coke particles (95). They also observed that, in spite of the increase of total surface area, the rate of gasification was independent of burn-off up to 50%.

The formation of new pores is mainly due to the action of the metal particles (84). However, if the particles are similar to those observed by Baker (circa 30 nm in diameter) (36), the creation of macropores is to be expected. As a result, the surface area should not increase significantly. Probably the gasification is revealing micro or transitional pores already existing in the carbon but hitherto unaccessible to the gas. The unaccessible areas are thus responsible for the saturation weights observed.

4.2.3 Gasification by hydrogen

The main features of the carbon dioxide gasification (including the existence of a saturation weight) were also observed in this system. This suggests that the mechanism previously described, involving bulk diffusion of carbon in nickel, is operative in the gasification of the carbon deposits, irrespective of the gasifying gas. The kinetics observed, however, will obviously depend on the nature of the rate controlling steps for particular conditions of gasification.

The most interesting feature observed in Fig. 3.40 is the decrease of the rate with increasing temperature above 650°C (Ea ≃ - 82 KJ mole^{-1}). Orders with respect to hydrogen close to 2 were observed in this zone. As the temperature decreased, the apparent activation energy increased sharply to 180 KJ mole^{-1} and then to 265 KJ mole^{-1}. At the same time, the orders decreased to one and fractional numbers, respectively.

In the lower temperature zone, the kinetics observed supports the view that the surface reaction is the rate controlling step. First, the apparent activation energy is similar to that reported by Nishyama et al. (71), under conditions where one of the surface reactions was stated to be rate controlling. Second, the orders showed the same "saturation effect" as was observed with carbon dioxide, decreasing from one to near zero as the partial pressure of hydrogen increased. This effect can be understood by considering a reaction scheme where hydrogen adsorbs and dissociates on the metal, giving atomic hydrogen that combines with carbon supplied from the bulk:

$$H_2 \rightleftharpoons 2(H)_M \qquad (1)$$

$$2(H)_M + C \longrightarrow (CH_2)_M \longrightarrow \cdots\cdots \longrightarrow (CH_4)_M \qquad (2)$$

$$(CH_4)_M \longrightarrow CH_4 \qquad (3)$$

If, in step (2), the simultaneous combination of two hydrogen atoms with carbon is assumed to be the rate controlling step, a rate expression can be derived using the Langmuir isotherm:

$$\text{Rate} \simeq k'(\theta)_M^2 = \frac{k' \, b_H P_H}{(1 + (b_H P_H)^{1/2} + c_x)^2}$$

where c_x stands for other species adsorbed at the same type of active sites on the metal surface.

The "saturation" effect will thus be explained by the increasing importance of the term $b_H P_H$ in the rate expression.

The explanation of the kinetic data determined above 550°C (see Fig. 3.40) has proved to be rather more difficult. The change in the apparent activation energy should not be due to mass transfer limitations because (a) the order with respect to hydrogen is > 1 and (b) the decrease in E_A is too small. It cannot also be explained by a change in the controlling mechanism to bulk diffusion of carbon in nickel(71). In fact, both the order and the activation energy would have to be different in this case (zero and 124 KJ $mole^{-1}$, respectively). Another explanation is a decrease in the adsorption on the surface with increasing temperature. For instance, as the temperature increases, the adsorption of hydrogen decreases and the term $(b_H P_H)^{1/2}$ in the denominator of the rate equation also decreases. This would imply an increase in the order and a decrease in activation energy. However, a limiting value of 1 would be expected, while orders greater than one are observed above 550°C. In spite of this, the last explanation is still the one that best fits the experimental evidence. But the argument remains to be proved.

The influence of the reverse reaction: $CH_4 \rightarrow C + H_2$ upon the rates measured at high temperatures has already been demonstrated in 3.3.2.2. Maxima in the Arrhenius plot of the rates of hydrogen gasification (at temperatures between 650 - 750°C) have been observed previously (71 , 89). Marsh et al. (90) rejected an explanation on the basis of competition between two processes on the carbon surface, and suggested instead that diffusion limitations above T_{max} were responsible for the maxima observed. However, this cannot be the case, because mass transfer limitations would not explain a decrease of the rate with increasing temperature (unless the structure of the deposit is changing). The explanation must be sought in terms of the effect on the rate of the

approach to equilibrium conditions. The gasification does not stop, only because the removal of methane from the reaction sites allows a certain distance to be kept from the equilibrium concentration (Δc). This distance will obviously depend on the contact times used. If Δc is supposed to remain practically the same above T_{max}, the amount of carbon gasified at a given temperature will depend only on the value of the equilibrium methane concentration. This would explain why the apparent activation energy is so close to the heat of reaction at these temperatures. Furthermore, at a given temperature, the equilibrium methane concentration will depend on the power 2 of the hydrogen pressure. Hence, if the partial pressure of hydrogen in the feed is decreased, the gasification rate will decrease proportionally (observed order: 1.8).

The equilibrium situation attained in Run 81 allows the determination of the molar excess free energy of the carbon formed (as compared to that of ideal graphite). According to Rostrup-Nielsen (10), the deviation from graphite data is explained by the structural incompleteness of the carbon and also by a contribution of the surface energy. The excess function can be calculated using a relationship involving only the surface tensions and the dimensions of a carbon whisker in contact with a nickel particle:

$$\Delta G_c \simeq \mu^* + 12\frac{\gamma}{d}$$

where μ^* - contribution from structural defects
γ - surface tension of the whisker
d - diameter of the nickel particle (assumed to be the same as the whisker).

Now in Run 81, at 750°C, the equilibrium methane concentration is $\simeq$ 9.5% (V/V). Then, at 750°C, the constant for the equilibrium:

$$CH_4 \longrightarrow C + 2H_2$$

will be: $K_p^{exp} = 6.90$ atm. From data in reference (9), the calculated value for the constant of the methane-hydrogen/graphite equilibrium at 750°C, is $K_p^{graphite} = 11.76$ atm. Then:

$$\Delta G_c = RT \ln \frac{K_p^{graph}}{K_p^{exp}} = 4.56 \text{ KJ mole}^{-1}$$

In Table 5 of reference (10), ΔG_c is seen to be approximately

constant above 500°C. Hence, it is reasonable to suggest that the correlation presented in Figure 8 (10) can also be used at 750°C:

$$\Delta G_c = 2.80 + \frac{915}{d} \qquad (\Delta G_c \text{ in KJ mole}^{-1}, \text{ d in } ^{o}A)$$

Then, in our case:

$$d \simeq 520^{o}A = 52 \text{ nm}$$

Considering the approximations involved in a calculation of this type, this value agrees quite well with the diameter of the "pear-shaped" particles actually observed Baker et al. (36) (circa 30 nm). With particles such as these, the surface to volume ratio should be in between that of a cylinder and a cone:

$$\frac{S}{V} = \frac{2}{d} \simeq 3.8 \times 10^{5} \text{ cm}^{-1}$$

In the case of foils, the average nickel concentration in the carbon is 1.5% (W/W) or 1.68×10^{-3} cm^3 Ni/g C. Hence, the total metal surface area will be 6.5×10^{-2} m^2 Ni/g C. In this way, by means of the excess free energy of formation, the carbon metal area, hitherto unknown, could be calculated. However, the use of this value to normalise the rate is limited. In fact, the fraction of the total metal surface involved in the gasification at a given stage is not known (cf. 4.2.2).

4.2.4 Gasification by steam

As in the case of carbon dioxide and hydrogen, the steam gasification rates remained constant for long periods of time, without deactivation being detected at intermediate values of carbon burn-off. The hydrogen produced in the reaction is probably sufficient to keep the metal in the reduced state, and thus prevent deactivation by the formation of a stable nickel oxide. Accordingly, the addition of hydrogen to the feed had no apparent effect in the gasification rate.

The main products of the reaction were hydrogen and carbon dioxide. Carbon monoxide was detected only in small amounts, although its concentration was still in excess of that corresponding to the equilibrium of the water-gas shift reaction. This indicates that carbon monoxide is produced directly in the gasification.

The kinetics described in 3.3.3 can be summarised as follows:

	Temperature (^{o}C)		
	T < 600	600 < T < ∿ 725	T > 725
Apparent activation energy (E_A) ($KJ\ moles^{-1}$)	164 ± 9	61 ± 4	∿ 0
Order with respect to steam	0.6	∿ 0.8	1

This data suggests that the effect of mass transfer in the gasification rate is becoming important as temperature increases. At 750°C, the rates increased appreciably with the inlet flow rate. The process is probably film-diffusion controlled in the higher temperature zone. In the lower temperature zone the value of E_A agrees quite well with recently published data for the steam gasification of nickel-doped graphite (93). The authors stated that the rate of gasification of carbons with 1.4% (W/W) nickel was affected by mass transfer within the pores of carbon from 525 to 840°C.

The Weisz and Prater criterion (133) was used to check for the existence of pore diffusion limitations below 600°C. The values obtained (assuming diffusion to occur in the transition regime between bulk and Knudsen diffusion) indicated, however, that these limitations should not be important in this zone.

With this result in mind, the surface reaction was assumed the rate controlling step at low temperatures. A mechanism can be envisaged where water dissociates at the metal surface producing chemisorbed oxygen and hydrogen atoms, and that the oxygen subsequently reacts with carbon to produce carbon monoxide. In the gas phase, carbon monoxide reacts with steam to produce carbon dioxide and hydrogen. The reaction rate should thus, depend on the partial pressure of steam and also on the relative coverages of the metal surface by oxygen and hydrogen. The fractional order observed agrees with this assumption.

The mechanism proposed in 4.2.2 is probably also operative in the steam-carbon system. If carbon is precipitated from the bulk of the metal, the reaction with adsorbed oxygen need not necessarily occur at carbon metal-interfaces (88). In this way, higher reactivities will be expected in the present system.

4.2.5 Comparison of the carbon gasification rates

There has been some interest over the years in the relative rates of gasification of carbon by steam, carbon dioxide and hydrogen (9,74,78, 94). Walker et al. (74) reviewed several previous investigations to show that, at 800°C and 10 KN m^{-2} gas pressure, the relative rates of the uncatalysed reaction were, respectively:

$$3 : 1 : 3 \times 10^{-3}$$

Although this relationship was drawn for a well defined set of conditions, in subsequent publications it has been formulated in general terms (1) and also used in the context of the metal catalysed reactions (94).

The results shown in Figs. 3.34, 3.41 and 3.45 allow the comparison of the rates of the gasification of the carbon deposits formed in the present work. This is shown in Fig. 4.4. The rates in the Arrhenius type plot were normalised with the initial amount of carbon in the usual way. The curve for steam refers to 100 KNm^{-2} pressure: this was obtained by extrapolation using the orders determined in the different temperature regimes.

The figure shows clearly that steam is the most effective gasifying agent for carbon at atmospheric pressure in the presence of nickel. Between 550 and 650°C, hydrogen is more effective than carbon dioxide, but this order is reversed at lower and higher temperatures. As the order of reactivity depends on the temperature, the value of generalised comparisons is limited. Furthermore, the relative rates of gasification may also be affected by an increase in pressure. Hydrogen gasification, the only case involving a decrease in the number of gas phase molecules, will be favoured by a shift of the equilibrium towards methane formation (cf. 4.2.3). Accordingly, Hedden (78), working with pressures between 10^3 and 10^4 KN m^{-2}, did not observe, at high temperatures, the decrease in the rate of hydrogen gasification shown in Fig. 4.4. As a result, hydrogen may be a more effective agent for high pressure gasification of carbon deposits such as ours.

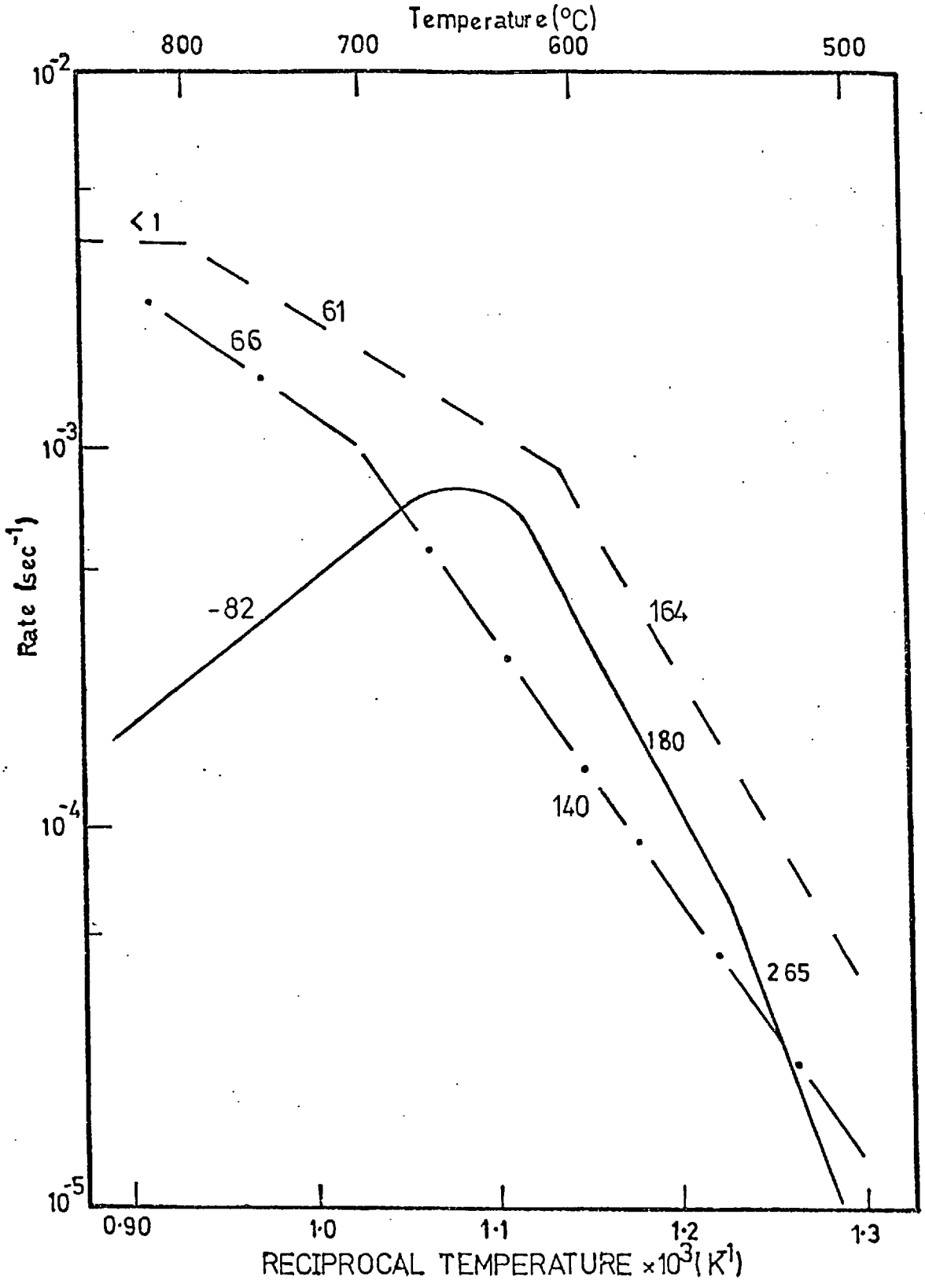

Fig. 4.4 Pseudo-Arrhenius plot of the rates of carbon gasification.
Atmospheric pressure; inlet flow = 3.3 cm^3 (STP) sec^{-1}
—— H_2; — — steam; —·— carbon dioxide
Rate expressed as g carbon gasified per g initial carbon deposited per second. (Numbers give apparent activation energies in KJ $mole^{-1}$)

4.3 CARBON DEPOSITION IN THE PRESENCE OF STEAM

The reaction of n-hexane with steam was mainly studied to obtain some information on the mechanism of coking of steam reforming catalysts.

The steam reforming reaction may be formally described by the initial breakdown of the hydrocarbon:

$$C_nH_{2n+2} + nH_2O \longrightarrow nCO + (2n + 1)H_2$$

followed by the water-gas shift and the methanation reactions. Carbon can be formed from the products of these reactions by any of the following equilibria:

$$2CO \rightleftharpoons C + CO_2$$

$$CO + H_2 \rightleftharpoons C + H_2O$$

$$CH_4 \rightleftharpoons C + 2H_2$$

In the presence of excess steam (and for low hexane conversions) the formation of carbon via the above equilibria is minimised. However, carbon deposits can also be formed by direct decomposition of the hydrocarbon over the catalyst and these deposits may be stable even if the equilibria predict no carbon formation (101). The present discussion is primarily concerned with this aspect of the coking of steam reforming catalysts.

The deposition of carbon in the presence of steam occurred without apparent loss of activity of the catalyst for the steam reforming reaction. However, under certain conditions, severe deactivation occurred and only minimal rates of deposition were detected. This is thought to be related with the oxidation of the catalyst by steam: $Ni + H_2O \longrightarrow NiO + H_2$ since, when hydrogen was added to the feed, no deactivation was detected.

The general features of the deposition of carbon were similar to those observed in the absence of steam. The deposition rate increased with temperature until 550°C ($E_A \simeq 119$ KJ mole^{-1}). Orders of 0.5 and 0 were determined with respect to the hydrocarbon and steam, respectively. Above 550°C the rate decreased with increasing temperature and orders of 1 in n-hexane and - 0.8 in steam were observed.

The results suggest a complex reaction mechanism, with steam possibly gasifying part of the carbon deposited at high temperatures. Ross and Steel (113) have shown that, at 873 K, the rate of carbon gasification by steam was greater than the rate of the reaction of steam reforming of methane. They suggested that carbon deposition does not occur significantly during the reaction because, even if carbon deposits were formed, they would be immediately gasified by steam.

The various mechanisms that have been proposed for the steam reforming of hydrocarbons higher than methane (134,135, 1 ,136) are fundamentally of two general types:

(1) Mechanisms that assume the complete breakdown of the hydrocarbon to carbon and hydrogen, followed by reaction of carbon with steam.

(2) Mechanisms that assume the sequential breakdown of the hydrocarbon to produce adsorbed surface intermediates followed by reaction with steam or further dehydrogenation to carbon.

If mechanism (1) were considered to apply to the reaction of n-hexane with steam, the net rate of carbon formation (in the presence of steam) could be calculated by subtracting the rate of steam gasification from the rate of deposition (in the absence of steam). Table 4.7 shows the balance of these rates at 550°C.

Table 4.7 Comparison of the rates of carbon deposition and gasification at 550°C.
(Catalyst : Ni/Al_2O_3 , 100 mg)

Process	Data from (section)	Inlet partial pressures (KN m^{-2})			Rate (μg sec^{-1})
		H_2O	H_2	C_6H_{14}	
Carbon Formation	3.2.2.1	-	15	3.1	16.1
Gasification by steam	3.3.3	25	-	-	3.60
Gasification by H_2	3.3.2	-	15	-	0.54
Calculated net rate	→				~12.0
Carbon formation (steam reforming)	3.2.2.4	25	15	3.1	1.95

The calculated rate of carbon deposition exceeds significantly the rate actually observed under steam reforming conditions. A similar result was obtained for the steam reforming of propylene (137).

The major problem when comparing the values of the rates is the uncertainty of the temperature at the catalyst surface, since the temperature drop across the gas film (caused by the endothermic reaction) is not known. Hence, the results shown in the table only allow a qualitative discussion. In spite of this limitation, the difference between the observed and the calculated values of the rate is so large that mechanism 1 (which implies that carbon formation is a necessary step in the over-all steam reforming process) is unlikely. Moseley et al. (100), studying the gasification of light hydrocarbons, showed that the coking reaction competed with the steam reforming reaction. Rostrup-Nielson (101) also considered competition between the two processes for the adsorbed hydrocarbon species. It could be argued that the difference observed in Table 4.7 was due to the fact that water and n-hexane were competing for the same sites on the catalyst surface. This would cause a decrease of the rate of the carbon forming reaction under steam reforming conditions. However, it has been suggested (136) that the dissociations of water and the hydrocarbon occur at different surface sites (possibly the support and the metal). Hence, the mechanism involving adsorbed hydrocarbon intermediate species as precursors for both the coking and the gasification seems to be the more likely. Accordingly, Lahaye et al. (104) concluded that, in the steam cracking of n-hexane, intermediate species react on the catalyst to form carbonaceous products.

CONCLUSIONS

1. The decomposition of acetylene on polycrystalline foils and nickel single crystals showed that carbon formation was enhanced if the surface was rough and there were grain boundaries present. The presence of grain boundaries facilitates the nucleation of carbon which, in turn, determines, to a great extent, the break-away of particles from the nickel surface, preventing the self-poisoning of the catalyst. Nickel particles were found in the carbon deposits, which were active for further carbon deposition when separated from the original foils. The orientation of the crystal faces was not related in a straightforward way with the observed rates of deposition. The initial rate was found to be greater on the (110) face of nickel than on the (111) face. However as carbon formation increased, this order was reversed.

2. Pyrolytic carbon was seen to grow on the face of a single crystal of nickel covered with a layer of amorphous carbon, whilst a clean face remained uncovered. In a series of experiments it was shown that the process of carbon diffusion through nickel is involved in the formation of heavy catalytic carbon deposits.

3. A successful autocalytic modelling and parameter estimation procedure was used to explain the kinetics of carbon formation from acetylene on polycrystalline nickel foils determined under batch conditions. The maximum in the curves of rate of deposition vs. conversion observed at low acetylene conversions was explained by the combined effects of nucleation and poisoning.

4. At low temperatures (below 500°C) the kinetics observed under flow conditions using a differential reactor were in agreement with a previously proposed mechanism for the process. This supposes that carbon diffusion through nickel is rate limiting. As the temperature increased above 500°C a change in rate controlling step occurred. The order of the reaction (with respect to both hydrogen and acetylene) increased and the apparent activation energy decreased becoming negative. In the presence of high partial pressures of hydrogen no deactivation effects were observed under these conditions: the deposition rates were reproducible when the temperatures were scanned upwards and downwards.

5. Successful theoretical models were derived to explain the negative apparent activation energies and the orders of the reaction observed above 550°C for the decomposition of acetylene, ethylene and 1-butene over nickel. The models suppose that the surface reaction is the rate controlling step and that the decrease in rate with increasing temperature is due to enhanced desorption of both hydrocarbon and hydrogen.

6. The kinetics of carbon deposition from aliphatic and aromatic hydrocarbons on polycrystalline foils and supported nickel catalysts could not be explained by the mechanism shown to apply in the case of acteylene and the olefins. Alternative mechanisms were discussed and the surface reaction was considered to be rate limiting at low temperatures.

7. Comparison of the deposition of carbon from n-hexane on polycrystalline foils and supported nickel catalysts showed that the support material had no significant influence on the kinetics of the process.

8. In the case of aliphatic and aromatic hydrocarbons some irreversible loss of activity was always observed above 550-600°C, even in the presence of high partial pressures of hydrogen. Deactivation of the catalyst by carbon (encapsulation) is considered to be the main cause for the decrease in the rate with increasing temperature observed with these hydrocarbons. A general scheme is proposed to explain the effect of hydrogen and the apparent negative activation energies observed with different systems.

9. The gasification of carbon deposits by steam, carbon dioxide and hydrogen was studied on both polycrystalline foils and supported nickel catalysts. Some of the main features of the gasification were similar to those of the deposition on the same type of catalysts. After a short induction period, the rate of gasification accelerated to a constant and reproducible value, which lasted until circa 70% of the deposit was burnt-off. Furthermore, common characteristics were also observed with different gasifying agents. This evidence was used to advance the idea that carbon diffusion through nickel is operative in both the formation and gasification of the carbon deposits studied in the present work.

10. The surface area and total pore volume of the deposits increased during gasification. This is probably due to the fact that part of the microporous structure of carbon was not initially reached by the adsorbate but became increasingly accessible as the deposit burn-off increased.

11. The kinetics of gasification by steam, carbon dioxide and hydrogen were determined. In all cases, the kinetic data obtained at low temperatures (below 600°C) was consistent with control of the process by the chemical reaction. As the temperature increased the rates of gasification by steam and carbon dioxide were affected by diffusion limitations. The concentration of methane near the reaction sites was shown to affect the rate of hydrogen gasification above 650°C.

12. The equilibrium of methane with hydrogen and carbon attained at high temperature allowed the calculation of the excess free energy of formation of carbon (with respect to that of ideal graphite). Using this value and an experimental correlation found in the literature, the maximum diameter and the surface area of the nickel particles in the carbon deposits were estimated to be 52 nm and 6.5×10^{-2} m^2 (grams of carbon)$^{-1}$, respectively.

13. The relative efficacies of steam, carbon dioxide and hydrogen for the nickel catalysed gasification of carbon deposits was determined over the range of temperatures 500-850°C and at atmospheric pressure. Steam is the most effective gasifying agent across the whole temperature range. Between 550 and 650°C, hydrogen is more effective than carbon dioxide, but at lower or higher temperatures this order is reversed.

14. The deposition of carbon on supported nickel catalyst during the steam-reforming of n-hexane was studied over the temperature range 450-600°C. No loss of activity for the steam reforming reaction was seen to accompany the coking of the catalysts. The rate of carbon deposition depended positively on the partial pressure of n-hexane and was nearly independent of the steam partial pressure. A maximum in the rate was observed at about 550°C. Above this temperature the coking rate still increased with the partial pressure of n-hexane but decreased when the

partial pressure of steam increased.

15. The mechanism of carbon deposition on steam reforming catalysts is thought to involve an adsorbed hydrocarbon intermediate that is also a precursor for the steam reforming reaction.

APPENDIX A

Comparison of different possible mechanisms

The different mechanisms presented in Table 4.2 were compared by means of a computer program (CARBON). The values of the constants in the rate expressions, as well as the standard deviation (σ), for each of the models were calculated via a minimisation sub-routine (CALCFX). The models were represented graphically by means of sub-routine GRAFICO (See Fig. 4.3). The models selected, presented in Table 4.3, were those with the smaller σ, for the smaller number of parameters.

The program is listed in the next pages. Subroutines VA04A and GRAPH2 were obtained directly from the Departmental Library.

```
      PROGRAM CARBON(INPUT,OUTPUT,TAPE5=INPUT,TAPE6=OUTPUT)
C
C
      EXTERNAL CALCFX
      DIMENSION X(10),E(10),W(160)
      COMMON M,MN,BN,PH(20),PC(20),BH,BC,AK,X1,X2,X3,X4,X5,NUMERO
     2  ,YE(50)
      N=0
      CALL CALCFX(N,X,F)
      ESCALE=10**5
      IPRINT=0
      ICON=1
      DO 7 J=1,9
      X(J)=1
      E(J)=0.001
    7 CONTINUE
      MAXIT=150
      MAXFUN=1500
      DO 2 I=1,MN
      M=I
      N=3
      IF(M.EQ.3) N=2
      BN=M
      N3N=N*(N+3)
      CALL VA04A(X,E,N,F,ESCALE,IPRINT,ICON,MAXIT,CALCFX,W,N3N,MAXFUN)
      N=11
      CALL CALCFX(N,X,F)
    2 CONTINUE
      STOP
      END



      SUBROUTINE  GRAFICO(Z,Y,MFIT,MMAX)
      DIMENSION Z(MFIT,MMAX),Y(MFIT,MMAX),ICON(10),RC(10),RH(10)
      COMMON M,MN,BN,PH(20),PC(20),BH,BC,AK,X1,X2,X3,X4,X5,NUMERO
     2  ,YE(50)
      ICON(1)=NUMERO
      DO 4 I=2,5
      ICON(I)=MMAX
    4 CONTINUE
      ICON(6)=2
      IPRINT=0
      RC(1)=25.0
      AUX=5.5/(FLOAT(MMAX-1))
      M1=MFIT-1
      DO 6 I=2,M1
      Z(I,1)=1.5
      IM=I-1
      RC(I)=RC(IM)*2.
      RCI=RC(I)
      DO 5 J=1,MMAX
      K=J+1
      IF(J.GT.NUMERO) GO TO 12
```

```
      Z(1,J)=ALOG(PH(J))
      Y(1,J)=YE(J)
   12 CONTINUE
C      PH(I)  TO USE IN RATE EXPRESSION IS EQUAL TO EXP(Z(I,J))
      ZIJ=Z(I,J)
      IF (K.GT.MMAX) GO TO 211
      Z(I,K)=ZIJ+AUX
  211 CONTINUE
      GO TO (1100,1200,1300,1400,1500,1600,1700,1800,1900),M
 1100 YIJ=X1+X2+X3+ZIJ+ALOG(RCI/((1.+PH*EXP(ZIJ)+BC*RCI)**2))
      GO TO 7
 1200 YIJ=X1+X2+X3+ZIJ+ALOG(RCI/((1.+BH*EXP(ZIJ))*
     4   (1.+BC*RCI)))
      GO TO 7
 1300 YIJ=X1+X2+X3+ZIJ+ALOG(RCI/(1.+BH*EXP(ZIJ)))
      GO TO 7
 1400 CONTINUE
 1500 CONTINUE
 1600 CONTINUE
 1700 CONTINUE
 1800 CONTINUE
 1900 CONTINUE
    7 IF(YIJ.GT.7.0) YIJ=7.0
      Y(I,J)=YIJ
    5 CONTINUE
    6 CONTINUE
      Z(6,1)=1.5
      Y(6,1)=0.
      Z(6,2)=7.0
      Y(6,2)=7.
      CALL GRAPH2(Z,Y,MFIT,ICON,MMAX,IPRINT)
      RH(1)=25.
      DO 9 I=2,M1
      IM=I-1
      RH(I)=RH(IM)*2.
      RHI=RH(I)
      DO 8 J=1,MMAX
      K=J+1
      IF (J.GT.NUMERO) GO TO 13
      Z(1,J)=ALOG(PC(J))
   13 CONTINUE
C     RC(I)  TO USE IN RATE CALCULATION IS EQUAL TO EXP(Z(I,J))
      ZIJ=Z(I,J)
      GO TO(2100,2200,2300,2400,2500,2600,2700,2800,2900),M
 2100 YIJ=X1+X2+X3+ZIJ+ALOG(RHI/((1.+BC*EXP(ZIJ)+BH*RHI)**2))
      GO TO 11
 2200 YIJ=X1+X2+X3+ZIJ+ALOG(RHI/((1.+BC*EXP(ZIJ))*
     5   (1.+BH*RHI)))
      GO TO 11
 2300 YIJ=X1+X2+X3+ZIJ+ALOG(RHI/(1.+BC*EXP(ZIJ)))
      GO TO 11
 2400 CONTINUE
 2500 CONTINUE
 2600 CONTINUE
 2700 CONTINUE
 2800 CONTINUE
 2900 CONTINUE
   11 IF(YIJ.GT.7.0) YIJ=7.0
      Y(I,J)=YIJ
    8 CONTINUE
    9 CONTINUE
      CALL GRAPH2(Z,Y,MFIT,ICON,MMAX,IPRINT)
      RETURN
      END
```

```
      SUBROUTINE CALCFX(N,X,F)
      DIMENSION Z(10,25),Y(10,25),QN(20),QH(20),QC(20),RATE(20),TEMP(20)
     1,X(10),YC(20),E(20),TINV(20) ,RATEC(20)
      COMMON M,MN,BH,PH(20),PC(20),BH,BC,AK,X1,X2,X3,X4,X5,NUMERO
     2  ,YE(50)
      IF (N) 1000,1000,1001
C
C ***  READ DATA AND CHANGE DIMENSIONS
C
 1000 CONTINUE
      READ(5,650)MFIT,MMAX
  650 FORMAT(2(X,I2))
      READ(5,700)MN
  700 FORMAT (I1)
      READ(5,100) NUMERO
  100 FORMAT(I2)
      READ(5,200)(QN(I),QH(I),QC(I),RATE(I),TEMP(I),I=1,NUMERO)
  200 FORMAT(2(5(F5.1,1X)))
      DO 22I=1,NUMERO
      TEMP(I)=TEMP(I)+273.
      TINV(I)=1./TEMP(I)
      S=QN(I)+QH(I)+QC(I)
      T=760./S
      PH(I)=QH(I)*T
      PC(I)=QC(I)*T
   22 CONTINUE
      WRITE(6,290)
  290 FORMAT(///////41X,
     1       50HQN        QH        QC       RATE    TEMP(K)                )
      WRITE(6,300)(QN(I),QH(I),QC(I),RATE(I),TEMP(I),I=1,NUMERO)
  300 FORMAT((35X,5(4X,F5.1)))
      RETURN
C
C ***  CALCULATION OF FUNCTION TO BE MINIMIZED
C
 1001 F=0.
      GO TO(10,20,30,40,50,60,70,80,90),M
C               3 PARAMETERS MODEL 1  L-H COMPETITIVE
C
   10 AK=EXP(X(1))
      BH=EXP(X(2))
      BC=EXP(X(3))
      DO 1 I=1,NUMERO
      YE(I)=ALOG(RATE(I))
      YC(I)=X(1)+X(2)+X(3)+ALOG(PC(I)*PH(I)/((1.+BH*PH(I)+BC*PC(I))**2))
      F(I)=YC(I)-YE(I)
      RATEC(I)=EXP(YC(I))
      E(I)=(EXP(F(I))-1.)*100.
      F=F+E(I)**2
      BN=3.
    1 CONTINUE
      GO TO 91
C
C               3 PARAMETERS MODEL 2  L-H NON-COMPETITIVE
C
   20 AK=EXP(X(1))
      BH=EXP(X(2))
      BC=EXP(X(3))
      DO 2 I=1,NUMERO
      YE(I)=ALOG(RATE(I))
      YC(I)=X(1)+X(2)+X(3)+ALOG(PC(I)*PH(I)/((1.+BH*PH(I))*(1.+BC*PC(I))
     1                                                                  ))
```

```
      E(I)=YC(I)-YE(I)
      RATEC(I)=EXP(YC(I))
      E(I)=(EXP(E(I))-1.)*100.
      F=F+E(I)**2
      BN=3.
    2 CONTINUE
      GO TO 91
C               2 PARAMETERS MODEL 3  RIDEAL-ELEY
C
   30 AK=EXP(X(1))
      BH=EXP(X(2))
      DO 3 I=1,NUMERO
      YE(I)=ALOG(RATE(I))
      YC(I)=X(1)+X(2)+ALOG(PC(I)*PH(I)/(1.+BH*PH(I)))
      E(I)=YC(I)-YE(I)
      RATEC(I)=EXP(YC(I))
      E(I)=(EXP(E(I))-1.)*100.
      F=F+E(I)**2
      BN=2
    3 CONTINUE
      GO TO 91
   40 CONTINUE
   50 CONTINUE
   60 CONTINUE
   70 CONTINUE
   80 CONTINUE
   90 CONTINUE
   91 AN=NUMERO
      F=SQRT(F/(AN-BN))
      IF(N-10) 1002,1002,1003
 1003 CONTINUE
      WRITE(6,500)
  500 FORMAT(////////40X,
     4       50HPH          PC        RATE     RATEC    TEMP(K)      ER
      WRITE(6,600)(PH(I),PC(I),RATE(I),RATEC(I),TEMP(I),E(I),I=1,NUMERO
  600 FORMAT((35X,6(4X,F5.1)))
      WRITE(6,900)
  900 FORMAT(///29X,1HK,10X,2HBH,10X,2HBC,6X,11HSTAND.DEV.  ,2X,
     67HTEMP(K)  ,6X,4HTINV)
      WRITE(6,400)AK,BH,BC,F,TEMP(1),TINV(1)
  400 FORMAT(21X,6E12.4)
      X1=X(1)
      X2=X(2)
      X3=X(3)
      X4=X(4)
      X5=X( 5)
      CALL GRAFICO(Z,Y,MFIT,MMAX)
 1002 CONTINUE
      RETURN
      END
```

REFERENCES

1. Catalyst Handbook, Wolfe Scientific Books, London (1970).

2. White, G.A., Roszkowski, T.R. and Stanbridge, D.W., Hydro-Carbon Processing 54, 130 (1975).

3. Szepe, S. and Levenspiel, O., Proc. 4th Symposium on Chemical Reaction Engineering, Brussels (1968), Pergamon Press (1971).

4. Satterfield, C.N., Mass Transfer in Heterogeneous Catalysis, MIT Press, Massachusetts (1970).

5. Thomas, J.M. and Thomas, W.J., Introduction to the Principles of Heterogeneous Catalysis, Academic Press, London (1967).

6. Presland, A.E.B. and Walker, Jr., P.L., Carbon 7, 1 (1969).

7. Figueiredo, J.L., Ph.D. Thesis, University of London (1975).

8. Dent, F.J., 49th Report of the Joint Research Committee, Trans. Inst. Gas Eng., p.602 (1945-6).

9. Gilliland, E.R. and Harriott, P., Ind. and Eng. Chem. 46, n.10, 2195 (1954).

10. Rostrup-Nielsen, J.R., J. Catal. 27, 343 (1972).

11. Renaud, M. and Bonnetain, L., J. Catal. 33, 160 (1974).

12. Hougen, O.A., Watson, K.M. and Ragatz, R.A., Chemical Process Principles, Part II, 2nd Ed., John Wiley and Sons, New York (1959).

13. Lobo, L.S., Ph.D. Thesis, University of London (1971).

14. Hirth, J.P. and Pound, G.M., Condensation and Evaporation. Nucleation and Growth Kinetics, Progress in Material Science 11, Pergamon Press (1963).

15. Strickland-Constable, R.F., Kinetics and Mechanism of Nucleation, Academic Press, London (1968).

16. Lane, G.E., Ph.D. Thesis, University of London (1972).

17. Hartman, P., Crystal Growth: An Introduction, North-Holland (1973).

18. Burke, J., The Kinetics of Phase Transformation in Metals, Pergamon Press, London (1965).

19. Frank, F.C., Discuss. Faraday Soc. 5, 48 (1949).

20. Sears, G.W., J. Chem. Phys. 31, 358 (1959).

21. Baird, R., Feates, F. and Harris, P., Carbon 10, 93 (1972).

22. Baker, R.T.K., Harris, P.S., Thomas, R.B. and Waite, R.J., J. Catal. 30, 86 (1973).

23. Biscoe, J. and Warren, B.E., J. Appl. Phys. 13, 364 (1942).

24. Franklin, R.E., Acta Crystallogr. 4, 253 (1951).

25. Takahashi, H., Kuroda, H. and Akamatu, H., Carbon 2, 432 (1964).

26. La Cava, A.I., Ph.D. Thesis, University of London (1976).

27. Conroy, J.S., Slysh, R.S., Murphy, D.B. and Kinney, C.R., Proc. Third Carbon Conf. (1957), p.395, Pergamon Press, London (1959).

28. Banarjee, B.C., Hirth, T.J. and Walker Jr., P.L., Nature 192, 450 (1961).

29. Robertson, S.D., Nature 221, 1044 (1969).

30. Moayeri, M., M.Sc. Thesis, University of London (1970).

31. Blau, G., D.I.C. Thesis, Imperial College (1969).

32. Presland, A., Roscoe, C. and Walker Jr., P.L., Proc. of 3rd Conf. on Ind. Carbons and Graphite, Soc. Chem. Ind., p.116 (1971).

33. Blau, G. and Presland, A., ibid., p.121.

34. Derbyshire, F.J., Ph.D. Thesis, University of London (1974).

35. Derbyshire, F.J. and Trimm, D.L., Carbon 13, 189 (1975).

36. Baker, R., Barber, M., Harris, P., Feates, F. and Waite, R., J. Catal. 26, 51 (1972).

37. Grenga, H.E. and Lawless, K.R., J. Appl. Phys. 43, 1508 (1972).

38. Karu, A. and Beer, M., J. Appl. Phys. 37, 2179 (1966).

39. Tomita, A., Yoshida, K., Nishiyama, Y. and Tamai, Y., Carbon 10, 601 (1972).

40. Tamai, Y., Nishiyama, Y. and Takahashi, M., Carbon 6, 593 (1968).

41. Leidheiser, H. and Gwathmey, A., J. Am. Chem. Soc. 70, 1206 (1948).

42. Cunningham, R. and Gwathmey, A., Adv. in Catalysis 9, 25 (1957).

43. Gwathmey, A. and Cunningham, R., Adv. in Catalysis 10, 57 (1958).

44. Robertson, S.D., Carbon 8, 365 (1970).

45. Rostrup-Nielsen, J.R. and Trimm, D.L., J. Catal. 48, 155 (1977).

46. Baker, R.T.K., Gadsby, G.R., Thomas, R.B. and Waite, R.J., Carbon 13, 211 (1975).

47. Escoubes, M., Quinson, J. and Eyraud, C., Bull. Soc. Chim. de France, 2435 (1967).

48. Lafitau, H. and Jacque, L., Bull. Soc. Chim. de France, 4779, (1968).

49. Patrikeev, V., Odyakov, V. and Balandin, A., Zh. Prikl. Khim. (Leninegrad) 41, 1063 (1968).

50. Tamai, Y., Nishiyama, Y. and Takahashi, M., Carbon 7, 209 (1969).

51. Tesner, P., Robinovich, E., Rafalkes, I. and Arefieva, E., Carbon 8, 435, (1970).

52. Newman, B., Kroger, C. and Fingas, E., Z. Anorg. Chem. 197, 321 (1931).

53. Lobo, L.S. and Trimm, D.L., Nature 234, 15 (1971).

54. Baker, R., Feates, J. and Harris, P., Carbon 10, 93 (1972).

55. Robertson, S.D., Carbon 10, 221 (1972).

56. Lobo, L.S., Trimm, D.L. and Figueiredo, J.L., Proc. 5th Int. Congr. Catal., 1972, p.1125 (1973).

57. Lobo, L.S. and Trimm, D.L., J. Catal. 29, 15 (1973).

58. Fryer, J. and Paal, Z., Carbon 11, 665 (1973).

59. Lobo, L.S., Proc. III Simpósio Iberoamericano de Catalisis, 1972, Acta Cientifica Venezolana, p.219 (1973).

60. Nishiyama, Y. and Tamai, Y., J. Catal. 33, 98 (1974).

61. Moayeri, M., Ph.D. Thesis, University of London (1974).

62. Figueiredo, J.L. and Trimm, D.L., Prepr. London Int. Carbon-Graphite Conf., 4th, 194 (1974).

63. Toei, R., Kazuhiro, N., Yamada, K. and Okazaki, M., J. Chem. Eng. of Japan 8, no.2, 131 (1975).

64. Baker, R.T.K., Gadsby, G.R. and Terry, S., Carbon 13, 245 (1975).

65. Baker, R.T.K. and Waite, R.J., J. Catal. 37, 101 (1975).

66. Nishiyama, Y. and Tamai, Y., J. Catal. 45, 1 (1976).

67. Wentreck, P.R., Wood, B.J. and Wise, H., J. Catal. 43, 363 (1976).

68. Keep, C.W., Baker, R.T.K. and France, J.A., J. Catal. 41, 232 (1977).

69. McCarty, J.G. and Madix, R.J., J. Catal. 48, 422 (1977).

70. Renshaw, G., Roscoe, C. and Walker Jr., P.L., J. Catal. 22, 394 (1971).

71. Nishiyama, Y. and Tamai, Y., Carbon 14, 13 (1976).

72. Palmer , H.B. and Dormish, F.L., J. Phys. Chem. 68, 1553 (1964).

73. Wada, T., Wada, H., Elliott, J.F. and Chipman, J., Metall. Trans. 2, 2199 (1971).

74. Walker Jr., P.L., Rusinko, F. and Austin, L.G., Adv. Catal. 11, 133 (1959).

75. Ergun, S. and Mentser, M., Chemistry and Physics of Carbon, Vol.1, p.203, Edward Arnold, London (1965).

76. Walker Jr., P.L., Shelef, M. and Anderson, R.A., Chemistry and Physics of Carbon, Vol.4, p.287, Edward Arnold, London (1968).

77. Stanier, H. and McKean, J.B., Gas Journal 265, 111 (1951).

78. Hedden, K., Proc. 5th Conf. on Carbon, Vol.1, p.125, Pergamon Press, New York (1962).

79. Gregg, S.J. and Sing, K.S., Adsorption, Surface Area and Porosity, Academic Press, London (1967).

80. Marsh, H. and Rand, B., J. Colloid Interface Sci. 33, 101 (1970).

81. Marsh, H. and Rand, B., Carbon 9, 47 (1971).

82. John, P.T., Chetty, V.G. and Datta, K.K., Carbon 15, 169, (1977).

83. Walker Jr., P.L., Austin, L.J. and Tietjen, J.J., Chemistry and Physics of Carbon, Vol.1, p.327, Edward Arnold, London (1965).

84. Marsh, H. and Rand, B., Carbon 9, 63 (1971).

85. Tomita, A. and Tamai, Y., J. Catal. 27, 293 (1972).

86. Gaidai, N.A. and Kiperman, L.S., Kin i Kat. 15, no.4, 954 (1974).

87. Tomita, A., Sato, N. and Tamai, Y., Carbon 12, 143 (1974).

88. McKee, D.W., Carbon 12, 453 (1974).

89. Rewick, R.T., Wentreck, P.R. and Wise, H., Fuel 53, 274 (1974).

90. Marsh, H. and Taylor, D.W., Fuel 54, 219 (1975).

91. Marsh, H. and Adair, R.R., Carbon 13, 327 (1975).

92. Figueiredo, J.L. and Trimm, D.L., J. Catal. 40, 154 (1975).

93. Otto, K. and Shelef, M., Proc. 6th Int. Congr. Catal., 1976, Vol.2, p.1082, The Chemical Society (1977).

94. Tamai. Y., Watanabe, H. and Tomita, A., Carbon 15, 103 (1977).

95. Hahn, R. and Hüttinger, K.J., Prepr. 13th Biennal Conf. on Carbon, Irvine, California, p.44 (1977).

96. Marsh, H. and Taylor, D.W., ibid., p.46.

97. Tuddenheim, W.M. and Hill, G.R., Ind. Eng. Chem. 47, 2129 (1955).

98. Macack, J., Licka, S. and Malecha, J., Chimie et Industrie, 105, no.9 (1972).

99. Bridger, G.W., Prepr. Symposium Der Internationalen Gas-Union, paper 7, Karlsruhe (1972).

100. Moseley, F., Stephens, R.W., Stewart, K.D. and Wood, J., J. Catal. 24, 18 (1972).

101. Rostrup-Nielsen, J.R., J. Catal. 33, 184 (1974).

102. Ross, J.R.H., The Steam Reforming of Hydrocarbons, Sepecialist Periodical Reports, Vol.4, p.34, The Chemical Society, London (1975).

103. Bridger, G.W., Inst. Chem. Eng., 3rd Annual Research Meeting, Salford (1976).

104. Lahaye, J., Badie, P. and Ducret, J., Carbon 15, 87 (1975).

105. Bhatta, K.S.M. and Dixon, G.M., Trans. Faraday Soc. 63, 2217 (1967).

106. Andrew, S.P.S., Chem. Eng. Progr. Symp. 63, 90 (1967).

107. Kaiser, R., Gas Phase Chromatography, Butterworths (1963).

108. Goldwasser, M., Ph.D. Thesis, University of London (1976).

109. Bridger, G.W. and Davies P., B.P., 1 003 702 (1965).

110. Kokes, R.J. and Emmet, P.H., J. Am Chem. Soc. 82, 1037 (1960).

111. Richardson, R.L. and Benson, S.W., J. Phys. Chem. 61, 405 (1957).

112. Walker Jr., P.L., Rakszawski, J.F. and Imperial, G.R., J. Phys. Chem. 63, 133 (1959).

113. Ross, J.R.H. and Steel, C.F., Trans. Faraday Soc. 69, 10 (1973).

114. Rao, Y.K. and Taplan, B.P., Metall. Trans. 3, 2465 (1972).

115. Perderau, M.M., Compt. Rendue Acad. Sci., Paris, 267, Serie C, 1288 (1968).

116. Baird, T., Fryer, J.R. and Grant, B., Carbon 12, 591 (1974).

117. Lander, J.J., Kern, H.E. and Beach, A.L., J. Appl. Phys. 23, 1305 (1952).

118. Shavensin, A.B., Minkevitch, A.H. and Scherbinski, G.B., Chern. Met. 1, 95 (1965).

119. Schenk, H., Arch. Eisenhuetternw. 36, 107 (1965).

120. Smith, R.P., Trans. Met. Soc. AIME 224, 1224 (1966).

121. Kovenskiy, I.I., Fiz. Metal. Metalloved. 16, 4, 613 (1963).

122. Massaro, T.A. and Petersen, E.E., J. Appl. Phys. 42, 5534 (1971).

123. Lavrovski, K.P., Kalinenko, R.A. and Shevelikova, L.V., Proc. 8th World Petroleum Congress, Vol.4, p.357, Appl. Science Publ., London (1971).

124. Hayward, D.L. and Trapnell, B.M.W., Chemisorption, Butterworths, London (1964).

125. Wedler, G. and Fisch, G., Ber. Kernforschungsanlage Juelich, No.6 (Vol.1), p.215 (1972).

126. Thomson, S.J. and Webb, G., Heterogeneous Catalysis, Oliver and Boyd, Edinburgh and London (1968).

127. Bond, G.C., Catalysis by Metals, Academic Press, London (1962).

128. Weeler, S.W., Chemical Reaction Eng. Reviews. Advances in Chemistry, Series 148, American Chemical Soc., p.26 (1975).

129. Boudart, M., AIChe J. 2, 62 (1956) and 18, 465 (1972).

130. Robinovich, E.Y. and Radionov, A.V., Trudy Vses. Issled, Inst. Prirod. Gazov. 6, 37 (1959).

131. Figueiredo, J.L. and Trimm, D.L., J. Catal. 40, 154 (1975).

132. Blakeley, T.H., Proc. 4th Conf. on Carbon (1959), p.95, Pergamon Press (1960).

133. Weisz, P.B. and Prater, C.D., Adv. in Catalysis 6, 143 (1954).

134. Gordon, A.S., Ind. Eng. Chem. 44, 1857 (1952).

135. Balashova, S.A., Slovokhotova, T.A. and Balandin, A.A., Kinetics and Catalysis 7, 273 (1966).

136. Rostrup-Nielsen, J.R., J. Catal. 31, 173 (1973).

137. Figueiredo, J.L. and Trimm, D.L., Prep. V. Simpósio Iberoamericano de Catálise, Lisbon (1976).

138. Baird, T., Fryer, J. and Grant, B., Nature 233, 329 (1971).